EFFECTS OF STRUCTURAL COMPONENTS ON RHEOLOGICAL AND MELTDOWN PROPERTIES OF ICE CREAM

by

Dieyckson Osvani Freire

A dissertation submitted in partial fulfillment of

the requirements for the degree of

Doctor of Philosophy

(Food Science)

at the

UNIVERSITY OF WISCONSIN-MADISON

2020

Date of final oral examination: 1/16/2020

The dissertation is approved by the following members of the Final Oral Committee:

Richard W. Hartel, Professor, Food Science

Scott A. Rankin, Professor, Food Science

Bradley W. Bolling, Assistant Professor, Food Science

Sundaram Gunasekaran, Professor, Biological Systems Engineering

DEDICATION

This thesis is dedicated to all my Family, in special to my wife, Tassy, daughters, Elisa and Isabela, parents, Joao and Conceicao, and sisters, Tati and Jessica, and is written in memory of my beloved ones Godfather, Antônio Jacinto de Souza,

uncle, Ademar Torres, and aunt, Maria Osani Torres.

ABSTRACT

Although ice phase plays a dominant role on the physical properties of ice cream, other structural components also affect rheological and meltdown properties. However, there is a lack of information about these relationships in literature. Thus, the objectives of this work were to assess the effects of structural components on the rheological and meltdown properties. It was hypothesized that (1) rheological and meltdown properties were affected by fat destabilization, overrun and mix viscosity, among other parameters, and (2) meltdown behavior was influenced by the rheological properties of the ice cream matrix. Ice creams were made with a wide range of extent of fat destabilization (partially coalesced fat globules), overrun and mix viscosity (serum phase viscosity) to provide a wide range of structures and rheological properties. The structural parameters affected not only the meltdown properties, such as drip-through rate and final height, but also the rheological properties, including storage modulus, residual viscosity, yield stress and rheological destruction, obtained as thixotropy. Good correlations between the rheological parameters at 0°C with meltdown parameters were found. Structural parameters also affected rheological and meltdown properties in commercial ice cream products. Remarkably, models from the study with ice creams with controlled structural formation were found to fit well the commercial sample data.

INTRODUCTION

Ice cream has an intricate multiphasic structure, which is formed mainly during dynamic freezing (churning and freezing at the same time) of the mix. The intrinsic arrangement of structural components governs its physical properties affecting directly meltdown behavior, texture and sensory properties during consumption. An unfrozen serum phase holds structural components dispersed together, such as ice crystals, air cells, and individual and clustered fat globules.

Although ice phase volume and ice crystal size distribution are important structural components in ice cream, other structural components from air, fat and serum phases also affect rheology and meltdown of ice cream. Moreover, although rheological properties are also a physical property of ice cream, rheological behavior of the initial structure formed during dynamic freezing affects not only equipment design and process adjustments in manufacturing, but also sensory, texture and meltdown properties.

Many studies have reported about ice cream rheology. However, the correlation between rheological and meltdown properties has been little explored in literature. The mechanical behavior strongly affects the performance of ice cream during meltdown test. Rheological parameters that are important for this mechanical performance during meltdown test of ice cream may provide more accurate instrumental characterization since many rheological measurements have their rheological constitutive equations. This accuracy in rheological measurements would be essential to further understand important empirical measurements for ice cream quality, such as sensory, texture and meltdown properties.

The use of model systems is important to control variables that would be impossible to control on an industrial scale, besides being economically unfeasible. However, although model

systems are important for studies in food science, the purpose of research is often their application in industry. Thus, the use of ice cream with controlled structural formation is essential to understand the influence of controlled variables on both structural formation and their physical properties. On the other hand, the evaluation of commercial ice cream products allows the practical validation of ice cream science.

In this context, the main objective of this study is to evaluate the effects of structural components on the rheological and meltdown properties and their correlations in ice cream. The study was divided into three parts: i) the effects of mix viscosity, extent of fat destabilization and overrun on rheological properties of ice creams with controlled structural formation, ii) the correlations between rheological and meltdown properties in those ice creams with controlled structural formation and iii) the effects of structural components on rheological and meltdown properties as well as their correlations in commercial ice cream products. In summary, the most important rheological parameters are presented in the three research chapters. However, specific rheological parameters were selected for further discussion so that the mechanical performance of the ice cream during meltdown tests could be highlighted. Furthermore, the first (Chapter 2) and second (Chapter 3) studies were used as foundation for the third study (Chapter 4), which evaluated commercial ice cream products available in grocery stores of a local market in the US.

ACKNOWLEDGEMENTS

First, I thank God for being present at every moment of my life. The completion of this work was made possible with the support and help of several people.

My deepest appreciation to my advisor, Professor Richard W. Hartel. First, for accepting me as a student in his research group. Second, for his great mentorship. The advice and opportunities that you allowed me to have during these years helped me become not only a better professional, but also a better person. It was really life changing. Last, for our great conversations about this complex product, ice cream!

Thanks to my committee members, Dr. Scott Rankin, Dr. Bradley Bolling and Dr. Sundaram Gunasekaran, for instructions, advice, time and for reviewing the thesis.

Thanks to my lab assistants/friends, in special, Rachel, Lexi, Morgan, Angie and Spring, for working with me during this time in Madison.

Thanks to all my lab friends for a great time in the basement, in special Jasmine, Maya, Amy, Sam, Abbey, Emily, Julia, Angel, Laura, Hassan, Vikash, Katie, Cara, Marielle, Mack, Katherine, Liana, CJ, Breeann, Kathleen, Yunna, Maddy, Kendra, Melanie, Margaret, Balaji, Karen, Lauren..

Thanks to all faculty and staff of the Department of Food Science that indirectly contributed to my journey in Madison.

Thanks to CNPq (National Council for Scientific and Technological Development – Brazil) for the scholarship and FDC (Frozen Dessert Center) for the financial support.

Thanks to my family for their support and prayers in the hard times, especially my mom, Conceição, my dad, João, my sisters, Tati and Jessica, and my grandma, Gloria.

Above all, I thank my beloved wife, Tassy, for her love and support over the years in good times and bad. I also thank God for the blessings and gifts poured into our lives, namely, my beloved daughters, Elisa and Isabela.

TABLE OF CONTENTS

Page

DEDICATION……i

ABSTRACT……...……ii

INTRODUCTION ……...……iii

ACKNOWLEDGEMENTS……..v

LIST OF TABLES……...xii

LIST OF FIGURES…….…...xiv

Chapter 1 Literature Review……1

1.1 Ice Cream……..……2

1.1.1 Ingredients of Ice Cream Mix……..…2

1.1.1.1 Milk Fat ……..……..…3

1.1.1.2 Milk Solids NonFat (MSNF) ……..……3

1.1.1.3 Sweeteners ……..……..…4

1.1.1.4 Emulsifiers ……..……..…4

1.1.1.5 Stabilizers ……..……..…5

1.1.2 Process ……..……..…5

1.1.2.1 Blending and Pasteurization…….……6

1.1.2.2 Homogenization……..… ……6

1.1.2.3 Cooling and Ageing…….…. ……...7

1.1.2.4 Dynamic Freezing……..… ……..7

1.1.2.5 Hardening and Storage…….…….. .8

1.2 Structural Components……..… …….8

1.2.1 Ice Phase…….……8

1.2.2 Air Phase…….……..10

1.2.3 Fat Phase ....…….…….....11

1.2.4 Serum Phase…….……13

1.3 Ice Cream Meltdown…….……...14

1.4 Ice Cream Rheology…….……...16

1.4.1 Oscillatory Thermo-Rheometry (OTR) …….……..16

1.4.2 Creep and Recovery…….……19

1.4.3 Stress Growth ……...21
1.4.4 Flow Ramp and Thixotropic Loop……25
1.5 Summary…….…….28
1.5 References…….……...28
Chapter 2 Effects of Serum Phase Viscosity, Partially-Coalesced Fat Globules and Overrun on the Rheological Properties of Ice Cream…..…….……..35
2.1 Abstract……..…….…36
2.2 Introduction…….…….37
2.3 Materials and Methods…….……38
2.3.1 Materials…….……...38
2.3.2 Experimental Design…….……39
2.3.3 Formulation and Processing…….… 39
2.3.4 Structural Components (Physical, Compositional and Structural Measurements) ……40
2.3.4.1 Ice Cream Mix Rheology ……..… 40
2.3.4.2 Overrun …….…….42
2.3.4.3 Particle/Fat Globule Size Distribution……42
2.3.4.4 Air Cell Size Distribution…….…. 42
2.3.4.5 Ice Crystal Size Distribution…….. 43
2.3.5 Ice Cream Rheological Properties……. 43
2.3.5.1 Oscillatory Thermo-Rheometry (OTR) ……. 44
2.3.5.2 Creep-Recovery…….…… 45
2.3.5.3 Stress Growth …….……... 45
2.3.5.4 Flow Ramp…….……46
2.3.6 Statistical Analysis……...……..…46
2.4 Results and Discussion……..…47
2.4.1 Structural Components (Structural Elements, Compositional and Physical Parameters) …47
2.4.1.1 Mix Rheology…….……47
2.4.1.2 Overrun…….…… 50
2.4.1.3 Percent of Partially Coalesced Fat Globules (Fat Destabilization) ……50
2.4.1.4 Air Cell Size…….……...……52
2.4.1.5 Ice Crystal Size……...……..…53

2.4.2 Rheological Properties of the Ice Cream Matrix……53
2.4.2.1 Oscillatory Thermo-Rheometry (OTR) ……53
2.4.2.2 Creep and Recovery Measurements ……58
2.4.2.3 Stress Growth (Constant Low Shear Rate) ……62
2.4.2.4 Flow Ramp (Shear Rate Ramp) and Thixotropy……66
2.5 Conclusions……72
2.6 Acknowledgements……73
2.7 References……73
Chapter 3 Correlations between Rheological Properties and Meltdown Behavior of Ice Cream……81
3.1 Abstract……82
3.2 Introduction……83
3.3 Materials and Methods……84
3.3.1 Materials……84
3.3.2 Experimental Design……85
3.3.3 Formulation and Processing……85
3.3.4 Physical, Compositional and Structural Measurements (Structural Components) ……86
3.3.4.1 Ice Cream Mix Viscosity ……86
3.3.4.2 Overrun ……87
3.3.4.3 Particle/Fat Globule Size Distribution……87
3.3.4.4 Air Cell Size Distribution……87
3.3.4.5 Ice Cell Size Distribution……88
3.3.5 Rheological properties……88
3.3.5.1 Oscillatory Thermo-Rheometry (OTR) ……89
3.3.5.2 Creep-Recovery……90
3.3.5.3 Stress Growth ……90
3.3.5.4 Flow Ramp……90
3.3.6 Statistical Analysis……91
3.4 Results and Discussion……91
3.4.1 Structural Components and their Correlations……91
3.4.2 Ice Cream Meltdown ……93

3.4.3 Ice Cream Rheology……..……93
3.4.4 Correlations between Rheology and Meltdown Behavior…….……94
3.4.4.1 Storage Modulus ($G'_{0°C}$) from Oscillatory Thermo-Rheometry (OTR) ……..…95
3.4.4.2 Residual Viscosity (η_0) from Generalized Kevin-Voigt Model (Creep Measurements)...103
3.4.4.3 Yield Stress (σ_Y) from Stress Growth Measurements……...……111
3.4.4.4 Thixotropy from Flow Measurements (Shear Rate Ramp) ……..……119
3.5 Conclusions……125
3.6 Acknowledgements……127
3.7 References……..……128
Chapter 4 Effects of Structural Elements, Compositional and Physical Parameters on Meltdown Behavior and Rheological Properties of Commercial Ice Cream Products……...……135
4.1 Abstract……..……136
4.2 Introduction……137
4.3 Materials and Methods……...……138
4.3.1 Materials……..……138
4.3.2 Compositional, Physical and Structural Measurements (Structural Components) ….....…138
4.3.2.1 Fat content…….……...……138
4.3.2.2 Total solids……...……138
4.3.2.3 Ice cream mix density……...……139
4.3.2.4 Overrun……139
4.3.2.5 Particle/Fat Globule Size Distribution……..……139
4.3.2.6 Air Cell Size Distribution…….……140
4.3.2.7 Ice Crystal Size Distribution…….……140
4.3.3 Drip-Through Rate……..……142
4.3.4 Rheological properties of Commercial Ice Cream Products……143
4.3.4.1 Oscillatory Thermo-Rheometry (OTR) ……...……144
4.3.4.2 Creep-Recovery……144
4.3.4.3 Stress Growth ……..……145
4.3.5 Statistical Analysis……..……145
4.4 Results and Discussion……...……146

4.4.1 Compositional/Physical Parameters and Structural Elements……146
4.4.1.1 Total Fat…… ...147
4.4.1.2 Total Solids……...147
4.4.1.3 Density of Ice Cream Mix ……147
4.4.1.4 Overrun…… 147
4.4.1.5 Percent of Partially-Coalesced Fat Globules (Fat Destabilization) …… 148
4.4.1.6 Air Cell Size…… 148
4.4.1.7 Ice Crystal Size…… 149
4.4.2 Drip-Through Rate ……..……...149
4.4.3 Rheological Properties of the Ice Cream Matrix…….……151
4.4.3.1 Oscillatory Thermo-Rheometry (OTR) ……...……151
4.4.3.2 Creep and Recovery Measurements ……156
4.4.3.3 Stress Growth (Constant Low Shear Rate) ……..……161
4.4.4 Correlations between Rheological Parameters and Drip-Through Rate (DT)….……166
4.5 Conclusions……169
4.6 Acknowledgements……170
4.7 References……..……171
Chapter 5 Conclusions and Recommendations ……..…… 177
5.1 Conclusions……178
5.2 Recommendations……..……181

LIST OF TABLES

Page

Table 2.1 Means and standard errors for mix viscosity at 50 s^{-1}, overrun, extent of fat destabilization (FD), air cell and ice crystal size from ice creams with manipulated structures. One-way ANOVA and Tukey's HSD ($\alpha = 0.05$) tests were performed to determine significant difference within the data……...….78

Table 2.2 Parameter estimates, coefficients of determination (R^2 and R^2_{Adj}) and F ratios of multiple linear regression (MLR) models (n=27) for rheological parameters from the oscillatory thermo-rheometry (OTR), creep/recovery, stress growth and flow ramp measurements……...……...…79

Table 2.3 Means and standard errors for $tan\delta_{Peak}$ from ice creams with manipulated structures. One-way ANOVA and Tukey's HSD ($\alpha = 0.05$) tests were performed to determine significant difference within the data ……....80

Table 3.1 Means and standard errors for mix viscosity at 50s^{-1}, overrun, extent of fat destabilization (FD), air cell and ice crystal sizes of the ice creams with controlled structural formation. One-way ANOVA and Tukey's HSD ($\alpha = 0.05$) tests were performed to determine significant difference within the data. Source: Wu, Freire and Hartel (2019) and Chapter 2….....…..……..…….131

Table 3.2 Means and standard errors for meltdown parameters (drip-through rate and final height) of the ice creams with controlled structural formation. One-way ANOVA and Tukey's HSD ($\alpha = 0.05$) tests were performed to determine differences within the data. Source: Wu, Freire and Hartel (2019)……..……..132

Table 3.3 Means and standard errors for rheological parameters measured at 0°C, storage modulus ($G'_{0°C}$), residual viscosity from the six-element model ($\eta_{0\,0°C}$) in creep data, yield stress from stress growth ($\sigma_{Y\,0°C}$) and thixotropy ($Thix_{0°C}$) from flow ramp. One-way ANOVA and Tukey's HSD ($\alpha = 0.05$) tests were performed to determine difference within the data. Source: Chapter 2. ……..133

Table 3.4 Parameter estimates and coefficients of determination (R^2) for three term exponential models (n=27), in which rheological parameters measured at 0°C, storage modulus ($G'_{0°C}$), residual viscosity from the creep data fitted by six-element model ($\eta_{0\,0°C}$), yield stress from stress growth ($\sigma_{Y\,0°C}$) and rheological destruction from up and down flow ramp ($Thix_{0°C}$ from FR). from the oscillatory thermo-rheometry (OTR), creep/recovery, stress growth and flow ramp measurements……..……..134

Table 3.5 Parameter estimates and coefficients of determination (R^2) for three term exponential models (n=27), in which rheological parameters measured at 0°C, storage modulus ($G'_{0°C}$), residual viscosity from the creep data fitted by six-element model ($\eta_{0\ 0°C}$), yield stress from stress growth ($\sigma_{Y\ 0°C}$) and rheological destruction ($Thix_{\ 0°C}$). from the oscillatory thermo-rheometry (OTR), creep/recovery, stress growth and flow ramp measurements……134

Table 4.1 Comparison of means using Tukey's HSD for total fat, total solids, ice cream mix density (ICM density), overrun, extent of fat destabilization (FD), air cell and ice crystal sizes of commercial ice creams products ($\alpha = 0.05$). ……174

Table 4.2 Parameter estimates, coefficients of determination (R^2 and R^2_{Adj}) of the multiple linear regression models for storage (G') and loss (G") moduli, loss tangent (tanδ), residual viscosity (η_0) and yield stress (σ_y) at 0 and 20°C. ……175

Table 4.3 Comparison of means using Tukey's HSD for storage (G') and loss (G") moduli, loss tangent (tanδ), residual viscosity (η_0) and yield stress (σ_{YS}) at 0 and 20°C of commercial ice cream products ($\alpha = 0.05$).……176

LIST OF FIGURES

Page

Figure 1.1 Schematic diagram of phenomenological analysis for stress overshoot data. Source: Elliott and Ganz (1977) mentioned in Rao (2007).……..……...….23

Figure 1.2 Shear diagram of shear rate versus shear stress for time-independent flow behavior, Newtonian, shear-thinning, and shear-thickening. Moreover, fluids with yield stress, Bingham and Herschel-Bulkley. Source: Rao (2007)……...26

Figure 1.3 Diagram for up and down curves of shear stress against shear rate from a stepped flow test (flow sweep) using parallel plates and steady state sensing (5% tolerance within 30 seconds in three consecutive sampling) for a typical thixotropic system with 40% overrun and low fat destabilization at 0°C…….……..…...….27

Figure 2.1 Particle size distributions for samples: (A) with different levels of stabilizer (S1, S2 and S3 refer to 0, 0.2 and 0.4%, respectively), and constant levels of PS80 (0.015%) and air flow (11L.h^{-1}); (B) with different levels of air flow (A1, A2 and A3 refer to 8, 11 and 15L.h^{-1}, respectively), and constant levels of stabilizer (0.2%) and PS80 (0.015%)……51

Figure 2.2 (A) Storage (G') and loss (G") moduli behavior for samples S1A1P1 (0% stabilizer, 8L.h^{-1} air flow and 0% PS80) and S3A3P3 (0.4% stabilizer, 15L.h^{-1} air flow and 0.03% PS80). (B) Tanδ behavior for the samples S1A1P1 and S3A3P3. ……...….54

Figure 2.3 (A) Sample S2A2P2 (0.2% stabilizer, 11L.h^{-1} air flow and 0.015% PS80) used as example for maximum creep strain (MCS) and recovery (%R); (B) Springs and dashpots of the six-element model (Maxwell model in series with two Kelvin-Voigt models); (C) sample S2A2P2 used as example for prediction of creep compliance by the six-element model……...….59

Figure 2.4 (A) Schematic diagram of phenomenological analysis adapted from Elliott and Ganz (1977) and Rao (2007) using sample S2A2P2 at 0°C. (B) Stress growth test at a constant shear rate of 0.01s^{-1} using steady state sensing (5% tolerance within 30 seconds in three consecutive sampling) for samples S1A1P1 and S3A3P3 at 0°C.…….……...….63

Figure 2.5 Log-log plot of up and down curves of shear stress against shear rate from a flow sweep test using parallel plates and steady state sensing (5% tolerance within 30 seconds in three consecutive sampling) for a melted ice cream with 40% overrun and low fat destabilization at 0°C.……..……...….67

Figure 2.6 (A) Shear stress (up and down) and (B) instantaneous viscosity (up and down) curves for the sample S2A2P2; and (C) schematic diagram to illustrate the parameters, such as maximum instantaneous viscosity (η_M), correspondent stress to the maximum instantaneous viscosity (σ_{MV}) and height of the stress peak (σ_{Peak}), were obtained from the up shear rate ramp……...….68

Figure 2.7 Correlation between rheological destruction measurement (Thix $_{0°C}$) and the observed peak at tanδ curve ($\tan\delta_{Peak}$) during oscillatory thermo-rheometry (OTR). ……..……...….71

Figure 3.1 Behavior of storage modulus ($G'_{0°C}$) versus drip-through rate (DT) for samples with controlled mix viscosity, overrun and extent of fat destabilization [Data compiled from Wu et al. (2019) and Chapter 2]. Line is fitted exponential model.……....……...….96

Figure 3.2 (A) Drip-through rate (grey circle) and G' at 0°C ($G'_{0°C}$) (black square) versus extent of fat destabilization; (B) Drip-through rate (grey triangle) and $G'_{0°C}$ (black circle) versus mix viscosity (at $50s^{-1}$); (C) Drip-through rate (grey diamond) and $G'_{0°C}$ (black triangle) versus overrun [Data compiled from Wu, Freire and Hartel (2019) and Chapter 2]……..……...….98

Figure 3.3 Behavior of storage modulus ($G'_{0°C}$) versus and final height (FH) for samples with controlled mix viscosity, overrun and extent of fat destabilization [Data compiled from Wu et al. (2019) and Chapter 2]. Line is fitted exponential model…….……...….101

Figure 3.4 (A) Final Height (hollow circle) and G' at 0°C ($G'_{0°C}$) (black square) versus extent of fat destabilization; (B) Final Height (hollow triangle) and $G'_{0°C}$ (black circle) versus mix viscosity (at $50s^{-1}$); (C) Final Height (hollow diamond) and $G'_{0°C}$ (black triangle) versus overrun [Data compiled from Wu et al. (2019) and Chapter 2].……...….102

Figure 3.5 Behavior of residual viscosity ($\eta_{0\ 0°C}$) from generalized Kelvin-Voigt model versus drip-through rate for samples with controlled mix viscosity, overrun and extent of fat destabilization [Data compiled from Wu et al. (2019) and Chapter 2]. Line is fitted exponential model.……...….106

Figure 3.6 (A) Drip-through rate (grey circle) and $\eta_{0\ 0°C}$ (black square) versus extent of fat destabilization; (B) Drip-through rate (grey triangle) and $\eta_{0\ 0°C}$ (black circle) versus mix viscosity (at $50s^{-1}$); (C) Drip-through rate (grey diamond) and $\eta_{0\ 0°C}$ (black triangle) versus overrun [Data compiled from Wu et al. (2019) and Chapter 2].…… ……...….107

Figure 3.7 Behavior of residual viscosity ($\eta_{0\ 0°C}$) from generalized Kelvin-Voigt model versus final height (FH) for samples with controlled serum phase viscosity, overrun and extent of fat destabilization [Data compiled from Wu et al. (2019) and Chapter 2]. Line is fitted exponential model……..….109

Figure 3.8 (A) Final Height (hollow circle) and $\eta_{0\ 0°C}$ (black square) versus extent of fat destabilization; (B) Final Height (hollow triangle) and $\eta_{0\ 0°C}$ (black circle) versus mix viscosity (at $50s^{-1}$); (C) Final Height (hollow diamond) and $\eta_{0\ 0°C}$ (black triangle) versus overrun [Data compiled from Wu et al. (2019) and Chapter 2].…… ……...……...….110

Figure 3.9 Behavior of yield stress ($\sigma_{Y\ 0°C}$) versus drip-through rate (DT) for samples with controlled mix viscosity, overrun and extent of fat destabilization [Data compiled from Wu et al. (2019) and Chapter 2]. Line is fitted exponential model.……..……...….112

Figure 3.10 (A) Drip-through rate (grey circle) and $\sigma_{Y\ 0°C}$ (black square) versus extent of fat destabilization; (B) Drip-through rate (grey triangle) and $\sigma_{Y\ 0°C}$ (black circle) versus mix viscosity (at $50s^{-1}$); (C) Drip-through rate (grey diamond) and $\sigma_{Y\ 0°C}$ (black triangle) versus overrun [Data compiled from Wu et al. (2019) and Chapter 2].……...….114

Figure 3.11 Behavior of yield stress ($\sigma_{Y\ 0°C}$) versus final height (FH) for samples with controlled mix viscosity, overrun and extent of fat destabilization [Data compiled from Wu et al. (2019) and Chapter 2]. Line is fitted Michaelis Menten model.……..…...….116

Figure 3.12 (A) Final Height (hollow circle) and $\sigma_{Y\ 0°C}$ (black square) versus extent of fat destabilization; (B) Final Height (hollow triangle) and $\sigma_{Y\ 0°C}$ (black circle) versus mix viscosity (at $50s^{-1}$); (C) Final Height (hollow diamond) and $\sigma_{Y\ 0°C}$ (black triangle) versus overrun [Data compiled from Wu et al. (2019) and Chapter 2].……..…...….117

Figure 3.13 Behavior of thixotropy ($Thix_{0°C}$) versus drip-through rate (DT) for samples with controlled mix viscosity, overrun and extent of fat destabilization [Data compiled from Wu et al. (2019) and Chapter 2]. Line is fitted exponential model.……...……..…….120

Figure 3.14 (A) Drip-through rate (grey circle) and $Thix_{0°C}$ (black square) versus extent of fat destabilization; (B) Drip-through rate (grey triangle) and $Thix_{0°C}$ (black circle) versus mix viscosity (at $50s^{-1}$); (C) Drip-through rate (grey diamond) and $Thix_{0°C}$ (black triangle) versus overrun [Data compiled from Wu et al. (2019) and Chapter 2].……...….122

Figure 3.15 Behavior of thixotropy (Thix $_{0°C}$) versus final height (FH) for samples with controlled mix viscosity, overrun and extent of fat destabilization [Data compiled from Wu et al. (2019) and Chapter 2]. Line is fitted exponential model.……..……...….124

Figure 3.16 (A) Final Height (hollow circle) and Thix $_{0°C}$ (black square) versus extent of fat destabilization; (B) Final Height (hollow triangle) and Thix $_{0°C}$ (black circle) versus mix viscosity (at $50s^{-1}$); (C) Final Height (hollow diamond) and Thix $_{0°C}$ (black triangle) versus overrun [Data compiled from Wu et al. (2019) and Chapter 2].……...….126

Figure 4.1 Particle size distribution of sample 129 used as example of melted ice cream products. Casein micelle peak between 0.1-0.3 µm, initial emulsion peak between 0.3-5 µm, and destabilized fat peak beginning around 5 µm…..….141

Figure 4.2 (A) Drip-through curves of samples 880 and 957. (B) Drip-through rate behavior of commercial ice cream products predicted by extent of fat destabilization. Triangles are ice cream sandwich samples.……...….150

Figure 4.3 Behavior of storage (G') and loss (G") moduli (A) as well as tanδ (B) during oscillatory thermo-rheometry (OTR) of the samples 880 and 957.……...….152

Figure 4.4 Example for behavior of storage (G') and loss (G") moduli, obtained from oscillatory thermo-rheometry (OTR), against extent of fat destabilization at (A) 0°C and (B) 20°C. Triangles are ice cream sandwich samples. Lines are linear trend line…….……..…...….155

Figure 4.5 (A) Creep and recovery measurements for sample 880 at 0°C used as example maximum creep strain (MCS) and recovery; (B) springs and dashpots of the generalized Kelvin-Voigt model (Maxwell unit in series with N Kelvin-Voigt units); (C) observed creep compliance data over time with six-element model for sample 880.…….……...….158

Figure 4.6 Influence of (A) fat destabilization, (B) overrun and (C) air cell size on residual viscosity (η_0) from six-element models at 0 and 20°C. Triangles are ice cream sandwich samples. Triangles are ice cream sandwich samples. Lines are linear trend line.…… …….……...….160

Figure 4.7 (A) Schematic diagram for phenomenological analysis using sample 880 at 0°C and (B) stress growth test for samples 957 at 0°C.…….….163

Figure 4.8 Influence of (A) fat destabilization, (B) overrun and (C) air cell size on residual viscosity (σ_Y) from six-element models at 0 and 20°C. Triangles are ice cream sandwich samples. Lines are linear trend line.…….…...….165

Figure 4.9 Correlations of drip-through rate with (A) storage modulus ($G'_{0°C}$), (B) residual viscosity **(**$\eta_{0\ 0°C}$) and (C) yield stress ($\sigma_{Y\ 0°C}$) at 0°C compared to exponential decay models for ice creams with controlled structural formation from previous work (Chapter 3). Triangles are ice cream sandwich samples. Lines and dotted lines are models and their 95% confidence intervals, respectively, from previous work (Chapter 3).……..……..……...….168

Chapter 1

1 Literature Review

1.1 Ice Cream

Ice cream is a complex product, which consists of a multiphasic microstructure formed mainly during freezing (churning and freezing at the same time) of ice cream mix (Goff and Hartel, 2013). Ice crystals, air cells, and individual and clustered fat globules are dispersed in an unfrozen serum phase (Goff and Hartel, 2013). Although ice phase affects physical behavior of ice cream products, such as meltdown and rheological properties, other structural components from air, fat and serum phase are also important for meltdown and rheology of ice cream.

The legal definition of ice cream is different for each country. In the United States, the Standard of Identity for ice cream (Code of regulations, Title 2 Food and Drugs, Part 135 Frozen Desserts) requires at least 10% milkfat and 20% total milk solids. Moreover, minimum requirements for density (0.54kg/L) and total solids (0.19kg/L) in ice cream leads to approximately a maximum of 100% overrun (Goff and Hartel, 2013). Formulation and process are the main variables that affect structural formation in ice cream during freezing.

1.1.1 Ingredients of Ice Cream Mix

Ingredients used in mix formulation depend on quality of suppliers, availability, cost, legal definitions and market demand (Goff and Hartel, 2013). The levels and nature of ingredients also affect formation of structural components in ice cream matrix. In turn, structural components and their arrangement influence meltdown behavior and rheology of ice cream. In this section, the main ingredients of ice cream mix that affect structure of ice cream will be discussed.

1.1.1.1 Milk Fat

Cream, butter and vegetal fat are the most common sources of fat for mix formulations. Total fat in ice cream is related to its quality and cost. For instance, ice creams with more than 14% total fat are considered a premium product (Goff and Hartel, 2013). Milk fat contributes to nutritional aspects, flavor, acts as a synergistic carrier for flavor ingredients added, provides smooth texture and body, and desirable rheological and melting behavior (Goff and Hartel, 2013; Hartel et al., 2017). During freezing, individual fat globules may be destabilized due to shear forces in the barrel promoted by dasher, ice crystal formation, air incorporation and increased viscosity combined with the membrane composition of fat globules (Goff and Hartel, 2013; Warren and Hartel, 2018). High fat content in mix may lead to a dry and grainy texture, whereas low fat levels may lead to a smooth, homogeneous and slightly viscous texture (Walstra et al., 2006).

1.1.1.2 Milk Solids NonFat (MSNF)

Skim or whole milk powder, skim or whole milk, whey powder and whey protein products are among the main sources of milk solids nonfat (MSNF) in ice cream formulations. Cream is also a secondary MSNF source when it is used as a milkfat source. MSNF includes casein, whey proteins, lactose, mineral salts, vitamins and other minor components of milk. MSNF contributes to flavor, body, texture, freezing point depression, air cell stability and serum phase viscosity (Goff and Hartel, 2013). Greater protein level increases serum phase viscosity, stabilizes air cells, and improves body and nutritional value of ice cream. However, increased milk proteins can also inhibit destabilization of fat globules during freezing, which leads to issues in body, melting and texture properties of the ice cream (Daw and Hartel, 2015; Segall and Goff, 1999). Lactose content decreases freezing point and partially contributes sweetness in ice cream. High content of lactose can lead to greater impact in freezing point depression, malabsorption issues in consumer as well

as possible sensory defect due its crystallization, known as sandiness (Goff and Hartel, 2013; Hartel et al., 2017). Minerals, mainly calcium and phosphorus, contribute to nutritional value and also decrease freezing point in ice cream (Goff and Hartel, 2013).

1.1.1.3 Sweeteners

In traditional ice cream, nutritive sugars used in ice cream formulations include cane and beet sugars, corn sweeteners, maple sugar, honey, and fructose, among others. Sweeteners provide sweetness, affect ice phase through freezing point depression and improve texture. It is also an economic source for total solids. Sweeteners also increase acceptability of ice cream by enhancing flavors, mainly delicate fruit flavors. Lack of sweeteners provides flat taste and harder texture, while very high levels hide pleasant flavors. High sweetener levels can also impact whippability, which mainly affects freezing in batch freezers (Goff and Hartel, 2013). Finally, high levels of sweeteners can also decrease shelf life since increased volume of unfrozen serum phase may also increase molecular mobility in ice cream.

1.1.1.4 Emulsifiers

Whole eggs or egg yolks were historically added as emulsifiers in frozen desserts to improve sensory properties (Goff and Hartel, 2013; Hartel et al., 2017). The main types of emulsifiers added to ice cream formulations in industry are mono- and diglycerides and sorbitan esters. Blends of mono- and diglycerides and polysorbate 80 (PS80) are commonly used in ice cream manufacture with ranges of 0.1-0.2% and 0.02-0.04%, respectively (Goff and Hartel, 2013). Milk proteins in milk are sufficient to stabilize fat globules. However, emulsifier addition improves stability of air cells and promotes partial coalescence of fat globules during freezing of ice cream

(Goff and Hartel, 2013; Hartel et al., 2017; Walstra et al., 2006). Emulsifiers also improve fat nucleation during ageing, whippability quality, produce drier and stiffer texture, increase number of air cells and thinner lamellae, increase resistance to shrinkage and meltdown and provide smoother texture in ice cream (Goff and Hartel, 2013).

1.1.1.5 Stabilizers

Polysaccharides, which are polymers of sugar residues, are the most common hydrocolloids used in stabilizer systems of ice cream. Guar gum, locust bean gum (LBG) and xanthan gum are among the common polysaccharides used as stabilizers. Some polysaccharides, such as carrageenan, are added as secondary stabilizers to prevent phase separation (Goff and Hartel, 2013). Proteins (e.g., gelatin), which is less common, has also been used in stabilizer systems (Hartel et al., 2017; Miller-Livney and Hartel, 1997). Stabilizers are added to primarily increase viscosity of serum phase in ice cream. This results in a stable foam and suspension of flavor components, a decrease in moisture migration and shrinkage, increased melting resistance, more stable melting (without phase separation), a smoother texture and, mainly, a decrease in ice recrystallization during temperature fluctuations (Goff and Hartel, 2013). Moreover, some stabilizers, such as LBG, may form a gel-like network in the serum phase, which helps further decrease ice recrystallization during temperature fluctuations (Goff et al., 1999).

1.1.2 Process

Besides formulation, process conditions can also affect structure formation in ice cream. Basically, ice cream manufacture operations can be divided into three steps, manufacturing of mix, dynamic freezing and hardening. In mix manufacture, ingredients are combined and mixed,

followed by pasteurization, homogenization and ageing. After that, mix is frozen, followed by packaging and hardening steps.

1.1.2.1 Blending and Pasteurization

In general, liquid ingredients, such as cream, milk, syrup, among others, are added first to the tank. Blending and heating are started at the same time. Then, dry ingredients, such as nonfat dry milk, sugar, stabilizers, emulsifiers, among others, are added before the mixture reaches 50°C (Goff and Hartel, 2013).

Batch or high temperature short time (HTST) pasteurization aims to primarily stabilize the product from a microbiological perspective. Mix is held at 69°C for 30min in batch pasteurization, while in HTST, mix is heated to 80°C and kept for 25s (Goff and Hartel, 2013).

1.1.2.2 Homogenization

Homogenization process reduces fat globule size to lower than 2μm and provides a stable and uniform mix (Goff and Hartel, 2013). Mix is forced to pass through a very tiny opening of one or two stages. As large fat globules pass through the orifice, their membranes are broken down and new tiny globules are formed. In the process, milk proteins are adsorbed to the newly formed interface (Goff and Hartel, 2013). Overall, homogenization pressure needs to be adapted to fat content, pasteurization intensity, and, sometimes, even to mix formulation (Walstra et al., 2006). In general, a pressure of 17MPa (14MPa in first stage and 3MPa in second stage) is used for mix homogenization (Goff and Hartel, 2013). The process is meant to provide a fine and smooth texture to the ice cream (Walstra et al., 2006).

1.1.2.3 Cooling and Ageing

After being homogenized, mix is cooled to 4°C and equilibrated (aged) for 4-24h. During ageing, fat partially crystalizes (Goff and Hartel, 2013) and as emulsifiers (e.g., PS80 or partially crystalline mono- and diglyceride) are more hydrophobic than milk proteins, they replace milk proteins in the membrane of the fat globule (Clarke, 2004). Moreover, mix viscosity increases as stabilizers are hydrated during ageing (Goff and Hartel, 2013). All these events are essential for the subsequent process.

1.1.2.4 Dynamic Freezing

Mix can be frozen in a batch or continuous freezer. The principles are similar, using a scraped-surface heat exchanger, with the main difference between batch and continuous being air incorporation. In a batch freezer, a specific amount of mix is frozen without controlling the volume of air incorporated (overrun). In a continuous freezer, mix is continuously fed from pumps and pressurized air is injected at a controlled rate at the inlet of the freezer (Goff and Hartel, 2013). Ice crystals (dendritic shape) are formed at the wall, scraped off by the dasher, and mixed into the center of the barrel, where the dendrite branches are separated by agitation and viscous heat. Some melting occurs due to viscous heat, and migration of water molecules to the partially melted ice dendrites increases (i.e., cryo-concentration) as temperature in the mixture of ice continues to decrease. As crystals ripen and become disc-shaped, they keep growing until the draw temperature (batch freezer) or exit (in continuous freezer) are reached. Therefore, ice crystal formation depends on dasher speed, overrun, shear forces, residence time in barrel and draw temperature (Cook and Hartel, 2010; Donhowe et al., 1991; Goff and Hartel, 2013; Hartel, 1996). Typically, draw temperature is between -5 and -6°C (Goff and Hartel, 2013).

1.1.2.5 Hardening and Storage

After collecting ice cream in a container, the product is soft. Ice crystals show mean size between 20 and 30μm, while after hardening ice crystal size increases to about 35-48μm (Cook and Hartel, 2011). In general, a blast-freezer is set between -25 and -30°C and ice creams are hardened for 12 to 24 hours. In the hardening chamber, ice cream freezes at a faster rate than in a regular freezer because of the cold temperatures and high air velocity (Goff and Hartel, 2013). Conditions of hardening can also affect the ice cream quality (Chang and Hartel, 2002a). This step is important to minimize ice crystal and air cell growth in the ice cream (Goff and Hartel, 2013).

1.2 Structural Components

Formulation and process affect structural formation of ice cream during freezing. In ice cream structure, ice crystals, individual and clustered fat globules and air cells are dispersed in an unfrozen serum phase (Goff and Hartel, 2013). Meltdown behavior and rheology of ice cream are influenced by the nature and arrangement of these structural components.

1.2.1 Ice Phase

Around 50% of water is frozen after dynamic freezing and about 75 to 80% after hardening (Goff and Hartel, 2013). Ice crystals vary in size from 1 to 150 μm in diameter (Cook and Hartel, 2010) and have a log normal distribution (Donhowe et al., 1991) with an average size from 35 to 67 μm (Cook and Hartel, 2010; Warren and Hartel, 2014). In general, ice crystals larger than 50μm can result in coarse or grainy texture if there are enough amount (Arbuckle, 1966; Donhowe et al., 1991). Several factors and their interactions, such as mix formulations and process conditions,

affect volume and formation of ice crystals in ice cream (Amador et al., 2017; Hartel, 1996; Muse and Hartel, 2004).

Formulation factors that affect ice crystal size distribution include total solids, sweetener types and level, among others. For example, Donhowe et al. (1991) found that decreased total solids of the mix increased mean ice crystal size, which was mainly due to greater ice phase volume in the system. Moreover, mono- and disaccharide sugars and milk minerals affect ice phase since they are main the main contributors to freezing point in mix formulation (Goff and Hartel, 2013).

The influence of process conditions on ice crystal size has been widely studied. Ice crystal size is affected by dasher speed (Russell et al., 1999), draw temperature (Amador et al., 2017; Muse and Hartel, 2004) as well as type of freezer (Wildmoser et al., 2004). Moreover, Russell et al. (1999) and Drewett and Hartel (2007) showed that longer residence time within the freezer results in larger ice crystal formation, which was mainly related to ice crystal ripening during freezing in the barrel. However, despite numerous advances on the mechanisms of ice crystallization in the last decades (Cook and Hartel, 2011, 2010; Donhowe et al., 1991), little is known about the influence of freezer design on ice crystal formation (Hartel et al., 2017). The effects of parameters such as type of blades, barrel size, and even dasher/beater design, among others, have not been properly studied.

During storage, recrystallization of ice crystals is probably the main parameter to determine shelf life of ice cream. Basically, recrystallization occurs due to melting of numerous small ice crystals, growth of large ice crystals and fusion/accretion of ice crystals (Hartel, 1998). Recrystallization rate depends on many factors, such as formulation, process and, mainly, storage conditions (Goff and Hartel, 2013). Recrystallization rate is close to zero at storage temperature close to glass transition temperature. However, recrystallization rate increases in warmer

temperature based on the thermodynamic ripening process (Hagiwara and Hartel, 1996; Hartel, 1998; Hartel et al., 2017). This process is further accelerated by temperature fluctuations (Donhowe and Hartel, 1996; Flores and Goff, 1999a; Goff and Hartel, 2013), which often occur in ice cream distribution chain and home freezers. Specifically, stabilizers are added to ice cream mix formulations to decrease recrystallization rate (Hartel, 1998; Hartel et al., 2017). Furthermore, ice structuring proteins and peptides have been reported to decrease ice recrystallization in ice cream (Regand and Goff, 2006) and frozen ice cream mix (Wang and Damodaran, 2009), respectively.

1.2.2 Air Phase

Air in ice cream affects texture, stability, sensory, rheology and meltdown (Eisner et al., 2005; Goff et al., 1995; Hartel et al., 2017; Sofjan and Hartel, 2004; Wildmoser et al., 2004). Air can be injected under pressure using a continuous freezer or incorporated by whipping mix under atmospheric pressure using a batch freezer (Goff and Hartel, 2013). Air phase is described by overrun, which can be easily controlled in scraped surface continuous freezers, and by air cell size distribution in ice cream.

Ice cream can have a maximum overrun of 100% in the United States, according to the Standard of Identity (Code of regulations, Title 2 Food and Drugs, Part 135 Frozen Desserts), whereas regulations for maximum overrun in ice cream vary in each country (Goff and Hartel, 2013). In a recent study, overrun in commercial ice cream products varied from 22 to 119% (Warren and Hartel, 2014). Indirectly, overrun can also affect formation of other structural components. Higher overrun can lead to formation of smaller ice crystals and air cell sizes (Flores

and Goff, 1999a; Sofjan and Hartel, 2004). Moreover, overrun can also affect the rheological properties of ice cream (Wildmoser et al., 2004).

In general, mean air cell size in ice cream is around 20µm (Chang and Hartel, 2002b; Goff and Hartel, 2013), with commercial ice cream products varying from 17.1 to 39.5µm (Warren and Hartel, 2014). Within an ice cream, the air cell size distribution can span from a few to over 100 µm (Goff and Hartel, 2013). Air incorporated increases shear forces in the freezer barrel, which leads to further breakdown of air cells in the freezer (Chang and Hartel, 2002c; Sofjan and Hartel, 2004; Warren and Hartel, 2018). After freezing, air cell size is influenced by hardening and storage conditions (Chang and Hartel, 2002a).

Air cell size changes during storage can lead to shrinkage of the ice cream. Specifically, this process can be accelerated by pressure changes during transport of ice cream (Dubey and White, 1997; Hartel et al., 2017). This defect leads to lower acceptability of the ice cream (Goff and Hartel, 2013; Hartel et al., 2017). Moreover, Chang and Hartel (2002c) observed that air cells became interconnected, and created channeling during long-term storage of ice cream. Lower storage temperatures increases the stability of air cells, by limiting diffusion rates.

1.2.3 Fat Phase

Fat content and type used in ice cream depends on regulations of each country. In the US, according to standard of identity (Code of regulations, Title 2 Food and Drugs, Part 135 Frozen Desserts), ice cream should have at least 10% milkfat. Milkfat content is often associated with quality and cost of ice cream. In general, premium and superpremium ice creams contain more than 12% fat (Goff and Hartel, 2013; Hartel et al., 2017). Fat provides smooth texture, body

retention and desirable melting properties as well as increases flavor richness and acts as carrier for added flavor compounds (Goff and Hartel, 2006).

Individual fat globule size can vary from 0.5 to 3μm, with a mean size of 0.8 μm in ice cream mix (Goff and Hartel, 2013). Emulsifiers partially replace proteins in the fat globule membrane during physical ageing. As ice crystals form and viscosity of slurry in the barrel increases, shearing forces increase, and chances of fat globules sharing liquid fat also increases. As there are fat crystals within those fat globules, a partial coalescence of globules occurs (Goff et al., 1987; Goff and Hartel, 2013; Muse and Hartel, 2004; Pawar et al., 2012). Besides interfacial tension (Goff and Hartel, 2013), this arrested coalescence among the fat globules is also affected by elastic moduli and radii of the droplets (Thiel et al., 2016). Fat globule clusters range from 5 to over 100μm (Goff and Hartel, 2013). The percentage of partially-coalesced fat globules, also known as extent of fat destabilization, is influenced by formulation and process conditions (Amador et al., 2017; Daw and Hartel, 2015; Granger et al., 2005; Warren and Hartel, 2018; Wildmoser et al., 2004). In addition, structural components, such as serum phase with different viscosity and overrun, were also reported to affect fat destabilization during freezing (Amador et al., 2017; Goff and Spagnuolo, 2001; Muse and Hartel, 2004; Warren and Hartel, 2018).

Fat destabilization is measured by the percentage of destabilized fat globules formed during dynamic freezing, which is calculated from the ratio of fat clusters in the ice cream to the initial emulsion globules in the mix. Fat destabilization ranges from 2.6 to 55.3% in commercial ice cream products (Warren and Hartel, 2014). The extent of fat destabilization was reported to affect ice cream rheology (Wildmoser et al., 2004). Moreover, high fat destabilization reduces sensory iciness (Amador et al., 2017) and decreases meltdown rate (Bolliger et al., 2000; Koxholt et al., 2001; Muse and Hartel, 2004; Segall and Goff, 2002; Warren and Hartel, 2018, 2014) in ice cream.

On the other hand, excess of fat destabilization can lead to buttery texture in ice cream (Goff and Hartel, 2013).

1.2.4 Serum Phase

Serum phase, or the unfrozen liquid phase, is a freeze-concentrated solution of sugars (sucrose and lactose) and salts with proteins and stabilizers. Other structural elements, such as ice crystals, air cells and fat globules, among others, are dispersed in this continuous phase and held together in the matrix (Goff and Hartel, 2013). Serum phase mechanical behavior depends primarily on mix formulation and temperature of the ice cream.

Freezing point depression, which is affected mainly by sugars and salts, in mix formulation determines the volume of ice phase in ice cream. Higher freezing point means greater ice phase volume, which directly affects the hardness of ice cream (Goff and Hartel, 2013; Hartel et al., 2017). Moreover, as temperature decreases, the volume of ice phase and serum phase viscosity increase. At some point, as freeze-concentration and serum phase viscosity increase, the system reaches the glass transition at temperatures from -32 to -40°C. At this temperature, molecular mobility is drastically reduced, and product is very stable (Goff and Hartel, 2013; Hartel et al., 2017).

Although stabilizers increase stability of ice cream at low temperatures, they do not affect the glass transition because they are added at such low levels (Goff et al., 1993). Stabilizers are added mainly to reduce ice recrystallization in ice cream (Flores and Goff, 1999b; Hagiwara and Hartel, 1996; Miller-Livney and Hartel, 1997; Regand and Goff, 2003). Higher mix viscosity also influences sensory (Amador et al., 2017) and rheological properties of ice cream (Goff et al., 1995). Furthermore, mix viscosity can also be affected by type and level of proteins in the mix

formulation, which can also affect fat destabilization and drip-through rate (Daw and Hartel, 2015).

On the other hand, depending on type and content, stabilizers can also present incompatibility with milk proteins in ice cream, which results in phase separation in the serum (Goff and Hartel, 2013). Another defect related to serum phase is the supersaturation of lactose dur to freeze concentration (Goff and Hartel, 2013; Hartel et al., 2017). Depending on formulation and storage conditions, lactose can crystallize during storage and lead to a coarse texture, with sandy feeling in the mouth.

1.3 Ice Cream Meltdown

Melting properties are probably among the most important quality parameters in ice cream. Melting characteristics are related not only to sensory properties (melting mouthfeel of ice cream), but also melting resistance during the consumption of ice cream. The melting behavior is measured mainly by meltdown tests. Many factors influence ice cream meltdown. Most of the structural components previously discussed, to a greater or lesser extent, affect meltdown behavior of ice cream. As heat penetrates the ice cream, ice crystals melt and dilute the freeze-concentrated serum phase. This lower viscosity serum phase then drains through the matrix lamellae. This drainage may be fast or slow depending on the obstacle nature faced by serum phase during meltdown in matrix. Thus, this matrix arrangement also affects the remnant foam on the top of the screen after the test (Goff and Hartel, 2013).

Heat transfer as well as melting and dispersing of melted ice (water) into serum phase is affected by ice phase nature (Goff and Hartel, 2013). Muse and Hartel (2004) found positive

correlation between ice crystal size and melting rate. In other words, larger ice crystals led to faster drip-through on the screen.

Higher overrun reduces meltdown rate in ice cream (Sakurai et al., 1996; Sofjan and Hartel, 2004; Warren and Hartel, 2018). Air phase affects not only thermal diffusivity, but also the rearrangement of the matrix during meltdown test. As ice cream collapses during the test, air cells stack on top of each other (Goff and Hartel, 2013). Smaller air cell size is expected to increase stability of ice cream during meltdown (Goff and Hartel, 2013). In addition to the lower melting rate of higher overrun ice cream, Sofjan and Hartel (2004) also found an inverse correlation between air cell size and overrun. Therefore, stability of air cells will determine the retention of structure on the screen, which, consequently, also affects meltdown rates (Goff and Hartel, 2013).

Partially-coalesced fat globules surrounding air cells provide more stability, hence greater meltdown resistance (Bolliger et al., 2000; Goff and Jordan, 1989; Muse and Hartel, 2004; Segall and Goff, 2002; Warren and Hartel, 2018). Fat clusters distributed through lamellae create a fat network and decrease melting rate in ice cream (Goff and Hartel, 2013; Muse and Hartel, 2004). Moreover, depending on the size, lamellae in the matrix can also be blocked by individual or clustered fat globules; thus, drainage during meltdown test is also reduced (Koxholt et al., 2001; Warren and Hartel, 2014).

Serum phase viscosity also influences melting rate (Amador et al., 2017; Muse and Hartel, 2004; Yuennan et al., 2014). After being diluted by melted ice, higher serum phase viscosity slows the drainage through the lamellae (Goff and Hartel, 2013). El-Nagar et al. (2002) found that increased mix viscosity with inulin added to formulation decreased meltdown rate. Huppertz et al. (2011) also found that increased mix viscosity, which was due to high pressure treatment of mix, increased melting resistance in ice cream.

Although many studies on meltdown behavior have been performed, little is known about its correlation with rheological properties of ice cream. Greater understanding of this correlation may aid in ice cream quality assessments since instrumental tests can provide more accurate information. In addition, a mapping of rheological and meltdown properties can assist in research and development of new products in the frozen dessert industry.

1.4 Ice Cream Rheology

Structural components and their arrangement in the ice cream matrix strongly affect ice cream rheology. Rheological behavior influences not only texture and sensory properties, but also melting behavior of ice cream. In other words, mechanical performance of an ice cream slab on the top of a screen during meltdown test depends on its elastic, viscous and viscoelastic behaviors. Although all structural components and their interactions in intrinsic structural arrangement are important for the overall mechanical behavior during meltdown, some components may have stronger or weaker influence depending on the rheological property evaluated. Different rheological tests presented in the next sections not only have similar rheological parameters that can confirm results with each other, but also have parameters that are unique to each test. These singular parameters may assist academia and industry to characterize important physical and meltdown properties evaluated in research and new product development.

1.4.1 Oscillatory Thermo-Rheometry (OTR)

Small amplitude oscillatory shear (SAOS), also known as dynamic rheological measurement, is among the most common methods to evaluate viscoelastic properties of ice cream and other food products (Dogan et al., 2013; Dolz et al., 2008; Goff et al., 1995; Gunasekaran and

Ak, 2000; Rao, 2007). This is a sensitive nondestructive method that allows rheological parameters to be related to molecular motion events, such as melting and glass transition (Gunasekaran and Ak, 2000). In SAOS, a small sinusoidal strain (γ) or stress (σ) with a frequency is applied to the sample and σ (or γ) is measured (Gunasekaran and Ak, 2000; Rao, 2007). These measurements are carried out within the Linear Viscoelastic Regime (LVR); that is, preset γ (or σ) are proportional to σ (or γ) (Gunasekaran and Ak, 2000). Initial sweeps of γ or σ amplitude are conducted to ensure the measurements are performed within the LVR. In a preset sinusoidal γ input within the LVR, the output σ is (Gunasekaran and Ak, 2000; Rao, 2007):

$$\sigma t = \gamma_o G' \sin(\omega t) + \gamma_o G^{"} \cos(\omega t) \quad (1.1)$$

Here, G' is shear elastic or storage modulus and G" is shear viscous or loss modulus, which are frequency dependent functions. After a complete cycle, the deformation energy is available and can be used as a driving force to either recover the initial shape, or to flow the sample completely or some combination of both. Some samples (truly elastic materials) present a reversible deformation, in which they store the whole deformation energy during the deformation cycle and use this energy to completely recover the structure (Gunasekaran and Ak, 2003; Mezger, 2006). However, food systems, such as ice cream, show an intermediate behavior. In other words, those samples will use one part of the deformation energy available to partially recover from the deformation and another part will be lost (Mezger, 2006). Thus, from an energy perspective, G' measures the stored and released deformation energy per deformation cycle per unit volume, which is related to elastic behavior of molecular events, and G" measures the dissipated deformation

energy as heat per deformation cycle per unit volume, which is related to viscous behavior of molecular events.

In OTR, mechanical and thermal analyses are carried out at the same time to obtain information about microstructure and sensory properties (Wildmoser et al., 2004). Wildmoser et al. (2004), using OTR from -20 to 10°C, correlated G' and G" with microstructure and quality (sensory) properties of ice cream. Higher overrun and smaller connectivity of ice crystals showed smaller G' and G" values below -10°C and both G' and G" were correlated with sensory properties of rigidity and scoopability of ice cream. Between -10 and 0°C, lower overrun led to steeper slopes of G' and G" and both G' and G" were correlated with sensory impression of coldness. Between 0 and 10°C, greater overrun led to greater G", which was correlated to enhanced creaminess. Granger et al. (2005), also using OTR, found that emulsifier with unsaturated fatty acids led to greater fat destabilization, increased melting time and giving higher G' values at 5°C. Goff et al. (1995) observed G' and G" in stabilized ice creams lower than unstabilized ice creams at temperatures between -15 and -8°C; also, higher overrun led to higher G'.

Another common parameter from SAOS is the ratio between viscous and elastic properties, loss tangent or damping factor (tanδ):

$$\tan\delta = {}^{G"}/_{G'} \tag{1.2}$$

Tanδ, also a function of frequency, provides information about the relative effects of viscous and elastic properties in a viscoelastic behavior (Gunasekaran and Ak, 2000). At low temperatures (between -15 and -6°C), tanδ was reported to be lower in stabilized ice creams than unstabilized ice creams due to elasticity from the gel network of proteins and polysaccharides (Goff et al.,

1995). Granger et al. (2005), investigating the influence of formulation on structure of ice cream using OTR, reported that a peak of tanδ between -10 and 0°C was related to a decrease in ice phase fraction. Tsevdou et al. (2015), using OTR, correlated tanδ to storage time of ice creams. The increased storage time of ice creams led to an exponential decrease of tanδ at -8°C.

In other dairy products, tanδ obtained from OTR measurements has been related to meltability of Cheddar cheese (Ustunol et al., 1995) as well as used to predict meltability of imitation cheese (Mounsey and O'Riordan, 1999). A peak of tanδ from OTR using vertical oscillation was found for Gouda cheese samples at different maturation stages (Taneya et al., 1979), as mentioned by Gunasekaran and Ak (2003). However, potential slippage and disruption of sample as well as the assertion that strain amplitude was within LVR were not addressed in the work. Wetton and Marsh (1990) also found peak of tanδ from OTR evaluating casein samples and showed plasticization effect in the samples with different moisture content. Moreover, tanδ obtained from frequency sweeps has been related to relaxation of bonds in milk gels (Lucey, 2002; van Vilet et al., 1989) and used to study viscoelastic properties of mozzarella (Ak and Gunasekaran, 1996).

Therefore, a better understanding of tanδ behavior will likely contribute to further knowledge of the structural arrangement in ice cream. Moreover, information about melting behavior of ice cream can probably be obtained from OTR by evaluating correlations between rheological and meltdown properties.

1.4.2 Creep and Recovery

In general, SAOS is among the most common methods to study viscoelastic properties of foods. However, another technique is needed to further understand internal structures due to

composition changes in a food product (Dogan et al., 2013; Dolz et al., 2008; Toker et al., 2013). A common technique for these studies is creep and recovery measurements (Dogan et al., 2013).

In a creep test, which is a transient method, the material at rest is submitted to a sudden step increase in stress (Steffe, 1996). The constant stress ($\sigma_{constant}$) is chosen within the LVR based on preliminary oscillatory stress amplitude sweeps. The $\sigma_{constant}$ is applied to the sample and strain (γ) is recorded over time (t) until the sample reaches steady state. In recovery, the load ($\sigma_{constant}$) is released, and the recovery of structure is measured until the sample again reaches steady state.

In data analysis, shear creep compliance (J) is commonly plotted over time (Steffe, 1996):

$$J = f(t) = {}^{\gamma}/_{\sigma_{constant}} \tag{1.3}$$

These data are described using mechanical models (spring and dashpots). In many situations, the simplest phenomenological-rheological model is chosen since there are no well-established criteria on physical principles for food and biological materials (Purkayastha et al., 1984). Creep behavior of biological and polymeric systems is often described by a generalized Kelvin-Voigt model (also known as discrete retardation spectrum) with more than one retardation time (Ahmed, 2015; Gunasekaran and Ak, 2003; Kaschta and Schwarzl, 1994; Purkayastha et al., 1984).

$$J(t) = J_0 + \sum_{i=1}^{N} J_i[1 - e^{-t/\tau_i}] + t/\eta_0 \tag{1.4}$$

Here, J(t) is shear creep compliance over time (t), τ_i are retardation times, J_i are retarded compliances (represent viscoelastic behavior), J_0 is instantaneous compliance (represents elastic

behavior) and η_0 is residual viscosity (represents viscous behavior). From the model, parameters of each element can be determined. G_0 (spring) and η_0 (dashpot) of the Maxwell unit are the elastic modulus and residual viscosity, respectively. From the Kelvin-Voigt units, G_i (springs) are the retarded elastic moduli and η_i (dashpots) are internal viscosities (Dogan et al., 2013).

A six-element model was used by Shama and Sherman (1966) as well as Sherman (1966) to describe creep behavior for ice cream and ice cream mix, respectively. Shama and Sherman (1966) suggested that each element of the six-element model represents mechanical behavior of one structural component in frozen ice cream. G_0 was primarily influenced by ice crystals, G_1 influenced by weak stabilizer gel, η_1 influenced by fat crystals, G_2 influenced by protein enveloped air cells, η_2 influenced by weak stabilizer gel as well as protein enveloped air cells and, η_0 influenced by ice and fat crystals. A four-element model, also known as Burgers model, was used by Sherman (1966) to study creep behavior of melted ice cream at 20°C. Furthermore, Sherman (1966) suggested that globules of 0.5µm or smaller were related to the second Kelvin-Voigt unit (G_2 and η_2) added to the six-element model to study creep behavior of mix. On the other hand, Dogan et al. (2013) used Burgers model to evaluate creep behavior of ice cream mixes with different concentrations of xanthan gum. Therefore, although there were studies on creep behavior of frozen and melted ice cream a few decades ago, some updates are needed since instrumental techniques have evolved over time.

1.4.3 Stress Growth

Stress growth, also commonly known as stress overshoot, is a start-up flow method, where material at rest is suddenly submitted to a constant shear rate (Steffe, 1996). Stress overshoot is common in a sample experiencing some structure breakdown (Elliott and Ganz, 1977). However,

this test has a singularity. It has been categorized based on transient viscoelastic flow of the sample (Rao, 2007; Steffe, 1996) as well as on large final deformation property of the sample after reaching the steady state (Lucey et al., 1997; Luyten et al., 1994). This measurement may not only validate results from other tests and obtain viscosity measurement at a low shear rate, but also obtain the yield stress (σ_y) of the matrix.

A phenomenological analysis has also been proposed for stress overshoot data (Elliott and Ganz, 1977; Rao, 2007). The schematic diagram obtained from Rao (2007) is presented in Figure 1.1: t is time, σ_A is stress at the end of the elastic portion, σ_P is peak shear stress, σ_∞ is equilibrium shear stress and σ_R is residual shear stress after shearing has stopped. Correspondent strains (γ) for those stress and time values are γ_{tA}, γ_P (which is the strain correspondent to the σ_P) and $\gamma_{t\infty}$. Furthermore, the product of the shear rate and time is the total deformation at different shear time. Therefore, equations for shear modulus (G), equilibrium viscosity (η_∞) and work of structure breakdown (W) can be determined from the previous definitions (Rao, 2007):

$$G = {d\sigma}/{d\gamma} = \sigma_A/\gamma_{t_A} \tag{2.2}$$

$$\eta_\infty = \sigma_\infty/\dot{\gamma} \tag{2.3}$$

$$W = \dot{\gamma}\int_A^B(\sigma - \sigma_\infty)\mathrm{dt} \tag{2.4}$$

Here, $\dot{\gamma}$ is constant shear rate, A is time that stress curve overshot σ_∞ and B is time that σ_∞ was achieved. Moreover, excess work of structure breakdown (W) is the area above the extrapolated σ_∞ line.

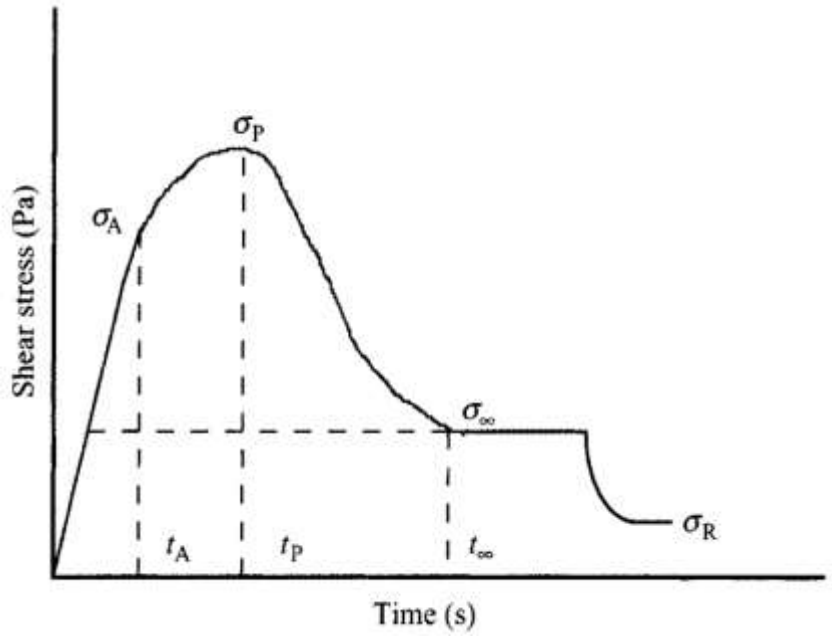

Figure 1.1 Schematic diagram of phenomenological analysis for stress overshoot data. Source: Elliott and Ganz (1977) mentioned in Rao (2007).

Yield stress (σ_y), which corresponds to σ_P in Figure 1.1, is the minimum stress required to initiate flow of a material (Sun and Gunasekaran, 2009). Measurements of σ_y and yield strain (γ_y) have been obtained from experiments at constant shear rate to evaluate mixtures of polysaccharides as well as acid gels made from heated milk (Lucey, 2001; Lucey et al., 1997; Luyten et al., 1994). Scoopability and ability to dip ice cream have been correlated to σ_y measurements (Briggs et al., 1996). Another possibility may relate σ_y to the ability of the ice cream matrix to remain on the top of the screen after a typical meltdown test.

Sherman (1966) compared mix to melted ice cream at 0.133 and 1.197s^{-1}. Interestingly, shear stress curves of mix at both shear rates presented stress values greater than melted ice cream. However, this was probably due to experimental conditions. The ice cream was placed to melt a few hours at 20-21°C. Then, mix and melted ice cream were cooled and evaluated at -5.5°C. Thus, two possibilities need to be considered here. First, the presence of possible bubbles in melted ice cream may have affected thermal conductivity during experiments; thus, greater formation of ice crystals probably occurred in mix compared to refrozen ice cream, and hence, greater stress values were probably presented by mix. Secondly, since samples were analyzed at -5.5°C, it is possible that ice crystal formation also led to some increase in normal force during shear; that is, shear stress measurements were probably distorted during the experiments. Therefore, although stress growth measurement has been reported to be a useful tool to evaluate food matrices, its potential to evaluate structure of ice cream products has not been completely explored yet. Moreover, σ_y could assist to further characterize and understand meltdown properties of ice cream.

1.4.4 Flow Ramp and Thixotropic Loop

Flow properties are a common tool for quality control of food products. In general, fluid flow behavior is characterized using a shear diagram with shear rate versus shear stress. Flow behaviors in Figure 1.2 illustrate time-independent fluids; that is, fluid does not depend on duration of shearing, it depends only on shear rate (Rao, 2007). In general, steady state flow measurements are not recommended for ice cream since, depending on temperature and shearing, ice phase can not only melt, but also create normal force during the measurements, hence giving unreliable rheological data.

A typical ice cream matrix at 0°C shows no ice phase as well as, depending on the sample preparation, no major structural damage in absence of ice crystals. The flow behavior of a thixotropic system is illustrated in Figure 1.3 using a stepped flow test (flow sweep) diagram. This system shows time-dependency in the upward curve. However, the downward curve of the matrix approaches a shear-thinning behavior. Overall, food products with time-dependent shear-thinning behavior show thixotropic flow behavior (Rao, 2007). In a fluid with thixotropic behavior, when forces during shear are high enough, inter-particle bonds are broken down, structural unit sizes are reduced and flow resistance is lowered during shear; after that, initial structure is slowly recovered at rest (Barnes, 1997; Rao, 2007).

Although it is known that the melted ice cream matrix at 0°C behaves as a weak gel (Goff and Hartel, 2013; Granger et al., 2005; Wildmoser et al., 2004), a flow ramp test could be used to evaluate time dependence of the remnant foam using large deformations. Furthermore, rheological destruction could be empirically quantified as thixotropy to infer information about initial structural formation in the melted matrix.

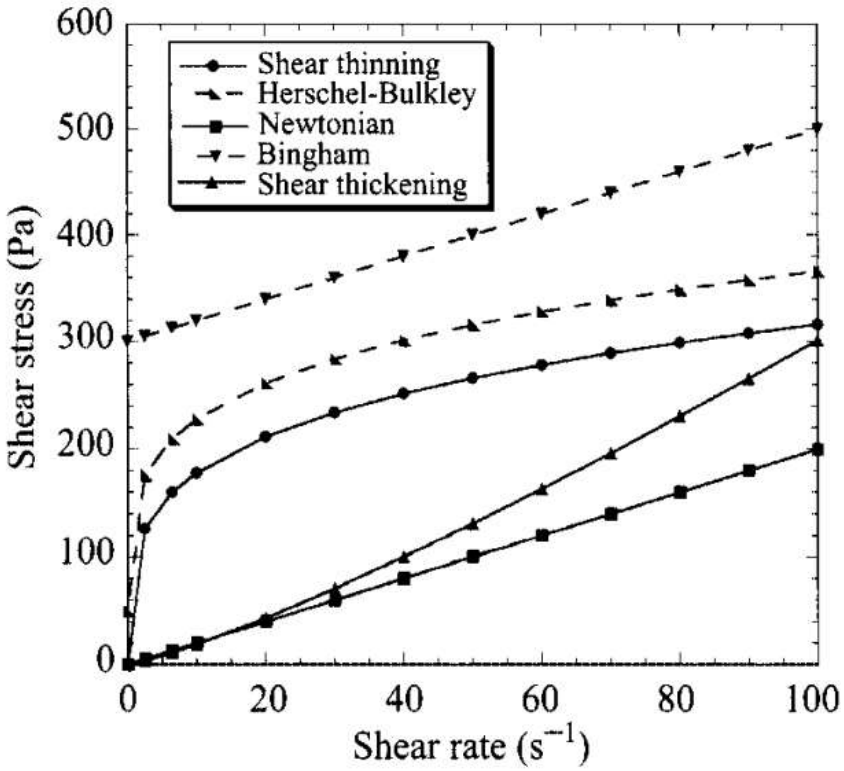

Figure 1.2 Shear diagram of shear rate versus shear stress for time-independent flow behavior, Newtonian, shear-thinning, and shear-thickening. Moreover, fluids with yield stress, Bingham and Herschel-Bulkley. Source: Rao (2007).

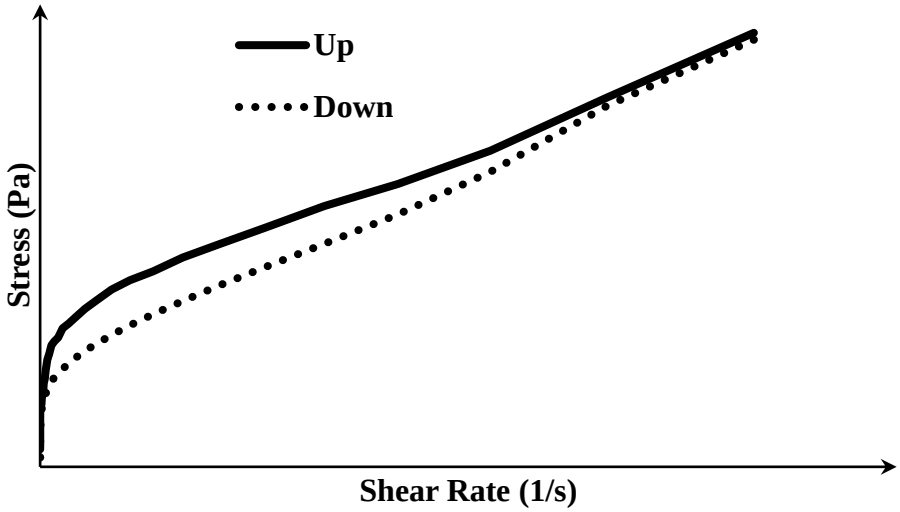

Figure 1.3: Diagram for up and down curves of shear stress against shear rate from a stepped flow test (flow sweep) using parallel plates and steady state sensing (5% tolerance within 30 seconds in three consecutive sampling) for a typical thixotropic system with 40% overrun and low fat destabilization at 0°C.

1.5 Summary

Numerous studies on meltdown behavior of ice cream have been performed. These studies generally correlate meltdown properties with structural elements. However, little is known about the correlation not only with rheological destruction, but also with other rheological properties of ice cream. Greater understanding of these correlations may aid in ice cream quality assessments since instrumental tests can provide more accurate information. In addition, a mapping of rheological and meltdown behaviors can assist in research and development of new products in frozen dessert industry.

1.5 References

Ahmed, J., 2015. Effect of Barley B-Glucan Concentrate On Oscillatory and Creep Behavior Of Composite Wheat Flour Dough. J. Food Eng. 152, 85–94. https://doi.org/https://doi.org/10.1016/j.jfoodeng.2014.11.018

Ak, M.M., Gunasekaran, S., 1996. Dynamic Rheological Properties of Mozzarella Cheese During Refrigerated Storage. J. Food Sci. 61, 566–569. https://doi.org/10.1111/j.1365-2621.1996.tb13159.x

Amador, J., Hartel, R., Rankin, S., 2017. The Effects of Fat Structures and Ice Cream Mix Viscosity on Physical and Sensory Properties of Ice Cream. J. Food Sci. 82, 1851–1860. https://doi.org/10.1111/1750-3841.13780

Arbuckle, W.S., 1966. Relation of Freezing and Hardening to the Body and Texture of Ice Cream. Ice Cream F. Trade J. 48, 34–47.

Barnes, H.A., 1997. Thixotropy—a Review. J. Nonnewton. Fluid Mech. 70, 1–33. https://doi.org/https://doi.org/10.1016/S0377-0257(97)00004-9

Bolliger, S., Goff, H.D., Tharp, B.W., 2000. Correlation between Colloidal Properties of Ice Cream Mix and Ice Cream. Int. Dairy J. 10, 303–309.

Briggs, J.L., Steffe, J.F., Ustunol, Z., 1996. Vane Method to Evaluate the Yield Stress of Frozen Ice Cream. J. Dairy Sci. 79, 527–531. https://doi.org/https://doi.org/10.3168/jds.S0022-0302(96)76395-6

Chang, Y., Hartel, R.W., 2002a. Stability of Air Cells in Ice Cream during Hardening and Storage. J. Food Eng. 55, 59–70.

Chang, Y., Hartel, R.W., 2002b. Development of Air Cells in a Batch Ice Cream Freezer. J. Food Eng. 55, 71–78. https://doi.org/https://doi.org/10.1016/S0260-8774(01)00243-6

Chang, Y., Hartel, R.W., 2002. Measurement of Air Cell Distributions in Dairy Foams. Int. Dairy J. 12, 463–472. https://doi.org/https://doi.org/10.1016/S0958-6946(01)00171-6

Clarke, C., 2004. **The Science of Ice Cream**, First. ed. The Royal Society of Chemistry, Cambridge.

Cook, K.L.K., Hartel, R.W., 2011. Effect of freezing temperature and warming rate on Dendrite Break-Up when Freezing Ice Cream Mix. Int. Dairy J. 21, 447–453. https://doi.org/https://doi.org/10.1016/j.idairyj.2011.01.007

Cook, K.L.K., Hartel, R.W., 2010. Mechanisms of Ice Crystallization in Ice Cream Production. Compr. Rev. Food Sci. Food Saf. 9, 213–222.

Daw, E., Hartel, R.W., 2015. Fat Destabilization and Melt-Down of Ice Creams with Increased Protein Content. Int. Dairy J. 43, 33–41.

Dogan, M., Kayacier, A., Toker, Ö.S., Yilmaz, M.T., Karaman, S., 2013. Steady, Dynamic, Creep, and Recovery Analysis of Ice Cream Mixes added with Different Concentrations of Xanthan Gum. Food Bioprocess Technol. 6, 1420–1433.

Dolz, M., Hernández, M.J., Delegido, J., 2008. Creep and recovery experimental investigation of low oil content food emulsions. Food Hydrocoll. 22, 421–427. https://doi.org/https://doi.org/10.1016/j.foodhyd.2006.12.011

Donhowe, D.P., Hartel, R.W., 1996. Recrystallization of ice in ice cream during controlled accelerated storage. Int. Dairy J. 6, 1191–1208.

Donhowe, D.P., Hartel, R.W., Bradley, R.L., 1991. Determination of ice crystal size distributions in frozen desserts. J. Dairy Sci. 74, 3334–3344.

Drewett, E.M., Hartel, R.W., 2007. Ice crystallization in a scraped surface freezer. J. Food Eng. 78, 1060–1066. https://doi.org/https://doi.org/10.1016/j.jfoodeng.2005.12.018

Dubey, U.K., White, C.H., 1997. Ice Cream Shrinkage: A Problem for the Ice Cream Industry1. J. Dairy Sci. 80, 3439–3444. https://doi.org/https://doi.org/10.3168/jds.S0022-0302(97)76320-3

Eisner, M.D., Wildmoser, H., Windhab, E.J., 2005. Air cell microstructuring in a high viscous ice cream matrix. Colloids Surfaces A Physicochem. Eng. Asp. 263, 390–399.

El-Nagar, G., Clowes, G., Tudorică, C.M., Kuri, V., Brennan, C.S., 2002. Rheological quality and stability of yog-ice cream with added inulin. Int. J. Dairy Technol. 55, 89–93. https://doi.org/10.1046/j.1471-0307.2002.00042.x

Elliott, J.H., Ganz, A.J., 1977. Salad dressings—preliminary rheological characterization. J. Texture Stud. 8, 359–371.

Flores, A.A., Goff, H.D., 1999a. Recrystallization in Ice Cream After Constant and Cycling Temperature Storage Conditions as Affected by Stabilizers. J. Dairy Sci. 82, 1408–1415. https://doi.org/https://doi.org/10.3168/jds.S0022-0302(99)75367-1

Flores, A.A., Goff, H.D., 1999b. Ice Crystal Size Distributions in Dynamically Frozen Model Solutions and Ice Cream as Affected by Stabilizers. J. Dairy Sci. 82, 1399–1407. https://doi.org/https://doi.org/10.3168/jds.S0022-0302(99)75366-X

Goff, H.D., Caldwell, K.B., Stanley, D.W., Maurice, T.J., 1993. The Influence of Polysaccharides on the Glass Transition in Frozen Sucrose Solutions and Ice Cream. J. Dairy Sci. 76, 1268–1277. https://doi.org/https://doi.org/10.3168/jds.S0022-0302(93)77456-1

Goff, H.D., Ferdinando, D., Schorsch, C., 1999. Fluorescence microscopy to study galactomannan structure in frozen sucrose and milk protein solutions. Food Hydrocoll. 13, 353–362. https://doi.org/https://doi.org/10.1016/S0268-005X(99)00017-X

Goff, H.D., Freslon, B., Sahagian, M.E., Hauber, T.D., Stone, A.P., Stanley, D.W., 1995. Structural Development in Ice Cream—Dynamic Rheological Measurements. J. Texture Stud. 26, 517–536. https://doi.org/10.1111/j.1745-4603.1995.tb00801.x

Goff, H.D., Hartel, R.W., 2013. **Ice Cream**, Seventh. ed. Springer Science & Business Media, New York.

Goff, H.D., Hartel, R.W., 2006. **154 Ice Cream and Frozen Desserts. Handb. Food Sci. Technol. Eng**. 149, 94. Boca Raton.

Goff, H.D., Jordan, W.K., 1989. Action of Emulsifers in Promoting Fat Destabilization During the Manufacture of Ice Cream. J. Dairy Sci. 72, 18–29. https://doi.org/https://doi.org/10.3168/jds.S0022-0302(89)79075-5

Goff, H.D., Liboff, M., Jordan, W.K., Kinsella, J.E., 1987. The Effects of Polysorbate 80 on the Fat Emulsion in Ice Cream Mix: Evidence from Transmission Electron Microscopy Studies. Food Struct. 6, 193–198.

Goff, H.D., Spagnuolo, P., 2001. Effect Of Stabilizers On Fat Destabilization Measurements In Ice Cream. Milchwissenschaft-Milk Sci. Int. 56, 450–453.

Granger, C., Leger, A., Barey, P., Langendorff, V., Cansell, M., 2005. Influence of formulation on the structural networks in ice cream. Int. Dairy J. 15, 255–262. https://doi.org/https://doi.org/10.1016/j.idairyj.2004.07.009

Gunasekaran, S., Ak, M.M., 2003. **Cheese Rheology and Texture.** CRC Press LLC, Boca Raton.

Gunasekaran, S., Ak, M.M., 2000. Dynamic oscillatory shear testing of foods — selected applications. Trends Food Sci. Technol. 11, 115–127. https://doi.org/https://doi.org/10.1016/S0924-2244(00)00058-3

Hagiwara, T., Hartel, R.W., 1996. Effect of sweetener, stabilizer, and storage temperature on ice recrystallization in ice cream. J. Dairy Sci. 79, 735–744.

Hartel, R.W., 1998. Mechanisms and kinetics of recrystallization in ice cream, in: Reid, D.S. (Ed.), The Properties of Water in Foods ISOPOW 6. Springer US, Boston, MA, pp. 287–319. https://doi.org/10.1007/978-1-4613-0311-4_14

Hartel, R.W., 1996. Ice crystallization during the manufacture of ice cream. Trends Food Sci. Technol. 7, 315–321.

Hartel, R.W., Rankin, S.A., Bradley, R.L., 2017. A 100-Year Review: Milestones in the development of frozen desserts. J. Dairy Sci. 100, 10014–10025. https://doi.org/https://doi.org/10.3168/jds.2017-13278

Huppertz, T., Smiddy, M.A., Goff, H.D., Kelly, A.L., 2011. Effects of high pressure treatment of mix on ice cream manufacture. Int. Dairy J. 21, 718–726. https://doi.org/https://doi.org/10.1016/j.idairyj.2010.12.005

Kaschta, J., Schwarzl, R.R., 1994. Calculation of discrete retardation spectra from creep data — I. Method. Rheol. Acta 33, 517–529. https://doi.org/10.1007/BF00366336

Koxholt, M.M.R., Eisenmann, B., Hinrichs, J., 2001. Effect of the Fat Globule Sizes on the Meltdown of Ice Cream. J. Dairy Sci. 84, 31–37. https://doi.org/https://doi.org/10.3168/jds.S0022-0302(01)74448-7

Lucey, J.A., 2002. Formation and Physical Properties of Milk Protein Gels. J. Dairy Sci. 85, 281–294. https://doi.org/https://doi.org/10.3168/jds.S0022-0302(02)74078-2

Lucey, J.A., 2001. The relationship between rheological parameters and whey separation in milk gels. Food Hydrocoll. 15, 603–608. https://doi.org/https://doi.org/10.1016/S0268-005X(01)00043-1

Lucey, J.A., Teo, C.T., Munro, P.A., Singh, H., 1997. Rheological properties at small (dynamic) and large (yield) deformations of acid gels made from heated milk. J. Dairy Res. 64, 591–600. https://doi.org/10.1017/S0022029997002380

Luyten, H., Kloek, W., Van Vliet, T., 1994. Yielding behaviour of mixtures of xanthan and enzyme-modified galactomannans. Food Hydrocoll. 8, 431–440.

Mezger, T.G., 2006. **The Rheology Handbook: For Users of Rotational and Oscillatory Rheometers**. Vincentz Network. Hanover.

Miller-Livney, T., Hartel, R.W., 1997. Ice recrystallization in ice cream: interactions between sweeteners and stabilizers. J. Dairy Sci. 80, 447–456.

Mounsey, J.S., O'Riordan, E.D., 1999. Empirical and Dynamic Rheological Data Correlation to Characterize Melt Characteristics of Imitation Cheese. J. Food Sci. 64, 701–703. https://doi.org/10.1111/j.1365-2621.1999.tb15114.x

Muse, M.R., Hartel, R.W., 2004. Ice Cream Structural Elements that Affect Melting Rate and Hardness. J. Dairy Sci. 87, 1–10. https://doi.org/https://doi.org/10.3168/jds.S0022-0302(04)73135-5

Pawar, A.B., Caggioni, M., Hartel, R.W., Spicer, P.T., 2012. Arrested coalescence of viscoelastic droplets with internal microstructure. Faraday Discuss. 158, 341–350. https://doi.org/10.1039/C2FD20029E

Purkayastha, S., Peleg, M., Normand, M.D., 1984. Presentation of the creep curves of solid biological materials by a simplified mathematical version of the generalized Kelvin-Voigt model. Rheol. Acta 23, 556–563. https://doi.org/10.1007/BF01329288

Rao, M.A.A., 2007. **Rheology of Fluid and Semisolid Foods: Principles and Applications**, Second. ed. Springer Science & Business Media, New York.

Regand, A., Goff, H.D., 2006. Ice Recrystallization Inhibition in Ice Cream as Affected by Ice Structuring Proteins from Winter Wheat Grass. J. Dairy Sci. 89, 49–57. https://doi.org/https://doi.org/10.3168/jds.S0022-0302(06)72068-9

Regand, A., Goff, H.D., 2003. Structure and ice recrystallization in frozen stabilized ice cream model systems. Food Hydrocoll. 17, 95–102. https://doi.org/https://doi.org/10.1016/S0268-005X(02)00042-5

Russell, A.B., Cheney, P.E., Wantling, S.D., 1999. Influence of freezing conditions on ice crystallisation in ice cream. J. Food Eng. 39, 179–191. https://doi.org/https://doi.org/10.1016/S0260-8774(98)00161-7

Sakurai, K., Kokubo, S., Hakamata, K., Tomita, M., Yoshida, S., 1996. Effect of production conditions on ice cream melting resistance and hardness. Milchwissenschaft 51, 451–454.

Segall, K.I., Goff, H.D., 2002. A modified ice cream processing routine that promotes fat destabilization in the absence of added emulsifier. Int. Dairy J. 12, 1013–1018. https://doi.org/https://doi.org/10.1016/S0958-6946(02)00117-6

Segall, K.I., Goff, H.D., 1999. Influence of adsorbed milk protein type and surface concentration on the quiescent and shear stability of butteroil emulsions. Int. Dairy J. 9, 683–691. https://doi.org/https://doi.org/10.1016/S0958-6946(99)00143-0

Shama, F., Sherman, P., 1966. The Texture of Ice Cream 2. Rheological Properties of Frozen Ice Cream. J. Food Sci. 31, 699–706. https://doi.org/10.1111/j.1365-2621.1966.tb01926.x

Sherman, P., 1966. The Texture of Ice Cream 3. Rheological Properties of Mix and Melted Ice Cream. J. Food Sci. 31, 707–716. https://doi.org/10.1111/j.1365-2621.1966.tb01927.x

Sofjan, R.P., Hartel, R.W., 2004. Effects of overrun on structural and physical characteristics of ice cream. Int. Dairy J. 14, 255–262.

Steffe, J.F., 1996. **Rheological Methods in Food Process Engineering**. Freeman Press, East Lansing.

Sun, A., Gunasekaran, S., 2009. Yield Stress in Foods: Measurements and Applications. Int. J. Food Prop. 12, 70–101. https://doi.org/10.1080/10942910802308502

Taneya, S., Izutsu, T., Sone, T., 1979. Dynamic Viscoelasticity of Natural Cheese and Processed Cheese, in: Sherman, P. (Ed.), Food Texture and Rheology, P. Sherman, Ed., 369–383. Academic Press, p. 456 pages.

Thiel, A.E., Hartel, R.W., Spicer, P.T., Hendrickson, K.J., 2016. Coalescence Behavior of Pure and Natural Fat Droplets Characterized via Micromanipulation. J. Am. Oil Chem. Soc. 93, 1467–1477. https://doi.org/10.1007/s11746-016-2896-4

Toker, O.S., Karaman, S., Yuksel, F., Dogan, M., Kayacier, A., Yilmaz, M.T., 2013. Temperature Dependency of Steady, Dynamic, and Creep-Recovery Rheological Properties of Ice Cream Mix. Food Bioprocess Technol. 6, 2974–2985. https://doi.org/10.1007/s11947-012-1005-4

Tsevdou, M., Gogou, E., Dermesonluoglu, E., Taoukis, P., 2015. Modelling the effect of storage temperature on the viscoelastic properties and quality of ice cream. J. Food Eng. 148, 35–42. https://doi.org/https://doi.org/10.1016/j.jfoodeng.2014.07.002

Ustunol, Z., Kawachi, K., Steffe, J., 1995. Rheological Properties of Cheddar Cheese as Influenced by Fat Reduction and Ripening Time. J. Food Sci. 60, 1208–1210. https://doi.org/10.1111/j.1365-2621.1995.tb04557.x

van Vliet, T., Roefs, S.P.F.M., Zoon, P., Walstra, P., 1989. Rheological properties of casein gels. J. Dairy Res. 56, 529–534. https://doi.org/10.1017/S0022029900029022

Walstra, P., Wouters, J.T.M., Geurts, T.J.C.N.-S.. D. 2006 S.. . W. 2006 S.. . D. 2006, 2006. Dairy science and technology. Second edition. Boca Raton : CRC/Taylor & Francis, 2006.

Wang, S., Damodaran, S., 2009. Ice-Structuring Peptides Derived from Bovine Collagen. J. Agric. Food Chem. 57, 5501–5509. https://doi.org/10.1021/jf900524y

Warren, M.M., Hartel, R.W., 2018. Effects of Emulsifier, Overrun and Dasher Speed on Ice Cream Microstructure and Melting Properties. J. Food Sci. 83, 639–647. https://doi.org/10.1111/1750-3841.13983

Warren, M.M., Hartel, R.W., 2014. Structural, Compositional, and Sensorial Properties of United States Commercial Ice Cream Products. J. Food Sci. 79, E2005–E2013. https://doi.org/10.1111/1750-3841.12592

Wetton, R., Marsh, R.C.N.-T.B. 1989 T.. B. 1989, 1990. Dynamic mechanical thermal analysis (DMTA) of food materials, in Rheology of Food, Pharmaceutical and Biological Materials with General Rheology , R. Carter, Ed., 231–247. London: Elsevier Applied Science.

Wildmoser, H., Scheiwiller, J., Windhab, E.J., 2004. Impact of disperse microstructure on rheology and quality aspects of ice cream. LWT-Food Sci. Technol. 37, 881–891.

Yuennan, P., Sajjaanantakul, T., Goff, H.D., 2014. Effect of Okra Cell Wall and Polysaccharide on Physical Properties and Stability of Ice Cream. J. Food Sci. 79, E1522–E1527. https://doi.org/10.1111/1750-3841.12539

Chapter 2

2 Effects of Serum Phase Viscosity, Partially-Coalesced Fat Globules and Overrun on the Rheological Properties of Ice Cream

2.1 Abstract

Ice cream rheology is strongly influenced by ice phase presence, although other structural components also affect its rheological behavior. Despite important advances in ice cream rheology in recent decades, the influence of structural components on rheological behavior of ice cream matrix has not yet been fully elucidated. Moreover, rheological parameters that may be important for mechanical performance of ice cream in its melting properties have not been studied yet. In this context, the effects of structural components were evaluated on rheological properties of ice cream. Polysorbate 80 (PS80), air flow and stabilizer aimed to change the extent of fat destabilization (FD), overrun and mix viscosity (serum phase viscosity), respectively, in ice creams. Rheological properties of ice creams were obtained from oscillatory thermo-rheometry (OTR), creep/recovery, stress growth and flow ramp measurements. In OTR, mix viscosity, followed by overrun, influenced G' and tanδ below -10°C. When ice phase decreased (between -10 and -2.7°C), mix viscosity had reduced effects, but continued to strongly affect G' and tanδ, followed by FD, and with lower effects from overrun. When the ice phase was completely melted at 0°C, FD had most influence on G' and tanδ, followed by overrun, and with lower effects from mix viscosity. Six-element model described well creep behavior of melted ice cream at 0°C. Viscous behavior at lower shear rate ($\eta_{0\ 0°C}$) was most influenced by mix viscosity, followed by FD, and lower overrun effects. Transient behavior, represented by $\sigma_{Y\ 0°C}$, of melted matrix at 0°C was most influenced by FD, followed by mix viscosity, with lower overrun effects. Thixotropy, from flow ramp measurement, was most affected by mix viscosity, followed by overrun, and with lower FD effects. Moreover, correlation between $Thix_{\ 0°C}$ and $tan\delta_{Peak}$ suggested that structure formation affected the magnitude of $tan\delta_{Peak}$. The most influential structural component on each rheological response varied on the type of shear applied to sample, which emphasized the importance of different rheological tests used to characterize the wide range of structures.

2.2 Introduction

The nature and intricate arrangement of structural components, such as ice crystals, partially-coalesced fat globules, air cells and unfrozen serum phase, affect directly the meltdown and rheological properties of the ice cream matrix. In fact, the rheological behavior of ice cream is mainly governed by ice phase presence (Goff et al., 1995; Granger et al., 2005; Shama and Sherman, 1966; Wildmoser et al., 2004). Nevertheless, other factors, such as partially coalesced fat globules, overrun and unfrozen serum phase, also affect the rheological behavior in the matrix (Goff et al., 1995; Goff and Hartel, 2013).

After the dynamic freezing, fat globules may stay either as individual fat globules or as partially-coalesced fat globules, with an average size from 0.5 to 3 μm and from 5 to 80 μm (Goff and Hartel, 2013), respectively. The fat destabilization influences sensory properties and melt resistance (Amador et al., 2017; Warren and Hartel, 2018, 2014). Consequently, fat destabilization also affects the rheological properties of the ice cream matrix.

The gas phase in ice cream can be represented by overrun (amount of air incorporated) and size distribution of air cells. Overrun can be easily controlled in scraped-surface continuous freezers. The air incorporated can provide smother texture, higher melt resistance and lower hardness (Sofjan and Hartel, 2004). Some secondary effects, such as smaller ice crystal and air cell sizes, have been also reported due to increased levels of overrun (Flores and Goff, 1999a; Sofjan and Hartel, 2004). Moreover, the overrun can also affect the rheological properties of ice cream (Goff et al., 1995; Wildmoser et al., 2004).

The unfrozen serum phase is a freeze-concentrated phase, with sugars (sucrose and lactose) and salts in solution. The serum phase interacts with other structural elements, such as ice crystals, air cells and fat globules, among others, and keeps them together in the matrix (Goff and Hartel,

2013). The addition of stabilizers has been reported to retard ice recrystallization (Flores and Goff, 1999b; Hagiwara and Hartel, 1996; Miller-Livney and Hartel, 1997; Regand and Goff, 2003) and decrease drip-through rates (Goff and Hartel, 2013; Muse and Hartel, 2004) in ice creams. In addition, the mix viscosity affects not only the sensory properties (Amador et al., 2017), but it also can affect the rheological properties in ice creams (Goff et al., 1995).

In this context, a combination of oscillatory, transient and rotational rheological measurements can provide substantial information about the structure and melting behavior as well as confirm the results of one test with another. The rheological characterization of ice creams with controlled structural formation can help elucidate the correlation between rheology and ice cream microstructure. Thus, the goal of this study was to assess the effects of partially-coalesced fat globules, overrun and serum phase on the rheological properties of full fat ice creams.

2.3 Materials and Methods

2.3.1 Materials

Cream, nonfat dry milk, sucrose, stabilizers and emulsifiers were used to make the ice cream mixes. Cream, sucrose (United Sugars, Edina, MN, USA) and nonfat dry milk (Dairy America, Fresno, CA, USA) were obtained from the Babcock Hall Dairy Plant (Madison, WI). A stabilizer blend (Germantown™ Premium I.C., New Century, KS, USA), including locust bean gum (LBG), guar gum, and carrageenan, and mono-and diglycerides (Grinsted® HV 52 K-A, New Century, KS, USA) (MDG) were purchased from Danisco USA. Polysorbate 80 (PS80) was obtained from Avatar® (Avapol™ 80K Sorbitan Ester, University Park, IL, USA).

2.3.2 Experimental Design

This study aimed to evaluate the effects of structural components, such as serum phase viscosity (mix viscosity), partially coalesced fat globules (fat destabilization) and overrun, on the rheological properties of full fat ice cream. For this purpose, a 3x3x3 factorial was designed with different levels of stabilizer, polysorbate 80 (PS80) and air flow (overrun). Different levels of stabilizer (0, 0.2 and 0.4%), PS80 (0, 0.015 and 0.030%) and air flow (8, 11 and 15L.h^{-1}) were utilized to change the mix viscosity, the extent of fat destabilization and overrun, respectively. Table 2.1 shows the experimental design and the controlled target structural components. The factorial was performed in duplicate. Ice cream mixes and ice creams were randomly made and randomly frozen, respectively.

2.3.3 Formulation and Processing

Formulation of the ice cream mixes included 12% fat, 11.3% milk solids nonfat, 16.9% sucrose, 0.15% MDG, 0 to 0.4% stabilizer and 0 to 0.03% PS80. Total solids were approximately 40.5% and freezing point was -2.72±0.06°C.

Dry and liquid ingredients were blended and heated to 85°C using a Stephan mixer (Stephan Food Processing Machinery, Hamelin, Germany), which was a batch-jacketed system. Then, the mixture was homogenized using a two-stage homogenizer (Manton-Gaulin MFG, Co. Inc., Everett, MA, USA) at 17.2 MPa (3.4 and 13.8MPa in the second and first stages, respectively). After that, the mixture was cooled to 10°C in the Stephan mixer and aged for approximately 24 hours at 4°C.

A Hoyer Frigus KF 80 F continuous freezer (Tetra Pak Hoyer Inc., Aarhus, Denmark) was operated in manual mode with 500RPM dasher speed to make the ice creams. The levels of air

flow were changed according to the target overrun (8, 11 and 15L.h^{-1} for 50, 75 and 100%, respectively) at constant pump ratio (0.99±0.00), which is the ratio between the mix and ice cream pump. Fine adjusts for the target overrun were made by controlling the flow of ice cream (pump system) in the freezer (22.0±0.4L.h^{-1}). After reaching the draw temperature (-6.05±0.01°C), which was measured by an internal thermometer upon exit of the barrel in the freezer, and overrun (50.2±0.2%, 75.1±0.2% and 99.6±0.2%), ice cream samples were collected in a container (473mL). The samples were placed in a hardening cabinet (-29°C). After around one hour, samples were transferred to a walk-in freezer at -29°C.

2.3.4 Structural Components (Physical, Compositional and Structural Measurements)

Ice cream mix before and after the homogenization were analyzed for fat globule size distribution, using light scattering analysis, and confirmed by using optical light microscopy. Moreover, the viscosity of the aged ice cream mixes was measured. During the dynamic freezing, draw temperatures and overrun were measured. After the hardening step, particle/fat globule size distribution, optical light microscopy, air cell size distribution, ice cell size distribution and rheological measurements were performed on the ice cream samples. All analyses were carried out in triplicate.

2.3.4.1 Ice Cream Mix Rheology

Flow sweep, flow ramp and oscillatory measurements of ice cream mixes were performed using a rotational rheometer (DHR-2, TA Instruments, New Castle, DE, USA) with cup and bob geometry at 0°C. This temperature of analysis was chosen to match with the temperature of the rheological measurements carried out on the melted ice cream. The mix was allowed to equilibrate

in temperature for 5 minutes. A logarithmic flow sweep, 10 data points per decade, was carried out from 100 to $1s^{-1}$ shear rate using steady state sensing (5% tolerance within 30 seconds in 3 consecutive sampling with 180 seconds maximum equilibration time). Apparent viscosity was recorded at $50s^{-1}$ shear rate and the Herschel-Bulkley model, which was found to be the best model, was used to fit the data:

$$\sigma = \sigma_0 + k \times \dot{\gamma}^n \quad (2.1)$$

Here, σ is the shear stress (Pa), σ_0 is the yield stress (Pa), k is the consistency coeffiecient ($Pa.s^n$), $\dot{\gamma}$ is the shear rate (s^{-1}) and n is the flow behavior index (dimensionless).

Flow ramp measurements were carried out at 0°C on mix formulations with 0, 0.2 or 0.4% stabilizer and 0.03% PS80. Shear rate was increased from 0.001 to 100 s^{-1} with 10 points per decade for 10 minutes, followed by a decreasing shear ramp from 100 to 0.001 s^{-1} for another 10 minutes. Instantaneous shear stress and viscosity were obtained over time. Thixotropy was obtained by calculating the area between the shear stress curves using the TRIOS software (2019 TA Instruments–Waters LLC, New Castle, USA).

Frequency sweep tests were performed in mix formulations with 0, 0.2 or 0.4% stabilizer and 0.03% PS80. Two mix samples with the extreme stabilizer levels, 0 and 0.4% (S1 and S3, respectively, see code in Table 2.1) were used to characterize the linear viscoelastic regime (LVR) of the mixes. After that, logarithmic frequency sweep, 10 points per decade, was performed using 0.1% strain from 0.5 to $628.3rad.s^{-1}$ at 0°C. Storage modulus (G'), loss modulus (G") and loss tangent (tanδ) were obtained.

2.3.4.2 Overrun

The same volumes of mix and ice cream (177.4mL) were weighed and the overrun obtained using the percentage difference between the mix and ice cream weights to the ice cream weight (Goff and Hartel, 2013). After reaching equilibrium temperature and overrun during freezing, overrun measurements were obtained prior to collecting samples from the beginning, middle and end of production.

2.3.4.3 Particle/Fat Globule Size Distribution

Laser light scattering (Malvern Mastersizer 2000, Malvern Instruments Ltd., Worcestershire, UK) was used to obtain the particle size distributions of the mix and melted ice cream (Goff and Hartel, 2013). Two to four drops of the sample (4°C) were used to obtain obscuration values from 13 to 15%. The refractive index for the dispersant (deionized water) was 1.33 and the refractive index for the dispersed phase (milk fat) was 1.47. Absorbance was set at 0.01.

The ice cream was melted at ambient temperature (22±1°C) and stored at 4°C until analysis. The percentage of fat destabilization was obtained by comparing the peak of destabilized fat from melted ice cream curve to the peak of initial emulsion from ice cream mix curve (Bolliger et al., 2000; Warren and Hartel, 2018).

2.3.4.4 Air Cell Size Distribution

Air cell analysis was performed within an insulated glove box (Donhowe et al., 1991) at -6°C, as described by Chang and Hartel (2002). An optical light microscope (Optiphot, Nikon, Inc., Garden City, NY, USA) with a 30W LED light system, solid state camera (Cohu Eletronics

Div., San Diego, CA, USA) and OPTIMAS software (OPTIMAS v6.1, Optimas Corp., Meyer Instruments Inc., Houston, Tex. U.S.A.) was used to obtain images at 40x magnification. At least 300 air cells were analyzed using Image Pro Plus software (Image Pro Plus 7.0, Media Cybernetics, Inc., Rockville, MD, USA) and results were collected in a Microsoft Excel spreadsheet for statistical analysis.

2.3.4.5 Ice Crystal Size Distribution

Ice crystal analysis was performed at -15°C in an insulated glove box, as described by Donhowe et al. (1991). OPTIMAS software (OPTIMAS v6.1, Optimas Corp., Meyer Instruments Inc., Houston, Tex. U.S.A.) was used to obtain images (40x magnification) from a solid state camera (Cohu Eletronics Div., San Diego, CA, USA), which was attached to an optical light microscope (Optiphot, Nikon, Inc., Garden City, NY, USA) with a 30W LED light system. At least 300 ice crystals were traced from the images using Microsoft Softonic Paintbrush for Mac. Image Pro Plus software (Image Pro Plus 7.0, Media Cybernetics, Inc., Rockville, MD, USA) was used to analyze the ice crystals. Then, the results were collected in a Microsoft Excel spreadsheet for statistical analysis.

2.3.5 Ice Cream Rheological Properties

A rotational rheometer with parallel plates of 25mm diameter with crosshatched surface (DHR-2, TA Instruments, New Castle, DE, USA) was used to obtain the rheological measurements. Stepped Peltier Plate system attached to a liquid recirculating chiller (ThermoCube, Solid State Cooling Systems, Wappingers Falls, NY, USA) with a 20% ethanol solution was used to control the lower plate temperature. Upper Heated Plate system attached to a liquid recirculating

chiller (Isotemp 4100 R35, Fisher Scientific, Waltham, MA, USA) with a 50% ethylene glycol solution was used to control the upper plate temperature. Ice cream disks of 25 and 2.5mm of diameter and height, respectively, were prepared within the insulated glove box at -20°C (Donhowe et al., 1991). The disks were obtained from ice cream slabs cut from the center of the containers using a cylindrical tool. The parallel plates were preset at -15 or -5°C, depending on the analysis. The 25mm ice cream disk was placed in the center of the lower plate and the upper plate was loaded into the sample without trimming. Protocols for each rheological measurement are described in the subsequent sections. The samples with extreme levels of stabilizer, air flow and PS80, S1A1P1 (0% stabilizer, 8L.h^{-1} air flow and 0% PS80) and S3A3P3 (0.4% stabilizer, 15L.h^{-1} air flow and 0.03% PS80) (Table 2.1), were used to confirm the suitability of the rheological protocols developed. Those ice creams were expected to cover the range of the structural variety of the ice creams assessed in this study.

2.3.5.1 Oscillatory Thermo-Rheometry (OTR)

The oscillatory thermo-rheometry (OTR) using controlled axial force was adapted from Wildmoser et al. (2004) and Granger et al. (2005). The OTR was carried out from -15 to 25°C. All OTR analyses were carried out within the Linear Viscoelastic Regime (LVR), which was characterized in preliminary tests and confirmed by samples S1A1P1 and S3A3P3. Strains (within the LVR) of 0.01 and 0.1% were used from -15 to 0°C and from 0 to 25°C, respectively. The parallel plates were preset at -15°C and the ice cream disk was loaded with initial gap of 1800µm. A sample cover used to minimize water evaporation (as the ice cream was exposed for long time in the ambient) was placed on top followed by an insulating thermal cover for the parallel plates. Continuous oscillation with 10 rad.s^{-1} angular frequency was applied on the sample using

automatic motor mode and 0N (±0.1N) normal force. G', G" and tanδ were obtained every 4 seconds using ramp rate of 0.5°C.min^{-1}. After that, one data point every 0.5°C was obtained by using the data reduction feature from the TRIOS software (2019 TA Instruments–Waters LLC, New Castle, USA).

2.3.5.2 Creep-Recovery

Creep and recovery tests were adapted from Steffe (1996) and Dogan et al. (2013). The plates were set to -5°C, the sample was loaded to 1800µm gap, an insulating thermal cover was placed, the temperature was adjusted to 0°C, and samples were equlibrated for 10min. A constant stress ($\sigma_{constant}$) of 1.2Pa, which was within the LVR, was applied for 150s. The load was relieved, and the structural recovery was recorded for another 150s. Data were recorded using fast sampling, with data points decreasing logarithmically over time. Maximum creep strain (MCS) and recovery (%R) were obtained, and creep compliance data were fitted by mechanical models using the TRIOS software (2019 TA Instruments–Waters LLC, New Castle, USA).

2.3.5.3 Stress Growth

Stress growth measurements were adapted from Elliott and Ganz (1977) and Rao (2007). The plates were preset at -5°C, the sample was loaded to 1800µm gap, an insulating thermal cover was placed on top, the temperature was ajusted to 0°C, and the sample was equilibrated for 10min. A constant shear rate of 0.01s^{-1} was applied; shear stress was obtained over 1800 seconds or until reaching the steady state flow, which was verified by using the steady state sensing in the rheometer software (5% tolerance within 30 seconds in three consecutive sampling) at 0°C. Shear modulus (G), equilibrium viscosity (η_∞) as well as work of structure breakdown (W) were

determined using a phenomenological analysis adapted from Elliott and Ganz (1977) and Rao (2007).

2.3.5.4 Flow Ramp

After setting the rheometer plates to -5°C, the samples were loaded and the flow ramp was carried out at 0°C. Shear rate was increased from 0.001 to 100 s^{-1} with 10 points per decade for 10 minutes, followed by a decreasing shear ramp from 100 to 0.001 s^{-1} for another 10 minutes. The instantaneous shear stress and viscosity were obtained over time. The area between the shear stress curves (up and down) was obtained using the thixotropy function in the TRIOS software (2019 TA Instruments–Waters LLC, New Castle, USA). Melted ice creams did not recover their initial structure after shearing the matrix at 0°C. Thus, the area between the curves was obtained as rheological destruction measurement.

2.3.6 Statistical Analysis

All data were analyzed using with JMP statistical software (JMP Pro 14.0, SAS Inst., Cary, N.C., U.S.A. 2018). The data analysis using multiple linear regression (MLR) provided a general overview of the effects of structural components on rheological properties, as the 27 samples were analyzed together. Mix viscosity, overrun and fat destabilization were kept in all MLR models since those variables were chosen to predict the rheological parameters in the ice cream matrix. Plots of actual by predicted values, residual by predicted values, studentized residuals and residual normal quantile were used as diagnostics for linearity, error independence, equal variance and normal distribution of errors. One-way ANOVA and Tukey's HSD tests were also performed to complement the data analysis. This combined analysis allowed assessment of which structural

components governed a rheological parameter and how the overlapping structural components influenced the same rheological parameter.

2.4 Results and Discussion

The levels of stabilizer, air flow and PS80 were chosen in order to build a wide variety of structures, which could cover the range of structures observed in full fat commercial ice cream products (Warren and Hartel, 2014). Therefore, the effects of the mix viscosity at $50s^{-1}$, overrun and fat destabilization extent on the rheological properties of ice creams with controlled structural formation were evaluated in this study.

2.4.1 Structural Components (Structural Elements, Compositional and Physical Parameters)

Table 2.1 shows the full factorial design with 3 levels of stabilizer, air flow and polysorbate 80 (PS80), as well as the correspondent mix viscosity, overrun and fat destabilization extent for each ice cream sample. Other structural components evaluated can also be found in the same table. Although these other structural components were not in the scope here, they are available in case the reader searches for further information about the ice cream samples.

2.4.1.1 Mix Rheology

The mix viscosity at $50s^{-1}$ increased mainly when the stabilizer levels were increased in the formulations (Table 2.1). The ability of stabilizers to modify rheological properties not only in ice cream mix, but also in other food products has been well established in the last decades (Cottrell et al., 1980; Goff and Hartel, 2013; Li and Nie, 2016; Saha and Bhattacharya, 2010). Stabilizers, such as LBG, guar gum and carrageenan, are polysaccharides with a large number of hydroxyl

(-OH) groups present in their molecules. This characteristic leads to greater affinity with water, hence increasing its ability to retain water (Li and Nie, 2016; Saha and Bhattacharya, 2010). Moreover, according to Li and Nie (2016), the increase of viscosity is promoted by the thickening process of the liquid phase, which is related to nonspecific entanglement of conformationally-disordered polymer chains and the polymer-solvent interaction (Saha and Bhattacharya, 2010). Thus, the mix viscosity increased not only due to the greater molecular interaction between water and stabilizer when the stabilizer levels increased (enhanced ability to hold water), but also due to the greater entanglement among the stabilizer molecules (which contributes to the flow resistance of the mix).

Although the Herschel-Bulkley parameters will be discussed here, only the mix viscosity at $50s^{-1}$ (serum phase viscosity) will be used to build the MLR models in the subsequent Sections. Moreover, as a typical commercial stabilizer blend of LBG, guar gum and carrageenan is used in this study, similar to other studies from our research group (Amador et al., 2017; Warren and Hartel, 2018), the Herschel–Bulkley parameters and curves (shear stress and apparent viscosity) will not be shown here.

In general, ice cream mix presents a non-Newtonian flow pseudoplastic behavior (Clarke, 2004; Goff and Hartel, 2013), which was observed for all formulations in this study. The shear thinning behavior was more pronounced when the levels of stabilizer were increased in the formulations. In the Herschel–Bulkley parameters (Equation 2.1), σ_0 and k increased, while the n decreased when the stabilizer levels were increased in the mixes, as seen in previous works (Hagiwara and Hartel, 1996; Muse and Hartel, 2004; Soukoulis et al., 2008; Stanley et al., 1996). Although some differences were observed for certain conditions with and without PS80 added,

these differences were random and not considered further. No differences were found in those formulations for k and n values.

As stabilizer increased, thixotropy increased in the three chosen mix formulations with 0.03% PS80. The mixes with 0, 0.2 or 0.4% stabilizer had thixotropy values of 6.0(±0.4), 20.7(±0.3) and 55.2(±3.0) $Pa.s^{-1}$, respectively. LBG at 0.03% concentration with xanthan gum was found to affect thixotropic behavior in food emulsions containing modified starch (Dolz et al., 2007). Guar gum at 0.35% concentration was found to affect the extent of thixotropy in full and low fat ice cream mixes (Javidi et al., 2016). Moreover, iota carrageenan in the presence of Ca^{2+} salt has been reported to form a thixotropic dispersion (Thomas, 1997). Although type and concentration of carrageenan as well as the other gum concentrations in the stabilizer blend were unknown, the different levels of this commercial blend were enough not only to change mix viscosity, but also the thixotropic behavior of the ice cream mixes.

As stabilizer increased, storage modulus (G') increased and loss tangent (tanδ) decreased in the three mix formulations with 0.03% PS80. The mixes with 0, 0.2 or 0.4% stabilizer showed 0(±0), 1(±0) and 5(±0) Pa, respectively, for G', and 2.38(±0.35), 1.06(±0.35) and 0.62(±21), respectively, for tanδ at $1rad.s^{-1}$. Low angular frequency was used to compare samples due to inertia limitation at higher angular frequency for samples with no stabilizer added. As stabilizer levels increased, polysaccharide interactions increased and, therefore, mixes with 0.4% stabilizer added showed G'>G" (formation of weak gel). Mixes with 0 and 0.2% stabilizer added showed G'<G" at low frequency and 0°C.

2.4.1.2 Overrun

As can be observed in Table 2.1, the different levels of air flow in the continuous freezer allowed good control of the target overruns (50, 75 and 100%) in the samples. Manual mode was used to avoid interference from the automated control during freezing. Even though differences were small, individual overrun measurements will be subsequently used as an independent variable to build the MLR models in the subsequent Sections.

2.4.1.3 Percent of Partially-Coalesced Fat Globules (Fat Destabilization)

In general, higher levels of stabilizer, air flow and PS80 all presented higher values for fat destabilization. Fat destabilization increased with increasing levels of PS80 (Table 2.1). The emulsifiers partially replace proteins in the fat globule membrane, which, combined with shear forces during dynamic freezing, can lead to partial coalescence as liquid fat is shared among the fat globules (Goff et al., 1987; Goff and Hartel, 2013; Muse and Hartel, 2004; Pawar et al., 2012). However, this trend was not observed in formulations with 0.4% stabilizer and 11L.h^{-1} air flow (refer to samples S3A2P1-S3A2P3 in Table 2.1). Moreover, no difference in partial coalescence between 0 and 0.015% PS80 was found in the formulations with 0 or 0.2% stabilizer (Figure 2.1A). Thus, 0.015% PS80 was not sufficient to destabilize the membrane of fat globules in this study (Table 2.1).

Fat destabilization extent increased as the mix viscosity at 50s^{-1} (serum phase viscosity) increased, as illustrated by particle size distributions in Figure 2.1B. In general, only a moderate correlation was found between fat destabilization and mix viscosity ($r=0.48$, $p=0.0113$). An increased mix viscosity associated with higher fat destabilization was also reported by other authors (Amador et al., 2017; Goff and Spagnuolo, 2001; Muse and Hartel, 2004). Higher viscosity

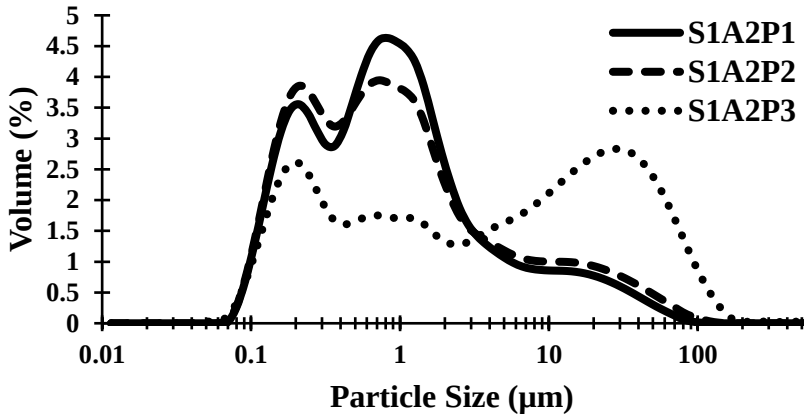

(A)

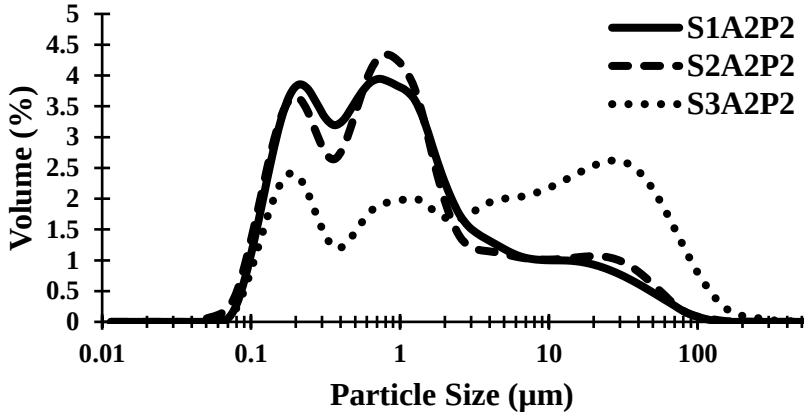

(B)

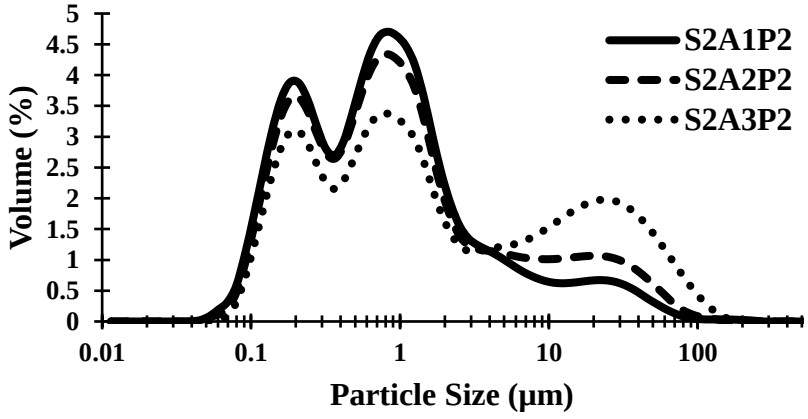

(C)

Figure 2.1: Particle size distributions for samples: (A) with different levels of PS80 (P1, P2 and P3 refer to 0, 0.015 and 0.03%, respectively), and constant levels of stabilizer (0%) and air flow (11L.h^{-1}); (B) with different levels of stabilizer (S1, S2 and S3 refer to 0, 0.2 and 0.4%, respectively), and constant levels of PS80 (0.015%) and air flow (11L.h^{-1}); (C) with different levels of air flow (A1, A2 and A3 refer to 8, 11 and 15L.h^{-1}, respectively), and constant levels of stabilizer (0.2%) and PS80 (0.015%).

of the slurry increases the shear forces in the barrel, which increases the collisions among the fat globules during dynamic freezing. Fat destabilization measurements will also be used as an independent variable to build MLR models in this study.

Fat destabilization extent increased as overrun increased, as illustrated by the particle size distributions in Figure 2.1C. Although a general correlation was found between fat destabilization and overrun (r=0.44, p=0.0207), the correlation was more prominent in the formulations with higher mix viscosity at $50s^{-1}$ (0.4% stabilizer) (r=0.86, p=0.0027). Warren and Hartel (2018), who also observed correlation between fat destabilization and overrun, reported that higher overrun led to higher probability of collisions among fat globules due to the thinner lamellae in those samples.

2.4.1.4 Air Cell Size

Air cell size increased as overrun decreased, especially in formulations with 0 (r=-0.80, p=0.0089) and 0.4% (r=-0.78, p=0.0134) stabilizer. This correlation is probably due to the increased shear stress as the incorporated air volume increases, which leads to the breakdown of air cells (Sofjan and Hartel, 2004; Warren and Hartel, 2018). Moreover, air cell size decreased as fat destabilization increased in the formulations with 0 (r=-0.80, p=0.0091), 0.2 (r=-0.76, p=0.0169) and 0.4% (r=-0.87, p=0.0022) stabilizer. This result corroborated previous work (Warren and Hartel, 2018). The shear forces that also promote fat destabilization lead to the breakdown of air cells. According to the work of Amador et al. (2017), the addition of stabilizers promoted smaller air cells at a draw temperature of -3°C. However, no trend was found either by the authors at draw temperature of -6°C nor in this study. Although there were slight differences among the air cell sizes, further studies are needed to elucidate the interactions between air cells and processing as well as between air cells and stabilizer levels. Finally, air cell size will not be

used to build MLR models due to the complexity to control this variable during the freezing as well as the collinearity in the MLR models, mainly between air cell size and overrun.

2.4.1.5 Ice Crystal Size

Only slight differences were found for the mean ice crystal size (Table 2.1), although no specific trends were found. Moreover, the control of ice crystal size was not in the scope of this study and has limited importance to melted ice cream. Therefore, ice crystal size will not be used to build MLR models in the next sections.

2.4.2 Rheological Properties of the Ice Cream Matrix

Structural components and their intrinsic arrangement determine rheological behavior in ice cream matrix, which directly influence melting and sensory properties. Different forces applied to the matrix can provide not only rheological parameters that confirm the mechanical role of these structural elements, but also parameters that help to understand the arrangement of these components in the ice cream matrix.

2.4.2.1 Oscillatory Thermo-Rheometry (OTR)

Since all dynamic rheological measurements are performed within LVR, storage (G') and loss (G") moduli provide information on solid-like and liquid-like behavior of the ice cream matrix with intact structure. In Figure 2.2A, the samples S1A1P1 and S3A3P3 (refer to codes in the Table 2.1), which represent the extreme levels of stabilizer, air flow and polysorbate 80 (PS80), illustrate the wide range of the G' and loss G" moduli presented by the ice cream samples. As proposed by Wildmoser et al. (2004), G’ and G” curves were divided into three zones. The tanδ (G”/G’) behavior, which is an important indicator of the phase melting (Granger et al., 2005) and structural

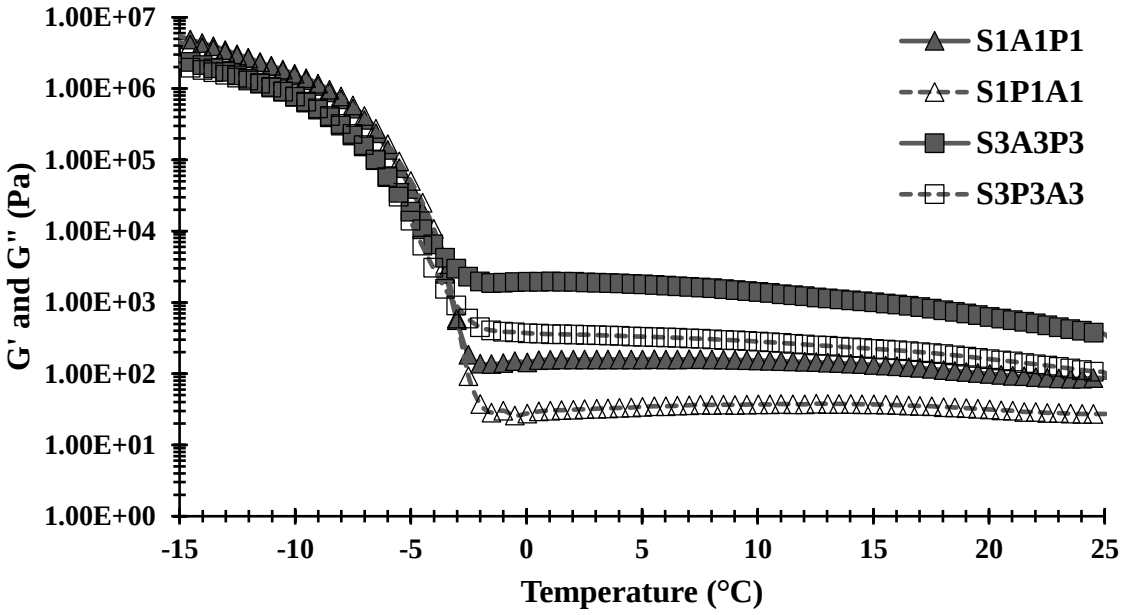

(A)

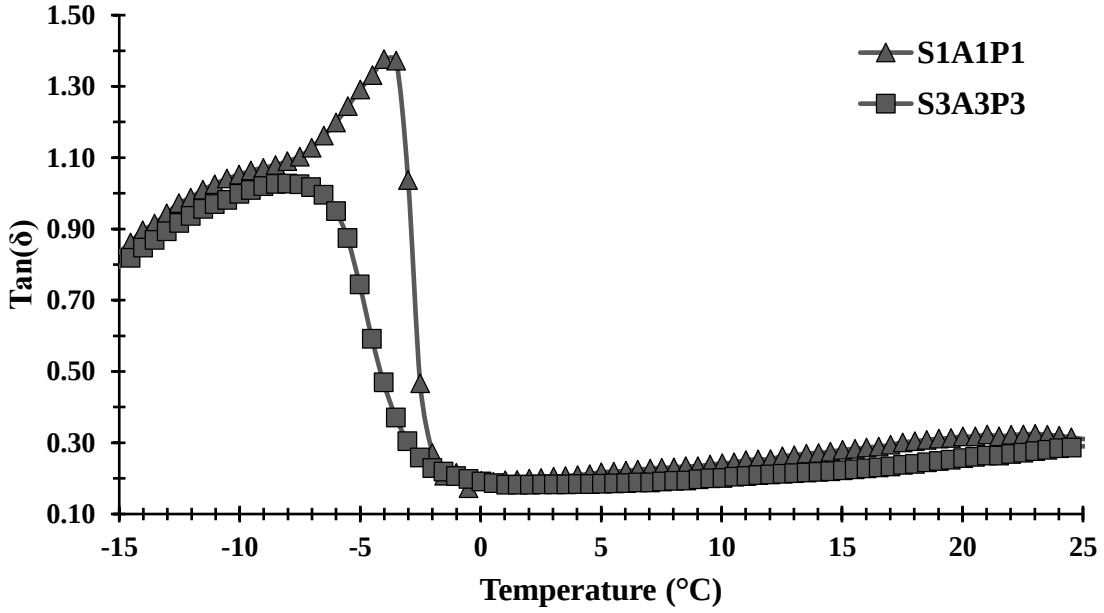

(B)

Figure 2.2: (A) Storage (G') and loss (G") moduli behavior for samples S1A1P1 (0% stabilizer, 8L.h^{-1} air flow and 0% PS80) and S3A3P3 (0.4% stabilizer, 15L.h^{-1} air flow and 0.03% PS80). (B) Tanδ behavior for the samples S1A1P1 and S3A3P3.

changes in the ice cream during the OTR, are also shown in Figure 2.2B for the same samples. The MLR models for the parameters obtained from OTR are shown in Table 2.2. The structural components similarly affected G' and G"; therefore, only MLR models for G' and tanδ are discussed in the text.

Zone I (from -15 to -10°C): All the samples showed G' slightly greater than G" at -15°C. Mix viscosity at $50s^{-1}$ inversely affected G' ($G'_{-15°C}$) and tanδ ($tan\delta_{-15°C}$) at -15°C, as observed in Table 2.2. The inverse correlation between mix viscosity (at $50s^{-1}$) and $tan\delta_{-15°C}$ aligned with Goff et al. (1995). As previously discussed, higher stabilizer levels led to lower tanδ values in ice cream mixes. Greater concentration of stabilizer molecules in serum phase also likely contributed to greater elasticity in the ice creams at -15°C. Tukey's HSD test was also used to complement the analysis for $G'_{-15°C}$ (Table 2.3).

As stabilizer level increased, $G'_{-15°C}$ decreased (Table 2.3), which corroborated the observations from the MLR model (Table 2.2). Goff et al. (1995) found that unstabilized ice cream showed G' and G" values significatively higher than stabilized ice cream at temperatures below--6°C. The authors related these correlations to the critical concentration (C*), also known as overlap concentration (Saha and Bhattacharya, 2010), reached by the guar gum used in their stabilizer system. Lower G' and G" in ice creams with higher stabilizer levels may be related to connectivity loss of ice crystals through the serum phase due to the higher entanglement of polysaccharides (as serum phase was freeze-concentrated). However, the mechanisms of how stabilizer molecules change G' and G" are still unclear and need further study.

As air flow (which efficiently controlled the overrun) increased, $G'_{-15°C}$ increased in samples with 0.4% stabilizer added (Table 2.3). As a weak gel formation was observed for mixes with 0.4% stabilizer added, the stabilizer entanglement probably affected the serum phase in those

ice creams. The thinner lamellae (smaller space) and smaller air cell size (as previously discussed) in ice creams with higher overrun probably increased the interactions of polysaccharide entanglements. Moreover, as the air surface area was increased with the higher overrun, interactions also increased at the serum phase/air cell interface.

Although samples with different levels of PS80 were different in formulations with no stabilizer and 11L.h^{-1} air flow added (Table 2.3), no trend was found in $G'_{-15°C}$ ($p=0.3296$). Direct correlation was found between fat destabilization and $G'_{-15°C}$ in samples with 0.2 ($r=0.81$, $p=0.0080$) and 0.4% ($r=0.86$, $p=0.0030$) stabilizer added. This was probably due to direct correlations of fat destabilization with mix viscosity and overrun, as previously discussed.

Zone II (from -10 to -2.7°C): As temperature increases from -10 to -2.7°C, melting of ice crystals and dilution of unfrozen serum phase are the main factors driving the structural changes in the ice cream matrix (Caldwell et al., 1992; Goff et al., 1995). As ice melts, G' and G" showed a sharp decrease (Figure 2.2A), which corroborated with previous findings (Eisner et al., 2005; Wildmoser et al., 2004). G' was approximately the same as G" during melting, which also agreed with other works (Goff and Hartel, 2013; Granger et al., 2005; Wildmoser et al., 2004). As a result, a peak was observed in tanδ for all samples. In this peak, G' was lower than G" in most samples, mainly in samples with low levels of stabilizer, and some samples with low PS80 and air flow levels. This suggests that the ice cream matrix increased in liquid-like behavior during melting of ice crystals (Goff and Hartel, 2013; Granger et al., 2005). In this temperature range, G' and G" were also found to be affected by formulation, such as stabilizer, and process, such as low-temperature extrusion (Goff et al., 1995; Goff and Hartel, 2013; Wildmoser et al., 2004). The viscous behavior in the peak of tanδ seemed related to the structure formation in the matrix. This will be discussed later in the text.

Zone III (from -2.7 to 25°C): Ice crystals were completely melted above -2.7°C. At 0°C, all samples showed G'>G". Extent of fat destabilization showed very strong direct effects on G' at 0°C ($G'_{0°C}$) in the MLR model (Table 2.2). The continuous 3-Dimensional fat network across the serum phase contributed to the elasticity of the melted matrix at 0°C, which corroborated with other works (Eisner et al., 2005; Granger et al., 2005; Wildmoser et al., 2004). Tukey's HSD test was also used to complement the analysis for $G'_{0°C}$, as shown in Table 2.3.

In general, as stabilizer increased, $G'_{0°C}$ also increased. It is known that water retention and stabilizer entanglements provide elasticity in the system (Goff et al., 1995; Li and Nie, 2016; Saha and Bhattacharya, 2010). Moreover, as previously discussed, gel formation was observed in the mixes with 0.4% stabilizer added, so greater G' is also expected for the respective ice creams with 0.4% stabilizer added. As air flow (which controlled overrun) increased, $G'_{0°C}$ increased. This is probably due to greater interactions of components of the serum phase as well as fat globules in the thinner lamellae in ice creams with high overrun. Moreover, this trend (direct correlation between air flow and $G'_{0°C}$) was slightly stronger in samples with 0.4% stabilizer added (Table 2.3), which was probably due to the gel formed in the serum phase through the lamellae, as observed in mixes with 0.4% stabilizer added. As PS80 increased, $G'_{0°C}$ increased. The PS80 destabilizes the membrane of fat globules in the mixes, leading to greater partial coalescence of fat globules during the dynamic freezing, and greater elasticity to the matrix at 0°C (P1-P3; see code in the Table 2.3). Thus, although G' was also affected by the mix viscosity (controlled by stabilizer levels) and overrun (controlled by the air flow), G' was most influenced by the extent of fat destabilization at 0°C.

The $\tan\delta_{0°C}$ ranged from 0.18 to 0.21, which was quite low compared to the $\tan\delta_{-15°C}$ range (from 0.76 to 0.85). This suggests that the ice cream matrix at -15°C showed highly concentrated

solution behavior, and when the ice phase was completely melted, the matrix turned to a gel at 0°C. No effect of structural components was found on $\tan\delta_{0°C}$, which suggests a relative stability of the structure at this temperature.

2.4.2.2 Creep and Recovery Measurements

Viscoelastic properties of food products are commonly studied by oscillatory tests. Nevertheless, another type of test is needed to better understand possible internal structures and their changes due to the composition (Dogan et al., 2013; Dolz et al., 2008; Toker et al., 2013). Thus, creep and recovery are among the most common tests for these investigations (Dogan et al., 2013).

In the creep test, a constant stress ($\sigma_{constant}$) of 1.2Pa, which was within the LVR based on oscillatory stress amplitude sweeps, was applied to the melted ice cream at 0°C, and the strain (γ) was recorded over time (t) for 150 seconds. In the recovery test, the load from the creep test was released, and the structural recovery was also measured for another 150 seconds. In the data analysis, the maximum creep strain (MCS) was obtained from the creep part and the percentage recovery (%R) after 150 seconds from the recovery part. All samples showed %R below 100%. In other words, although the constant stress applied to sample was within the LVR, the structure deformed did not recover its initial structure after releasing the load, hence, melted ice cream yielded over time. The sample S2A2P2 (refer to code in the Table 2.1), which represents the middle levels for stabilizer, air flow and PS80, is used as example for MCS and %R measurements in Figure 2.3A.

The shear creep compliance (J), which is γ divided by $\sigma_{constant}$ (1.2Pa), was determined over time (Steffe, 1996). From that, the generalized Kelvin-Voigt model (also known as discrete

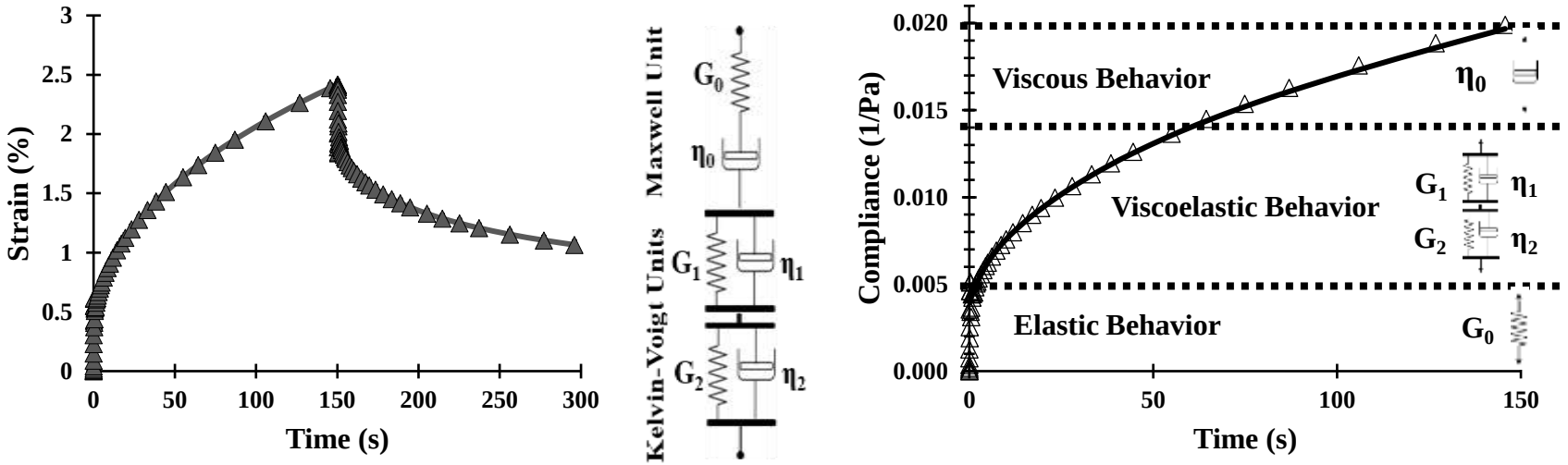

(A) **(B)** **(C)**

Figure 2.3: (A) Sample S2A2P2 (0.2% stabilizer, 11L.h^{-1} air flow and 0.015% PS80) used as example for maximum creep strain (MCS) and recovery (%R); (B) Springs and dashpots of the six-element model (Maxwell model in series with two Kelvin-Voigt models); (C) sample S2A2P2 used as example for prediction of creep compliance by the six-element model.

retardation spectrum) was used to fit the creep data (Ahmed, 2015; Gunasekaran and Ak, 2003; Kaschta and Schwarzl, 1994; Purkayastha et al., 1984).

$$J(t) = J_0 + \sum_{i=1}^{N} J_i[1 - e^{-t/\tau_i}] + t/\eta_0 \quad (2.2)$$

Here, J(t) is compliance over time (t), τ_i are the retardation times, J_i are the retarded compliances (represent the viscoelastic behavior), J_0 is the instantaneous compliance (represents the elastic behavior) and η_0 is the residual viscosity (represents the viscous behavior). Usually, the Kelvin-Voigt model is used to describe the creep behavior of biological and polymeric systems, which often present more than one retardation time (Gunasekaran and Ak, 2003; Purkayastha et al., 1984). The selected six-element model (Figure 2.3B), which was the simplest possible model (Purkayastha et al., 1984), provided a good fit (R^2>0.99) and described well the creep data, as can be observed in Figure 2.3C using the sample S2A2P2 as example. G_0 (spring) and η_0 (dashpot) of the Maxwell unit are the elastic modulus and residual viscosity, respectively. In the first and second Kelvin-Voigt units, G_1 and G_2 (springs) are the retarded elastic moduli, η_1 and η_2 (dashpots) are internal viscosities (Dogan et al., 2013). Shama and Sherman (1966) as well as Sherman (1966) also used a six-element model to describe the creep behavior for ice cream and ice cream mix, respectively. Shama and Sherman (1966), studying frozen ice cream, suggested that G_0 was mainly affected by ice crystals, G_1 affected by weak stabilizer gel, η_1 affected by fat crystals, G_2 affected by protein enveloped air cells, η_2 affected by weak stabilizer gel as well as protein enveloped air cells and, η_0 affected by ice and fat crystals. Sherman (1966) also studied melted ice cream and used a four-element model, also known as Burgers model, to evaluate the structure at 20°C.

Moreover, the author suggested that second Kelvin-Voigt unit (G_2 and η_2) in six-element model (Figure 2.3B) for mix was related to globules of 0.5µm or smaller.

In general, the extent of fat destabilization was the only structural component that had an effect on elastic (G_0) and viscoelastic (G_1, G_2, η_1 and η_2) behaviors in MLR models; that is, fat destabilization had most influence on these rheological parameters (data not shown here). As the greatest coefficient of determination (R^2=0.74) was from $\eta_{0\ 0°C}$, the MLR model for $\eta_{0\ 0°C}$ is presented as an example not only for the parameters obtained in the transient measurements, but also for viscous behavior of melted ice cream at 0°C in Table 2.2. Moreover, η_0 will be also used to confirm yield stress measurements in the subsequent Section.

The mix viscosity at $50s^{-1}$ (serum phase viscosity) and the extent of fat destabilization showed strong direct effects on $\eta_{0\ 0°C}$ (Table 2.2), which corroborated with the Tukey HSD test in Table 2.3. As the stabilizer and PS80 contents increased, $\eta_{0\ 0°C}$ increased, which were due to increased viscosity in the mix (an increased viscosity of serum phase was also expected in the melted ice cream) and to the elasticity provided by the 3D network of fat globules through the lamellae (no structure disruption was expected as measurements were performed within the LVR and at low shear rate), respectively. As air flow (overrun) increased, $\eta_{0\ 0°C}$ also increased (Table 2.3). This was probably due not only to the higher interactions at the serum phase/air cell interface (as the surface area was increased in higher overrun samples), but also to the more structured matrix by itself in the higher overrun samples (as correlation was found between overrun and air cell size). It is worth noting that other structural components, such as fat globules (extent of fat destabilization) and volume of air cells (overrun) could also affect the viscous behavior of melted ice cream at low shear rate. Thus, the greatest influence on $\eta_{0\ 0°C}$ was from the mix viscosity (which

coefficient was the most significant in MLR model), followed by the extent of fat destabilization and overrun.

2.4.2.3 Stress Growth (Constant Low Shear Rate)

Stress growth or stress overshoot is a singular test. Some authors categorize the test based on transient viscoelastic flow of the sample (Rao, 2007; Steffe, 1996), while others categorize the test due to the large final deformation property of the sample at the end of the test (Lucey et al., 1997; Luyten et al., 1994). Parameters obtained with this measurement could not only confirm the results of other tests as well as obtain the steady state viscosity at a low shear rate ($0.01s^{-1}$), but also present information about the yield stress (σ_y). Briggs et al. (1996) related σ_y to the ability of ice cream to dip or scoop.

A phenomenological analysis was adapted from Elliott and Ganz (1977) and Rao (2007). The schematic diagram using sample S2A2P2 (see code in Table 2.1) was adapted and used as example in Figure 2.4A: t is time, σ_A is the stress at the end of the elastic portion, σ_y is correspondent to the yield stress (stress peak) and σ_∞ is the equilibrium shear stress. The correspondent deformations (γ, strain), such as γ_{tA}, γ_y (which is the strain correspondent to the σ_y) and $\gamma_{t\infty}$, for those stress and time values were also found. Furthermore, the product of the shear rate and time is the total deformation at different shear time. Thus, from the previous definitions, equations for shear modulus (G), equilibrium viscosity (η_∞) and work of structure breakdown (W) can be determined (Rao, 2007):

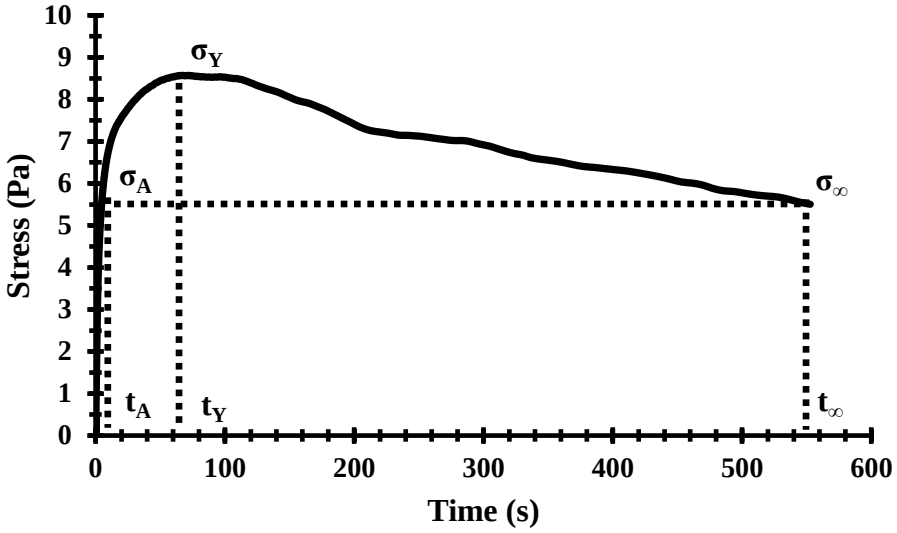

(A)

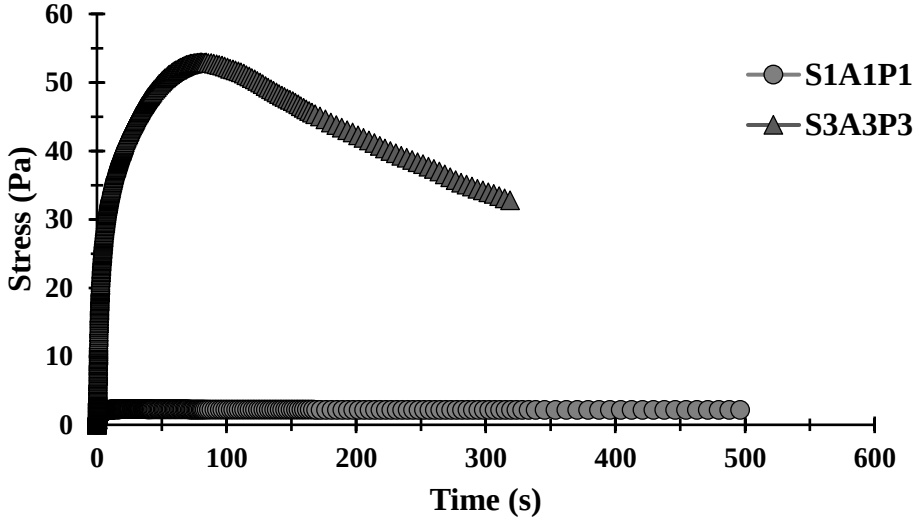

(B)

Figure 2.4: (A) Schematic diagram of phenomenological analysis adapted from Elliott and Ganz (1977) and Rao (2007) using sample S2A2P2 at 0°C. (B) Stress growth test at a constant shear rate of $0.01s^{-1}$ using steady state sensing (5% tolerance within 30 seconds in three consecutive sampling) for samples S1A1P1 and S3A3P3 at 0°C.

$$G = {}^{d\sigma}/_{d\gamma} = \sigma_A/\gamma_{t_A} \quad (2.3)$$

$$\eta_\infty = \sigma_\infty / \dot{\gamma} \quad (2.4)$$

$$W = \dot{\gamma} \int_A^B (\sigma - \sigma_\infty)\mathrm{d}t \quad (2.5)$$

Here, $\dot{\gamma}$ is the constant shear rate, A is the time that stress curve overshot σ_∞ and B is the time that σ_∞ was reached. Thus, W, which is area above the extrapolated σ_∞ line, was assessed as excess work of structure breakdown.

When a small $\dot{\gamma}$ is applied to the sample (Figure 2.4A), if σ curve is plotted against γ, $G_{0°C}$ can be obtained by calculating the initial slope on the curve of σ_A against γ. The matrix is assumed to be intact at the beginning of the curve and $G_{0°C}$ is related to the elastic property of the sample. As $\dot{\gamma}$ is kept constant, the structure enters into a transition range from intact structure to flow start. Over time, the structure eventually breaks and begins to flow (t_y). After the initial structure is broken, as constant $\dot{\gamma}$ is applied to sample, the structure continues to flow until reaching equilibrium (t_∞) at that specific $\dot{\gamma}$. After this point, σ becomes independent over time. Samples S1A1P1 and S3A3P3 (refer to codes in the Table 2.1), which represent the extreme levels of the formulations, illustrate the effects of structural components on stress growth parameters at 0°C in Figure 2.4B.

Overall, G (shear modulus) showed a similar trend to G' (storage modulus from OTR) and G_0 (elastic modulus of the six-element model from creep test) at 0°C (data not shown here). In addition, equilibrium viscosity (η_∞) also showed similar trend to η_0 (residual viscosity of the six-element model from creep test) at 0°C (data not shown here). The MLR model for σ_y, which

predicted 82% of the variability explained by the structural components, is presented in Table 2.2 as an example for the parameters obtained from the stress growth measurements. Extent of fat destabilization and mix viscosity at $50s^{-1}$ showed strong effects on σ_y. The effect of fat destabilization was probably due to the 3-D network of partially-coalesced fat globules through the lamellae, which provide structural resistance to initiate flow of the matrix. The effect of mix viscosity was probably due to increased LBG and carrageenan concentrations. In general, LBG and carrageenan present yield stress in emulsions (Turquois et al., 1992). A more detailed analysis was performed using Tukey's HSD test (Table 2.3).

As stabilizer and PS80 contents increased, which aimed to directly change the mix viscosity at $50s^{-1}$ and fat destabilization, respectively, σ_y also increased. In addition, as air flow (overrun) increased, σ_y also increased. This was probably due to the higher interactions at the serum phase/air cell interface as well as the more structured matrix in the samples with higher overrun (as ice creams with higher overrun showed smaller air cell size). Thus, mix viscosity at $50s^{-1}$ (which was the most significant coefficient from MLR model in Table 2.2) had the most effect on σ_y behavior, followed by the extent of fat destabilization and overrun.

Last, creep and recovery test were used to confirm the σ_y measurements of melted ice creams. At the end of the creep test the melted matrix yielded since %R values were below 100% for all samples, as previously discussed. The constant load (1.2Pa) applied to sample in creep test lower than $\sigma_{y\ 0°C}$ for all samples, which ranged from 2.2 to 53.8Pa, confirmed time-dependent nature of melted ice cream matrix. Among all six-elements parameters (creep data), $\eta_{0\ 0°C}$ presented the highest correlation with $\sigma_{y\ 0°C}$ (R^2=0.94, $p<0.0001$). Although the constant stress used in creep test was within the LVR, the Newtonian component in the six-element model, $\eta_{0\ 0°C}$, was measured when deformation reached equilibrium. In other words, the sample probably yielded in the viscous

behavior range shown in Figure 2.3C. Although creep and stress growth tests have different inputs, constant stress and shear rate, respectively, $\eta_{0\ 0°C}$ was probably obtained close to the $\sigma_{y\ 0°C}$ measurements. Therefore, this linear correlation could indirectly validate $\sigma_{y\ 0°C}$ measurements for melted ice cream samples.

2.4.2.4 Flow Ramp (Shear Rate Ramp) and Thixotropy

A typical thixotropic structure is broken down under shearing, and slowly, its initial structure is recovered at rest (Barnes, 1997). In preliminary tests, using a random ice cream sample with 40% overrun, the melted ice cream sample were subjected to upward and downward shear rate sweeps, as illustrated in a log-log plot in Figure 2.5. Time-dependency is clearly observed at low shear rates (below $1s^{-1}$) in upward curve (Figure 2.5). As hydrodynamic forces during upward shear reach a sufficient level, structural components, such as air cells, individual and clustered fat globules, flow freely through the disrupted matrix. In the downward curve (Figure 2.5), the disrupted matrix approaches a shear-thinning behavior and does not recover its initial structure. In other words, rheological destruction occurred after large deformation was applied to melted ice cream. Here, the flow ramp test was chosen to assess the time dependence of breakdown of the remnant foam using large deformations. In addition, a thixotropic loop was used to characterize the rheological destruction of the melted ice cream matrix at 0°C.

The larger the area between the up and down curves, the greater the rheological destruction, suggesting a greater initial structural formation in the melted matrix. The shear stress and instantaneous viscosity curves (up and down) for the sample S2A2P2 are shown as example in Figure 2.6A and 2.6B, respectively. The up shear stress and up viscosity curves were again plotted in Figure 2.6C to illustrate additional parameters that were obtained from the up shear rate ramps,

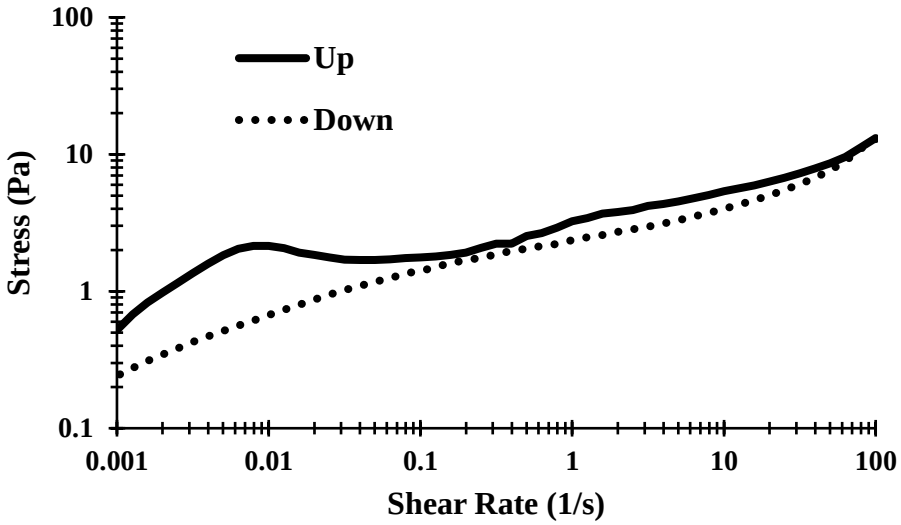

Figure 2.5: Log-log plot of up and down curves of shear stress against shear rate from a stepped flow test (flow sweep) using parallel plates and steady state sensing (5% tolerance within 30 seconds in three consecutive sampling) for a melted ice cream with 40% overrun and low fat destabilization at 0°C.

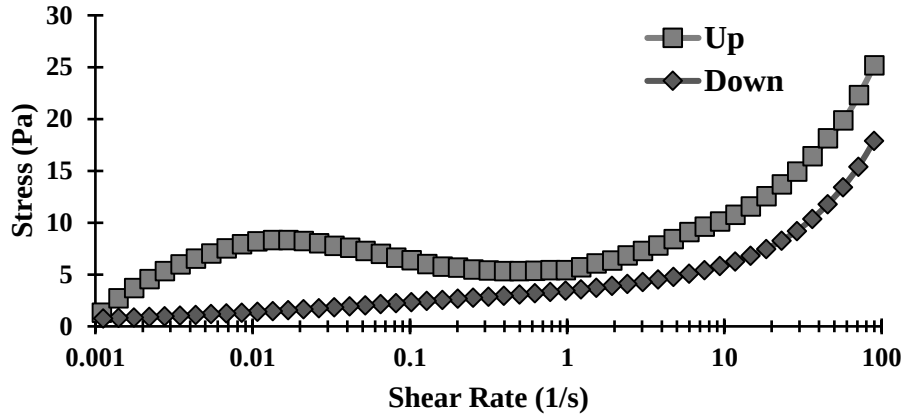

(A)

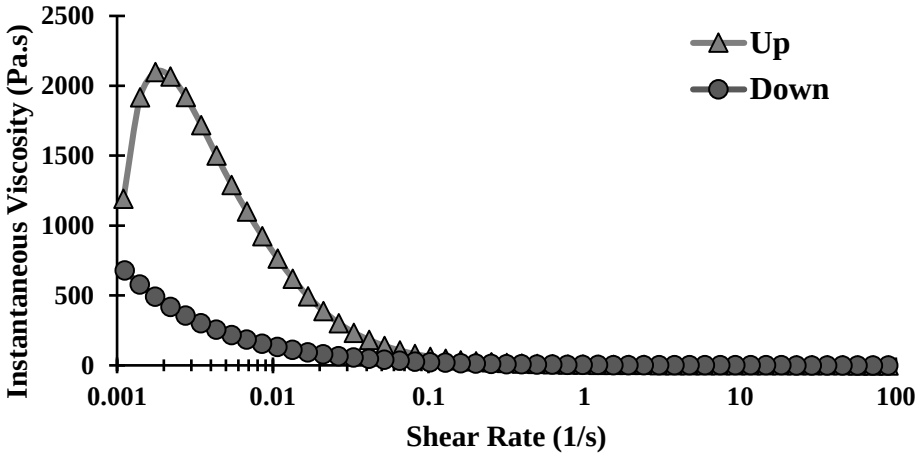

(B)

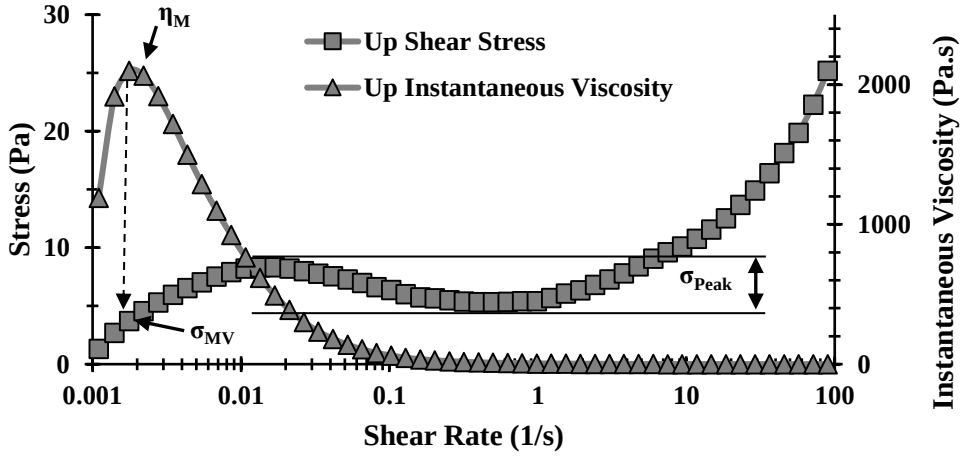

(C)

Figure 2.6: (A) Shear stress (up and down) and (B) instantaneous viscosity (up and down) curves for the sample S2A2P2; and (C) schematic diagram to illustrate the parameters, such as maximum instantaneous viscosity (η_M), correspondent stress to the maximum instantaneous viscosity (σ_{MV}) and height of the stress peak (σ_{Peak}), were obtained from the up shear rate ramp.

such as maximum instantaneous viscosity (η_M), correspondent stress to the η_M (σ_{MV}), and height of the stress peak (σ_{Peak}). The σ_{Peak} shown in Figure 2.6C was determined as:

$$\sigma_{Peak} = \sigma_{M\_0.001 \rightarrow 0.1} - \sigma_{m\_0.1 \rightarrow 10} \quad (2.6)$$

Here, $\sigma_{M\_0.001 \rightarrow 0.1}$ is the maximum shear stress from 0.001 to 0.1s^{-1} and $\sigma_{m\_0.1 \rightarrow 10}$ is the minimum shear stress from 0.1 to 10s^{-1}. This peak observed in the stress curve at lower shear rates (<1s^{-1}) must be related to the structure formation after freezing, mainly due to the fat destabilization and overrun, since no such peak was observed for mix.

As rheological destruction measurement (Thix $_{0°C}$) showed the greatest variability (89%) explained by the structural components, the MLR model for Thix $_{0°C}$ was shown as example for the parameters obtained in the flow ramp measurements (Table 2.2). Thix $_{0°C}$ ranged from 300 to 1420Pa.s^{-1}. After the dynamic freezing, the main structural formation is from the ice, air, fat and serum phases. As ice crystals were completely melted and viscosity of the mix and melted ice cream at 0°C were the same, Thix $_{0°C}$ was affected by the degree of disruption of air cells and network of fat globules through the lamellae. Mix viscosity at 50s^{-1} and extent of fat destabilization showed very strong direct effects on the Thix $_{0°C}$ (Table 2.2). The Tukey's HSD test was used to complement this analysis (Table 2.3).

As stabilizer increased, Thix $_{0°C}$ increased. This was probably due to the presence of LBG (Dolz et al., 2007), guar gum (Javidi et al., 2016) and iota carrageenan (Thomas, 1997) in the stabilizer system used in this study, as previously discussed. As increasing stabilizer affected thixotropic behavior in mixes, an increase in stabilizer was also expected to affect Thix $_{0°C}$ in melted ice creams containing stabilizer. Moreover, an increase in Thix $_{0°C}$ (Table 2.3) was observed

mainly in samples with 0.4% stabilizer added. This was probably due to the weak gel formation in the serum phase of those samples. As previously discussed, mixes with 0.4% stabilizer added presented weak gel formation (G>G"). As PS80 increased, Thix $_{0°C}$ increased slightly. Since PS80 is related to fat destabilization, the disruption of the 3-D network of partially-coalesced fat globules through the lamellae was directly responsible for this Thix $_{0°C}$. Furthermore, lower influence of PS80 was observed in samples with 0.4% stabilizer added. Weak gel formation in those samples probably exceeded the mechanical role of the fat network in the melted matrix at large deformations. As air flow (overrun) increased, Thix $_{0°C}$ showed slight increases, mainly in samples with 0.4% stabilizer added. Thinner lamellae in ice creams with higher overrun and greater number of smaller air cells (as previously discussed, inverse correlation was found between overrun and air cell size) provided greater structure formation (greater strength) due to more interactions of molecules as well as particles in the serum phase, and larger surface area at air/serum phase interface. However, in samples with 0.4% stabilizer added, weak gel formed in serum phase probably also exceeded the mechanical role of air phase in matrix at large deformations. Therefore, mix viscosity at $50s^{-1}$ (which coefficient was the most significant from MLR model in Table 2.2) showed most influence on thixotropic behavior, followed by the overrun and extent of fat destabilization.

As rheological destruction measurement (Thix $_{0°C}$) provided good information about the structure formation in the matrix at 0°C, the correlation between Thix $_{0°C}$ and the $\tan\delta_{Peak}$ was evaluated to help explain the tanδ behavior during OTR. The correlation between Thix $_{0°C}$ and $\tan\delta_{Peak}$ is presented in the Figure 2.7, which is also represented by the equation (R^2=0.92) below:

$$\tan\delta_{Peak} = 1.00 + 4.00 \cdot exp(-0.0077 \cdot \text{Thix}_{0°C}) \quad (2.7)$$

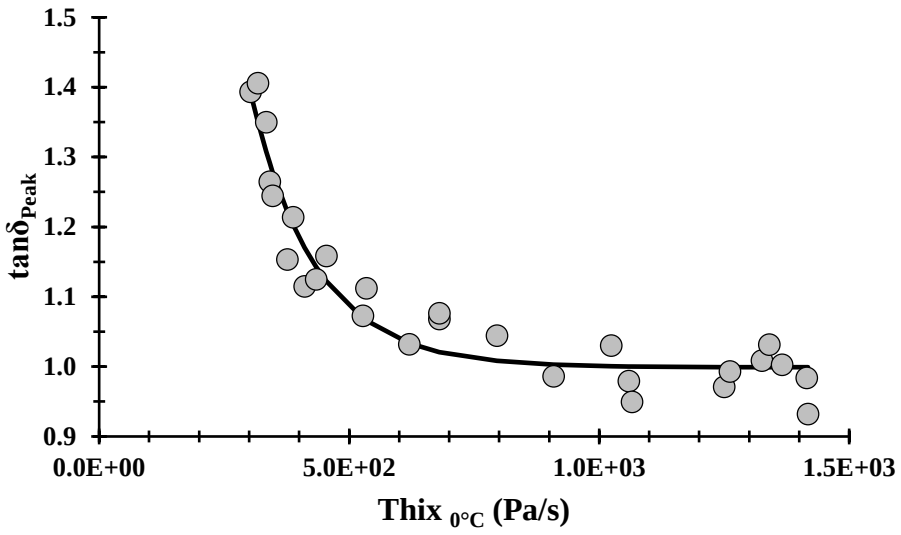

Figure 2.7: Correlation between rheological destruction measurement (Thix $_{0°C}$) and the observed peak at tanδ curve (tanδ$_{Peak}$) during oscillatory thermo-rheometry (OTR). Line is fitted exponential model from Equation 2.7.

As seen, there is an excellent correlation between the $tan\delta_{Peak}$ from OTR and $Thix_{0°C}$, where samples that showed the least thixotropy were those that had the highest $tan\delta_{Peak}$, most fluid-like. As measurements from OTR were performed within the LVR, structure is assumed to be undisrupted. As ice is completely melted, even though the fat network is slightly changed due to temperature, a similar structure to that when $tan\delta_{Peak}$ was measured is also assumed to be undisrupted without ice phase at 0°C. Moreover, samples prior to $Thix_{0°C}$ measurement also presented a similar initial structure to that when $tan\delta_{Peak}$ was measured (without ice phase). Therefore, this suggests that structure that affected $tan\delta_{Peak}$ magnitude during ice melting and dilution of serum phase in OTR is similar to the initial structure that was disrupted during the thixotropic loop.

2.5 Conclusions

In conclusion, the wide variety of structural components provided good correlations with rheological parameters. Importantly, all structural components (mix viscosity at $50s^{-1}$, fat destabilization and overrun), to a greater or lesser extent, showed influence on most rheological properties, which was a useful tool to characterize the structural arrangement in the ice cream samples. Structural components other than ice crystals were also important in dynamic oscillatory measurements of ice cream at low temperature (-15°C). Mix viscosity at $50s^{-1}$ had most effects on elastic behavior (G') in the presence of ice phase; in ice phase absence, fat destabilization showed the most influence on elastic behavior during OTR. In transient behavior, mix viscosity influence was slightly more significant than fat destabilization on viscous behavior (η_0) at low shear rate as well as on stress required to initiate the flow (σ_Y) of the melted matrix. The values of η_0 not only provided important insights about structural components, but also indirectly validated yield stress

measurements by its linear correlation. Although mix viscosity at $50s^{-1}$ and fat destabilization both showed strong effects on rheological destruction (thixotropy), mix viscosity at $50s^{-1}$ had the most influence. This more accurate instrumental characterization will help further understand important empirical measurements for ice cream quality, such as sensory, texture and meltdown properties.

The six-element model (generalized Kelvin-Voigt model) represented well creep behavior of melted ice cream. The thixotropic loop showed to be useful for assessing structure of ice cream and other frozen desserts since structural responses from low to high shear rates are covered in this test. Finally, as $\tan\delta_{Peak}$ showed a good correlation with Thix, it is possible that this phenomenon is related not only to ice melting and serum phase dilution from -10 to -2.7°C, but also to structural components and their arrangement formed during freezing of the ice cream.

2.6 Acknowledgements

The authors thank Lexi Florac for her help in data collection and tracing of ice crystals and air cells. D.O. Freire would like to thank his scholarship from CNPq (National Council for Scientific and Technological Development – Brazil) and financial support from FDC (Frozen Dessert Center).

2.7 References

Ahmed, J., 2015. Effect of Barley B-Glucan Concentrate On Oscillatory and Creep Behavior Of Composite Wheat Flour Dough. J. Food Eng. 152, 85–94. https://doi.org/https://doi.org/10.1016/j.jfoodeng.2014.11.018

Amador, J., Hartel, R., Rankin, S., 2017. The Effects of Fat Structures and Ice Cream Mix Viscosity on Physical and Sensory Properties of Ice Cream. J. Food Sci. 82, 1851–1860. https://doi.org/10.1111/1750-3841.13780

Barnes, H.A., 1997. Thixotropy—a Review. J. Nonnewton. Fluid Mech. 70, 1–33. https://doi.org/https://doi.org/10.1016/S0377-0257(97)00004-9

Bolliger, S., Goff, H.D., Tharp, B.W., 2000. Correlation between Colloidal Properties of Ice Cream Mix and Ice Cream. Int. Dairy J. 10, 303–309.

Briggs, J.L., Steffe, J.F., Ustunol, Z., 1996. Vane Method to Evaluate the Yield Stress of Frozen Ice Cream. J. Dairy Sci. 79, 527–531. https://doi.org/https://doi.org/10.3168/jds.S0022-0302(96)76395-6

Caldwell, K.B., Goff, H.D., Stanley, D.W., 1992. A Low-Temperature Scanning Electron Microscopy Study of Ice Cream. I Techniques and General Microstructure. Food Struct. Vol. 11, 1–9.

Chang, Y., Hartel, R.W., 2002. Measurement of Air Cell Distributions in Dairy Foams. Int. Dairy J. 12, 463–472. https://doi.org/https://doi.org/10.1016/S0958-6946(01)00171-6

Clarke, C., 2004. **The Science of Ice Cream**, First. ed. The Royal Society of Chemistry, Cambridge.

Cottrell, J.I.L., Pass, G., Phillips, G.O., 1980. The effect of stabilisers on the viscosity of an ice cream mix. J. Sci. Food Agric. 31, 1066–1070. https://doi.org/10.1002/jsfa.2740311015

Dogan, M., Kayacier, A., Toker, Ö.S., Yilmaz, M.T., Karaman, S., 2013. Steady, dynamic, creep, and recovery analysis of ice cream mixes added with different concentrations of xanthan gum. Food Bioprocess Technol. 6, 1420–1433.

Dolz, M., Hernández, M.J., Delegido, J., 2008. Creep and recovery experimental investigation of low oil content food emulsions. Food Hydrocoll. 22, 421–427. https://doi.org/https://doi.org/10.1016/j.foodhyd.2006.12.011

Dolz, M., Hernández, M.J., Delegido, J., Alfaro, M.C., Muñoz, J., 2007. Influence of xanthan gum and locust bean gum upon flow and thixotropic behaviour of food emulsions containing modified starch. J. Food Eng. 81, 179–186. https://doi.org/https://doi.org/10.1016/j.jfoodeng.2006.10.020

Donhowe, D.P., Hartel, R.W., Bradley, R.L., 1991. Determination of ice crystal size distributions in frozen desserts. J. Dairy Sci. 74, 3334–3344.

Eisner, M.D., Wildmoser, H., Windhab, E.J., 2005. Air cell microstructuring in a high viscous ice cream matrix. Colloids Surfaces A Physicochem. Eng. Asp. 263, 390–399.

Elliott, J.H., Ganz, A.J., 1977. Salad dressings—preliminary rheological characterization. J. Texture Stud. 8, 359–371.

Flores, A.A., Goff, H.D., 1999a. Ice Crystal Size Distributions in Dynamically Frozen Model Solutions and Ice Cream as Affected by Stabilizers. J. Dairy Sci. 82, 1399–1407. https://doi.org/https://doi.org/10.3168/jds.S0022-0302(99)75366-X

Flores, A.A., Goff, H.D., 1999b. Recrystallization in Ice Cream After Constant and Cycling Temperature Storage Conditions as Affected by Stabilizers. J. Dairy Sci. 82, 1408–1415. https://doi.org/https://doi.org/10.3168/jds.S0022-0302(99)75367-1

Goff, H.D., Freslon, B., Sahagian, M.E., Hauber, T.D., Stone, A.P., Stanley, D.W., 1995. Structural Development in Ice Cream—Dynamic Rheological Measurements. J. Texture Stud. 26, 517–536. https://doi.org/10.1111/j.1745-4603.1995.tb00801.x

Goff, H.D., Hartel, R.W., 2013. **Ice Cream**, Seventh. ed. Springer Science & Business Media, New York.

Goff, H.D., Liboff, M., Jordan, W.K., Kinsella, J.E., 1987. The Effects of Polysorbate 80 on the Fat Emulsion in Ice Cream Mix: Evidence from Transmission Electron Microscopy Studies. Food Struct. 6, 193–198.

Goff, H.D., Spagnuolo, P., 2001. Effect of stabilizers on fat destabilization measurements in ice cream. Milchwissenschaft-Milk Sci. Int. 56, 450–453.

Granger, C., Leger, A., Barey, P., Langendorff, V., Cansell, M., 2005. Influence of formulation on the structural networks in ice cream. Int. Dairy J. 15, 255–262. https://doi.org/https://doi.org/10.1016/j.idairyj.2004.07.009

Gunasekaran, S., Ak, M.M., 2003. **Cheese Rheology and Texture.** CRC Press LLC, Boca Raton.

Hagiwara, T., Hartel, R.W., 1996. Effect of sweetener, stabilizer, and storage temperature on ice recrystallization in ice cream. J. Dairy Sci. 79, 735–744.

Javidi, F., Razavi, S.M.A., Behrouzian, F., Alghooneh, A., 2016. The influence of basil seed gum, guar gum and their blend on the rheological, physical and sensory properties of low fat ice cream. Food Hydrocoll. 52, 625–633. https://doi.org/https://doi.org/10.1016/j.foodhyd.2015.08.006

Kaschta, J., Schwarzl, R.R., 1994. Calculation of discrete retardation spectra from creep data — I. Method. Rheol. Acta 33, 517–529. https://doi.org/10.1007/BF00366336

Li, J.-M., Nie, S.-P., 2016. The functional and nutritional aspects of hydrocolloids in foods. Food Hydrocoll. 53, 46–61. https://doi.org/https://doi.org/10.1016/j.foodhyd.2015.01.035

Lucey, J.A., Teo, C.T., Munro, P.A., Singh, H., 1997. Rheological properties at small (dynamic) and large (yield) deformations of acid gels made from heated milk. J. Dairy Res. 64, 591–600. https://doi.org/10.1017/S0022029997002380

Luyten, H., Kloek, W., Van Vliet, T., 1994. Yielding behaviour of mixtures of xanthan and enzyme-modified galactomannans. Food Hydrocoll. 8, 431–440.

Miller-Livney, T., Hartel, R.W., 1997. Ice recrystallization in ice cream: interactions between sweeteners and stabilizers. J. Dairy Sci. 80, 447–456.

Muse, M.R., Hartel, R.W., 2004. Ice Cream Structural Elements that Affect Melting Rate and Hardness. J. Dairy Sci. 87, 1–10. https://doi.org/https://doi.org/10.3168/jds.S0022-0302(04)73135-5

Pawar, A.B., Caggioni, M., Hartel, R.W., Spicer, P.T., 2012. Arrested coalescence of viscoelastic droplets with internal microstructure. Faraday Discuss. 158, 341–350. https://doi.org/10.1039/C2FD20029E

Purkayastha, S., Peleg, M., Normand, M.D., 1984. Presentation of the creep curves of solid biological materials by a simplified mathematical version of the generalized Kelvin-Voigt model. Rheol. Acta 23, 556–563. https://doi.org/10.1007/BF01329288

Rao, M.A.A., 2007. **Rheology of Fluid and Semisolid Foods: Principles and Applications**, Second. ed. Springer Science & Business Media, New York.

Regand, A., Goff, H.D., 2003. Structure and ice recrystallization in frozen stabilized ice cream model systems. Food Hydrocoll. 17, 95–102. https://doi.org/https://doi.org/10.1016/S0268-005X(02)00042-5

Saha, D., Bhattacharya, S., 2010. Hydrocolloids as thickening and gelling agents in food: a critical review. J. Food Sci. Technol. 47, 587–597. https://doi.org/10.1007/s13197-010-0162-6

Shama, F., Sherman, P., 1966. The Texture of Ice Cream 2. Rheological Properties of Frozen Ice Cream. J. Food Sci. 31, 699–706. https://doi.org/10.1111/j.1365-2621.1966.tb01926.x

Sherman, P., 1966. The Texture of Ice Cream 3. Rheological Properties of Mix and Melted Ice Cream. J. Food Sci. 31, 707–716. https://doi.org/10.1111/j.1365-2621.1966.tb01927.x

Sofjan, R.P., Hartel, R.W., 2004. Effects of overrun on structural and physical characteristics of ice cream. Int. Dairy J. 14, 255–262.

Soukoulis, C., Chandrinos, I., Tzia, C., 2008. Study of the functionality of selected hydrocolloids and their blends with κ-carrageenan on storage quality of vanilla ice cream. LWT - Food Sci. Technol. 41, 1816–1827. https://doi.org/https://doi.org/10.1016/j.lwt.2007.12.009

Stanley, D.W., Goff, H.D., Smith, A.K., 1996. Texture-structure relationships in foamed dairy emulsions. Food Res. Int. 29, 1–13. https://doi.org/https://doi.org/10.1016/0963-9969(95)00063-1

Steffe, J.F., 1996. **Rheological Methods in Food Process Engineering**. Freeman Press, East Lansing.

Thomas, W.R., 1997. Carrageenan, in: Imeson, A.P. (Ed.), Thickening and Gelling Agents for Food. Springer US, Boston, MA, pp. 45–59. https://doi.org/10.1007/978-1-4615-2197-6_3

Toker, O.S., Karaman, S., Yuksel, F., Dogan, M., Kayacier, A., Yilmaz, M.T., 2013. Temperature Dependency of Steady, Dynamic, and Creep-Recovery Rheological Properties of Ice Cream Mix. Food Bioprocess Technol. 6, 2974–2985. https://doi.org/10.1007/s11947-012-1005-4

Turquois, T., Rochas, C., Taravel, F.R., 1992. Rheological studies of synergistic kappa carrageenan-carob galactomannan gels. Carbohydr. Polym. 17, 263–268. https://doi.org/https://doi.org/10.1016/0144-8617(92)90168-P

Warren, M.M., Hartel, R.W., 2018. Effects of Emulsifier, Overrun and Dasher Speed on Ice Cream Microstructure and Melting Properties. J. Food Sci. 83, 639–647. https://doi.org/10.1111/1750-3841.13983

Warren, M.M., Hartel, R.W., 2014. Structural, Compositional, and Sensorial Properties of United States Commercial Ice Cream Products. J. Food Sci. 79, E2005–E2013. https://doi.org/10.1111/1750-3841.12592

Wildmoser, H., Scheiwiller, J., Windhab, E.J., 2004. Impact of disperse microstructure on rheology and quality aspects of ice cream. LWT-Food Sci. Technol. 37, 881–891.

Table 2.1 Means and standard errors for mix viscosity at 50 s^{-1}, overrun, extent of fat destabilization (FD), air cell and ice crystal size from ice creams with manipulated structures. One-way ANOVA and Tukey's HSD ($\alpha = 0.05$) tests were performed to determine significant difference within the data.

Stabilizer[1]	Air Flow	Polysorbate 80	Code	Viscosity (mPa.s)	Overrun (%)	FD (%)	Air Cell Size (μm)	Ice Crystal Size (μm)
0%	8L.h^{-1}	0%	S1A1P1	22.0±0.3^{X,A}	50.1±0.8^{X,a,A}	10.1±2.0^{X,a,A}	22.4±1.1^{XY,b,A}	28.5±1.7^{X,a,A}
		0.015%	S1A1P2	24.4±0.5^{X,A}	49.0±0.5^{X,a,A}	11.2±1.8^{X,a,A}	24.3±1.4^{Y,b,A}	33.9±0.2^{Y,a,A}
		0.03%	S1A1P3	21.7±0.8^{X,A}	50.7±0.3^{X,a,A}	48.1±10.9^{Y,a,A}	18.1±1.0^{X,b,A}	32.3±0.5^{XY,a,A}
	11L.h^{-1}	0%	S1A2P1	22.0±0.3^{X,A}	75.9±0.6^{X,b,A}	17.6±0.6^{X,b,A}	18.3±1.5^{X,ab,A}	31.6±0.5^{X,a,A}
		0.015%	S1A2P2	24.4±0.5^{X,A}	74.6±0.7^{X,b,A}	21.8±1.5^{X,b,A}	20.1±1.1^{X,ab,A}	35.8±0.1^{Y,b,B}
		0.03%	S1A2P3	21.7±0.8^{X,A}	75.0±0.4^{X,b,AB}	65.7±5.7^{Y,a,A}	16.1±0.5^{X,ab,A}	35.4±0.6^{Y,b,A}
	15L.h^{-1}	0%	S1A3P1	22.0±0.3^{X,A}	99.0±0.5^{X,c,A}	27.7±0.9^{X,c,A}	16.0±1.0^{X,a,A}	31.0±0.3^{XY,a,A}
		0.015%	S1A3P2	24.4±0.5^{X,A}	100.4±0.9^{X,c,A}	28.2±2.2^{X,b,A}	16.2±1.1^{X,a,A}	33.4±0.6^{Y,a,A}
		0.03%	S1A3P3	21.7±0.8^{X,A}	99.4±0.8^{X,c,A}	73.9±4.5^{Y,a,A}	11.8±1.7^{X,a,A}	29.8±1.0^{X,a,A}
0.2%	8L.h^{-1}	0%	S2A1P1	88.6±3.4^{X,B}	49.8±0.4^{X,a,A}	14.6±1.7^{X,a,A}	30.1±0.2^{Y,c,C}	31.9±0.5^{X,a,A}
		0.015%	S2A1P2	95.7±0.9^{X,B}	50.0±0.7^{X,a,A}	14.3±3.5^{X,a,A}	24.8±0.3^{X,b,A}	37.7±0.8^{Y,b,B}
		0.03%	S2A1P3	89.4±3.3^{X,B}	50.2±0.4^{X,a,A}	46.6±6.1^{Y,a,A}	24.4±0.3^{X,c,B}	33.1±0.5^{X,a,A}
	11L.h^{-1}	0%	S2A2P1	88.6±3.4^{X,B}	75.4±0.5^{X,b,A}	24.8±1.1^{X,b,B}	24.6±0.3^{Y,a,B}	32.6±1.1^{X,a,A}
		0.015%	S2A2P2	95.7±0.9^{X,B}	74.8±0.5^{X,b,A}	22.7±4.7^{X,a,A}	20.5±0.7^{X,a,A}	38.2±0.2^{Y,b,C}
		0.03%	S2A2P3	89.4±3.3^{X,B}	75.8±0.3^{X,b,B}	57.2±3.5^{Y,ab,A}	18.8±0.7^{X,b,B}	33.2±1.0^{X,a,A}
	15L.h^{-1}	0%	S2A3P1	88.6±3.4^{X,B}	100.2±0.5^{X,c,A}	35.7±3.0^{X,c,B}	26.9±0.4^{Z,b,C}	32.1±0.5^{X,a,A}
		0.015%	S2A3P2	95.7±0.9^{X,B}	98.8±0.5^{X,c,A}	42.9±3.5^{X,b,B}	18.3±1.0^{Y,a,A}	33.0±0.7^{X,a,A}
		0.03%	S2A3P3	89.4±3.3^{X,B}	99.4±0.6^{X,c,A}	69.5±3.0^{Y,b,A}	13.9±0.7^{X,a,A}	33.4±0.3^{X,a,AB}
0.4%	8L.h^{-1}	0%	S3A1P1	264.2±5.3^{X,C}	50.3±0.4^{X,a,A}	38.3±3.2^{X,a,B}	26.8±0.5^{X,c,B}	32.9±0.2^{X,b,A}
		0.015%	S3A1P2	290.4±2.1^{Y,C}	50.3±0.3^{X,a,A}	51.6±2.2^{Y,a,B}	25.3±0.7^{X,b,A}	31.9±0.3^{X,b,A}
		0.03%	S3A1P3	288.2±1.4^{Y,C}	51.2±0.8^{X,a,A}	46.1±2.4^{XY,a,A}	25.3±0.7^{X,a,B}	37.1±0.9^{Y,a,B}
	11L.h^{-1}	0%	S3A2P1	264.2±5.3^{X,C}	75.4±0.5^{X,b,A}	53.3±1.7^{X,b,C}	23.2±0.4^{X,b,B}	30.7±0.4^{X,a,A}
		0.015%	S3A2P2	290.4±2.1^{Y,C}	75.0±0.5^{X,b,A}	58.8±1.6^{X,a,B}	22.8±0.4^{X,a,A}	29.5±0.4^{X,a,A}
		0.03%	S3A2P3	288.2±1.4^{Y,C}	74.3±0.4^{X,b,A}	56.1±1.7^{X,b,A}	23.0±0.5^{X,a,C}	35.3±0.7^{Y,a,A}
	15L.h^{-1}	0%	S3A3P1	264.2±5.3^{X,C}	100.4±1.3^{X,c,A}	65.9±1.7^{XY,c,C}	21.1±0.4^{X,a,B}	32.0±0.3^{X,b,A}
		0.015%	S3A3P2	290.4±2.1^{Y,C}	99.2±0.1^{X,c,A}	57.9±3.7^{X,a,C}	24.4±0.3^{Y,ab,B}	37.0±0.2^{Y,c,B}
		0.03%	S3A3P3	288.2±1.4^{Y,C}	99.3±0.6^{X,c,A}	71.6±1.6^{Y,c,A}	22.4±1.0^{XY,a,B}	36.6±1.3^{Y,a,B}

Legend: [1]Stabilizer is a commercial blend that includes locust bean gum, guar gum and carrageenan. $^{X, Y, Z}$ denote significant differences among ice cream with different levels of polysorbate 80. $^{a, b, c}$ denote significant differences among ice cream with different levels of air flow. $^{A, B, C}$ denote significant differences among ice cream with different levels of stabilizer.

Table 2.2 Parameter estimates, coefficients of determination (R^2 and R^2_{Adj}) and F ratios of multiple linear regression (MLR) models (n=27) for rheological parameters from the oscillatory thermo-rheometry (OTR), creep/recovery, stress growth and flow ramp measurements.

Rheological Test	Y	Coefficients				R^2	R^2_{Adj}	F Ratio
		Intercept	Visc	FD	OR			
OTR	$G'_{-15°C}$	3580000^{***}	-10260000^{***}	0	10000	0.63	0.58	13.1203
	$\tan\delta_{-15°C}$	0.84^{***}	-0.14^{**}	0	0	0.53	0.46	8.5146
	$G'_{0°C}$	-640	410	30^{***}	0	0.60	0.55	11.6154
Creep	$\eta_{0\ 0°C}$	-43700	154000^{**}	900^{**}	400	0.74	0.70	21.2755
Stress Growth	$\sigma_{Y\ 0°C}$	-15.5^{*}	0.1^{***}	0.4^{***}	0.1	0.82	0.80	35.5645
Flow Ramp	$Thix_{0°C}$	0	2480^{***}	10^{***}	0	0.89	0.87	59.8792

Legend: Visc is mix viscosity, FD is fat destabilization and OR is overrun.
$^{*}p<0.05$, $^{**}p<0.01$; $^{***}p<0.001$.

Table 2.3 Means and standard errors for $tan\delta_{Peak}$ from ice creams with manipulated structures. One-way ANOVA and Tukey's HSD ($\alpha = 0.05$) tests were performed to determine significant difference within the data.

Stabilizer[1]	Air System	Polysorbate 80	Code	G'$_{-15°C}$ (MPa)	G'$_{0°C}$ (kPa)	$\eta_{0\ 0°C}$ (kPa.s)	$\sigma_{Y\ 0°C}$ (Pa)	Thix$_{0°C}$ (Pa.s^{-1})
0%	8L.h^{-1}	0%	S1A1P1	$5.4\pm0.7^{X,b,B}$	$0.16\pm0.01^{X,a,A}$	$1.2\pm0.1^{X,a,A}$	$2.3\pm0.2^{X,a,A}$	$303\pm4^{X,a,A}$
		0.015%	S1A1P2	$5.1\pm0.5^{X,a,C}$	$0.17\pm0.01^{X,a,A}$	$2.1\pm0.2^{X,a,A}$	$2.2\pm0.1^{X,a,A}$	$317\pm4^{X,a,A}$
		0.03%	S1A1P3	$4.6\pm0.6^{X,a,B}$	$0.25\pm0.02^{Y,a,A}$	$5.6\pm0.3^{Y,a,A}$	$3.2\pm0.2^{Y,a,A}$	$347\pm7^{Y,a,A}$
	11L.h^{-1}	0%	S1A2P1	$6.1\pm0.7^{Y,b,B}$	$0.16\pm0.01^{X,ab,A}$	$2.0\pm0.2^{X,a,A}$	$2.4\pm0.2^{X,a,A}$	$334\pm4^{X,b,A}$
		0.015%	S1A2P2	$6.1\pm0.7^{Y,a,B}$	$0.18\pm0.01^{X,a,A}$	$3.0\pm0.2^{X,a,A}$	$3.1\pm0.2^{X,b,A}$	$341\pm5^{X,b,A}$
		0.03%	S1A2P3	$3.7\pm0.3^{X,a,B}$	$0.44\pm0.08^{Y,ab,A}$	$10.0\pm1.3^{Y,a,A}$	$6.7\pm1.2^{Y,a,A}$	$411\pm14^{Y,a,A}$
	15L.h^{-1}	0%	S1A3P1	$2.9\pm0.4^{X,a,A}$	$0.20\pm0.02^{X,b,A}$	$5.9\pm0.5^{X,b,A}$	$3.3\pm0.3^{X,b,A}$	$376\pm11^{X,c,A}$
		0.015%	S1A3P2	$4.8\pm0.8^{X,a,B}$	$0.27\pm0.04^{X,b,A}$	$7.4\pm0.7^{X,b,A}$	$4.1\pm0.3^{X,c,A}$	$388\pm7^{X,c,A}$
		0.03%	S1A3P3	$5.1\pm0.5^{X,a,B}$	$1.81\pm0.67^{Y,b,A}$	$45.5\pm13.9^{Y,b,A}$	$26.9\pm8.1^{Y,b,A}$	$680\pm117^{Y,a,A}$
0.2%	8L.h^{-1}	0%	S2A1P1	$1.9\pm0.2^{X,a,A}$	$0.28\pm0.02^{X,a,A}$	$11.0\pm0.9^{X,a,B}$	$4.9\pm0.4^{X,a,A}$	$434\pm13^{X,a,A}$
		0.015%	S2A1P2	$2.6\pm0.3^{XY,a,B}$	$0.26\pm0.03^{X,a,A}$	$10.7\pm1.2^{X,a,A}$	$4.6\pm0.4^{X,a,A}$	$454\pm36^{X,a,B}$
		0.03%	S2A1P3	$3.2\pm0.3^{Y,a,B}$	$1.66\pm0.32^{Y,a,B}$	$50.5\pm3.0^{Y,a,B}$	$20.4\pm2.8^{Y,a,B}$	$795\pm26^{Y,a,B}$
	11L.h^{-1}	0%	S2A2P1	$3.1\pm0.4^{X,a,A}$	$0.58\pm0.04^{X,b,B}$	$21.2\pm1.7^{X,b,B}$	$8.5\pm1.2^{X,ab,A}$	$527\pm24^{X,ab,B}$
		0.015%	S2A2P2	$3.4\pm0.3^{X,a,A}$	$0.40\pm0.06^{X,a,A}$	$18.6\pm1.5^{X,b,B}$	$8.7\pm0.3^{X,b,A}$	$534\pm31^{X,a,B}$
		0.03%	S2A2P3	$3.3\pm0.3^{X,a,B}$	$2.84\pm0.19^{Y,b,C}$	$94.4\pm6.3^{Y,b,B}$	$34.0\pm1.8^{Y,a,B}$	$1059\pm44^{Y,a,B}$
	15L.h^{-1}	0%	S2A3P1	$3.2\pm0.4^{X,a,A}$	$0.87\pm0.03^{X,c,B}$	$41.6\pm4.2^{X,c,B}$	$13.3\pm2.0^{X,b,A}$	$620\pm40^{X,b,B}$
		0.015%	S2A3P2	$3.9\pm0.5^{XY,a,AB}$	$0.72\pm0.10^{X,b,A}$	$30.5\pm2.4^{X,c,A}$	$11.4\pm0.9^{X,c,A}$	$680\pm30^{X,b,B}$
		0.03%	S2A3P3	$5.0\pm0.5^{Y,b,B}$	$3.46\pm0.29^{Y,b,B}$	$133.2\pm15.3^{Y,c,B}$	$53.8\pm6.4^{Y,b,B}$	$1325\pm114^{Y,b,B}$
0.4%	8L.h^{-1}	0%	S3A1P1	$1.1\pm0.1^{X,a,A}$	$0.61\pm0.06^{X,a,B}$	$34.6\pm3.7^{X,a,C}$	$19.5\pm2.6^{X,a,B}$	$909\pm85^{X,a,B}$
		0.015%	S3A1P2	$1.2\pm0.2^{X,a,A}$	$0.99\pm0.15^{X,a,B}$	$53.8\pm4.8^{X,a,B}$	$35.6\pm2.5^{Y,a,B}$	$1261\pm50^{Y,a,C}$
		0.03%	S3A1P3	$1.2\pm0.2^{X,a,A}$	$0.81\pm0.09^{X,a,A}$	$60.1\pm14.3^{X,a,B}$	$28.7\pm2.0^{Y,a,C}$	$1024\pm121^{XY,a,B}$
	11L.h^{-1}	0%	S3A2P1	$2.2\pm0.2^{X,b,A}$	$1.26\pm0.08^{X,b,C}$	$66.6\pm3.2^{X,b,C}$	$31.0\pm3.9^{X,ab,B}$	$1065\pm46^{X,ab,C}$
		0.015%	S3A2P2	$2.6\pm0.4^{X,b,A}$	$1.69\pm0.10^{Y,b,B}$	$75.0\pm3.6^{X,a,C}$	$39.3\pm4.1^{X,a,B}$	$1415\pm59^{Y,a,C}$
		0.03%	S3A2P3	$2.0\pm0.1^{X,b,A}$	$1.42\pm0.15^{XY,b,B}$	$78.1\pm5.9^{X,ab,B}$	$32.1\pm1.8^{X,a,B}$	$1365\pm111^{Y,a,C}$
	15L.h^{-1}	0%	S3A3P1	$3.1\pm0.2^{X,c,A}$	$1.69\pm0.08^{X,c,C}$	$84.3\pm6.0^{X,c,C}$	$40.6\pm4.9^{X,b,B}$	$1250\pm65^{X,b,C}$
		0.015%	S3A3P2	$2.5\pm0.2^{X,b,A}$	$1.88\pm0.21^{X,b,B}$	$113.2\pm13.9^{X,b,B}$	$43.0\pm3.7^{X,a,B}$	$1418\pm61^{X,a,C}$
		0.03%	S3A3P3	$2.6\pm0.3^{X,b,A}$	$1.96\pm0.14^{X,c,AB}$	$113.5\pm9.2^{X,b,B}$	$53.8\pm5.4^{X,b,B}$	$1340\pm94^{X,a,B}$

Legend: [1]Stabilizer is a commercial blend that includes locust bean gum, guar gum and carrageenan. $^{X, Y, Z}$ denote significant differences among ice cream with different levels of polysorbate 80. $^{a, b, c}$ denote significant differences among ice cream with different levels of air flow. $^{A, B, C}$ denote significant differences among ice cream with different levels of stabilizer.

Chapter 3

3 Correlations between Rheological Properties and Meltdown Behavior of Ice Cream

3.1 Abstract

Meltdown behavior is among the most important characteristics for quality control in ice cream. However, although the meltdown test provides important information on melting behavior, this test also has its limitations, such as sample size, heat transfer rate, sample volume and weight, among others. Both rheological and melting properties are affected by structural components and their intrinsic arrangement in the ice cream matrix. The characterization of the mechanical behavior of these structural components and their interactions by instrumental tests, such as rheometry, can help in understanding the melting behavior in ice cream. Thus, this study aimed to evaluate the correlation between rheological properties and parameters from meltdown test in ice cream. Meltdown and rheological parameters, such as drip-through rate (DT) and final height (FH) as well as storage modulus ($G'_{0°C}$), residual viscosity ($\eta_{0\ 0°C}$), yield stress ($\sigma_{Y\ 0°C}$) and thixotropy ($Thix_{\ 0°C}$), were obtained from previous work. DT or FH were predicted by $G'_{0°C}$, $\eta_{0\ 0°C}$, $\sigma_{Y\ 0°C}$ and $Thix_{\ 0°C}$. An exponential decay or growth was observed in DT or FH, respectively, when $G'_{0°C}$, $\eta_{0\ 0°C}$, $\sigma_{Y\ 0°C}$ or $Thix_{\ 0°C}$ was increased. Exponential decay or growth in DT or FH, respectively, was observed in samples with no stabilizer added (low mix viscosity) and as fat destabilization and/or overrun increased. Then, a plateau was observed in DT as $G'_{0°C}$, $\eta_{0\ 0°C}$, $\sigma_{Y\ 0°C}$ or $Thix_{\ 0°C}$ increased, mainly in samples with 0.2 and 0.4% stabilizer added; a shorter plateau was observed in FH as $G'_{0°C}$, $\eta_{0\ 0°C}$, $\sigma_{Y\ 0°C}$ or $Thix_{\ 0°C}$ increased, mainly in samples with 0.4% stabilizer added. $G'_{0°C}$ reasonably explained DT and FH, while $\eta_{0\ 0°C}$, $\sigma_{Y\ 0°C}$ or $Thix_{\ 0°C}$ satisfactorily explained the variability (>80%) in both DT and FH. Therefore, $\eta_{0\ 0°C}$, $\sigma_{Y\ 0°C}$ or $Thix_{\ 0°C}$ measurements could be reliably used to correlate to DT and FH, which could reduce time and increase the accuracy to obtain information from the physical properties of ice cream.

3.2 Introduction

The physical properties of ice cream, such as meltdown and rheology, are strongly influenced by the ice phase presence. However, other structural components from air, fat and serum phases also affect meltdown and rheology of ice cream. In previous work, the effects of extent of fat destabilization, mix viscosity and overrun on the entire meltdown (Wu et al., 2019) and rheological properties (Chapter 2) of full fat ice creams were studied. Nevertheless, the correlation between rheological and meltdown properties from those ice creams was not yet explored.

In fact, although it is known that rheological properties affect ice cream meltdown (Goff and Hartel, 2013), there is a lack of information about their correlations in literature. It is known that mix viscosity and other structural components affect melting rate of ice cream (El-Nagar et al., 2002; Huppertz et al., 2011; Muse and Hartel, 2004). Furthermore, although several studies have investigated ice cream rheology in recent decades (Goff et al., 1995; Granger et al., 2005; Wildmoser et al., 2004), the relationship between rheology and meltdown has been little explored. Mechanical behavior strongly affects ice cream performance during meltdown. Correlations between rheological and meltdown properties can provide information not only about which rheological parameters are important in ice cream meltdown, but also which magnitude ranges are required to change this meltdown behavior. Thus, these rheological parameters may be important as reference for other research on structure development in ice cream.

Wu et al. (2019) found important information on melting behavior studying the entire meltdown and height collapse curves of ice creams. They found mix viscosity and fat destabilization had significant effects on both drip-through rate (DT) and final height (FH), while overrun affected the meltdown behavior in ice creams with no stabilizer added. That is, meltdown

of samples with low mix viscosity was influenced by overrun, but not when serum viscosity was high.

From our previous work (Chapter 2), at 0°C, extent of fat destabilization had most effects on storage modulus ($G'_{0°C}$, which was obtained from oscillatory thermo-rheometry from -15 to 25°C) and yield stress ($\sigma_{Y\ 0°C}$, which was obtained from stress growth measurements). The effects on $G'_{0°C}$ were followed by overrun with lower effects from mix viscosity, while the effects on $\sigma_{Y\ 0°C}$ were followed by mix viscosity with lower overrun effects. On the other hand, from creep tests, the residual viscosity ($\eta_{0\ 0°C}$), which was obtained from the Maxwell unit in series with two Kelvin-Voigt units (six-element model), and rheological destruction ($Thix_{0°C}$), which was obtained from thixotropic loops, was mainly affected by mix viscosity, followed by fat destabilization extent, and with lower overrun effects. Therefore, this study aimed to compile the findings reported by Wu et al. (2019) and our previous work (Chapter 2) to evaluate the correlations between meltdown behavior and rheological properties of full fat ice creams.

3.3 Materials and Methods

3.3.1 Materials

Ice cream mixes were made using cream, nonfat dry milk, sucrose, stabilizers and emulsifiers. Cream, sucrose (United Sugars, Edina, MN, USA) and nonfat dry milk (Dairy America, Fresno, CA, USA) were obtained from the Babcock Hall Dairy Plant (Madison, WI). A stabilizer blend (Germantown™ Premium I.C., New Century, KS, USA), which included locust bean gum (LBG), guar gum, and carrageenan, and mono-and diglycerides (Grinsted® HV 52 K-A, New Century, KS, USA) (MDG), was purchased from Danisco USA. Polysorbate 80 (PS80) was purchased from Avatar® (Avapol™ 80K Sorbitan Ester, University Park, IL, USA).

3.3.2 Experimental Design

This study aimed to evaluate the correlations between melting behavior and rheological properties of ice cream, which has not yet been studied. A 3x3x3 full factorial design with different levels of stabilizer (0, 0.2 and 0.4%), PS80 (0, 0.015 and 0.030%) and air flow (2, 3 and 4gal.h^{-1}) was used to control mix viscosity, extent of fat destabilization and overrun. The experimental design combined to the structural components, meltdown and rheological properties are presented in Tables 3.1, 3.2 and 3.3, respectively. The experiments were performed in duplicate. Mixes and ice creams were randomly made and frozen, respectively.

3.3.3 Formulation and Processing

Mix formulation included 12% fat, 11.3% milk solids nonfat, 16.9% sucrose, 0.15% MDG, 0 to 0.4% stabilizer and 0 to 0.03% PS80. Total solids were around 40.5% and freezing point was -2.7±0.1°C.

Ingredients were blended and heated to 85°C using a batch-jacketed mixer (Stephan Food Processing Machinery, Hamelin, Germany). After that, a two-stage homogenizer (Manton-Gaulin MFG, Co. Inc., Everett, MA, USA) at 17.2 MPa (3.4 and 13.8MPa in the second and first stages, respectively) was used to homogenize the mixture. Then, the homogenized mixture was cooled to 10°C in the mixer and aged for approximately 24 hours at 4°C.

Mixes were frozen in a Hoyer Frigus KF 80 F continuous freezer (Tetra Pak Hoyer Inc., Aarhus, Denmark), which was operated in manual mode at 500RPM dasher speed. Air flow was changed according to the target for overrun (8, 11 or 15L.h^{-1} aimed to reach 50, 75 and 100%, respectively) using constant pump ratio (0.99±0.00), as described in the previous work (Chapter 2). Flow of ice cream (pump system) in the freezer (22.0±0.4L.h^{-1}) was used for the fine adjusts of

overrun. When the ice cream reached the equilibrium temperature (-6.05±0.01°C) upon exit of the freezer barrel and equilibrium overrun (50.2±0.2%, 75.1± 0.2% and 99.6±0.2%), the ice cream was collected in containers (473mL), which were placed in a hardening cabinet (-29°C) for one hour and transferred to a walk-in freezer at -29°C.

3.3.4 Physical, Compositional and Structural Measurements (Structural Components)

Ice cream mixes were analyzed for fat globule size distribution, both by light scattering and optical light microscopy. The aged ice cream mixes were also analyzed for viscosity. For ice cream, draw temperatures and overrun were measured during the dynamic freezing. After hardening, particle/fat globule size distribution, optical light microscopy, air cell size distribution, ice cell size distribution and rheological measurements were performed on the ice creams. The analyses were performed in triplicate.

3.3.4.1 Ice Cream Mix Viscosity

A rotational rheometer (DHR-2, TA Instruments, New Castle, DE, USA) with cup and bob geometry preset at 0°C was used to measure the viscosity of the ice cream mixes. Mix temperature was equilibrated for 5 minutes. After that, 10 data points per decade were obtained using a flow sweep performed from 100 to $1s^{-1}$ shear rate with steady state sensing (5% tolerance within 30 seconds in 3 consecutive data points and 180s for maximum equilibration time). The apparent viscosity at 50s-1 shear rate was used as an approximation for the serum phase viscosity of the melted ice cream at 0°C.

3.3.4.2 Overrun

The weight of the same volume of mix and ice cream (177.4mL) was obtained. The percentage of the weight difference between the mix and ice cream to the ice cream weight was used to obtain the overrun (Goff and Hartel, 2013). After reaching equilibrium for draw temperature and ice cream weight, overrun values were obtained before collecting samples from the beginning, middle and end of the production.

3.3.4.3 Particle/Fat Globule Size Distribution

Particle size distributions were obtained using laser light scattering (Malvern Mastersizer 2000, Malvern Instruments Ltd., Worcestershire, UK) for mix and melted ice cream (Goff and Hartel, 2013). Obscuration from 13 to 15% was reached by using around three drops of sample (4°C); 1.33 was used as refractive index for dispersant (deionized water), 1.47 was used as refractive index for dispersed phase (milk fat), and 0.01 was used for absorbance.

Ice cream was placed at ambient temperature (22±1°C) to melt and then stored at 4°C until analysis. The peak of the destabilized fat from melted ice cream sample was compared to the peak of the initial emulsion from that respective mix sample to obtain the extent of fat destabilization (Bolliger et al., 2000; Warren and Hartel, 2018).

3.3.4.4 Air Cell Size Distribution

In the insulated glove box Donhowe et al. (1991) set at -6°C air cell size distribution was analyzed, as detailly described by (Chang and Hartel, 2002). Images at 40x magnification were taken using OPTIMAS software (OPTIMAS v6.1, Optimas Corp., Meyer Instruments Inc., Houston, Tex. U.S.A.) and a solid state camera (Cohu Eletronics Div., San Diego, CA, USA)

attached to an optical light microscope (Optiphot, Nikon, Inc., Garden City, NY, USA) with 30W LED light system. Images were analyzed using Image Pro Plus software (Image Pro Plus 7.0, Media Cybernetics, Inc., Rockville, MD, USA), from which results were collected in a Microsoft Excel spreadsheet. It was analyzed at least 300 air cells.

3.3.4.5 Ice Cell Size Distribution

In the same insulated glove box, ice crystal images were taken at -15°C, as described by Donhowe et al. (1991). Images at 40x magnification were taken using OPTIMAS software (OPTIMAS v6.1, Optimas Corp., Meyer Instruments Inc., Houston, Tex. U.S.A.) and a solid state camera (Cohu Eletronics Div., San Diego, CA, USA) attached to an optical light microscope (Optiphot, Nikon, Inc., Garden City, NY, USA) with 30W LED light system. After that, ice crystals (at least 300) from the images were traced using Microsoft Softonic Paintbrush for Mac. The images were processed using Image Pro Plus software (Image Pro Plus 7.0, Media Cybernetics, Inc., Rockville, MD, USA), and the results were collected in a Microsoft Excel spreadsheet.

3.3.5 Rheological properties

Rheological measurements were performed using parallel plates of 25mm diameter with crosshatched surface attached to a rotational rheometer (DHR-2, TA Instruments, New Castle, DE, USA). A liquid recirculating chiller (ThermoCube, Solid State Cooling Systems, Wappingers Falls, NY, USA) with a 20% ethanol solution attached to the Stepped Peltier Plate system was used to control the temperature in the lower plate. A liquid recirculating chiller (Isotemp 4100 R35, Fisher Scientific, Waltham, MA, USA) with a 50% ethylene glycol solution attached to the

Upper Heated Plate system was used to control the temperature in the upper plate. As detailed described in the previous work (Chapter 2), disks of ice cream with 25 and 2.5mm of diameter and height, respectively, were prepared using a cylindrical tool within insulated glove box at -20°C. The ice cream disk was taken to the rheometer with parallel plates preset at -15 or -5°C. Then, the upper plate was loaded into the disk without trimming. Preliminary tests using ice creams with the lowest (S1A1P1, refer to code in the Table 3.1) and the highest (S3A3P3, refer to code in the Table 3.1) levels of stabilizer, air flow and PS80 were performed to test the parameters used in each rheological protocol subsequently described.

3.3.5.1 Oscillatory Thermo-Rheometry (OTR)

As described in the previous work (Chapter 2), oscillatory thermo-rheometry (OTR), which used controlled axial force, was adapted from Wildmoser et al. (2004) and (Granger et al., 2005). The OTR performed from -15 to 25°C was performed within the Linear Viscoelastic Regime (LVR) for all samples, as confirmed in preliminary tests using the samples S1A1P1 and S3A3P3. From -15 to 0°C and from 0 to 25°C strain values of 0.01 and 0.1%, respectively, were used. Ice cream disk was loaded at -15°C with initial gap of 1800µm. A sample cover, which was developed to minimize water evaporation (as previously described in Chapter 2), followed by an insulating thermal cover for the parallel plates was placed over the sample. When the axial force was lower than 10N, the test began with a gap of 1800µm for 2 minutes. At 0N (±0.1 N) axial force, the sample was equilibrated for other 15 minutes. As described in the previous work (Chapter 2), a continuous oscillation using 10 $rad.s^{-1}$ at 0.5°C.min^{-1} was applied to the sample. Storage modulus ($G'_{0°C}$) was collected at 0°C.

3.3.5.2 Creep-Recovery

Creep measurements were adapted from Steffe (1996) and Dogan et al. (2013). The sample was loaded at -5°C and 1800µm gap, which was followed by an insulating thermal cover. Temperature was set to 0°C, and samples were equlibrated for 10min. After that, a constant stress of 1.2Pa ($\sigma_{constant}$), which was chosen within the LVR, was applied to the sample for 150s. The stress was relieved, and the structure recovered for another 150s. As observed in preliminary tests using samples S1A1P1 and S3A3P3, the equilibrium was reached with those measurements. Data points collected decreased logarithmically over time (fast sampling). Creep compliance data were fitted to a six-element model (generalized Kelvin-Voigt model) using the TRIOS software (2019 TA Instruments–Waters LLC, New Castle, USA).

3.3.5.3 Stress Growth

Stress growth measurements, which were adapted from Elliott and Ganz (1977) and (Rao, 2007), were performed at 0°C. Sample was loaded at -5°C and 1800µm gap. An insulating cover was placed over the sample and equilibrated for 10min at 0°C. A constant $0.01s^{-1}$ shear rate was applied to the sample. The stress was recorded over 1800 seconds or until the sample reached steady state flow (5% tolerance within 30 seconds in three consecutive sampling). The stress peak was taken as the yield stress (σ_y).

3.3.5.4 Flow Ramp

The sample was loaded at -5°C, temperature was set to 0°C and shear rate ramp was performed from 0.001 to 100 s^{-1}. The instantaneous shear stress and viscosity were obtained with 10 points per decade for 10 minutes. The up shear rate ramp was followed by down shear rate ramp

from 100 to 0.001 s^{-1} for another 10 minutes. The area between the curves was obtained as an empirical measurement of rheological destruction, as thixotropy, in the melted ice cream.

3.3.6 Statistical Analysis

Data were analyzed using JMP statistical software (JMP Pro 14.0, SAS Inst., Cary, N.C., U.S.A. 2018). The data analysis was performed using nonlinear regressions for rheological and meltdown properties from the 27 ice cream samples. Drip-through rate (DT) or final height (FH) were predicted by $G'_{0°C}$, $\sigma_{Y\ 0°C}$, $\eta_{0\ 0°C}$ or $Thix_{0°C}$. The final nonlinear model was chosen based on the lowest Schwarz's Bayesian information criterion (BIC) as well as R^2.

3.4 Results and Discussion

Structural components, rheological and meltdown properties of ice cream were compiled and discussed from Wu et al. (2019) and previous work (Chapter 2). Structural components and their correlations as well as rheological and meltdown properties will be briefly discussed. Then, correlations between rheology and meltdown of ice cream using nonlinear equations are presented and discussed.

3.4.1 Structural Components and their Correlations

As correlations, mainly between extent of fat destabilization with mix viscosity and overrun, among the structural components were expected, the structural formation was controlled within a certain range. The wide structural range of ice cream samples due to the different levels of stabilizers, airflow and PS80 were compiled from Wu et al. (2019) and previous work (Chapter 2) in Table 3.1.

As stabilizer levels increased, mix viscosity (at $50s^{-1}$) also increased (Table 3.1), which is well established in the literature for ice cream and other food products (Cottrell et al., 1980; Goff and Hartel, 2013; Li and Nie, 2016; Saha and Bhattacharya, 2010). As mentioned previously (Chapter 2), ice cream mixes showed non-Newtonian flow behavior, with an increase in pseudoplastic behavior (shear-thinning) as levels of stabilizer increased. Moreover, samples with 0.4% stabilizer added were reported to form a weak gel (Chapter 2). Also, PS80 had no significant effect on mix viscosity.

As air flow in the continuous freezer increased, overrun increased (Table 3.1). The air flow levels (8, 11 and $15L.h^{-1}$) using manual mode, which was used to avoid automation interferences from the freezer, provided good control for the target overrun (50, 75 and 100%, respectively).

Overall, as stabilizer, air flow and PS80 increased, extent of fat destabilization also increased (Table 3.1). Increased levels of PS80 generally enhanced fat destabilization during dynamic freezing, except for the samples with 0.4% stabilizer. As the mix viscosity (at $50s^{-1}$) increased, extent of fat destabilization increased (Table 3.1), which agreed with other authors (Amador et al., 2017; Goff and Spagnuolo, 2001; Muse and Hartel, 2004). Shear forces in the barrel increase due to the increased viscosity and lead to an increase of fat globule collisions during freezing. As overrun increased, fat destabilization extent also increased (Table 3.1), which was more prominent in samples with 0.4% stabilizer added ($r=0.86$, $p=0.0027$). This correlation (overrun and fat destabilization) corroborated with other studies (Warren and Hartel, 2018). Higher overrun increases fat globule collisions during freezing due to the thinner lamella.

Air cell size generally decreased as overrun increased (Table 3.1), which corroborated with previous studies (Sofjan and Hartel, 2004; Warren and Hartel, 2018). This was probably due to increased shear stress during freezing that leads to further breakdown of air cells. As stabilizer was

added, slight differences among air cell size was found. Amador et al. (2017) found smaller air cells using -3°C as draw temperature, but not at -6°C as draw temperature, which corroborated to this study. More research is required to understand the correlations between air cell size and processing as well as air cell size and stabilizer levels.

Although slight differences were found in the ice crystal size, no trend was found among the ice cream samples. Thus, any small differences in ice crystal size will not be considered further.

3.4.2 Ice Cream Meltdown

Drip-through rate (DT) and final height (FH), which were obtained from Wu et al. (2019), represent the change of ice cream matrix during meltdown test (Table 3.2). As ice cream melts at ambient temperature (~22°C) under the force of gravity, DT represents the flow of the matrix, while FH represents the remnant foam on the top of screen at the end of the meltdown test. In summary, DT or FH were most influenced by mix viscosity (at 50 s^{-1}) and fat destabilization, which both presented inverse correlations with DT and direct correlations with FH. Overall, overrun influenced DT or FH only in samples with no stabilizer added. An inverse correlation was found between overrun and DT, whereas a direct relationship was found between overrun and FH.

3.4.3 Ice Cream Rheology

Storage modulus ($G'_{0°C}$), residual viscosity ($\eta_{0\ 0°C}$), yield stress ($\sigma_{Y\ 0°C}$) and thixotropy ($Thix_{\ 0°C}$), shown in Table 3.3 from previous work (Chapter 2), were evaluated at 0°C since it was intended to highlight the controlled structural components (mix viscosity, overrun and extent of fat destabilization) across the different formulations at a temperature where the melted ice cream matrix had yet to experience major damage. From Chapter 2, $G'_{0°C}$ represents elastic behavior,

$\eta_{0\ 0°C}$ represents viscous behavior at low shear rate, $\sigma_{Y\ 0°C}$ represents the transient flow behavior and Thix $_{0°C}$ represents rheological destruction, which allude to strength of the initial structural formation. Overall, direct correlations were found between mix viscosity, fat destabilization or overrun with G'$_{0°C}$, $\eta_{0\ 0°C}$, $\sigma_{Y\ 0°C}$ or Thix $_{0°C}$. Fat destabilization had the most influence among structural components on G'$_{0°C}$, followed by overrun and mix viscosity. Mix viscosity showed the most influence on $\eta_{0\ 0°C}$, followed by fat destabilization, and with lower effects of overrun. Among the structural components, fat destabilization showed the most influence on $\sigma_{Y\ 0°C}$, followed by mix viscosity and overrun. The mix viscosity showed the most influence on Thix $_{0°C}$, followed by overrun and FD effects. Here, rheological parameters will be correlated to the mechanical performance of ice cream during the drip test (DT) or remnant foam height at the end of the meltdown test (FH).

3.4.4 Correlations between Rheology and Meltdown Behavior

Nonlinear models (presented in Tables 3.4 and 3.5) were used to evaluate correlations between rheological parameters obtained at 0°C and meltdown parameters. Here, extent of fat destabilization, mix viscosity (at $50s^{-1}$) and overrun are the main structural components discussed (Wu et al., 2019; Chapter 2). The rheological measurements were evaluated at 0°C since it was intended to highlight the controlled structural components (mix viscosity, overrun and extent of fat destabilization) across the different formulations at a temperature where the melted ice cream matrix had yet to experience major damage. Here, it is assumed that the slab of ice cream on the top of the screen during the meltdown test was represented by the melted ice cream disk between the parallel plates at 0°C in the rheometer. Even though this is not strictly true, no other way to compare the rheology of the remnant foam was possible. Moreover, relationships between

composition (which directly affected the structural components) with meltdown and rheological parameters are detailed in Tables 3.2 and 3.3, respectively.

3.4.4.1 Storage Modulus ($G'_{0°C}$) from Oscillatory Thermo-Rheometry (OTR)

Storage modulus ($G'_{0°C}$) is the measurement of deformation energy stored and recovered per cycle of deformation in the matrix (Ferry, 1980; Gunasekaran and Ak, 2003, 2000). The ability to retain the initial shape of the ice cream slab during dripping or remnant foam at the end of meltdown test is due to the elastic properties of the matrix. This property is directly related to $G'_{0°C}$.

The relationships of all rheological parameters against DT (Tables 3.2 and 3.3) generally shows an exponential decay, which can be represented by a generic exponential model with three parameters:

$$DT = a + b \cdot \exp\left(c \cdot Rheological\ Parameter\right) \quad (3.1)$$

Here, a is asymptote, b is scale and c is growth rate.

As seen in Figure 3.1, at low $G'_{0°C}$, samples showed high DT. That is, samples with weak structure dripped rapidly through the screen. As $G'_{0°C}$ increased, DT first showed an exponential decay and then reached a lower asymptote, where DT was independent of $G'_{0°C}$. Samples with $G'_{0°C}$ below 175Pa showed high DT. As $G'_{0°C}$ increased up to around 400Pa, exponential decay in DT was seen**.** $G'_{0°C}$ values above 400Pa led to DT below 0.6g.min^{-1}, where, except sample S1A3P3 (see code in Table 3.3), most samples presented a plateau with DT below 0.3g.min^{-1}. Above 440Pa,

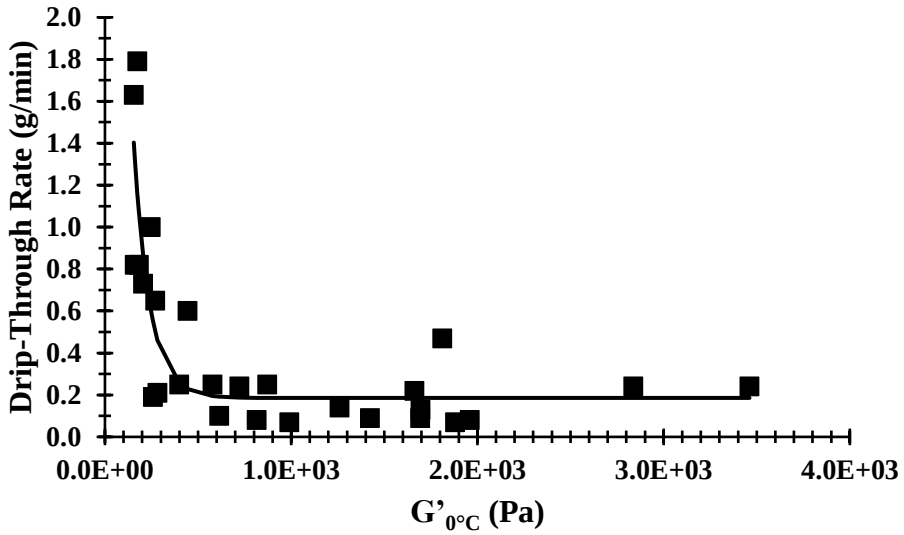

Figure 3.1 Behavior of storage modulus ($G'_{0°C}$) versus drip-through rate (DT) for samples with controlled mix viscosity, overrun and extent of fat destabilization [Data compiled from Wu et al. (2019) and Chapter 2]. Line is fitted exponential model.

DT changed only slightly. With higher $G'_{0°C}$, the remnant foam had greater solid-like behavior and hence, lower DT. A nonlinear model is presented in Table 3.4 to describe the correlation between $G'_{0°C}$ and DT, which is also represented in Figure 3.1.

As can be observed in Figure 3.2A, as fat destabilization increased, in general, DT decreased and $G'_{0°C}$ increased, respectively, although there were numerous outliers. Other studies also found this relationship between fat destabilization and DT (Bolliger et al., 2000; Muse and Hartel, 2004; Warren and Hartel, 2018) and $G'_{0°C}$ (Eisner et al., 2005; Granger et al., 2005; Wildmoser et al., 2004). The fat clusters connected through the lamellae probably increased the elasticity of the ice cream matrix, which were able to partially decrease the serum phase drip on the top of the screen. In the transition zone, from the exponential decay to plateau, samples S1A1P2 and S2A1P2 (see codes in Table 3.2 or 3.3), which presented low fat destabilization, showed low DT with $G'_{0°C}$ below 400Pa (Figure 3.2A). This was probably related to other structural components, which were directly affected by the formulations (Table 3.3), that also affected $G'_{0°C}$ to a lower degree, such as viscosity and overrun.

From Figure 3.2B, as mix viscosity (at $50s^{-1}$) increased, DT clearly decreased, showing a significant effect of the mix viscosity on rate of DT. At the same time, $G'_{0°C}$ increased, but data became more scattered. These relationships between mix viscosity with DT (Amador et al., 2017; Muse and Hartel, 2004) and $G'_{0°C}$ (Dogan et al., 2013) were found in previous studies. At low viscosity (code S1 in the Tables 3.2 and 3.3), $G'_{0°C}$ was low and DT was high in most samples. At higher mix viscosity (at $50s^{-1}$), $G'_{0°C}$ increased further and DT showed a strong decrease, which was almost independent of fat destabilization and overrun (Wu et al., 2019). The

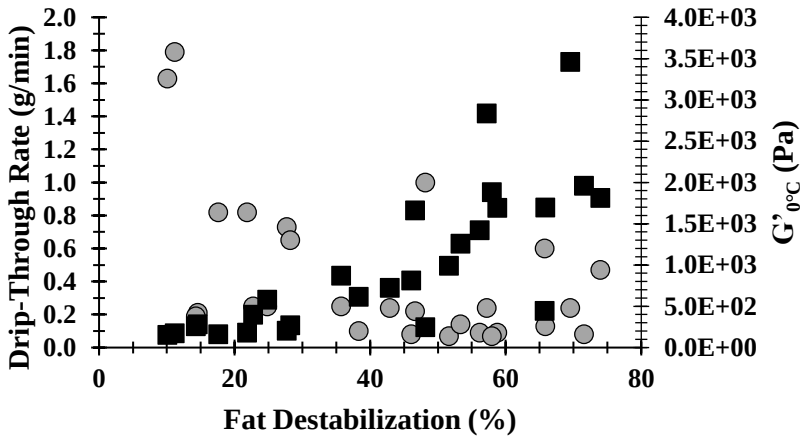

(A)

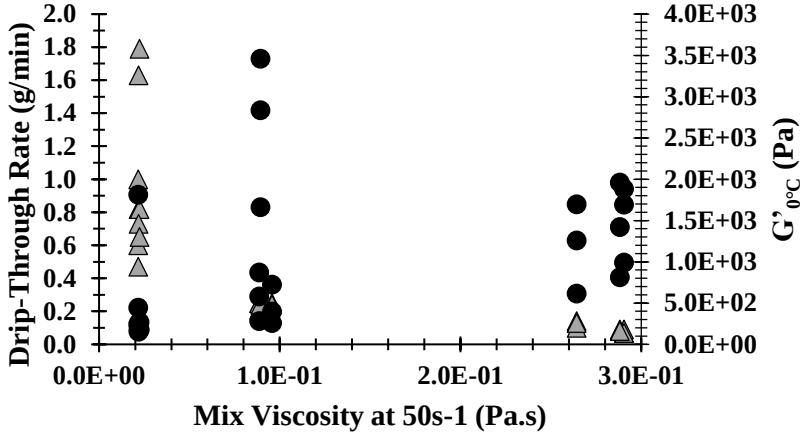

(B)

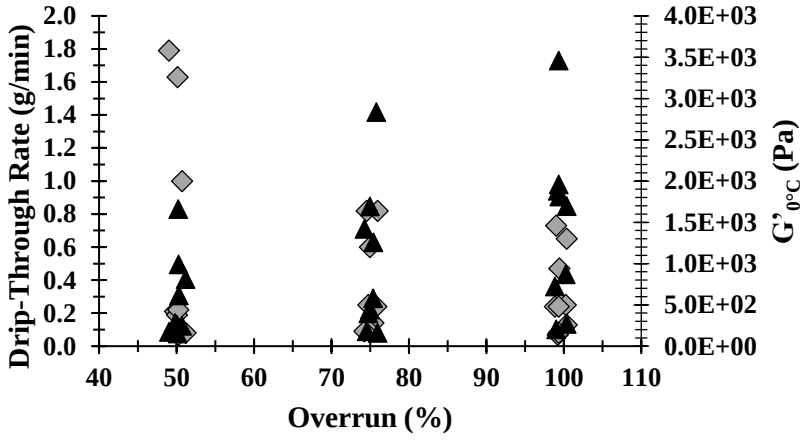

(C)

Figure 3.2 (A) Drip-through rate (grey circle) and G' at 0°C ($G'_{0°C}$) (black square) versus extent of fat destabilization; (B) Drip-through rate (grey triangle) and $G'_{0°C}$ (black circle) versus mix viscosity (at $50s^{-1}$); (C) Drip-through rate (grey diamond) and $G'_{0°C}$ (black triangle) versus overrun [Data compiled from Wu, Freire and Hartel (2019) and Chapter 2].

water retention and higher entanglement of polysaccharides provided elasticity to the matrix, which was potentialized by fat destabilization and overrun, so that flow of the serum phase was limited and reduced ice cream dripping.

As overrun increased, $G'_{0°C}$ generally increased and DT generally decreased, although there was significant scatter in the data, as observed in Figure 3.2C. These general relationships between overrun with DT (Sakurai et al., 1996; Sofjan and Hartel, 2004) and $G'_{0°C}$ (Wildmoser et al., 2004) were found in previous work. In DT, this trend was observed mainly in samples with no stabilizer added, the trends decreased with 0.2% and almost no differences were found with 0.4% stabilizer added (Table 3.2). In $G'_{0°C}$, this trend was reversed (Table 3.3). Although samples with 0.4% stabilizer added showed a lower range of $G'_{0°C}$, greater influence on $G'_{0°C}$ was found from overrun. As previously discussed, weak gel formation was observed in mix formulations with 0.4% stabilizer added. This gel formation, associated with larger volume of smaller air cells, provided greater structural strength to the ice cream matrix due to greater interaction of structural components in the thinner lamellae and larger surface area in the interface air cell/serum phase. Thus, this low range of $G'_{0°C}$ was not enough to see a difference in the DT. Finally, it is worth recalling from previous work (Chapter 2) that fat destabilization most influenced $G'_{0°C}$ behavior and that $G'_{0°C}$ above 400Pa led to a stable DT below 0.3g.min^{-1} in most samples.

Moving on to FH, overall, data for most of the rheological parameters versus FH (Tables 3.2 and 3.3) presented an exponential increase, which could be represented by a generic exponential model:

$$FH = a + b \cdot \exp\left(c \cdot Rheological\ Parameter\right) \quad (3.2)$$

Here, a is asymptote, b is scale and c is growth rate.

As $G'_{0°C}$ increased, FH initially showed an exponential increase and then reached an upper asymptote (Figure 3.3). Samples with $G'_{0°C}$ below 155Pa showed no FH (0%), meaning the entire sample completely dripped through the screen. As $G'_{0°C}$ increased further, up to around 750Pa, FH showed an exponential increase**.** The higher variability in FH at low $G'_{0°C}$ is probably due to greater dependence of FH on other mechanical components, such as viscous and viscoelastic behavior. $G'_{0°C}$ values above 750Pa led to FH above 40% (Figure 3.3), where, except sample S3A1P1 (see code in Table 3.2), most samples with 0.4% stabilizer added presented FH above 50%. Above 750Pa, FH changed slightly from 40 to 60%. A higher $G'_{0°C}$ means greater solid-like behavior of the microstructure, which directly increased the FH of the remnant foam on the top of the screen. A nonlinear model is shown in Table 3.4 to describe the correlation between $G'_{0°C}$ and FH, which is also represented in Figure 3.3.

As fat destabilization increased, both FH and $G'_{0°C}$ (previously discussed) generally increased (Figure 3.4A), although there was significant variability. This relationship between fat destabilization and shape retention was also suggested from other studies (Bolliger et al., 2000; Warren and Hartel, 2018). Although fat destabilization generally correlated with mix viscosity and overrun (Table 3.3), PS80 levels influenced the FH less than mix viscosity and overrun. Thus, the network of fat clusters increased the $G'_{0°C}$ of the ice cream matrix and partially increased the FH.

Overall, as mix viscosity (at $50s^{-1}$) increased, FH and $G'_{0°C}$ (previously discussed) increased slightly (Figure 3.4B), although the values were quite scattered. The relationship

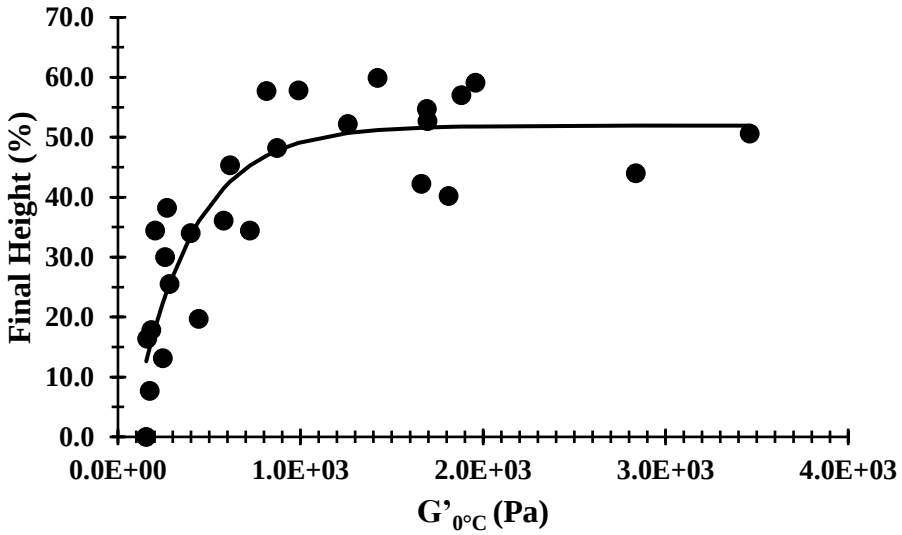

Figure 3.3 Behavior of storage modulus ($G'_{0°C}$) versus and final height (FH) for samples with controlled mix viscosity, overrun and extent of fat destabilization [Data compiled from Wu et al. (2019) and Chapter 2]. Line is fitted exponential model.

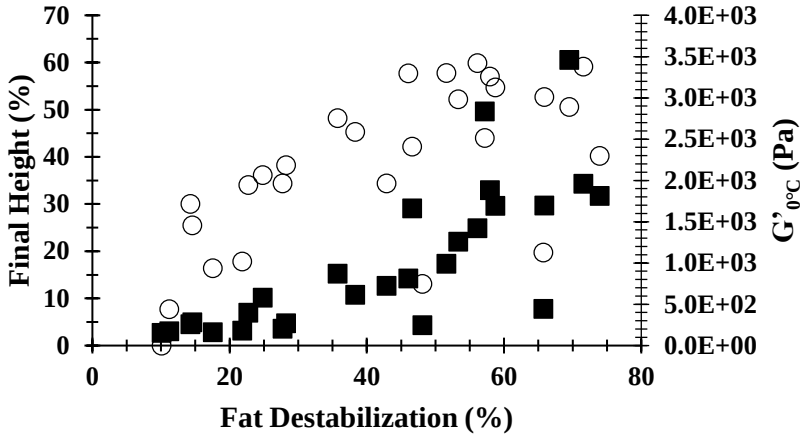

(A)

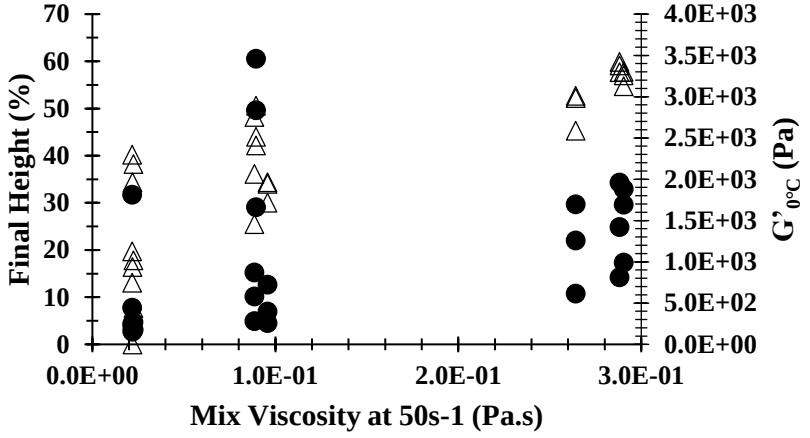

(B)

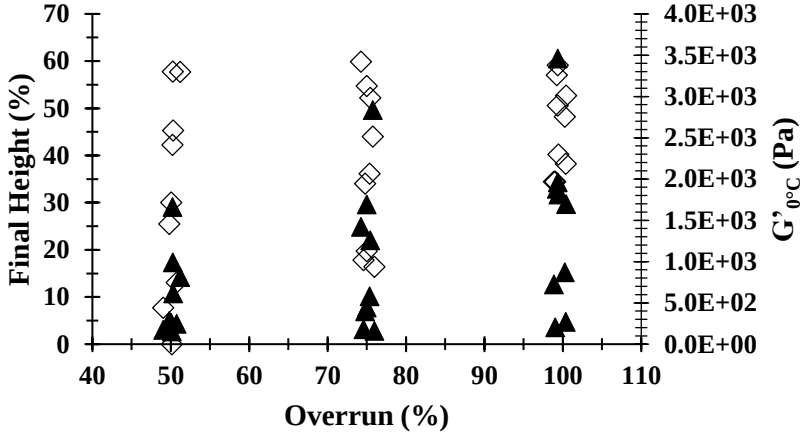

(C)

Figure 3.4 (A) Final Height (hollow circle) and G' at 0°C ($G'_{0°C}$) (black square) versus extent of fat destabilization; (B) Final Height (hollow triangle) and $G'_{0°C}$ (black circle) versus mix viscosity (at $50s^{-1}$); (C) Final Height (hollow diamond) and $G'_{0°C}$ (black triangle) versus overrun [Data compiled from Wu et al. (2019) and Chapter 2].

between mix viscosity and shape retention was probably due to the drainage resistance (Wu et al., 2019). This shape retention was more prominent in the samples with 0.4% stabilizer added (Table 3.2), where a weak gel formation was observed in their respective mix formulations, as previously discussed. Therefore, the water retention and higher entanglement of polysaccharides partially increased $G'_{0°C}$, but directly affected the flow as well as drainage resistance and increased the FH.

In general, as overrun increased, FH and $G'_{0°C}$ (previously discussed) increased slightly (Figure 3.4C), although the results were highly scattered. This relationship between overrun (air flow) and FH was more prominent in samples with no stabilizer added (Table 3.2). In other words, the higher overrun increased $G'_{0°C}$ and FH, but only when viscosity was low. Thus, $G'_{0°C}$ was most affected by fat destabilization, and DT as well as FH were most affected by mix viscosity.

The variability of DT (73% explained variability) and FH (75% explained variability) were satisfactorily predicted by $G'_{0°C}$ (Table 3.4). However, the use of other mechanical parameters, which include viscous and viscoelastic behavior, might possibly improve the variability prediction of DT or FH.

3.4.4.2 Residual Viscosity (η_0) from Generalized Kevin-Voigt Model (Creep Measurements)

Gravitational force is the only load applied to ice cream during a typical meltdown test. In this condition, as ice melts and dilutes the serum phase, shear rate should be quite low. In creep test from previous work (Chapter 2), since constant stress value was chosen within the LVR, the load applied to the sample also produced low shear rates. Thus, parameters obtained from the creep test may correlate with the mechanical performance of ice cream in meltdown test.

From the previous work (Chapter 2), shear creep compliance (J) was obtained for melted ice creams at 0°C from the structure study. The generalized Kelvin-Voigt model with six

parameters (one Maxwell unit in series with two Kelvin units) was found to describe well those creep compliance data for the melted ice cream (Chapter 2):

$$J(t) = J_0 + J_1\left[1 - e^{-\frac{t}{\tau_1}}\right] + J_2\left[1 - e^{-\frac{t}{\tau_2}}\right] + t/\eta_0 \quad (3.3)$$

Here, J(t) is the compliance over time (t), τ_1 and τ_2 are retardation times, J_1 and J_2 are retarded compliances, J_0 is instantaneous compliance and η_0 is the residual viscosity. J_1 and J_2 represent the viscoelastic behavior (from the two Kelvin-Voigt units). J_0 and η_0 represent the elastic and viscous behaviors (from the Maxwell unit), respectively. From this mechanical model (Equation 3.1), parameters of each element (one Maxwell unit and two Kelvin units) were obtained. G_0 (spring) is elastic modulus and η_0 (dashpot) is residual viscosity from Maxwell unit, G_1 (spring) is retarded elastic modulus and η_1 (dashpot) is internal viscosity from first Kelvin-Voigt unit, G_2 (spring) is retarded elastic modulus, and η_2 (dashpot) is internal viscosity from second Kelvin-Voigt unit (Dogan et al., 2013). While other parameters are discussed elsewhere in this dissertation, here, η_0 will be discussed further since it represents viscous behavior at low shear rate and may possibly present good correlation with viscous behavior of the ice cream matrix in meltdown test. Moreover, from our previous work (Chapter 2), η_0 was also used to validate $\sigma_{Y\,0°C}$ measurements. Therefore, here, the correlations of both $\eta_{0\,0°C}$ and $\sigma_{Y\,0°C}$ with meltdown parameters will also be compared to each other.

A nonlinear model to describe the correlation between $\eta_{0\,0°C}$ and DT is presented in Table 3.4; this correlation is also represented in Figure 3.5. The exponential decay model has three parameters, growth rate, scale and asymptote (Equation 3.1). At low $\eta_{0\,0°C}$, DT is high. As $\eta_{0\,0°C}$ increases slightly, DT presents an exponential decay and reaches a lower asymptote, where DT is

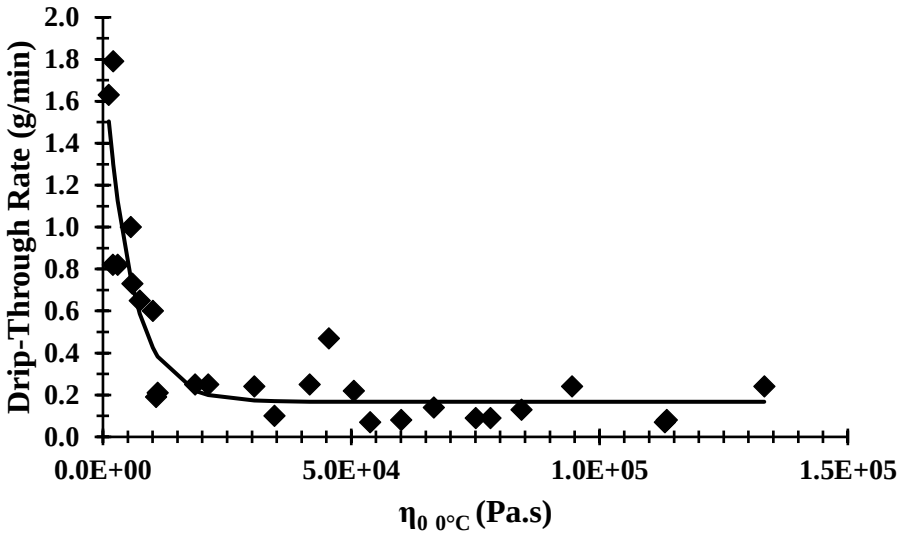

Figure 3.5 Behavior of residual viscosity ($\eta_{0\ 0°C}$) from generalized Kelvin-Voigt model versus drip-through rate for samples with controlled mix viscosity, overrun and extent of fat destabilization [Data compiled from Wu et al. (2019) and Chapter 2]. Line is fitted exponential model.

almost independent of $\eta_{0\,0°C}$. As observed in Figure 3.5, samples with $\eta_{0\,0°C}$ below 2000Pa.s showed DT above 0.8g.min^{-1}. As $\eta_{0\,0°C}$ increased up to around 11000Pa.s, DT showed an exponential decay**.** For $\eta_{0\,0°C}$ values above 11000Pa.s, DT was below 0.3g.min^{-1}, except for sample S1A3P3 (see code in Table 3.3 and Figure 3.5). Higher $\eta_{0\,0°C}$ means greater flow resistance and lower DT.

In general, as fat destabilization increased, DT decreased (previously discussed) and $\eta_{0\,0°C}$ increased, which is represented in Figure 3.6A. The relationship between fat destabilization and $\eta_{0\,0°C}$ is due to the elastic properties provided by the network of fat globules to the melted matrix. Moreover, as PS80 increased (increased fat destabilization), no differences were found for $\eta_{0\,0°C}$ in samples with 0.4% stabilizer added (Table 3.3), which was probably due to gel (weak) formation in those respective mixes, as showed in previous work (Chapter 2).

As mix viscosity (at 50s^{-1}) increased, DT decreased (previously discussed) and $\eta_{0\,0°C}$ increased (Figure 3.6B) although there was significant scatter in the data. Dogan et al. (2013) reported that the increase of xanthan gum concentration increased mix viscosity as well as residual viscosity (η_0). The ability of stabilizers to affect mix viscosity is well established in the literature.

Therefore, an increase of $\eta_{0\,0°C}$ in melted ice cream due to increase of mix viscosity was expected. In general, as overrun increased, DT decreased (previously discussed) and $\eta_{0\,0°C}$ increased; however, DT (previously discussed) and $\eta_{0\,0°C}$ values were very scattered, as observed in Figure 3.6C. This relationship between overrun (air flow) and $\eta_{0\,0°C}$ (Table 3.3) was probably due to the greater surface area at the air cell/serum phase interface in samples with higher overrun, which led to greater interactions of molecules and particles in the matrix. Furthermore, a correlation was found between overrun and air cell size, the greater volume of small air cells probably led to a more structured melted matrix, which increased the $\eta_{0\,0°C}$. However, further study is required to better comprehend the correlation between overrun and $\eta_{0\,0°C}$.

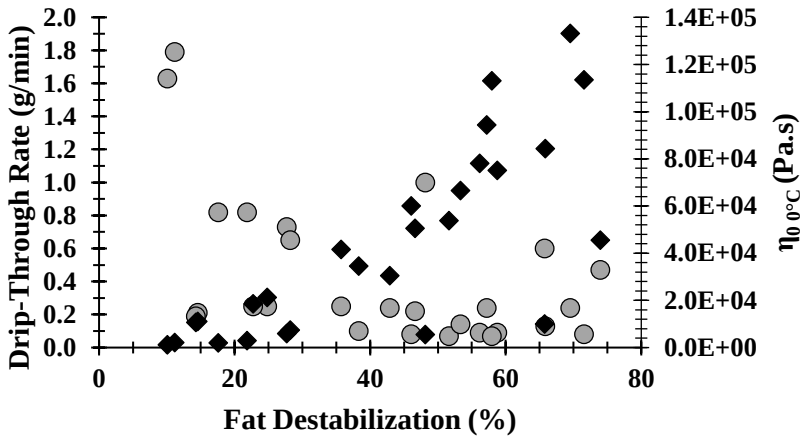

(A)

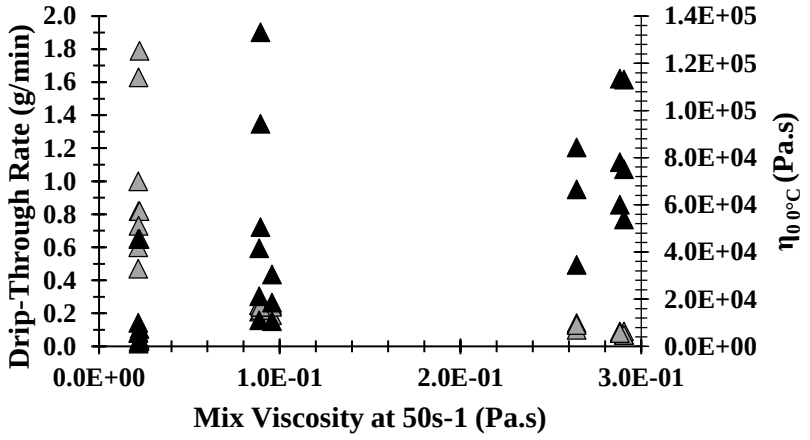

(B)

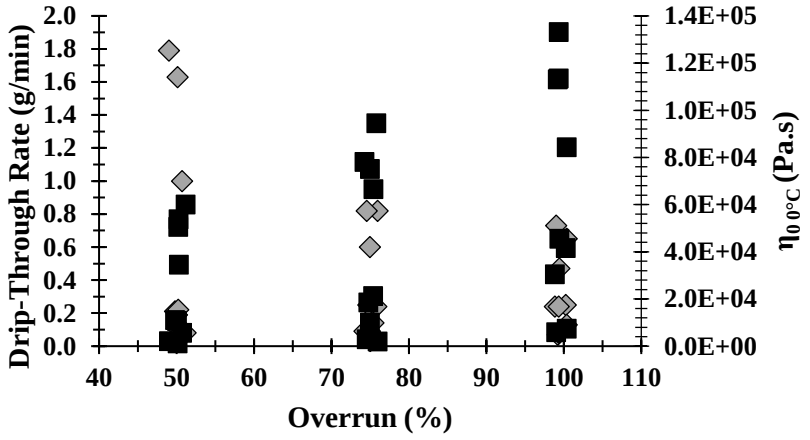

(C)

Figure 3.6 (A) Drip-through rate (grey circle) and $\eta_{0\ 0°C}$ (black square) versus extent of fat destabilization; (B) Drip-through rate (grey triangle) and $\eta_{0\ 0°C}$ (black circle) versus mix viscosity (at $50s^{-1}$); (C) Drip-through rate (grey diamond) and $\eta_{0\ 0°C}$ (black triangle) versus overrun [Data compiled from Wu et al. (2019) and Chapter 2].

Moving on to FH, a nonlinear model (Table 3.4) describes the correlation between $\eta_{0\ 0°C}$ and FH. This correlation is also represented in Figure 3.7. The model shows an exponential decay with three parameters, growth rate, scale and asymptote (Equation 3.2). At low $\eta_{0\ 0°C}$, FH is low. As $\eta_{0\ 0°C}$ increases slightly, FH shows an exponential increase. After that, an upper asymptote in FH is reached. As observed in Figure 3.7, no remnant foam (0% FH) was found in samples with $\eta_{0\ 0°C}$ below 1200Pa.s. Samples with no stabilizer added, except sample S1A3P3 (see code in the Table 3.2), showed exponential increase of FH, as $\eta_{0\ 0°C}$ increased up to around 11000Pa.s. A transition zone between 11000 and 50500Pa.s (FH ranged from 34 to 48%) was mainly observed for samples with 0.2% stabilizer added. After that, samples with 0.4% stabilizer added, except sample S3A1P1 (see code in the Table 3.2), presented $\eta_{0\ 0°C}$ above 53800Pa.s and a plateau in FH, which ranged from 50 to 60%. Higher $\eta_{0\ 0°C}$ provided greater structure retention due to flow and drainage resistance, which directly affected FH of remnant foam.

As observed in Figure 3.8A, overall, as fat destabilization extent increased FH (previously discussed) and $\eta_{0\ 0°C}$ (previously discussed) also increased. In other words, fat destabilization increased $\eta_{0\ 0°C}$ of melted matrix at 0°C and partially increased structure retention at the end of the test.

As mix viscosity (at $50s^{-1}$) increased, FH (previously discussed) and $\eta_{0\ 0°C}$ (previously discussed) generally increased, as observed in Figure 3.8B, although there was again significant scatter. Increased stabilizer levels increased viscosity, which increased $\eta_{0\ 0°C}$ and FH.

In general, as overrun increased, FH (previously discussed) increased, which was mainly in samples with no stabilizer added, and $\eta_{0\ 0°C}$ (previously discussed) increased, as observed in

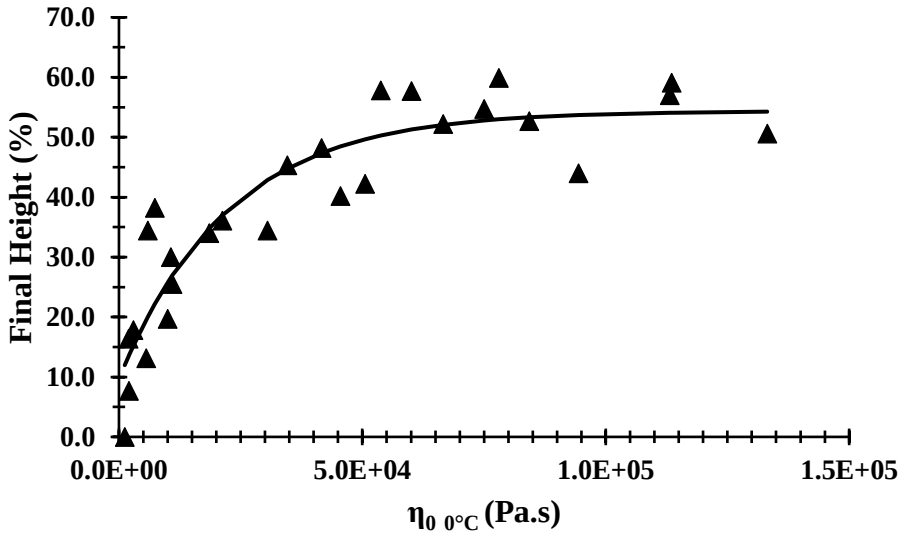

Figure 3.7 Behavior of residual viscosity ($\eta_{0\,0°C}$) from generalized Kelvin-Voigt model versus final height (FH) for samples with controlled mix viscosity, overrun and extent of fat destabilization [Data compiled from Wu et al. (2019) and Chapter 2]. Line is fitted exponential model.

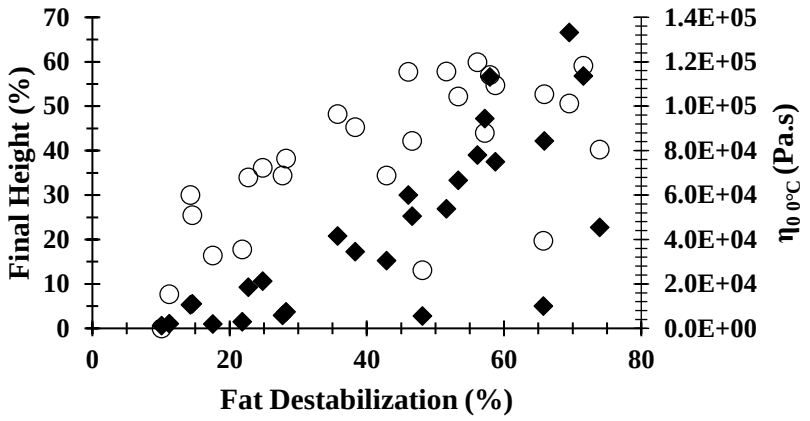

(A)

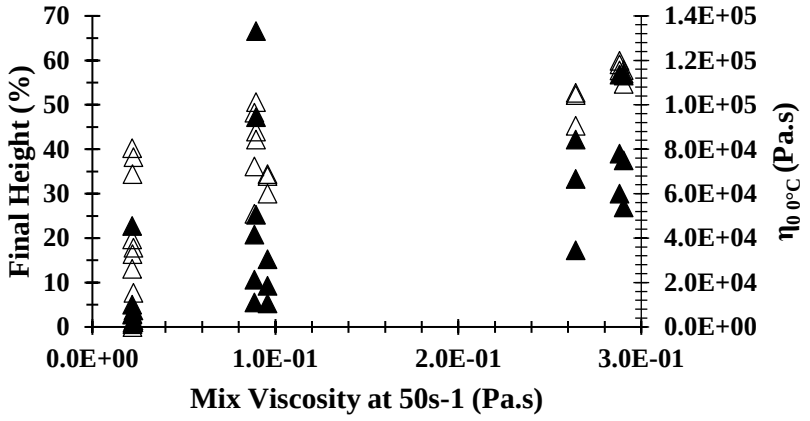

(B)

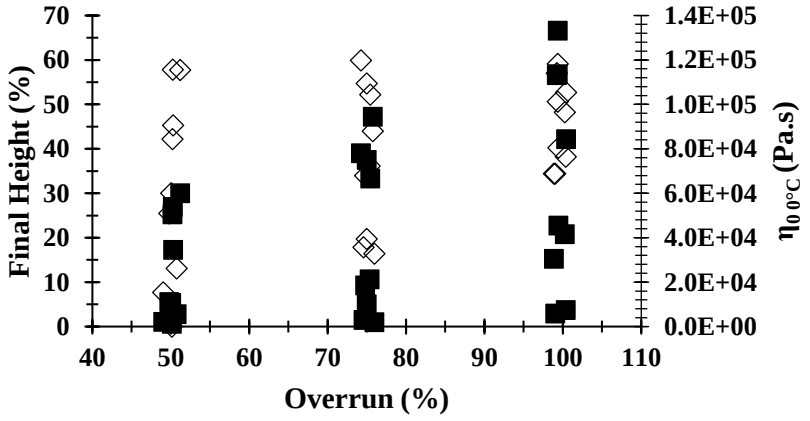

(C)

Figure 3.8 (A) Final Height (hollow circle) and $\eta_{0\ 0°C}$ (black square) versus extent of fat destabilization; (B) Final Height (hollow triangle) and $\eta_{0\ 0°C}$ (black circle) versus mix viscosity (at $50s^{-1}$); (C) Final Height (hollow diamond) and $\eta_{0\ 0°C}$ (black triangle) versus overrun [Data compiled from Wu et al. (2019) and Chapter 2].

Figure 3.8C. Again, there was significant scatter in the data. Samples with higher overrun probably had greater interactions of molecules and particles at the air/serum phase interface due to not only thinner lamellae, but also greater volume of smaller air cells, as previously discussed.

The $\eta_{0\ 0°C}$ explained 83 and 84% of the variability in DT and FH, respectively. In other words, the fitted exponential models presented in Table 3.4 provided reliable correlations with meltdown parameters in studied system. Therefore, in systems with mix formulations, process and hardening conditions similar to the one used in this study, $\eta_{0\ 0°C}$ measurements could be used to replace DT and FH measurements, which could reduce time in ice cream research.

3.4.4.3 Yield Stress (σ_Y) from Stress Growth Measurements

Yield stress (σ_Y) is defined as minimum shear stress required to a sample initiate flow (Sun and Gunasekaran, 2009). Moreover, σ_Y is also referred to as transient stress, where the sample shows elastic solid-like or viscous liquid-like behavior; this occurs in a stress interval where the sample presents viscoelastic behavior (Sun and Gunasekaran, 2009). In ice cream and other frozen desserts, σ_Y has been related to the ability to dip or scoop (Briggs et al., 1996). Here, σ_y was related to the ability of the ice cream matrix to drip and remain during and after, respectively, meltdown test on the top of the screen.

The DT data predicted by $\sigma_{Y\ 0°C}$ presents an exponential decay (refer to Equation 3.1), as seen in Figure 3.9. At low $\sigma_{Y\ 0°C}$, DT was high. As $\sigma_{Y\ 0°C}$ slightly increased, an exponential decay was seen in DT. As $\sigma_{Y\ 0°C}$ increased, DT reached a lower asymptote, where $\sigma_{Y\ 0°C}$ had little effect

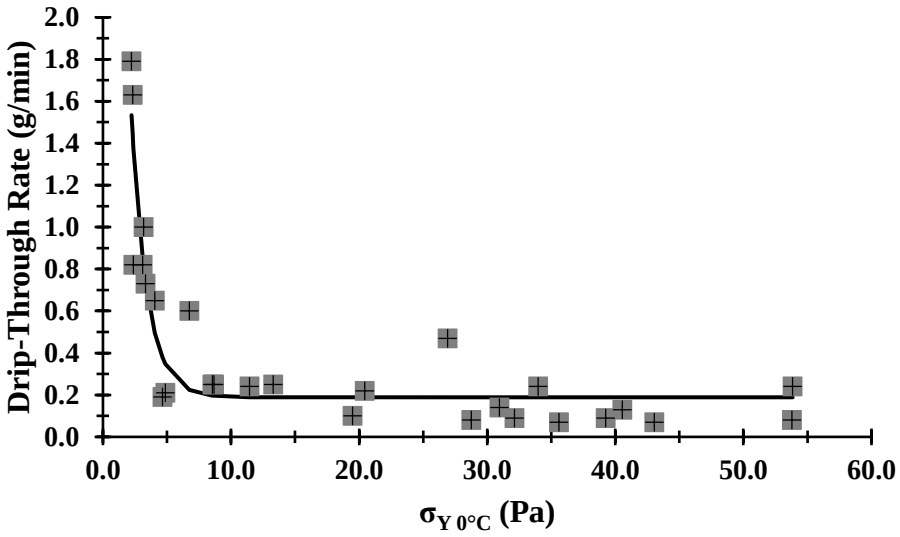

Figure 3.9 Behavior of yield stress ($\sigma_{Y\ 0°C}$) versus drip-through rate (DT) for samples with controlled mix viscosity, overrun and extent of fat destabilization [Data compiled from Wu et al. (2019) and Chapter 2]. Line is fitted exponential model.

on DT. At σ_Y below 2.0Pa, samples showed high DT(>1.7g.min^{-1}). When σ_Y increased to 4.0Pa, an exponential decay was observed in DT, mainly in samples with no stabilizer added. Above 4.0Pa, except samples S1A2P3 and S1A3P3 (see codes in Table 3.3), most samples presented a plateau with DT below 0.3g.min^{-1}. In general, the greater σ_Y, the greater stress required to initiate flow, and the lower DT. A nonlinear model is presented in Table 3.4 to describe correlation between $\sigma_{Y\ 0°C}$ and DT, which is also represented in Figure 3.9.

In general, as fat destabilization increased, DT (previously discussed) decreased and $\sigma_{Y\ 0°C}$ generally increased, as showed in Figure 3.10A. The relationship between fat destabilization and σ_Y is due to structured fat globules through lamellae, which provide elastic properties to the melted matrix that require more force to initiate flow. In addition, other factors, such as mix viscosity, overrun, among others, as well as their intrinsic array arrangement with the network of destabilized fat globules (fat destabilization), should also affect $\sigma_{Y\ 0°C}$, which might explain the outliers in Figure 3.10A. Therefore, higher fat destabilization generally decreased DT (Table 3.2) and strongly affected $\sigma_{Y\ 0°C}$ (Chapter 2).

As mix viscosity (at 50s^{-1}) increased, DT (previously discussed) decreased and $\sigma_{Y\ 0°C}$ generally increased (Figure 3.10B), although with significant scatter in the data. The correlation between mix viscosity (at 50s^{-1}) and $\sigma_{Y\ 0°C}$ was probably related to increased concentration of LBG and carrageenan in formulations. These polysaccharides were reported to present yield stress in emulsions (Turquois et al., 1992). Thus, increased mix viscosity led to increased σ_Y and decreased DT in samples.

Generally, as overrun increased, DT decreased (previously discussed) and $\sigma_{Y\ 0°C}$ increased (Figure 3.10C), although significant scatter was observed. The relationship between overrun and

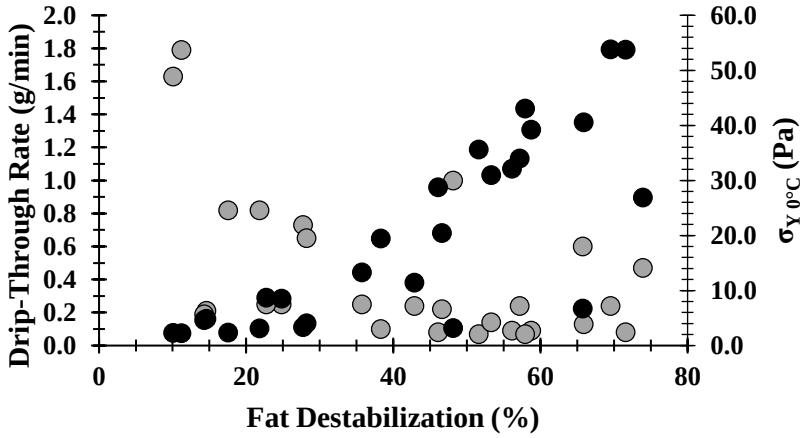

(A)

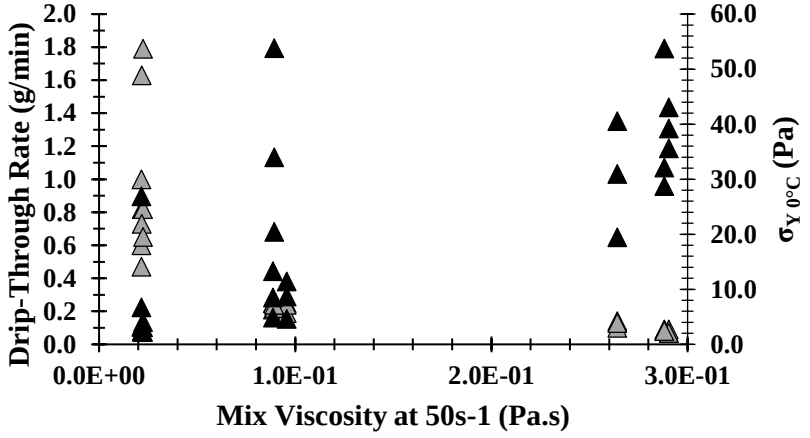

(B)

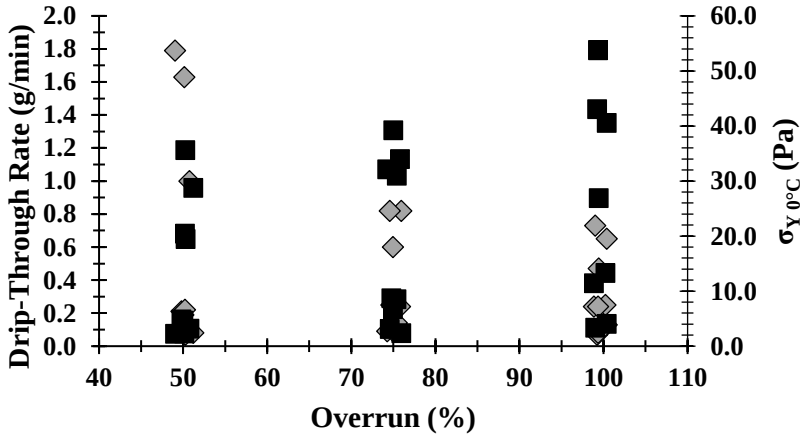

(C)

Figure 3.10 (A) Drip-through rate (grey circle) and $\sigma_{Y\ 0°C}$ (black square) versus extent of fat destabilization; (B) Drip-through rate (grey triangle) and $\sigma_{Y\ 0°C}$ (black circle) versus mix viscosity (at $50s^{-1}$); (C) Drip-through rate (grey diamond) and $\sigma_{Y\ 0°C}$ (black triangle) versus overrun [Data compiled from Wu et al. (2019) and Chapter 2].

σ_Y is probably related to greater interactions of components at the air cell/serum phase interface in samples with greater volume of smaller air cells (as previously discussed). This interaction could lead to strengthening of elastic behavior, which required greater force to initiate flow. Therefore, higher overrun increased $\sigma_{Y\ 0°C}$ and decreased DT to some extent.

Moving on to FH, a nonlinear model, shown in Table 3.5, was used to depict the relationship between $\sigma_{Y\ 0°C}$ and FH, which is also illustrated in Figure 3.11. This correlation was well explained by a Michaelis Menten type model that had two parameters:

$$FH = {(a \cdot \sigma_{Y\ 0°C})}\Big/{(b + \sigma_{Y\ 0°C})} \tag{3.4}$$

Here, a is maximum reaction rate and b is inverse affinity.

At low $\sigma_{Y\ 0°C}$, FH was low. As $\sigma_{Y\ 0°C}$ increased slightly, a strong increase in FH was seen. Then, as $\sigma_{Y\ 0°C}$ increased further, FH slowly reached a plateau. When σ_Y was below 2.0Pa, samples showed no remnant foam at the end of the meltdown test (FH=0%). When σ_Y increased to 4.0Pa, an exponential increase in the FH was observed in samples with no stabilizer added, except samples S1A2P3 and S1A3P3 (refer to codes in the Table 3.3). Between 4.0 and 27.0Pa, samples with 0.2% stabilizer added, except samples S2A2P3, S2A3P3 and S3A1P1 (refer to codes in Table 3.3), presented a less marked increase in remnant foam. Above 27.0Pa, a relative plateau was observed in FH between 44.0 and 60.0%. Therefore, the greater σ_Y, the greater stress required to initiate the flow, the greater FH, and the greater remnant structure at the end of the meltdown test.

As illustrated in Figure 3.12A, generally, as extent of fat destabilization increased, both FH (previously discussed) and $\sigma_{Y\ 0°C}$ (previously discussed) increased. A network of partially-coalesced fat globules increased the σ_Y of the matrix and remnant structure at the end of

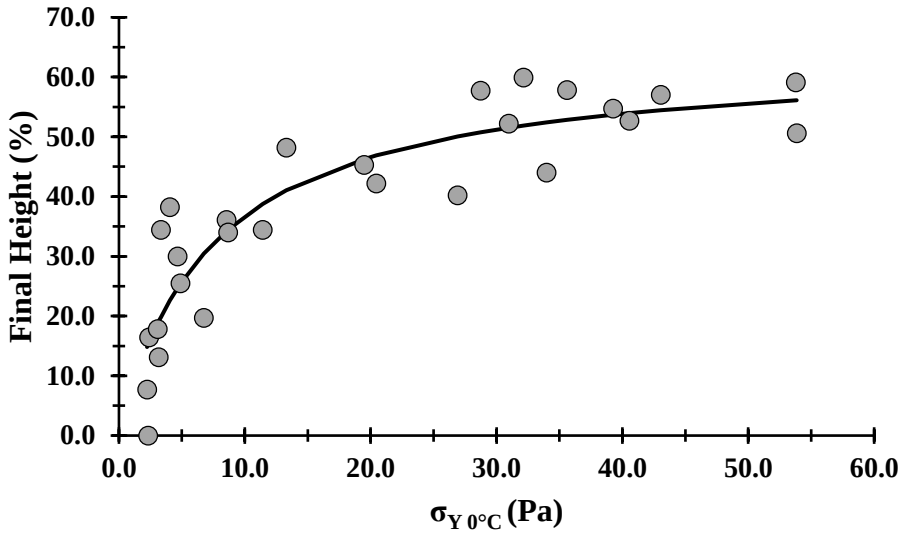

Figure 3.11 Behavior of yield stress ($\sigma_{Y\ 0°C}$) versus final height (FH) for samples with controlled mix viscosity, overrun and extent of fat destabilization [Data compiled from Wu et al. (2019) and Chapter 2]. Line is fitted Michaelis Menten model.

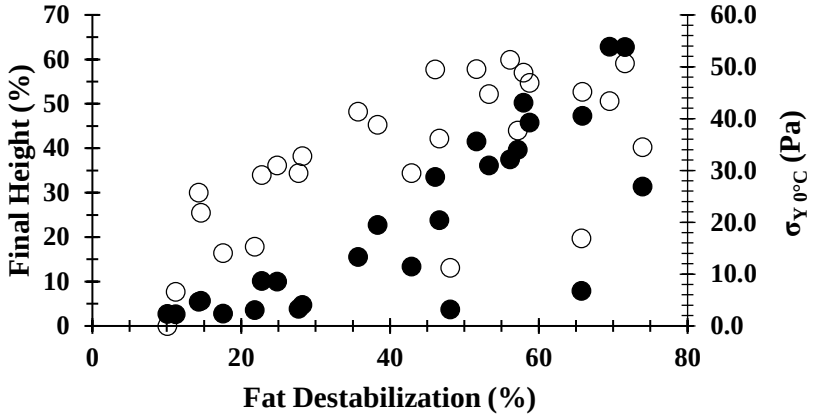

(A)

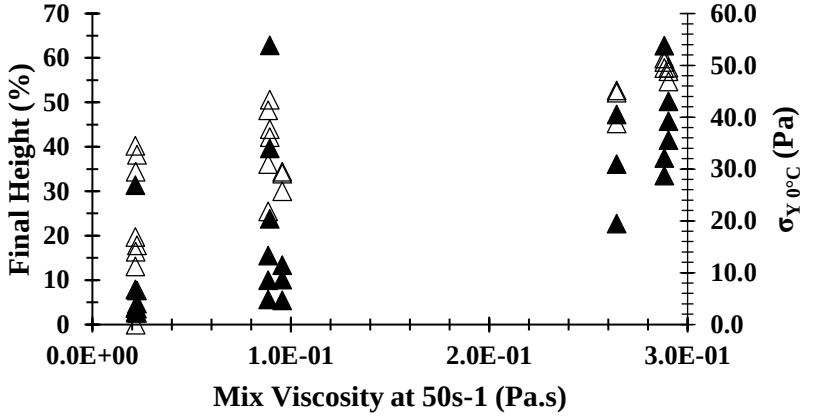

(B)

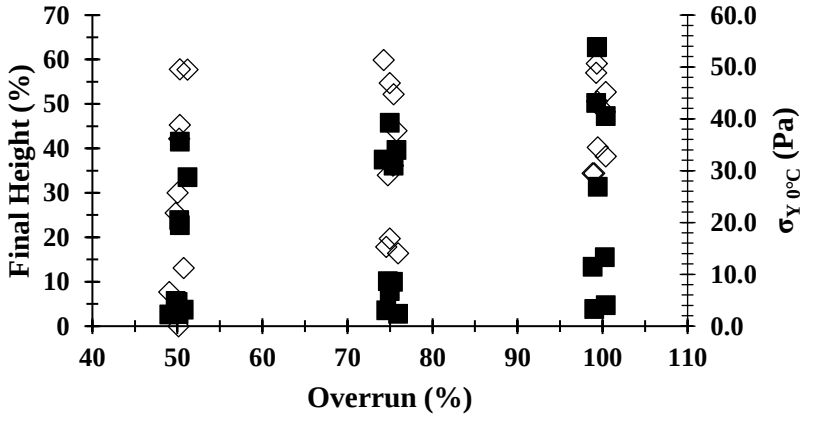

(C)

Figure 3.12 (A) Final Height (hollow circle) and $\sigma_{Y\ 0°C}$ (black square) versus extent of fat destabilization; (B) Final Height (hollow triangle) and $\sigma_{Y\ 0°C}$ (black circle) versus mix viscosity (at $50s^{-1}$); (C) Final Height (hollow diamond) and $\sigma_{Y\ 0°C}$ (black triangle) versus overrun [Data compiled from Wu et al. (2019) and Chapter 2].

the test. Other components, such as mix viscosity, overrun, among others, and their role in the intrinsic arrangement could have also affected $\sigma_{Y\ 0°C}$, which led to the outliers observed in Figure 3.12A.

As observed in Figure 3.12B, as mix viscosity (at $50s^{-1}$) increased, FH (previously discussed) and $\sigma_{Y\ 0°C}$ (previously discussed) both generally increased, although there was significant scatter in the data. Higher mix viscosity provided greater σ_Y, which directly affected FH and the height of the remnant structure. Here, the scatter data also means that other components and their arrangement in the matrix affected the relationship between mix viscosity (at $50s^{-1}$) with $\sigma_{Y\ 0°C}$ and FH.

Overall**,** as observed in Figure 3.12C, higher overrun led to higher FH (previously discussed), mainly in samples with no stabilizer added, and higher $\sigma_{Y\ 0°C}$ (previously discussed). The higher mix viscosity probably overlapped the mechanical role of overrun in the $\sigma_{Y\ 0°C}$ of the matrix. Consequently, mechanical performance of the matrix in FH was also affected. Thinner lamellae in samples with higher overrun probably led to greater interactions of structural components at the air/serum phase interface, which also presented smaller air cells, as previously discussed. Here again, the scatter data is probably due to other components and their arrangement in the matrix that affected relationship between overrun with FH and $\sigma_{Y\ 0°C}$.

In our previous work (Chapter 2), although the structural arrangement showed different responses due to the distinct inputs, such as constant shear rate (from $\sigma_{Y\ 0°C}$ measurements) and constant stress load (from $\eta_{0\ 0°C}$ measurements), the linear correlation between $\eta_{0\ 0°C}$ and $\sigma_{Y\ 0°C}$ ($R2=0.94$, $p<0.0001$) was used to validate the observed yield stress. The DT predicted by $\eta_{0\ 0°C}$ and $\sigma_{Y\ 0°C}$ showed asymptotes close to each other (Table 3.4). The scale and growth rate for DT predicted by $\eta_{0\ 0°C}$ were lower and higher, respectively, compared to DT predicted by $\sigma_{Y\ 0°C}$.

Moreover, although different model types were used to predict FH by $\eta_{0\ 0°C}$ (Table 3.4) and $\sigma_{Y\ 0°C}$ (Table 3.5), both presented a direct correlation with FH. Furthermore, fat destabilization, mix viscosity and overrun showed visually similar trends in DT (Figure 3.10) and FH (Figure 3.12).

DT and FH were well explained by $\sigma_{Y\ 0°C}$, which predicted 85 and 82% of variability, respectively. This is relatively high for a biological system such as ice cream (Tables 3.4 and 3.5, respectively). Thus, $\sigma_{Y\ 0°C}$ measurements could be a good alternative to DT and FH measurements from meltdown test; this could increase the knowledge of physical attributes of ice cream during melting.

3.4.4.4 Thixotropy from Flow Measurements (Shear Rate Ramp)

As reported in a previous chapter (Chapter 2), melted ice cream samples showed time dependence in flow sweep tests. Moreover, rheological destruction was also observed after the melted matrix was subjected to upward and downward shear rate sweeps; that is, the sample did not recover its initial structure. Therefore, a flow ramp test was used to evaluate time dependence using large deformations and the thixotropic loop between upward and downward shear rate ramps was used to empirically evaluate rheological destruction. In other words, greater rheological destruction presented by a sample suggests greater initial structure.

The nonlinear model (Table 3.4) described the correlation between $Thix_{0°C}$ and DT, which was also represented in Figure 3.13. The model shows an exponential decay and three parameters, growth rate, scale and asymptote (refer to Equation 3.1). DT was high at low $Thix_{0°C}$, followed by an exponential decay as $Thix_{0°C}$ slightly increased. After that, DT reached a lower asymptote, as $Thix_{0°C}$ increased further. Samples with $Thix_{0°C}$ measurements below 300Pa.s^{-1} showed high DT.

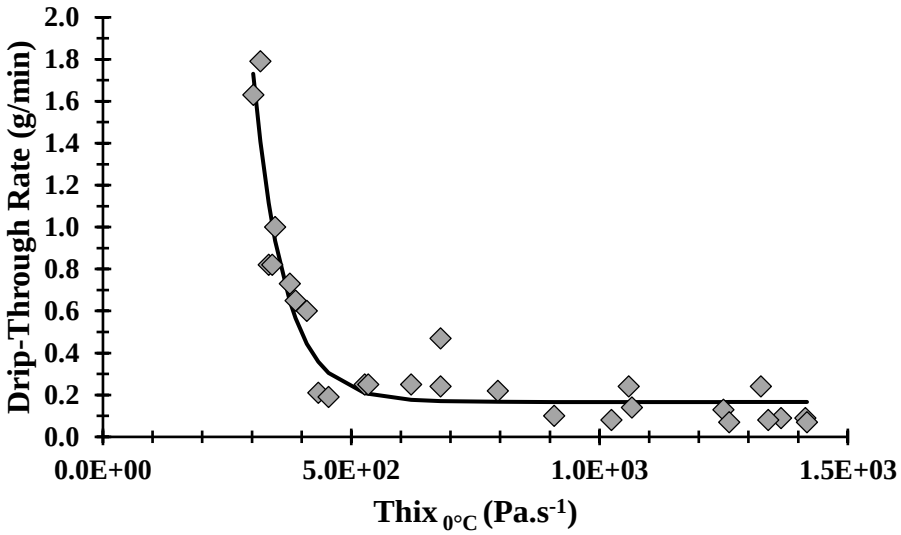

Figure 3.13 Behavior of thixotropy (Thix $_{0°C}$) versus drip-through rate (DT) for samples with controlled mix viscosity, overrun and extent of fat destabilization [Data compiled from Wu et al. (2019) and Chapter 2]. Line is fitted exponential model.

When Thix $_{0°C}$ increased to 410Pa.s^{-1} in samples, an exponential decay was observed in DT, which occurred mainly in samples with no stabilizer added in formulation. Samples with Thix $_{0°C}$ above 410Pa.s^{-1}, except sample S1A3P3 (see code in Table 3.3), presented a plateau in DT, which ranged from 0.1 to 0.3g.min^{-1}. Therefore, higher Thix $_{0°C}$, or greater rheological destruction, indicated greater structural formation and lower DT.

Overall, as fat destabilization extent increased, DT (previously discussed) decreased and Thix $_{0°C}$ increased, as illustrated in Figure 3.14A. This correlation between fat destabilization and Thix $_{0°C}$ was probably due to disruption of a 3-D network of fat globules through the lamellae (Chapter 2). In other words, greater strength of fat globule network led to greater Thix $_{0°C}$ measurements (Table 3.3). Therefore, greater strength of fat globule network generally decreased DT and increased Thix $_{0°C}$. The outliers observed in DT and Thix $_{0°C}$ were probably due to the influence of other factors, such as mix viscosity, overrun, among others, in the mechanical behavior of the matrix.

As observed in Figure 3.14B, higher mix viscosity (at 50s^{-1}) led to lower DT (previously discussed) and higher Thix $_{0°C}$, although the data were fairly scattered. The relationship between mix viscosity and Thix $_{0°C}$ was due to the greater concentrations of LBG (Dolz et al., 2007), guar gum (Javidi et al., 2016) and iota carrageenan (Thomas, 1997) in the stabilizer system of this study, as reported in previous work (Chapter 2). These polysaccharides present thixotropic behavior in emulsions or suspensions. The levels used (0.2 and 0.4%) were sufficient to increase mix viscosity and thixotropic behavior in respective mixes (data not shown here). Moreover, it is worth recalling that correlations between mix viscosity and fat destabilization were found. Therefore, mix viscosity increased Thix $_{0°C}$ of ice cream, which increased structural resistance, and hence, decreased drainage and DT (Figure 3.14B).

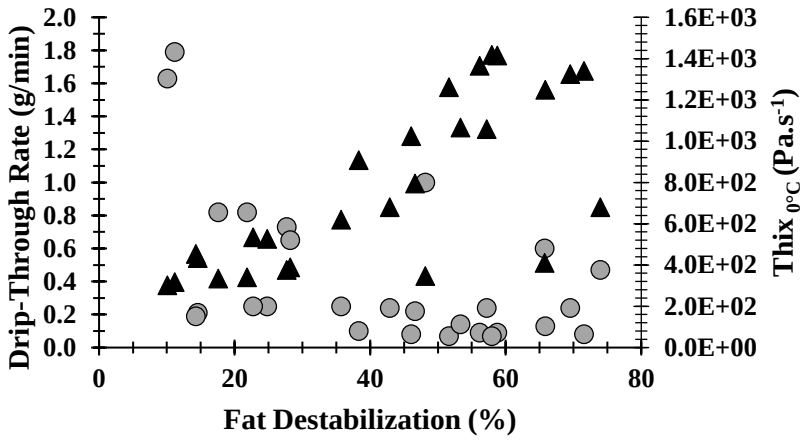

(A)

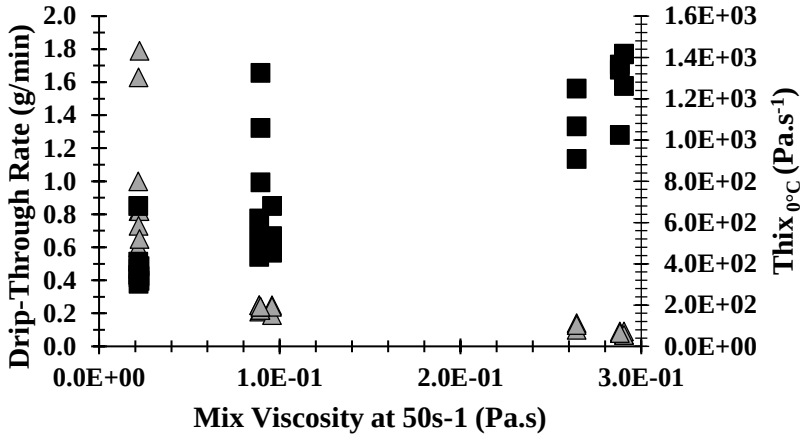

(B)

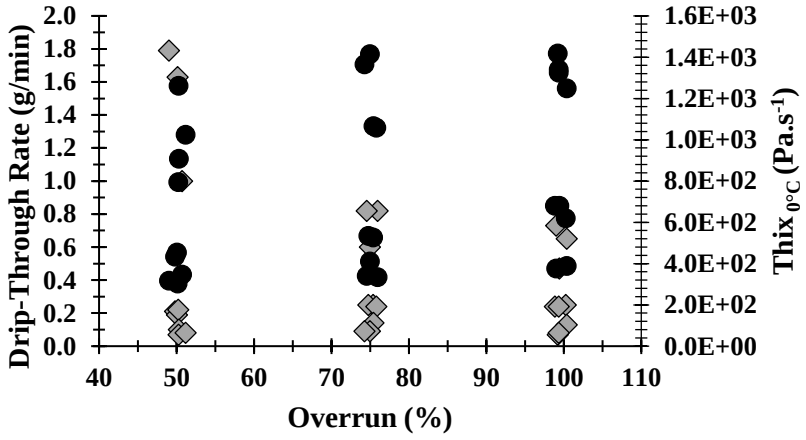

(C)

Figure 3.14 (A) Drip-through rate (grey circle) and Thix $_{0°C}$ (black square) versus extent of fat destabilization; (B) Drip-through rate (grey triangle) and Thix $_{0°C}$ (black circle) versus mix viscosity (at $50s^{-1}$); (C) Drip-through rate (grey diamond) and Thix $_{0°C}$ (black triangle) versus overrun [Data compiled from Wu et al. (2019) and Chapter 2].

Overall, as illustrated in Figure 3.14C, higher overrun led to lower DT (previously discussed) and higher Thix $_{0°C}$, although there was very wide scatter in the data points. Ice cream samples with higher overrun presented larger number of smaller air cells (previously discussed) and thinner lamella, which provided larger surface area at air/serum phase interface and greater interactions of components through the lamellae. An increase of air phase structure, which also showed correlation with fat destabilization (previously discussed), led to greater Thix $_{0°C}$ values. Interestingly, except samples S1A1P3-S1A3P3 (see codes in Table 3.3), overrun showed more influence on Thix $_{0°C}$ in samples with no stabilizer added in formulation. The same was observed for DT (Table 3.2). Thus, overrun presented more influence on DT and Thix $_{0°C}$ in samples with no stabilizer added in formulation.

Moving on to FH, a nonlinear model was used to describe the correlation between Thix $_{0°C}$ and FH (Table 3.4), which is also represented in Figure 3.15. An exponential decay model with three parameters, growth rate, scale and asymptote (refer to Equation 3.2) was fitted to the data. At low Thix $_{0°C}$, low FH was seen. As Thix $_{0°C}$ slightly increased, FH showed an exponential increase. Then, FH increased at lower rate and reached an upper asymptote, as Thix $_{0°C}$ increased further. No remnant foam (0% FH) was found in samples with Thix $_{0°C}$ below 300Pa.s^{-1}. Samples with no stabilizer added, except samples S1A2P3 and S1A3P3 (see codes in the Table 3.2), presented exponential increase in FH as Thix $_{0°C}$ increased from 300 to 390Pa.s^{-1}. A less pronounced increase in FH between 390 and 1000Pa.s^{-1} was mainly observed for samples with 0.2% stabilizer added. Above 1000Pa.s^{-1}, which included mainly samples with 0.4% stabilizer added, a levelling off in FH was reached, which ranged from 44 to 60%. Samples with higher Thix $_{0°C}$ presented greater structural disruption, which directly increased FH of remnant structure at the end of the meltdown test.

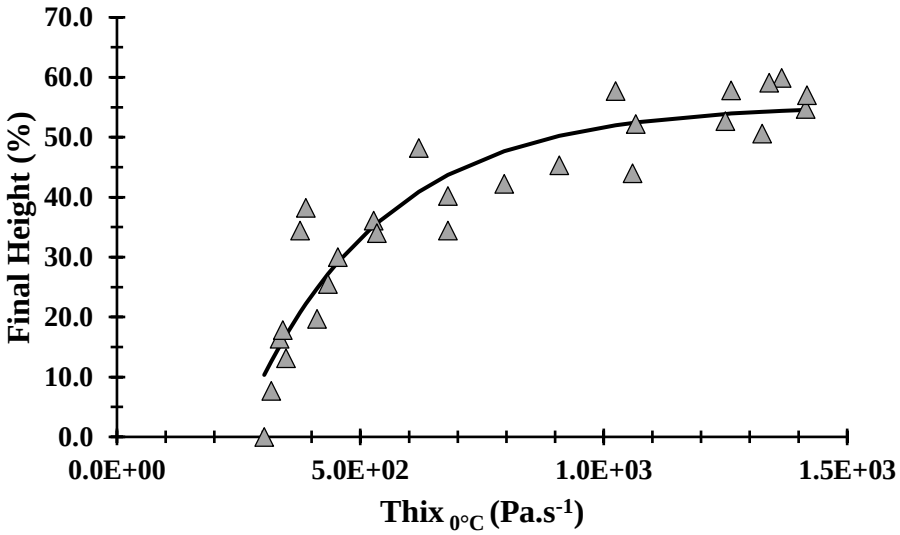

Figure 3.15 Behavior of thixotropy (Thix $_{0°C}$) versus final height (FH) for samples with controlled mix viscosity, overrun and extent of fat destabilization [Data compiled from Wu et al. (2019) and Chapter 2]. Line is fitted exponential model.

In general, as observed in Figure 3.16A, higher fat destabilization extent led to higher FH (previously discussed) and Thix $_{0°C}$ (previously discussed). Fat destabilization (Table 3.1) influenced FH less than Thix $_{0°C}$, as can be seen in Tables 3.2 and 3.3, respectively. Again, other components, such as mix viscosity, overrun, among others, and their arrangement probably influenced FH and Thix $_{0°C}$, which led to outliers observed in Figure 3.16A.

As observed in Figure 3.16B, higher mix viscosity (at $50s^{-1}$) led to higher FH (previously discussed) and Thix $_{0°C}$ (previously discussed), but with some scatter in the data. Mix viscosity (Table 3.1) strongly affected FH and Thix $_{0°C}$, as observed in Tables 3.2 and 3.3, respectively.

Overall, as illustrated in Figure 3.16C, increased overrun led to a slight increase of FH (previously discussed) and Thix $_{0°C}$ (previously discussed), mainly in samples with no stabilizer added in formulation. Here, mix viscosity also overlapped the mechanical role of overrun in the matrix, and hence, FH and Thix $_{0°C}$ values. Therefore, more scattered data were observed in FH and Thix $_{0°C}$.

Finally, 90 and 87% of variability in DT and FH were explained by Thix $_{0°C}$ (Table 3.4), respectively, which were relatively high considering the biological origin of ice cream ingredients. These were the best fitted models in this study. Thus, Thix $_{0°C}$ could be a promising parameter for correlations not only with DT and FH, but also with other meltdown parameters.

3.5 Conclusions

In conclusion, all of the measured rheological properties of ice cream correlated reasonably well with meltdown parameters. G'$_{0°C}$ gave good correlations with DT and FH, although not as good as some of the other rheological parameters. This suggested that the elastic nature of the structural arrangement in the melted ice cream matrix is important, but other mechanical

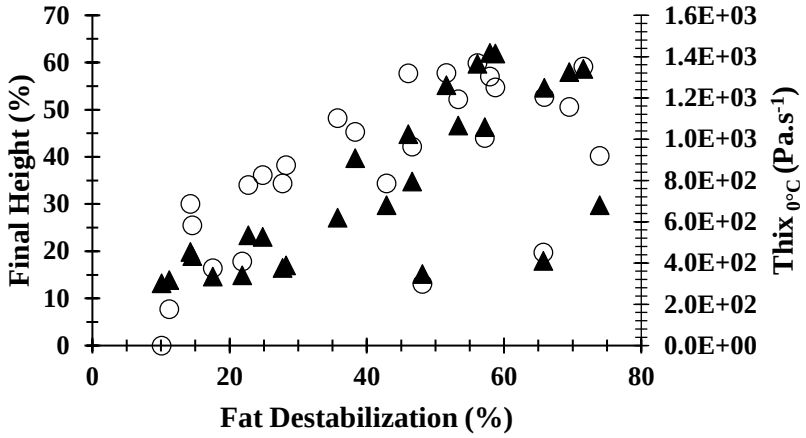

(A)

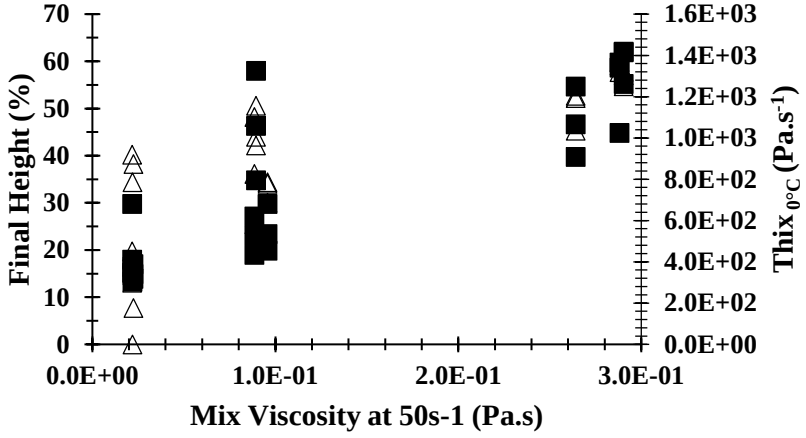

(B)

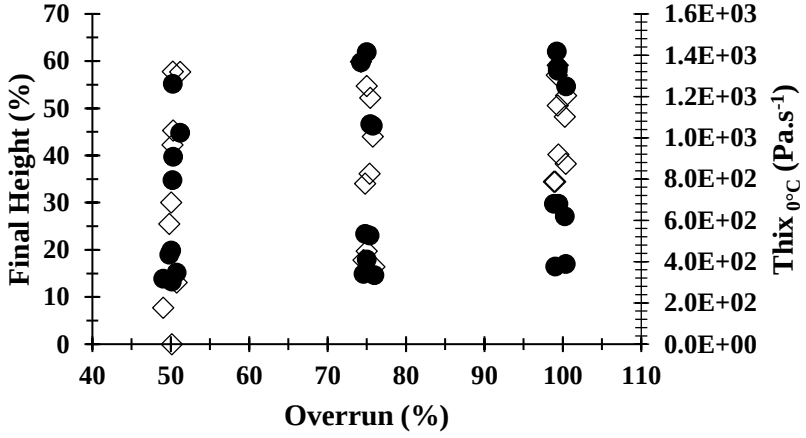

(C)

Figure 3.16 (A) Final Height (hollow circle) and Thix $_{0°C}$ (black square) versus extent of fat destabilization; (B) Final Height (hollow triangle) and Thix $_{0°C}$ (black circle) versus mix viscosity (at $50s^{-1}$); (C) Final Height (hollow diamond) and Thix $_{0°C}$ (black triangle) versus overrun [Data compiled from Wu et al. (2019) and Chapter 2].

parameters are needed to better explain behavior of DT and FH in meltdown test. Variability of DT and FH were well explained by $\eta_{0\ 0°C}$. The value of $\eta_{0\ 0°C}$ provided insights on the viscous behavior of the matrix at low shear rate, which is important in both the drip during the meltdown test, DT, and structure retention after the test, FH. $\sigma_{Y\ 0°C}$, which represents the force needed for the melted ice cream to yield, also explained well both DT and FH. Correlations of $\eta_{0\ 0°C}$ and $\sigma_{Y\ 0°C}$ with meltdown parameters showed similar trends as well as correlations of structural components with $\eta_{0\ 0°C}$ and $\sigma_{Y\ 0°C}$ also showed similar trends. These observations validated $\sigma_{Y\ 0°C}$ measurements observed in our previous work (Chapter 2). The rheological parameter, $Thix_{\ 0°C}$, was the best to explain DT and FH. The greater initial structural formation observed in the melted matrix was highly related for DT and FH measurements in meltdown test. Thus, the thixotropic loop of melted ice cream is a promising parameter for correlating with DT and FH in ice cream melt tests, which could improve our knowledge of the physical properties of ice cream. Last, mix viscosity, extent of fat destabilization and overrun are important components in the structural arrangement of the ice cream matrix, which influence not only the mechanical behavior during the drip, but also of the structure retention after the meltdown test.

3.6 Acknowledgements

The authors thank Lexi Florac for her help in data collection and tracing of ice crystals and air cells. D.O. Freire would like to thank his scholarship from CNPq (National Council for Scientific and Technological Development – Brazil) and financial support from FDC (Frozen Dessert Center).

3.7 References

Amador, J., Hartel, R., Rankin, S., 2017. The Effects of Fat Structures and Ice Cream Mix Viscosity on Physical and Sensory Properties of Ice Cream. J. Food Sci. 82, 1851–1860. https://doi.org/10.1111/1750-3841.13780

Bolliger, S., Goff, H.D., Tharp, B.W., 2000. Correlation between Colloidal Properties of Ice Cream Mix and Ice Cream. Int. Dairy J. 10, 303–309.

Briggs, J.L., Steffe, J.F., Ustunol, Z., 1996. Vane Method to Evaluate the Yield Stress of Frozen Ice Cream. J. Dairy Sci. 79, 527–531. https://doi.org/https://doi.org/10.3168/jds.S0022-0302(96)76395-6

Chang, Y., Hartel, R.W., 2002. Measurement of Air Cell Distributions in Dairy Foams. Int. Dairy J. 12, 463–472. https://doi.org/https://doi.org/10.1016/S0958-6946(01)00171-6

Cottrell, J.I.L., Pass, G., Phillips, G.O., 1980. The effect of stabilisers on the viscosity of an ice cream mix. J. Sci. Food Agric. 31, 1066–1070. https://doi.org/10.1002/jsfa.2740311015

Dogan, M., Kayacier, A., Toker, Ö.S., Yilmaz, M.T., Karaman, S., 2013. Steady, dynamic, creep, and recovery analysis of ice cream mixes added with different concentrations of xanthan gum. Food Bioprocess Technol. 6, 1420–1433.

Dolz, M., Hernández, M.J., Delegido, J., Alfaro, M.C., Muñoz, J., 2007. Influence of xanthan gum and locust bean gum upon flow and thixotropic behaviour of food emulsions containing modified starch. J. Food Eng. 81, 179–186. https://doi.org/https://doi.org/10.1016/j.jfoodeng.2006.10.020

Donhowe, D.P., Hartel, R.W., Bradley, R.L., 1991. Determination of ice crystal size distributions in frozen desserts. J. Dairy Sci. 74, 3334–3344.

Eisner, M.D., Wildmoser, H., Windhab, E.J., 2005. Air cell microstructuring in a high viscous ice cream matrix. Colloids Surfaces A Physicochem. Eng. Asp. 263, 390–399.

El-Nagar, G., Clowes, G., Tudorică, C.M., Kuri, V., Brennan, C.S., 2002. Rheological quality and stability of yog-ice cream with added inulin. Int. J. Dairy Technol. 55, 89–93. https://doi.org/10.1046/j.1471-0307.2002.00042.x

Elliott, J.H., Ganz, A.J., 1977. Salad dressings—preliminary rheological characterization. J. Texture Stud. 8, 359–371.

Ferry, J.D., 1980. Viscoelastic Properties of Polymers. New York: John Wiley & Sons.

Goff, H.D., Freslon, B., Sahagian, M.E., Hauber, T.D., Stone, A.P., Stanley, D.W., 1995. Structural Development in Ice Cream—Dynamic Rheological Measurements. J. Texture Stud. 26, 517–536. https://doi.org/10.1111/j.1745-4603.1995.tb00801.x

Goff, H.D., Hartel, R.W., 2013. **Ice Cream**, Seventh. ed. Springer Science & Business Media, New York.

Goff, H.D., Spagnuolo, P., 2001. Effect of stabilizers on fat destabilization measurements in ice cream. Milchwissenschaft-Milk Sci. Int. 56, 450–453.

Granger, C., Leger, A., Barey, P., Langendorff, V., Cansell, M., 2005. Influence of formulation on the structural networks in ice cream. Int. Dairy J. 15, 255–262. https://doi.org/https://doi.org/10.1016/j.idairyj.2004.07.009

Gunasekaran, S., Ak, M.M., 2003. **Cheese Rheology and Texture.** CRC Press LLC, Boca Raton.

Gunasekaran, S., Ak, M.M., 2000. Dynamic oscillatory shear testing of foods — selected applications. Trends Food Sci. Technol. 11, 115–127. https://doi.org/https://doi.org/10.1016/S0924-2244(00)00058-3

Huppertz, T., Smiddy, M.A., Goff, H.D., Kelly, A.L., 2011. Effects of high pressure treatment of mix on ice cream manufacture. Int. Dairy J. 21, 718–726. https://doi.org/https://doi.org/10.1016/j.idairyj.2010.12.005

Javidi, F., Razavi, S.M.A., Behrouzian, F., Alghooneh, A., 2016. The influence of basil seed gum, guar gum and their blend on the rheological, physical and sensory properties of low fat ice cream. Food Hydrocoll. 52, 625–633. https://doi.org/https://doi.org/10.1016/j.foodhyd.2015.08.006

Li, J.-M., Nie, S.-P., 2016. The functional and nutritional aspects of hydrocolloids in foods. Food Hydrocoll. 53, 46–61. https://doi.org/https://doi.org/10.1016/j.foodhyd.2015.01.035

Muse, M.R., Hartel, R.W., 2004. Ice Cream Structural Elements that Affect Melting Rate and Hardness. J. Dairy Sci. 87, 1–10. https://doi.org/https://doi.org/10.3168/jds.S0022-0302(04)73135-5

Rao, M.A.A., 2007. **Rheology of Fluid and Semisolid Foods: Principles and Applications**, Second. ed. Springer Science & Business Media, New York.

Saha, D., Bhattacharya, S., 2010. Hydrocolloids as thickening and gelling agents in food: a critical review. J. Food Sci. Technol. 47, 587–597. https://doi.org/10.1007/s13197-010-0162-6

Sakurai, K., Kokubo, S., Hakamata, K., Tomita, M., Yoshida, S., 1996. Effect of production conditions on ice cream melting resistance and hardness. Milchwissenschaft 51, 451–454.

Sofjan, R.P., Hartel, R.W., 2004. Effects of overrun on structural and physical characteristics of ice cream. Int. Dairy J. 14, 255–262.

Steffe, J.F., 1996. **Rheological Methods in Food Process Engineering**. Freeman Press, East Lansing.

Sun, A., Gunasekaran, S., 2009. Yield Stress in Foods: Measurements and Applications. Int. J. Food Prop. 12, 70–101. https://doi.org/10.1080/10942910802308502

Thomas, W.R., 1997. Carrageenan, in: Imeson, A.P. (Ed.), Thickening and Gelling Agents for Food. Springer US, Boston, MA, pp. 45–59. https://doi.org/10.1007/978-1-4615-2197-6_3

Turquois, T., Rochas, C., Taravel, F.R., 1992. Rheological studies of synergistic kappa carrageenan-carob galactomannan gels. Carbohydr. Polym. 17, 263–268. https://doi.org/https://doi.org/10.1016/0144-8617(92)90168-P

Warren, M.M., Hartel, R.W., 2018. Effects of Emulsifier, Overrun and Dasher Speed on Ice Cream Microstructure and Melting Properties. J. Food Sci. 83, 639–647. https://doi.org/10.1111/1750-3841.13983

Warren, M.M., Hartel, R.W., 2014. Structural, Compositional, and Sensorial Properties of United States Commercial Ice Cream Products. J. Food Sci. 79, E2005–E2013. https://doi.org/10.1111/1750-3841.12592

Wildmoser, H., Scheiwiller, J., Windhab, E.J., 2004. Impact of disperse microstructure on rheology and quality aspects of ice cream. LWT-Food Sci. Technol. 37, 881–891.

Wu, B., Freire, D.O., Hartel, R.W., 2019. The Effect of Overrun, Fat Destabilization, and Ice Cream Mix Viscosity on Entire Meltdown Behavior. J. Food Sci. 84, 2562–2571. https://doi.org/10.1111/1750-3841.14743

Table 3.1 Means and standard errors for viscosity (mix viscosity at $50s^{-1}$), overrun, extent of fat destabilization (FD), air cell and ice crystal sizes of the ice creams with controlled structural formation. One-way ANOVA and Tukey's HSD ($\alpha = 0.05$) tests were performed to determine significant difference within the data. Source: Wu, Freire and Hartel (2019) and Chapter 2.

Stabilizer[1]	Air Flow	PS80	Code	Viscosity (mPa.s)	Overrun (%)	FD (%)	Air Cell Size (μm)	Ice Crystal Size (μm)
0%	8L.h^{-1}	0%	S1A1P1	22.0±0.3^{X,A}	50.1±0.8^{X,a,A}	10.1±2.0^{X,a,A}	22.4±1.1^{XY,b,A}	28.5±1.7^{X,a,A}
		0.015%	S1A1P2	24.4±0.5^{X,A}	49.0±0.5^{X,a,A}	11.2±1.8^{X,a,A}	24.3±1.4^{Y,b,A}	33.9±0.2^{Y,a,A}
		0.03%	S1A1P3	21.7±0.8^{X,A}	50.7±0.3^{X,a,A}	48.1±10.9^{Y,a,A}	18.1±1.0^{X,b,A}	32.3±0.5^{XY,a,A}
	11L.h^{-1}	0%	S1A2P1	22.0±0.3^{X,A}	75.9±0.6^{X,b,A}	17.6±0.6^{X,b,A}	18.3±1.5^{X,ab,A}	31.6±0.5^{X,a,A}
		0.015%	S1A2P2	24.4±0.5^{X,A}	74.6±0.7^{X,b,A}	21.8±1.5^{X,b,A}	20.1±1.1^{X,ab,A}	35.8±0.1^{Y,b,B}
		0.03%	S1A2P3	21.7±0.8^{X,A}	75.0±0.4^{X,b,AB}	65.7±5.7^{Y,a,A}	16.1±0.5^{X,ab,A}	35.4±0.6^{Y,b,A}
	15L.h^{-1}	0%	S1A3P1	22.0±0.3^{X,A}	99.0±0.5^{X,c,A}	27.7±0.9^{X,c,A}	16.0±1.0^{X,a,A}	31.0±0.3^{XY,a,A}
		0.015%	S1A3P2	24.4±0.5^{X,A}	100.4±0.9^{X,c,A}	28.2±2.2^{X,b,A}	16.2±1.1^{X,a,A}	33.4±0.6^{Y,a,A}
		0.03%	S1A3P3	21.7±0.8^{X,A}	99.4±0.8^{X,c,A}	73.9±4.5^{Y,a,A}	11.8±1.7^{X,a,A}	29.8±1.0^{X,a,A}
0.2%	8L.h^{-1}	0%	S2A1P1	88.6±3.4^{X,B}	49.8±0.4^{X,a,A}	14.6±1.7^{X,a,A}	30.1±0.2^{Y,c,C}	31.9±0.5^{X,a,A}
		0.015%	S2A1P2	95.7±0.9^{X,B}	50.0±0.7^{X,a,A}	14.3±3.5^{X,a,A}	24.8±0.3^{X,b,A}	37.7±0.8^{Y,b,B}
		0.03%	S2A1P3	89.4±3.3^{X,B}	50.2±0.4^{X,a,A}	46.6±6.1^{Y,a,A}	24.4±0.3^{X,c,B}	33.1±0.5^{X,a,A}
	11L.h^{-1}	0%	S2A2P1	88.6±3.4^{X,B}	75.4±0.5^{X,b,A}	24.8±1.1^{X,b,B}	24.6±0.3^{Y,a,B}	32.6±1.1^{X,a,A}
		0.015%	S2A2P2	95.7±0.9^{X,B}	74.8±0.5^{X,b,A}	22.7±4.7^{X,a,A}	20.5±0.7^{X,a,A}	38.2±0.2^{Y,b,C}
		0.03%	S2A2P3	89.4±3.3^{X,B}	75.8±0.3^{X,b,B}	57.2±3.5^{Y,ab,A}	18.8±0.7^{X,b,B}	33.2±1.0^{X,a,A}
	15L.h^{-1}	0%	S2A3P1	88.6±3.4^{X,B}	100.2±0.5^{X,c,A}	35.7±3.0^{X,c,B}	26.9±0.4^{Z,b,C}	32.1±0.5^{X,a,A}
		0.015%	S2A3P2	95.7±0.9^{X,B}	98.8±0.5^{X,c,A}	42.9±3.5^{X,b,B}	18.3±1.0^{Y,a,A}	33.0±0.7^{X,a,A}
		0.03%	S2A3P3	89.4±3.3^{X,B}	99.4±0.6^{X,c,A}	69.5±3.0^{Y,b,A}	13.9±0.7^{X,a,A}	33.4±0.3^{X,a,AB}
0.4%	8L.h^{-1}	0%	S3A1P1	264.2±5.3^{X,C}	50.3±0.4^{X,a,A}	38.3±3.2^{X,a,B}	26.8±0.5^{X,c,B}	32.9±0.2^{X,b,A}
		0.015%	S3A1P2	290.4±2.1^{Y,C}	50.3±0.3^{X,a,A}	51.6±2.2^{Y,a,B}	25.3±0.7^{X,b,A}	31.9±0.3^{X,b,A}
		0.03%	S3A1P3	288.2±1.4^{Y,C}	51.2±0.8^{X,a,A}	46.1±2.4^{XY,a,A}	25.3±0.7^{X,a,B}	37.1±0.9^{Y,a,B}
	11L.h^{-1}	0%	S3A2P1	264.2±5.3^{X,C}	75.4±0.5^{X,b,A}	53.3±1.7^{X,b,C}	23.2±0.4^{X,b,B}	30.7±0.4^{X,a,A}
		0.015%	S3A2P2	290.4±2.1^{Y,C}	75.0±0.5^{X,b,A}	58.8±1.6^{X,a,B}	22.8±0.4^{X,a,A}	29.5±0.4^{X,a,A}
		0.03%	S3A2P3	288.2±1.4^{Y,C}	74.3±0.4^{X,b,A}	56.1±1.7^{X,b,A}	23.0±0.5^{X,a,C}	35.3±0.7^{Y,a,A}
	15L.h^{-1}	0%	S3A3P1	264.2±5.3^{X,C}	100.4±1.3^{X,c,A}	65.9±1.7^{XY,c,C}	21.1±0.4^{X,a,B}	32.0±0.3^{X,b,A}
		0.015%	S3A3P2	290.4±2.1^{Y,C}	99.2±0.1^{X,c,A}	57.9±3.7^{X,a,C}	24.4±0.3^{Y,ab,B}	37.0±0.2^{Y,c,B}
		0.03%	S3A3P3	288.2±1.4^{Y,C}	99.3±0.6^{X,c,A}	71.6±1.6^{Y,c,A}	22.4±1.0^{XY,a,B}	36.6±1.3^{Y,a,B}

Legend: [1]Stabilizer is a commercial blend that includes locust bean gum, guar gum and carrageenan. $^{X, Y, Z}$ denote significant differences among ice cream with different levels of polysorbate 80. $^{a, b, c}$ denote significant differences among ice cream with different levels of air flow. $^{A, B, C}$ denote significant differences among ice cream with different levels of stabilizer.

Table 3.2 Means and standard errors for meltdown parameters (drip-through rate and final height) of the ice creams with controlled structural formation. One-way ANOVA and Tukey's HSD ($\alpha = 0.05$) tests were performed to determine differences within the data. Source: Wu, Freire and Hartel (2019).

Stabilizer[1]	Air Flow	PS80	Code	Drip-Through Rate ($g.min^{-1}$)	Final Height (%)
0%	8L.h^{-1}	0%	S1A1P1	$1.63\pm0.02^{X,a,A}$	$0.0\pm0.0^{X,a,A}$
		0.015%	S1A1P2	$1.79\pm0.07^{X,a,A}$	$7.7\pm1.2^{Y,a,A}$
		0.03%	S1A1P3	$1.00\pm0.11^{Y,a,A}$	$13.1\pm2.4^{Y,a,A}$
	11L.h^{-1}	0%	S1A2P1	$0.82\pm0.01^{X,b,A}$	$16.4\pm0.9^{X,b,A}$
		0.015%	S1A2P2	$0.82\pm0.02^{X,b,A}$	$17.8\pm1.1^{X,b,A}$
		0.03%	S1A2P3	$0.60\pm0.04^{Y,b,A}$	$19.7\pm1.5^{X,a,A}$
	15L.h^{-1}	0%	S1A3P1	$0.73\pm0.02^{X,c,A}$	$34.4\pm0.8^{X,c,A}$
		0.015%	S1A3P2	$0.65\pm0.01^{X,c,A}$	$38.2\pm1.8^{XY,c,A}$
		0.03%	S1A3P3	$0.47\pm0.04^{Y,b,A}$	$40.2\pm1.6^{Y,b,A}$
0.2%	8L.h^{-1}	0%	S2A1P1	$0.21\pm0.01^{X,a,B}$	$25.5\pm1.6^{X,a,B}$
		0.015%	S2A1P2	$0.19\pm0.01^{X,a,B}$	$30.0\pm2.0^{X,a,B}$
		0.03%	S2A1P3	$0.22\pm0.01^{X,a,B}$	$42.2\pm1.8^{Y,a,B}$
	11L.h^{-1}	0%	S2A2P1	$0.25\pm0.00^{X,b,B}$	$36.1\pm2.6^{X,b,B}$
		0.015%	S2A2P2	$0.25\pm0.00^{X,b,B}$	$34.0\pm6.2^{X,a,B}$
		0.03%	S2A2P3	$0.24\pm0.00^{X,b,B}$	$44.0\pm1.0^{X,a,B}$
	15L.h^{-1}	0%	S2A3P1	$0.25\pm0.00^{X,b,B}$	$48.2\pm1.8^{X,c,B}$
		0.015%	S2A3P2	$0.24\pm0.00^{X,b,B}$	$34.4\pm3.5^{Y,a,A}$
		0.03%	S2A3P3	$0.24\pm0.00^{X,b,B}$	$50.6\pm1.3^{X,b,B}$
0.4%	8L.h^{-1}	0%	S3A1P1	$0.10\pm0.01^{X,a,C}$	$45.3\pm2.1^{X,a,C}$
		0.015%	S3A1P2	$0.07\pm0.00^{Y,a,B}$	$57.8\pm1.4^{Y,a,C}$
		0.03%	S3A1P3	$0.08\pm0.00^{Y,a,B}$	$57.7\pm2.7^{Y,a,C}$
	11L.h^{-1}	0%	S3A2P1	$0.14\pm0.01^{X,a,C}$	$52.2\pm1.8^{X,b,C}$
		0.015%	S3A2P2	$0.09\pm0.00^{Y,b,C}$	$54.7\pm0.6^{X,a,C}$
		0.03%	S3A2P3	$0.09\pm0.00^{Y,a,C}$	$59.9\pm0.9^{Y,a,C}$
	15L.h^{-1}	0%	S3A3P1	$0.13\pm0.02^{X,a,C}$	$52.7\pm1.0^{X,b,B}$
		0.015%	S3A3P2	$0.07\pm0.01^{Y,a,C}$	$57.0\pm1.7^{XY,a,B}$
		0.03%	S3A3P3	$0.08\pm0.00^{Y,a,C}$	$59.1\pm2.2^{Y,a,C}$

Legend: [1]Stabilizer is a commercial blend that includes locust bean gum, guar gum and carrageenan. $^{X, Y, Z}$ denote significant differences among ice cream with different levels of polysorbate 80. $^{a, b, c}$ denote significant differences among ice cream with different levels of air flow. $^{A, B, C}$ denote significant differences among ice cream with different levels of stabilizer.

Table 3.3 Means and standard errors for rheological parameters measured at 0°C, storage modulus ($G'_{0°C}$), residual viscosity from the six-element model ($\eta_{0\ 0°C}$) in creep data, yield stress from stress growth ($\sigma_{Y\ 0°C}$) and thixotropy (Thix $_{0°C}$) from flow ramp. One-way ANOVA and Tukey's HSD ($\alpha = 0.05$) tests were performed to determine difference within the data. Source: Chapter 2.

Stabilizer[1]	Air System	PS80	Code	$G'_{0°C}$ (kPa)	$\eta_{0\ 0°C}$ (kPa.s)	$\sigma_{Y\ 0°C}$ (Pa)	Thix (Pa.s^{-1})
0%	8L.h^{-1}	0%	S1A1P1	$0.16\pm0.01^{X,a,A}$	$1.19\pm0.11^{X,a,A}$	$2.3\pm0.2^{X,a,A}$	$303\pm4^{X,a,A}$
		0.015%	S1A1P2	$0.17\pm0.01^{X,a,A}$	$2.07\pm0.25^{X,a,A}$	$2.2\pm0.1^{X,a,A}$	$317\pm4^{X,a,A}$
		0.03%	S1A1P3	$0.25\pm0.02^{Y,a,A}$	$5.58\pm0.33^{Y,a,A}$	$3.2\pm0.2^{Y,a,A}$	$347\pm7^{Y,a,A}$
	11L.h^{-1}	0%	S1A2P1	$0.16\pm0.01^{X,ab,A}$	$1.99\pm0.17^{X,a,A}$	$2.4\pm0.2^{X,a,A}$	$334\pm4^{X,b,A}$
		0.015%	S1A2P2	$0.18\pm0.01^{X,a,A}$	$2.98\pm0.23^{X,a,A}$	$3.1\pm0.2^{X,b,A}$	$341\pm5^{X,b,A}$
		0.03%	S1A2P3	$0.44\pm0.08^{Y,ab,A}$	$10.03\pm1.53^{Y,a,A}$	$6.7\pm1.2^{Y,a,A}$	$411\pm14^{Y,a,A}$
	15L.h^{-1}	0%	S1A3P1	$0.20\pm0.02^{X,b,A}$	$5.90\pm0.50^{X,b,A}$	$3.3\pm0.3^{X,b,A}$	$376\pm11^{X,c,A}$
		0.015%	S1A3P2	$0.27\pm0.04^{X,b,A}$	$7.41\pm0.68^{X,b,A}$	$4.1\pm0.3^{X,c,A}$	$388\pm7^{X,c,A}$
		0.03%	S1A3P3	$1.81\pm0.67^{Y,b,A}$	$45.49\pm13.87^{Y,b,A}$	$26.9\pm8.1^{Y,b,A}$	$680\pm117^{Y,a,A}$
0.2%	8L.h^{-1}	0%	S2A1P1	$0.28\pm0.02^{X,a,A}$	$11.02\pm0.88^{X,a,B}$	$4.9\pm0.4^{X,a,A}$	$434\pm13^{X,a,A}$
		0.015%	S2A1P2	$0.26\pm0.03^{X,a,A}$	$10.68\pm1.16^{X,a,A}$	$4.6\pm0.4^{X,a,A}$	$454\pm36^{X,a,B}$
		0.03%	S2A1P3	$1.66\pm0.32^{Y,a,B}$	$50.55\pm2.96^{Y,a,B}$	$20.4\pm2.8^{Y,a,B}$	$795\pm26^{Y,a,B}$
	11L.h^{-1}	0%	S2A2P1	$0.58\pm0.04^{X,b,B}$	$21.23\pm1.70^{X,b,B}$	$8.5\pm1.2^{X,ab,A}$	$527\pm24^{X,ab,B}$
		0.015%	S2A2P2	$0.40\pm0.06^{X,a,A}$	$18.58\pm1.47^{X,b,B}$	$8.7\pm0.3^{X,b,A}$	$534\pm31^{X,a,B}$
		0.03%	S2A2P3	$2.84\pm0.19^{X,b,C}$	$94.44\pm6.31^{Y,b,B}$	$34.0\pm1.8^{Y,a,B}$	$1059\pm44^{Y,a,B}$
	15L.h^{-1}	0%	S2A3P1	$0.87\pm0.03^{X,c,B}$	$41.60\pm4.23^{X,c,B}$	$13.3\pm2.0^{X,b,A}$	$620\pm40^{X,b,B}$
		0.015%	S2A3P2	$0.72\pm0.10^{X,b,A}$	$30.51\pm2.41^{X,c,A}$	$11.4\pm0.9^{X,c,A}$	$680\pm30^{X,b,B}$
		0.03%	S2A3P3	$3.46\pm0.29^{Y,b,B}$	$133.17\pm15.33^{Y,c,B}$	$53.8\pm6.4^{Y,b,B}$	$1325\pm114^{Y,b,B}$
0.4%	8L.h^{-1}	0%	S3A1P1	$0.61\pm0.06^{X,a,B}$	$34.57\pm3.73^{X,a,C}$	$19.5\pm2.6^{X,a,B}$	$909\pm85^{X,a,B}$
		0.015%	S3A1P2	$0.99\pm0.15^{X,a,B}$	$53.80\pm4.83^{X,a,B}$	$35.6\pm2.5^{Y,a,B}$	$1261\pm50^{Y,a,C}$
		0.03%	S3A1P3	$0.81\pm0.09^{X,a,A}$	$60.08\pm14.32^{X,a,B}$	$28.7\pm2.0^{Y,a,C}$	$1024\pm121^{XY,a,B}$
	11L.h^{-1}	0%	S3A2P1	$1.26\pm0.08^{X,b,C}$	$66.60\pm3.23^{X,b,C}$	$31.0\pm3.9^{X,ab,B}$	$1065\pm46^{X,ab,C}$
		0.015%	S3A2P2	$1.69\pm0.10^{Y,b,B}$	$75.05\pm3.57^{X,a,C}$	$39.3\pm4.1^{X,a,B}$	$1415\pm59^{Y,a,C}$
		0.03%	S3A2P3	$1.42\pm0.15^{XY,b,B}$	$78.06\pm5.90^{X,ab,B}$	$32.1\pm1.8^{X,a,B}$	$1365\pm111^{Y,a,C}$
	15L.h^{-1}	0%	S3A3P1	$1.69\pm0.08^{X,c,C}$	$84.30\pm5.98^{X,c,C}$	$40.6\pm4.9^{X,b,B}$	$1250\pm65^{X,b,C}$
		0.015%	S3A3P2	$1.88\pm0.21^{X,b,B}$	$113.15\pm13.91^{X,b,B}$	$43.0\pm3.7^{X,a,B}$	$1418\pm61^{X,a,C}$
		0.03%	S3A3P3	$1.96\pm0.14^{X,c,AB}$	$113.53\pm9.21^{X,b,B}$	$53.8\pm5.4^{X,b,B}$	$1340\pm94^{X,a,B}$

Legend: [1]Stabilizer is a commercial blend that includes locust bean gum, guar gum and carrageenan. $^{X, Y, Z}$ denote significant differences among ice cream with different levels of polysorbate 80. $^{a, b, c}$ denote significant differences among ice cream with different levels of air flow. $^{A, B, C}$ denote significant differences among ice cream with different levels of stabilizer.

Table 3.4 Parameter estimates and coefficients of determination (R^2) for three term exponential models (n=27), in which rheological parameters measured at 0°C, storage modulus ($G'_{0°C}$), residual viscosity from the creep data fitted by six-element model ($\eta_{0\ 0°C}$), yield stress from stress growth ($\sigma_{Y\ 0°C}$) and rheological destruction from up and down flow ramp ($Thix_{\ 0°C}$ from FR). from the oscillatory thermo-rheometry (OTR), creep/recovery, stress growth and flow ramp measurements.

Y (Meltdown Parameters)	X (Rheological Parameters)	Coefficients a	b	c	R^2
Drip-Through Rate ($g.min^{-1}$)	$G'_{0°C}$ (Pa) from OTR	0.19^{**}	7.40	$-1.2E\text{-}02^{**}$	0.73
Final Height (%)	$G'_{0°C}$ (Pa) from OTR	51.93^{***}	-63.87^{***}	$-3.1E\text{-}03^{**}$	0.75
Drip-Through Rate ($g.min^{-1}$)	$\eta_{0\ 0°C}$ (Pa.s) from Creep	0.17^{***}	1.67^{***}	$-1.9E\text{-}04^{***}$	0.83
Final Height (%)	$\eta_{0\ 0°C}$ (Pa.s) from Creep	54.38^{***}	-44.71^{***}	$-4.4E\text{-}05^{***}$	0.84
Drip-Through Rate ($g.min^{-1}$)	$\sigma_{Y\ 0°C}$ (Pa) from Stress Growth	0.19^{***}	8.18^{*}	$-8.1E\text{-}01^{***}$	0.85
Drip-Through Rate ($g.min^{-1}$)	$Thix_{\ 0°C}$ ($Pa.s^{-1}$) from FR	0.17^{***}	198.99	$-1.6E\text{-}02^{***}$	0.90
Final Height (%)	$Thix_{\ 0°C}$ ($Pa.s^{-1}$) from FR	55.42^{***}	-132.68^{***}	$-3.6E\text{-}03^{***}$	0.87

Legend: "a" is asymptote, "b" is scale and "c" is growth rate from three term exponential (TTE) models.
$^{*}p_{ChiSquare}<0.05$, $^{**}p_{ChiSquare}<0.01$; $^{***}p_{ChiSquare}<0.001$.

Table 3.5 Parameter estimates and coefficients of determination (R^2) for three term exponential models (n=27), in which rheological parameters measured at 0°C, , storage modulus ($G'_{0°C}$), residual viscosity from the creep data fitted by six-element model ($\eta_{0\ 0°C}$), yield stress from stress growth ($\sigma_{Y\ 0°C}$) and rheological destruction ($Thix_{\ 0°C}$). from the oscillatory thermo-rheometry (OTR), creep/recovery, stress growth and flow ramp measurements.

Y (Meltdown Parameters)	X (Rheological Parameters)	Coefficients d	e	R^2
Final Height (%)	$\sigma_{Y\ 0°C}$ (Pa) from Stress Growth	63.8^{***}	7.4^{***}	0.82

Legend: "d" is maximum reaction rate and "e" is inverse affinity from Michaelis Menten model.
$^{*}p(_{ChiSquare}<0.05$, $^{**}p_{ChiSquare}<0.01$; $^{***}p_{ChiSquare}<0.001$.

Chapter 4

4 Effects of Structural Elements, Compositional and Physical Parameters on Melting Behavior and Rheological Properties of Commercial Ice Cream Products

4.1 Abstract

Effects of formulation, process and storage conditions on ice cream structure and sensory properties were studied in previous work. Moreover, effects of structural properties on rheological and meltdown properties as well as correlations between rheology and meltdown behavior of ice creams with controlled structural formation were also studied. However, effects of structural properties on rheology as well as correlations between rheology and meltdown properties of commercial ice cream products have not yet been studied. Thus, fifteen full fat commercial ice cream products from the United States were analyzed for total fat, total solids, mix density, overrun, extent of fat destabilization, air cell size, ice crystal size and drip-through (DT) rate. Fat destabilization was the main structural component to influence DT as well as rheological parameters, such as storage modulus (G'), residual viscosity (η_0) from six-element model (generalized Kelvin-Voigt model with six elements fitted in creep data) and yield stress (σ_Y), at 0 and 20°C. Other structural parameters, such as overrun, air cell size, total solids and mix density, depending on conditions, also affected DT and rheological properties. Between DT and rheological parameters ($G'_{0°C}$, $\eta_{0\,0°C}$ and $\sigma_{Y\,0°C}$), an exponential decay was generally observed for both data of commercial samples and previous models proposed for ice creams with controlled structural formation. Finally, from the observed data for commercial samples and the model suggested from previous work, it is suggested that $G'_{0°C}$ was a satisfactory rheological parameter to predict DT of ice cream products.

4.2 Introduction

The ice cream matrix is, at the same time, an emulsion, dispersion and foam (Cook and Hartel, 2010). Structural elements, such as ice crystals, partially-crystalline emulsified fat globules (individual and clustered globules) and air cells, are dispersed in an unfrozen serum phase (Goff and Hartel, 2013). Those structural components greatly depend on the formulation, process (Warren and Hartel, 2014), hardening and storage conditions (Chang and Hartel, 2002a).

The nature and intricate arrangement of these structural elements directly affect the meltdown and rheological properties of the ice cream matrix. In fact, the rheological behavior of ice cream is mainly governed by the ice phase (Goff et al., 1995; Granger et al., 2005; Shama and Sherman, 1966; Wildmoser et al., 2004), although the other structural elements can also affect the rheological behavior of both ice cream and melted foam (Goff et al., 1995; Goff and Hartel, 2013).

In previous work, Wu et al. (2019) made ice cream with different mix viscosity, fat destabilization and overrun, and explored the melting behavior of the ice cream, while the effects of those same structural components on rheological properties were studied in another work (Chapter 2). The correlation between rheological and meltdown properties was also previously studied (Chapter 3). Moreover, Warren and Hartel (2014) characterized the wide range of microstructure, behavior and sensory properties of full fat, low fat and nonfat commercial ice cream products. However, the meltdown and rheological properties as well as their correlation in commercial ice cream products have not yet been studied.

In this context, a combination of oscillatory, transient and rotational rheological measurements at different temperatures can provide substantial information about the structure and melting behavior, as well as confirm the results of one test with another. This study aimed to evaluate the effects of structural elements, compositional and physical parameters on the melting

behavior and rheological properties of commercial ice cream products. Last, the study was restricted to full fat ice cream since the wider variety of formulations could make the interpretation of the rheological data even more complex.

4.3 MATERIALS AND METHODS

4.3.1 Materials

Fifteen different full fat ice cream products (vanilla flavor) were purchased from 4 local grocery stores in Madison, Wisconsin, USA. Samples included 2 types of ice cream sandwiches and 13 full fat ice creams (≥10% milkfat content). Three samples from the same lot were purchased of each brand. The samples were stored at -28.9°C until analysis. Prior to analysis, samples were equilibrated at -20°C for at least 12 hours. Samples were analyzed in triplicate and at random. Specific formulations, process and storage conditions of each product were unknown.

4.3.2 Compositional, Physical and Structural Measurements (Structural Components)

4.3.2.1 Fat content

Total fat was measured using the Mojonnier Extraction Method (adapted from AOAC Method 989.05).

4.3.2.2 Total solids

Total solids were measured by microwave method using the “Ice Cream Mix Application” in the CEM SMART System 5 Microwave Moisture/Solids Analyzer (CEM Corporation, Matthews, N.C., U.S.A.).

4.3.2.3 Ice cream mix density

Ice cream mix density was calculated according to Equation 4.1, which utilizes fat content and total solids (Hui, 2006):

$$\rho_{Mix}\left[\frac{\text{Wt.}}{\text{L mix}}\right] = \frac{\text{(Wt. per liter of water)}}{\left[\frac{\%\text{ fat}}{100}\times 1.07527 + \left(\frac{\%\text{ total solids}}{100} - \frac{\%\text{ Fat}}{100}\right)\times 0.6329 + \frac{\%\text{ Water}}{100}\right]} \quad (4.1)$$

4.3.2.4 Overrun

Overrun was calculated using the volume displacement method (Archimedes' Principle), according to (Clarke, 2004). The method was also detailed in the previous work by Warren and Hartel (2014).

4.3.2.5 Particle/Fat Globule Size Distribution

Particle size distribution of the melted ice creams was obtained by laser light diffraction and light scattering using the Malvern Mastersizer 2000 (Malvern Instruments Ltd., Worcestershire, United Kingdom). Two to four drops of melted ice cream (4°C) were loaded into the cell to obtain obscuration values between 13 and 15%. The refractive indexes of 1.33 and 1.47 were set for the dispersant (deionized water) and dispersed phase (milk fat). Absorbance was set at 0.01.

In general, the extent of fat destabilization is obtained by comparing the peak of initial emulsion from ice cream mix curve to the peak of destabilized fat from melted ice cream curve (Bolliger et al., 2000). As described by Warren and Hartel (2014), some assumptions were made to obtain the extent of destabilized fat since the ice cream mixes were not available in this study. Sample 129 is used as example for a typical particle size distribution curve of the commercial

samples in Figure 4.1. The peak between 0.1-0.3μm represents the casein micelles. The extent of fat destabilization was calculated by dividing the percent volume of the destabilized fat peak, which is the third peak (beginning around 5 μm), by the total percent volume of fat particles, which is the initial emulsion peak (second peak between 0.3-5 μm) plus the destabilized fat peak (third peak).

4.3.2.6 Air Cell Size Distribution

Air cell size analysis was performed at -6°C in a temperature controlled, insulated glove box as described by Chang and Hartel (2002b). Images were taken using a solid state camera (Cohu Eletronics Div., San Diego, CA, USA) attached to an optical light microscope (Optiphot, Nikon, Inc., Garden City, NY, USA), and recorded using OPTIMAS software (OPTIMAS v6.1, Optimas Corp., Meyer Instruments Inc., Houston, Tex. U.S.A.). Six images approximately were taken at 40x magnification to ensure at least 300 air cells were counted from each container. Air cells were analyzed using Image Pro Plus software (Image Pro Plus 7.0, Media Cybernetics, Inc., Rockville, MD, USA) and results were collected in a Microsoft Excel spreadsheet.

4.3.2.7 Ice Crystal Size Distribution

Ice crystal analysis was carried out at -15°C in a temperature controlled, insulated glove box, as described by Donhowe et al. (1991). Images were taken using a solid state camera (Cohu Eletronics Div., San Diego, CA, USA) attached to an optical light microscope (Optiphot, Nikon, Inc., Garden City, NY, USA), which had a 30W LED light system, and recorded using OPTIMAS software (OPTIMAS v6.1, Optimas Corp., Meyer Instruments Inc., Houston, Tex. U.S.A.). Fifteen

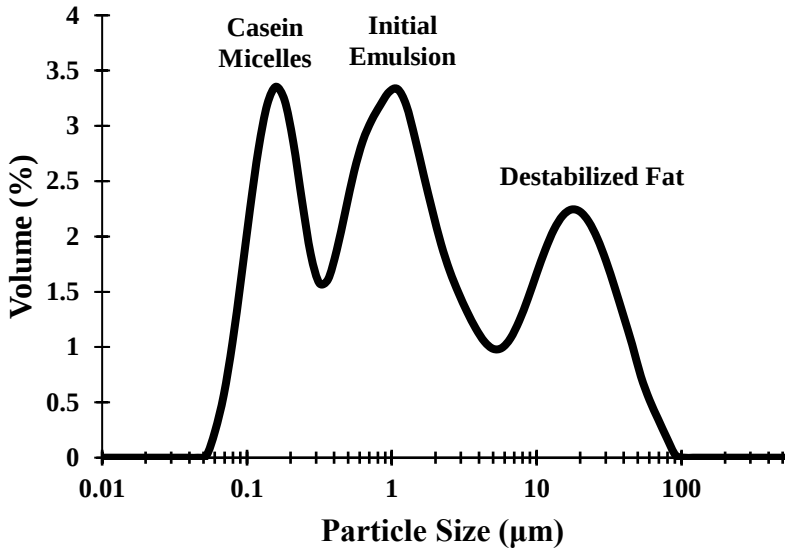

Figure 4.1: Particle size distribution of sample 129 used as example of melted ice cream products. Casein micelle peak between 0.1-0.3 µm, initial emulsion peak between 0.3-5 µm, and destabilized fat peak beginning around 5 µm.

images approximately were taken at 40x magnification to ensure at least 300 ice crystals were counted from each container. Ice crystals were traced using Microsoft Softonic Paintbrush for Mac. Then, traced images were analyzed using Image Pro Plus software (Image Pro Plus 7.0, Media Cybernetics, Inc., Rockville, MD, USA) and results were collected in a Microsoft Excel spreadsheet.

4.3.3 Drip-Through Rate

Slabs of ice cream weighing approximately 80g (dimensions varied slightly from each other due to the different overruns) were cut into cylindrical shape from the center of ice cream containers (pints). The meltdown tests were performed at ambient temperature (22.3±0.3°C). Samples were placed on a metal screen (3holes.cm^{-1}) supported by a metal ring. The melted ice cream dripped through the screen and was collected in a 1000mL beaker, which was placed on a scale (Pioneer^{TM}, Ohaus, Pine Brook, NJ, USA). The weight was recorded for 2 hours. In addition, pictures were taken during the test every minute for visual comparisons. The weight (g) of the melted ice cream on the scale was plotted as a function of time (minutes). The slope of the linear part of the curve was obtained as the drip-through rate (Bolliger et al., 2000).

Preparation of ice cream sandwiches for the meltdown test: First, wafers were removed and discarded from the ice cream sandwiches before the test. Three ice cream portions, which weighed approximately 80 g in total, from 3 sandwiches were placed as a stack on metal screen for the test. Surface area of the 3 rectangular bars stacked (around 161 cm^2) was inside the surface area range of cylindrical samples (from 139 to 195 cm^2) in this study. A pretest was performed by comparing drip-through of an ice cream (pint) that was cut in both cylinders and standard rectangular bars (mimicking the ice cream portion from sandwiches). The drip-through rate of the

stack of ice cream bars (1.69±0.14 $g.min^{-1}$) was similar to the ice cream cylinder (1.53±0.17 $g.min^{-1}$); thus, the modified test for sandwich shapes was considered comparable to other products

4.3.4 Rheological properties of Commercial Ice Cream Products

The rheological properties of commercial ice cream products were measured using a rotational rheometer and parallel plate of 25mm diameter with crosshatched surface (DHR-2, TA Instruments, New Castle, DE, USA). The temperature of the lower plate was controlled by Stepped Peltier Plate system, which was attached to a liquid recirculating chiller (ThermoCube, Solid State Cooling Systems, Wappingers Falls, NY, USA) with a 20% ethanol solution. The temperature of the upper plate was controlled by Upper Heated Plate system for Peltier Plate, which was attached to a liquid recirculating chiller (Isotemp 4100 R35, Fisher Scientific, Waltham, MA, USA) with a 50% ethylene glycol solution. From the center of the ice cream container was cut a slice, which was transferred to an insulated glove box at -20°C. A cylindrical tool was used to obtain disks of 25 and 2.5mm of diameter and height, respectively. The temperature of the parallel plates in the rheometer was preset at -15 or -5°C. The ice cream disk was placed in the center of the lower plate. The upper plate was loaded onto the ice cream disk without trimming the disk. Protocols of each test are described in the subsequent sections. Two ice creams with a wide range of fat destabilization (9 and 71% fat destabilization) were used to develop protocols for the rheological tests. These ice creams were made to cover the broad structural variety of the commercial ice creams evaluated in this study.

4.3.4.1 Oscillatory Thermo-Rheometry (OTR)

The oscillatory thermo-rheometry (OTR) adapted from Wildmoser et al. (2004) and Granger et al. (2005) was performed from -15 to 25°C. Preliminary tests were performed to ensure all OTR analyses were performed within the Linear Viscoelastic Regime (LVR). From -15 to 0°C and from 0 to 25°C, strains of 0.01 and 0.1%, respectively, were used. The sample was loaded at -15°C using 1800µm as initial gap. An insulating thermal cover for the Peltier Plate Systems was placed on top of the sample (Chapter 2). The experiment started when the axial force was lower than 10N. After that, the sample was held for 2 minutes at a gap of 1800 µm, which ensured the full contact of the upper plate to the ice cream disk; the axial force was set to 0N (±0.1 N) and a soak time of 15 minutes was used to equilibrate temperature and axial force. A continuous oscillation at 10rad.s^{-1} angular frequency was applied to the sample. The sampling time was adjusted to 4 seconds at a temperature ramp rate of 0.5°C.min^{-1}. The storage (G') and loss (G") moduli as well as loss tangent (tanδ) were obtained; subsequently, the data were reduced to obtain one data point every 0.5°C.

4.3.4.2 Creep-Recovery

Creep and recovery measurements, adapted from Steffe (1996) and Dogan et al. (2013), were carried out at 0 and 20°C. Parallel plates were preset at -5°C and an ice cream disk was loaded to a 1800µm gap. Temperature was adjusted to 0 or 20°C and held for 10 minutes to equlibrate the sample. A constant stress of 0.15 or 0.05Pa at 0 or 20°C, respectively, (both stress loads were within the LVR) was applied to the sample and the deformation (% strain) was recorded during 150 seconds. The load was relieved, and the structure recovery (% strain) was recorded for another 150 seconds. The collected data points decreased logarithmically with time (fast sampling).

Maximum creep strain (MCS) and recovery were obtained. Moreover, a generalized Kelvin-Voigt model, a mechanical model composed of one Maxwell unit (one spring and one dashpot linked in series) in series with one or more Kelvin-Voigt (one spring and one dashpot linked in parallel) units, was fitted to the creep compliance data using the TRIOS software (2019 TA Instruments–Waters LLC, New Castle, USA).

4.3.4.3 Stress Growth

Stress growth test was performed at 0 and 20°C. The sample was loaded at -5°C and upper plate was loaded to 1800µm. An insulating thermal cover was placed on top, temperature was adjusted to 0 or 20°C, and the sample was equilibrated for 10 minutes. A constant shear rate of 0.01 s^{-1} was applied and stress was recorded as function of time for 1800 seconds or until the sample reached the steady state flow (5% tolerance within 30 seconds in three consecutive sampling). Shear modulus (G), equilibrium viscosity (η_∞) and work of structure breakdown (W) were obtained from a phenomenological analysis adapted from Elliott and Ganz (1977) and Rao (2007).

4.3.5 Statistical Analysis

All data were analyzed using JMP statistical software (JMP Pro 14.0, SAS Inst., Cary, N.C., U.S.A. 2018). In the first part, drip-through rate and rheological parameters were explained or predicted by structural components using simple (SLR) or multiple (MLR) linear regression models. All possible models with up to seven of those structural components were fitted. Three models with the lowest Schwarz's Bayesian information criterion (BIC) were selected. If a model showed variance inflation factor (VIF) above 10, it was replaced by the next model with the lowest

BIC. A diagnostic was performed to evaluate the linear behavior, independent errors, constant variance and normal distribution of the errors in those three models. The final model was chosen by the lowest BIC value, but other criteria, such as lower p-value, Akaike's information criterion (AIC) and adjusted coefficient of determination (R^2_{adj}), were also used to check the consistency of the final model. After that, correlations between rheological responses and drip-through rate by using linear or nonlinear equations were used to better understand the melting behavior of the commercial samples. The final nonlinear / linear model was chosen based on the lowest BIC value and R^2.

4.4 Results and Discussion

The effects of structural components (compositional, physical and structural parameters), on the drip-through rate and rheological properties of commercial ice cream products were evaluated. In addition, linear/nonlinear models using selected rheological parameters as predictors of the drip-through rate were used to provide indirect associations between those structural components and drip-through rate of the commercial samples.

4.4.1 Compositional/Physical Parameters and Structural Elements

Table 4.1 provides an overview of the structural components of ice creams available in the national (United States) and local markets (Wisconsin). As observed by Warren and Hartel (2014), the wide range of structure is due to the formulations, equipment and process conditions used in the manufacture of each product. In the same way, as the hardening and storage conditions were unknown, structural changes probably occurred until the samples were purchased.

4.4.1.1 Total Fat

Total fat presented narrow range varying from 9.8 to 14.2% and overall mean 11.1±0.1%. This range was expected for the full fat ice creams, including standard, premium and sandwich versions, and agreed in general with the ice creams (full fat) assessed by Warren and Hartel (2014).

4.4.1.2 Total Solids

Total solids ranged from 37.0 to 40.7% and presented an overall mean of 38.6±0.1%. Warren and Hartel (2014) found correlation between total fat and total solids, which was not corroborated by this study (p=0.0792). This result may be due to the unknown formulations of the full fat commercial ice cream products.

4.4.1.3 Density of Ice Cream Mix

Ice cream mix density ranged from 1.082 to 1.110kgL^{-1} and presented an overall mean of 1.102±0.001kgL^{-1}. Mix density showed very strong inverse correlation with total fat (r=-0.8444, p=<0.0001). This correlation aligned with the observations from Warren and Hartel (2014). Since fat has lower density than the serum phase of ice cream mix, higher fat content led to lower density.

4.4.1.4 Overrun

Overrun measurements extended from 32.6 to 121.4% and presented an overall mean of 83.1±2.3%. Overrun showed strong inverse and moderate direct correlations with total fat (r=-0.7381, p=0.0017) and ice cream mix density (r=0.6329, p=0.0113), respectively. The inverse correlation between overrun and total fat corroborated with Warren and Hartel (2014). This correlation may be due to higher overrun levels in standard versions (or economy versions)

associated with the minimum standard requirements for milk fat based on the Standard of Identity for ice cream (Code of Regulations, Title 2 Food and Drugs, Part 135 Frozen Desserts) in the United States. In the same way, the correlation between overrun and mix density may also be related to the lower cost. In general, standard versions of full fat ice creams are associated with lower total solids and total fat content (~10%), which is correlated to the higher values of mix density.

4.4.1.5 Percent of Partially-Coalesced Fat Globules (Fat Destabilization)

Fat destabilization spanned from 4.5 to 77.0% and presented an overall mean of 42.1±1.6%. No correlation was found between fat destabilization and overrun ($p=0.9541$) in this study, whereas Segall and Goff (2002) and Warren and Hartel (2018) found a direct correlation using batch and continuous freezers, respectively. This is probably due to the use of different formulations and unknown manufacturing processes of the commercial ice cream products.

4.4.1.6 Air Cell Size

Mean air cell size for the commercial ice creams extended from 10.5 to 31.0μm, with an overall mean size of 18.3±1.6μm. There was a moderate inverse correlation with fat destabilization ($r=-0.5951$, $p=0.0193$). This corroborated with Warren and Hartel (2018), who reported that higher shear forces and/or emulsifiers (types and levels) benefit the formation of smaller air cells during the dynamic freezing. No correlation was found between air cell size and overrun ($p=0.1875$) in this study, which aligns with the observations from Warren and Hartel (2014). On the other hand, this correlation is not supported by Sofjan and Hartel (2004) and Warren and Hartel (2018). As observed by Chang and Hartel (2002a), the air cell size also depends on hardening step and storage

conditions. Therefore, although the hardening step and storage conditions are unknown, it is possible the air cell size changed since those factors were not controlled before purchasing the ice cream products.

4.4.1.7 Ice Crystal Size

Mean ice crystal size ranged from 32.6 to 53.5μm with overall mean size of 39.0±1.8μm. No correlation was found between ice crystal size and other structural components. This was probably due to either the random formulation, process and storage conditions or the narrow ranges of structural components presented by full fat commercial ice cream products.

4.4.2 Drip-Through Rate

The drip-through rate ranged from 2.00 (very rapid) to 0.13 (very slow) $g.min^{-1}$. Samples 880 and 957 are used to illustrate the drip-through rate behavior of the ice cream products in Figure 4.2A. Above 20% fat destabilization extent (FD), drip-through rate (DT) was low in the commercial samples, which is also illustrated in Figure 4.2B. This correlation aligned with Warren and Hartel (2014) and other previous work (Bolliger et al., 2000; Muse and Hartel, 2004; Segall and Goff, 2002; Warren and Hartel, 2018, 2014). Fat destabilization was the only structural component to affect DT. Warren and Hartel (2014), studying structural, compositional, and sensorial properties of commercial ice cream products (full fat, low fat and nonfat), also found that higher total fat and total solids as well as smaller ice crystal size led to slower drip-through rate. The authors also found positive correlation between overrun and drip-through rate. Here, DT was not affected by these other parameters probably due to the narrow range of total solids, total fat and ice crystal size observed in the products evaluated in this study.

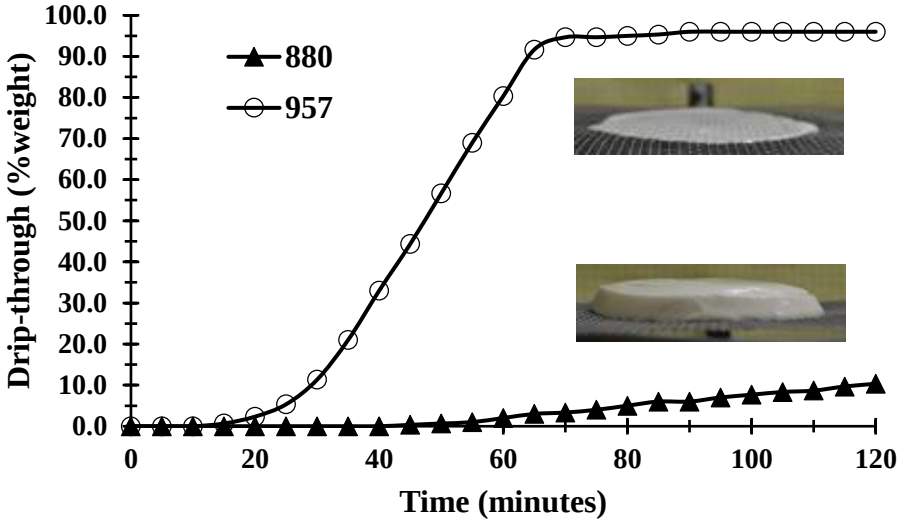

(A)

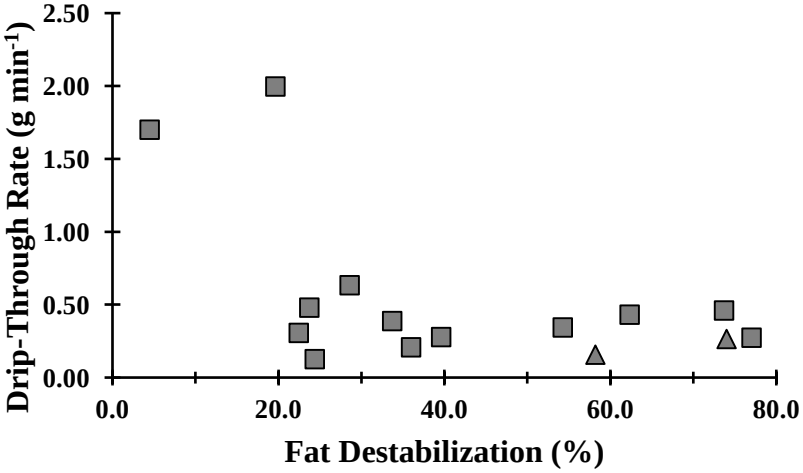

(B)

Figure 4.2: (A) Drip-through curves of samples 880 and 957. (B) Drip-through rate behavior of commercial ice cream products predicted by extent of fat destabilization. Triangles are ice cream sandwich samples.

It is possible that mix viscosity also had some effect on the DT in commercial products. As observed in previous work (Chapter 2), mix viscosity affected the rheological behavior of ice cream. In Chapter 3, excellent correlations were found between rheological parameters and meltdown behavior. Furthermore, Wu et al. (2019) found mix viscosity as an important structural component in the meltdown behavior of ice cream. However, more studies are required since mix viscosity was not evaluated in these commercial ice cream products.

4.4.3 Rheological Properties of the Ice Cream Matrix

Specific rheological measurements, namely storage modulus (G') and loss tangent (tanδ) from oscillatory thermo-rheometry (OTR), residual viscosity (η_0) from six-element model (generalized Kelvin-Voigt model) fitted in creep compliance data, and yield stress (σ_Y) from stress growth measurements at 0°C, were studied based on previous work (Chapter 2) for comparison purposes. These measurements were then correlated with the measured structural components.

4.4.3.1 Oscillatory Thermo-Rheometry (OTR)

Samples 880 and 957, which showed the lowest and the highest DT, were also chosen to represent the behavior of the storage (G') and loss (G") moduli of the commercial samples during the OTR (Figure 4.3A). The G' and G" curves were separated in three zones, as proposed by Wildmoser et al. (2004).

In zone I, at -15°C, G' ($G'_{-15°C}$) was greater than G" ($G"_{-15°C}$) in all ice cream products. The difference (between G' and G") ranged from 0.1 to 2.4MPa. These findings were close to previous work (Chapter 2), which ranged from 0.2 to 1.2MPa. The $\tan\delta_{-15°C}$ ranged from 0.76 to 0.94. However, no structural component was found to affect $G'_{-15°C}$, $G"_{-15°C}$ and $\tan\delta_{-15°C}$ (α=0.05). The

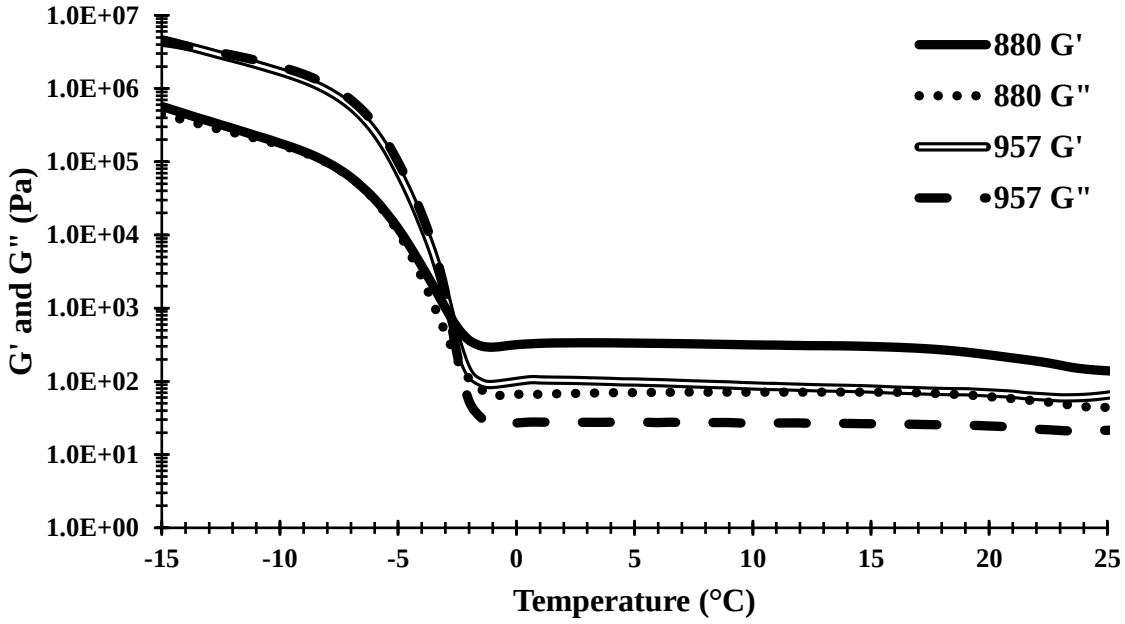

(A)

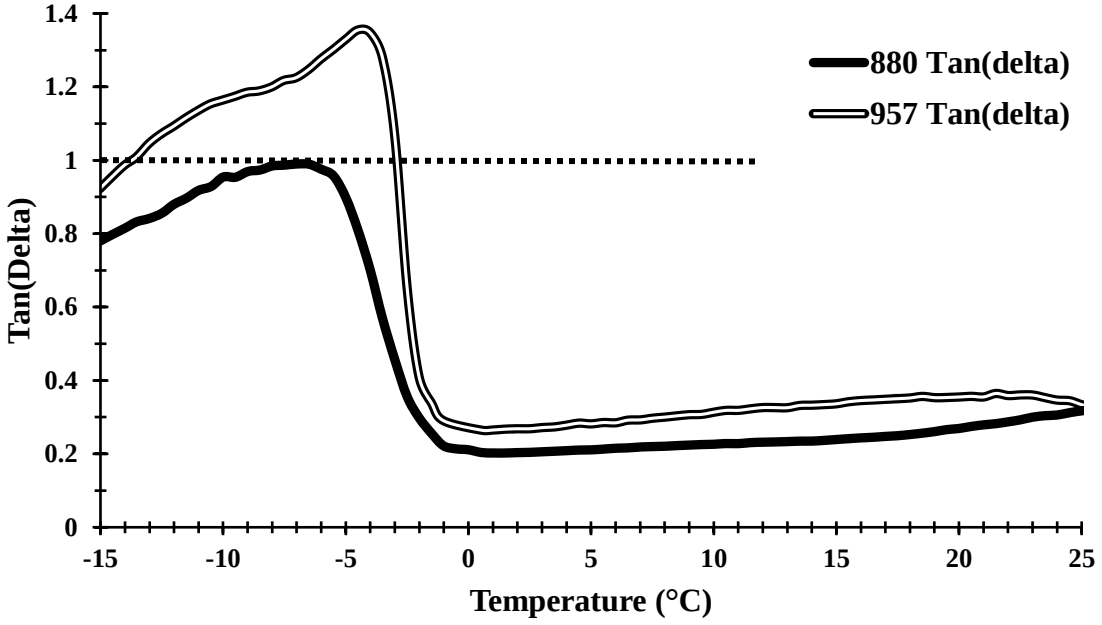

(B)

Figure 4.3: Behavior of storage (G') and loss (G") moduli (A) as well as tanδ (B) during oscillatory thermo-rheometry (OTR) of the samples 880 and 957.

same behavior was observed at -10°C. This is probably due to the unknown formulation, process, storage conditions as well as strong influence of ice phase on rheology of the commercial samples.

In zone II, as observed in previous work (Eisner et al., 2005; Wildmoser et al., 2004; Chapter 2), G' and G" showed a sharp decrease and G' approached G" in all samples; therefore, tanδ (G"/G') presented a peak during OTR, which was also observed in previous work (Granger et al., 2005; Chapter 2). At the peak in tanδ, G' was lower than G" in most samples, except sample 880, where tanδ was at 1.00. As ice melts, the ice cream matrix increases in liquid-like behavior (Goff and Hartel, 2013; Granger et al., 2005; Chapter 2). In previous work (Chapter 2), mix viscosity, overrun and fat destabilization were suggested to affect tanδ peak magnitude. Formulation, such as stabilizer (Goff et al., 1995), and process, such as low-temperature extrusion (Wildmoser et al., 2004), were also found to affect G' and G" from -10 to -6°C and from -10 to 0°C, respectively. Formation of a tanδ peak is probably related to structural rearrangement as ice melts in the matrix. Samples with more elastic behavior would have less structural rearrangement and hence, lower tanδ peak. However, further studies are required to describe the specific structural events that influence the peak formation observed in tanδ during OTR.

In zone III, all commercial samples showed solid-like behavior (G'>G") at 0°C. The difference between G' and G" ranged from 0.08 to 1.43kPa. This range is quite different compared to previously discussed difference at -15°C, where the difference ranged from 0.2 to 1.2MPa (Chapter 2). This difference at -15°C compared to 0°C is due to the strong influence of ice phase on G' and G" of the frozen matrix. After the ice crystals melted, the structure depends on the melted serum phase, fat globules, proteins and air phase (Goff and Hartel, 2013).

MLR models between G' and G" at 0°C and the structural composition/structure parameters are shown in Table 4.2. Fat destabilization presented strong direct effects on G' and G", while mix density presented moderate direct effects on $G'_{0°C}$ and $G"_{0°C}$. Results of the Tukey's HSD test are presented in Table 4.3 for $G'_{0°C}$ and $G"_{0°C}$. As illustrated in Figure 4.4A, direct correlations, but with a lot of scatter, were observed between fat destabilization and both $G'_{0°C}$ and $G"_{0°C}$, which aligned with other work (Eisner et al., 2005; Granger et al., 2005; Wildmoser et al., 2004; Chapter 2).

The $\tan\delta_{0°C}$ ranged from 0.19 to 0.26 (Table 4.3). This range was quite different from $\tan\delta_{-15°C}$ previously discussed, which ranged from 0.76 to 0.94. The greater values of $\tan\delta_{-15°C}$ when compared to $\tan\delta_{0°C}$ suggests a behavior transition of a highly concentrated solution at -15°C to a weak gel at 0°C. This aligned with previous work (Chapter 2) and suggested that the melted ice cream matrix had turned to a weak gel at 0°C. Moreover, no effect of structural components was found to influence $\tan\delta_{0°C}$.

As observed in MLR models at 20°C (Table 4.2), fat destabilization showed strong and very strong direct effects on $G'_{20°C}$ and $G"_{20°C}$, respectively, and total solids and overrun showed moderate direct effects on $G'_{20°C}$ and $G"_{20°C}$. Tukey's HSD test was also used to complement the analysis for $G'_{20°C}$ and $G"_{20°C}$ (Table 4.3). The effects of fat destabilization on $G'_{20°C}$ and $G"_{20°C}$ are illustrated in Figure 4.4B. The stronger correlations (significant coefficients in MLR) between fat destabilization with $G'_{0°C}$ and $G'_{20°C}$ when compared to $G"_{0°C}$ and $G"_{20°C}$ are probably due to the physical properties of milk fat, which contribute more to the elastic than viscous behavior of the melted ice cream. Moreover, the network of fat crystals in the partially-coalesced fat globules led to greater elasticity at 0°C when compared to 20°C. There was also a direct correlation between total solids and $G'_{20°C}$ or $G"_{20°C}$, which might be related to levels of stabilizer, milk solids nonfat,

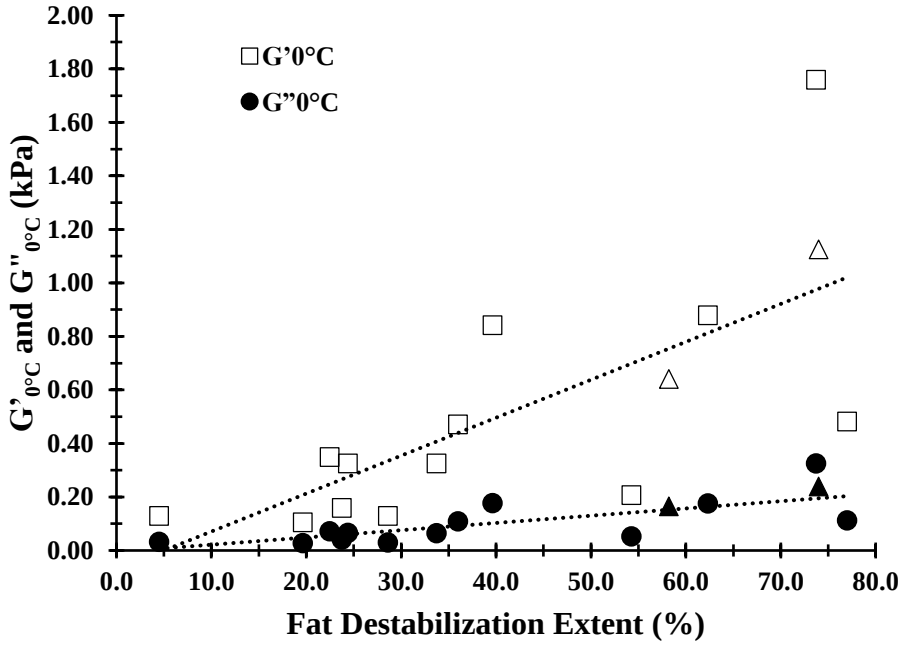

(A)

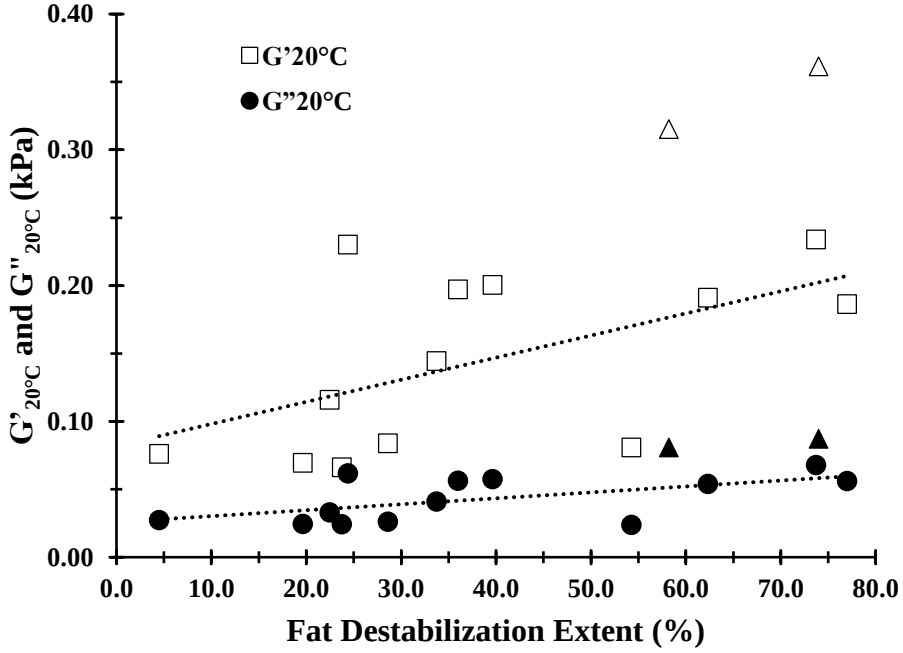

(B)

Figure 4.4: Example for behavior of storage (G') and loss (G") moduli, obtained from oscillatory thermo-rheometry (OTR), against extent of fat destabilization at (A) 0°C and (B) 20°C. Triangles are ice cream sandwich samples. Lines are linear trend line.

among other solids. A moderate direct correlation between $G'_{20°C}$ and overrun was probably related to greater interactions of serum phase components as well as fat globules within a thinner lamella in high overrun ice creams. Apparently, as fat destabilization decreased in impact on the elasticity, the role of other structural components, such as total solids and overrun, became more important in the melted matrix at 20°C.

As observed in previous work (Chapter 2), after a sharp decline from its peak during ice melting, tanδ achieved a minimum value and then started to increase slightly. At 20°C, $\tan\delta_{20°C}$ ranged from 0.24 to 0.37 (up from 0.19 to 0.26 at 0°C). This confirmed that the melted matrix had lost elasticity as temperature increased from 0 to 20°C. As observed in Table 4.3, $\tan\delta_{20°C}$ values increased in all samples, except sample 410 (ice cream sandwich), compared to $\tan\delta_{0°C}$. According to MLR, only fat destabilization affected $\tan\delta_{20°C}$ (Table 4.2). As observed in Tables 4.1 and 4.3, samples with lower fat destabilization showed higher $\tan\delta_{20°C}$. As the network of partially-coalesced fat globules decreased (lower fat destabilization), elasticity was lowered in the melted matrix. Low coefficient of determination was observed for $\tan\delta_{20°C}$ (Table 4.2). Moreover, although sample 410 showed relatively high fat destabilization (58.2%), the stability of $\tan\delta_{20°C}$ compared to $\tan\delta_{0°C}$ (Table 4.3) suggests that other structural components, such as mix viscosity, may also play important role in the melted matrix at 20°C. However, further studies are needed to identify which other structural components may also affect $\tan\delta_{20°C}$.

4.4.3.2 Creep and Recovery Measurements

In general, oscillatory tests are used to study viscoelastic properties of food products. However, another type of test is required to understand possible internal structures in food matrix and their changes, depending on composition (Dogan et al., 2013; Dolz et al., 2008; Toker et al.,

2013) or process. Therefore, creep and recovery tests are often used for these types of investigation (Dogan et al., 2013).

Oscillatory stress amplitude sweeps were used to characterize the LVR. After that, a constant stress ($\sigma_{constant}$), which was within the LVR, was applied to the melted sample at 0 or 20°C in creep measurement. Strain (γ) was obtained over time (t) for 150s. In the recovery measurement, stress was released, and recovery of structure was measured for another 150s. Maximum creep strain (MCS) and percentage recovery were obtained from creep and recovery measurement, respectively, as illustrated by sample 880 at 0°C in Figure 4.5A. Moreover, shear creep compliance (J) over time was also obtained by dividing γ by $\sigma_{constant}$ (Steffe, 1996). Creep compliance data were fitted using generalized Kelvin-Voigt model (Ahmed, 2015; Gunasekaran and Ak, 2003; Kaschta and Schwarzl, 1994; Purkayastha et al., 1984).

$$J(t) = J_0 + \sum_{i=1}^{N} J_i[1 - e^{-t/\tau_i}] + t/\eta_0 \quad (4.4)$$

Here, J(t) is compliance over time (t), τ_i is retardation times correspondent to compliances J_i (represent viscoelastic behavior), J_0 is instantaneous compliance (represent elastic behavior) and η_0 is steady-state viscosity or residual viscosity (represent viscous flow). Kelvin-Voigt model with more than one retardation time is often used to describe creep behavior of biological and polymeric systems (Gunasekaran and Ak, 2003; Purkayastha et al., 1984). In general, the simplest possible model is chosen to represent creep behavior (Purkayastha et al., 1984). A six-element model was chosen, as illustrated in Figure 4.5B. Spring, G_0, and dashpot, η_0, are elastic modulus and residual viscosity of the Maxwell unit, respectively. Springs, G_1 and G_2, and dashpots, η_1 and η_2, are retarded elastic moduli and internal viscosities of first and second Kelvin-Voigt units, respectively

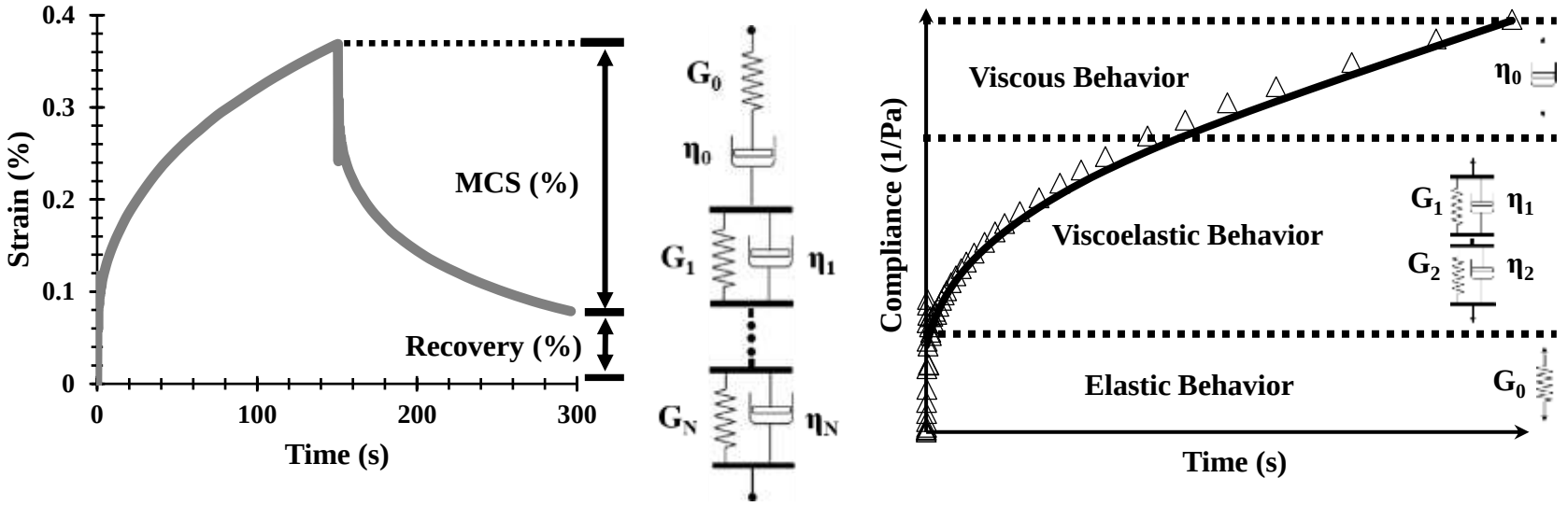

(A) (B) (C)

Figure 4.5: (A) Creep and recovery measurements for sample 880 at 0°C used as example maximum creep strain (MCS) and recovery; (B) springs and dashpots of the generalized Kelvin-Voigt model (Maxwell unit in series with N Kelvin-Voigt units); (C) observed creep compliance data over time with six-element model for sample 880.

(Dogan et al., 2013). Observed data from sample 880 were fitted by the six-element model (R^2>0.99) in Figure 4.5C as example. The six-element model was also used in previous work to describe creep behavior of ice cream mix as well as melted ice cream (Shama and Sherman, 1966; Sherman, 1966; Chapter 2).

At 0°C, fat destabilization was the only structural component to affect $G_{0\ 0°C}$, $G_{1\ 0°C}$ and $G_{2\ 0°C}$ in their respective MLR model (data not shown here). The most significant effect of fat destabilization was on $G_{0\ 0°C}$, which is the spring of the Maxwell unit in Figure 4.5C. Fat destabilization was also the only parameter to affect $\eta_{0\ 0°C}$, $\eta_{1\ 0°C}$ and $\eta_{2\ 0°C}$ at 0°C (data not shown here). Interestingly, among all six-element model parameters at 0°C, the MLR model for $\eta_{0\ 0°C}$ was the only model that was not found significant (p=0.0514). This is probably due to the more elastic than viscous behavior of the matrix at 0°C. In Chapter 2, after ice was melted, a greater elasticity was also found at lower temperatures, which was mainly related to milkfat properties. For comparison purposes with previous work (Chapter 2 and 3), although the MLR model for $\eta_{0\ 0°C}$ was not found significant, η_0 is discussed as example for six-element model parameters as well as creep and recovery measurements at 0 and 20°C. Moreover, here, as in Chapter 2, η_0 will be also compared to yield stress since both measurements were probably obtained under near transient conditions. Tukey's HSD test is used to complement the analysis for $\eta_{0\ 0°C}$ in Table 4.3.

In general, both $\eta_{0\ 0°C}$ and $\eta_{0\ 20°C}$ increased as fat destabilization increased, with a slightly greater effect on $\eta_{0\ 0°C}$, as observed in Figure 4.6A. This is probably due to greater elasticity of milk fat at 0°C compared to 20°C. Overall, as overrun increased, both $\eta_{0\ 0°C}$ and $\eta_{0\ 20°C}$ increased slightly, as observed in Figure 4.6B. Direct correlation between overrun and $\eta_{0\ 0°C}$ aligned with previous work (Chapter 2). This is probably due to greater interactions of serum phase molecules, fat globules, among other components, within a thinner lamella in ice creams with higher overrun.

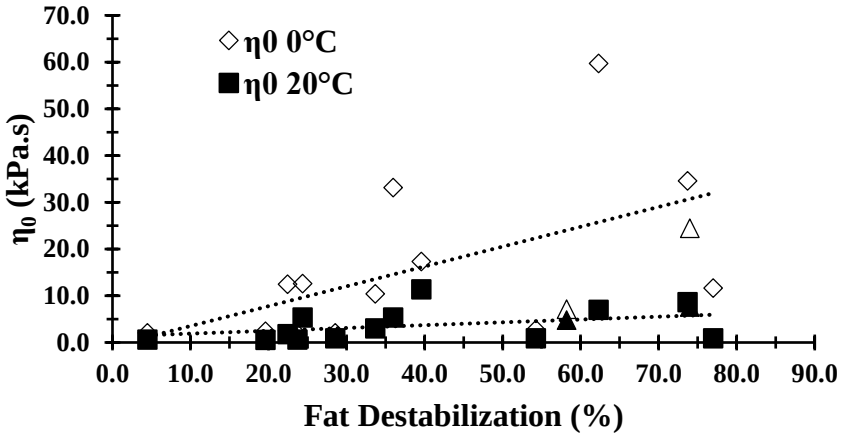

(A)

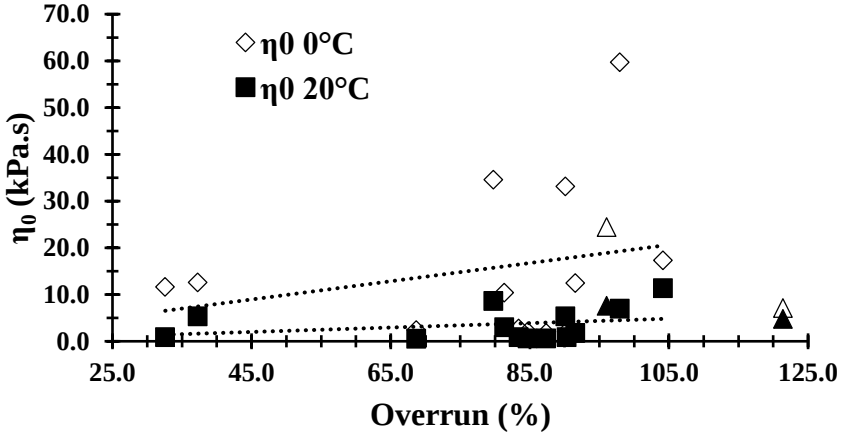

(B)

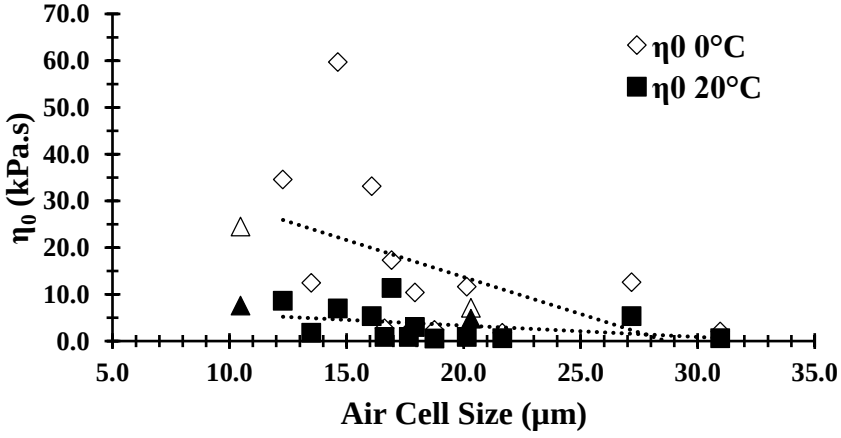

(C)

Figure 4.6: Influence of (A) fat destabilization, (B) overrun and (C) air cell size on residual viscosity (η_0) from six-element models at 0 and 20°C. Triangles are ice cream sandwich samples. Triangles are ice cream sandwich samples. Lines are linear trend line.

Further, both $\eta_{0\ 0°C}$ and $\eta_{0\ 20°C}$ increased, in general, as air cell size decreased (Figure 4.6C). The smaller air cells, with greater air surface area, probably led to greater molecular interactions at the serum phase/air cell interface.

In addition, both $\eta_{0\ 0°C}$ and $\eta_{0\ 20°C}$ increased (Table 4.3) as total solids increased (Table 4.1). Those correlations are probably related to higher levels of components, such as milk solids nonfat, stabilizer, among other solids. Although Dogan et al. (2013) studied mix formulations with different concentrations of xanthan gum, they reported an increase in η_0 (obtained from four-component Burger model) as xanthan gum levels increased. As was observed in Figures 4.6A, 4.6B and 4.6C, structural components showed impact on $\eta_{0\ 0°C}$ greater than $\eta_{0\ 20°C}$. This was probably related to changes in structure as temperature increased. Moreover, in previous work (Chapter 2), mix viscosity was also found to affect $\eta_{0\ 0°C}$. It is possible that mix viscosity may affect $\eta_{0\ 0°C}$ in this study as well. However, more studies are needed since mix viscosity was not analyzed in these commercial ice cream products.

4.4.3.3 Stress Growth (Constant Low Shear Rate)

Stress growth, also known as stress overshoot, encompasses rheological measurements with matrix intact, and in transient and equilibrium flows. In literature, the test is described both based on transient viscoelastic flow that occurs in the sample (Rao, 2007; Steffe, 1996) and on steady state flow reached at the end of the test, where due to large deformation, the sample is completely disrupted (Lucey et al., 1997; Luyten et al., 1994). Thus, parameters obtained from this test could confirm results of other tests and provide information about the yield stress (σ_y). In previous work, σ_y was related to the ability of ice cream to dip or scoop (Briggs et al., 1996) and to the ability of the matrix to remain on the top of the screen after meltdown test (Chapter 2).

Phenomenological analysis from Elliott and Ganz (1977) and Rao (2007) was adapted using stress growth measurement at 0°C. As observed in Figure 4.7A for sample 880, t is time when constant shear rate ($\dot{\gamma}$) is applied to the sample 880, σ_A is the stress at the end of elastic portion of the curve, σ_y is peak stress (which corresponds to yield stress) and σ_∞ is equilibrium shear stress. From those stress values and their respective times, their correspondent deformations, such as γ_{tA}, γ_y (which is strain correspondent to σ_y) and $\gamma_{t\infty}$, were found. Moreover, total deformation that occurs at different shearing time is the product of shear rate and time. Therefore, equations for shear modulus (G), equilibrium viscosity (η_∞) and work of structure breakdown (W) can be calculated from the previous definitions:

$$G = {d\sigma}/{d\gamma} = \sigma_A/\gamma_{t_A} \tag{4.5}$$

$$\eta_\infty = \sigma_\infty/\dot{\gamma} \tag{4.6}$$

$$W = \dot{\gamma}\int_A^B(\sigma - \sigma_\infty)\mathrm{dt} \tag{4.7}$$

Here, A is time that stress curve overshot σ_∞ and B is time that σ_∞ was reached. Therefore, the area above the extrapolated σ_∞ line was obtained as excess work of structure breakdown, W.

Stress growth measurement for sample 957, which showed the highest drip-through rate, is also presented in Figure 4.7B for comparison purposes. Overall, the effects of structural components on shear modulus (G) and equilibrium viscosity (η_∞) corroborated previous

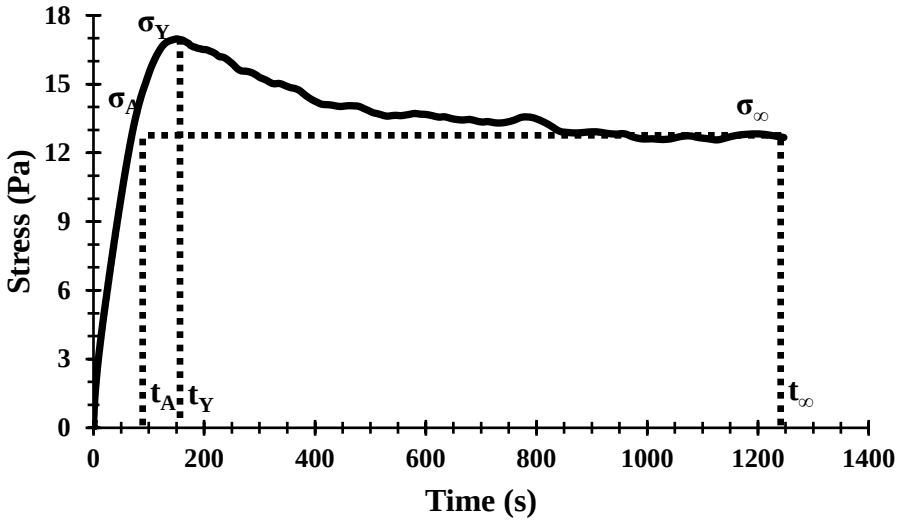

(A)

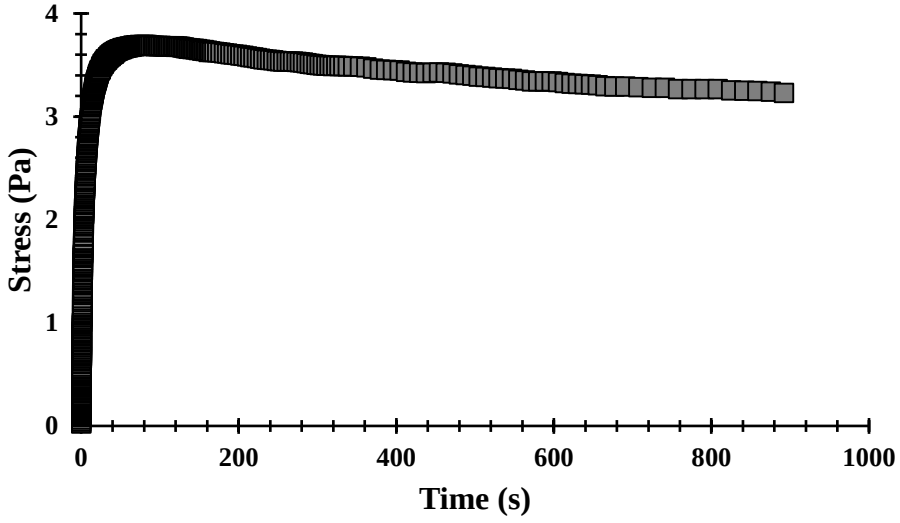

(B)

Figure 4.7: (A) Schematic diagram for phenomenological analysis using sample 880 at 0°C and (B) stress growth test for samples 957 at 0°C.

measurements of G' (from OTR) and η_0 (from six-element model in creep test), respectively, at both 0 and 20°C. This was also observed in the previous work (Chapter 2). Measurements of σ_y are presented to illustrate parameters obtained in stress growth measurements.

The MLR model for $\sigma_{y\ 20°C}$ at 20°C is presented in Table 4.2. Extent of fat destabilization and total solids showed moderate direct effects on $\sigma_{y\ 20°C}$. Although the MLR model for $\sigma_{y\ 0°C}$ at 0°C was not significant (p=0.0871), fat destabilization extent showed a moderate direct effect on $\sigma_{y\ 0°C}$. Thus, Tukey's HSD test is also used to complement the analysis for $\sigma_{y\ 0°C}$ and $\sigma_{y\ 20°C}$ in Table 4.3.

Overall, as fat destabilization increased, $\sigma_{y\ 0°C}$ and $\sigma_{y\ 20°C}$ increased, similar to previous work (Chapter 2). As shown in Figure 4.8A, fat destabilization had more effect on σ_y at 0°C compared to 20°C. In this transient flow zone, an increased network of fat globules provided greater elasticity to the matrix, requiring greater force to initiate the flow. Greater impact of fat destabilization at 0°C is probably related to more fat crystals as compared to 20°C. Generally, as overrun increased, both $\sigma_{y\ 0°C}$ and $\sigma_{y\ 20°C}$ increased, as observed in Figure 4.8B, which agreed with previous work (Chapter 2). The thinner lamellae with higher overrun increased the strength of serum phase/air cell interface to provide greater resistance to initiate flow. In general, as air cell size decreased, both $\sigma_{y\ 0°C}$ and $\sigma_{y\ 20°C}$ increased (Figure 4.8C). Greater air surface area provided by smaller air cells probably promoted greater interactions at the serum phase/air cell interface, which could increase σ_y measurements. As either mix density or total solids increased, $\sigma_{y\ 0°C}$ or $\sigma_{y\ 20°C}$ increased. These correlations were probably related to higher levels of unknown components that could contribute to mix density and total solids, such as milk solids nonfat and stabilizer, among others. Therefore, correlations of $\sigma_{y\ 0°C}$ or $\sigma_{y\ 20°C}$ with mix density or total solids are not further

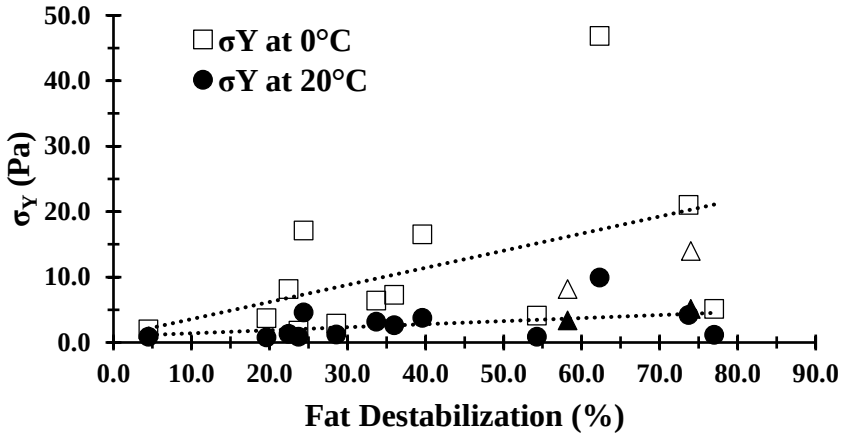

(A)

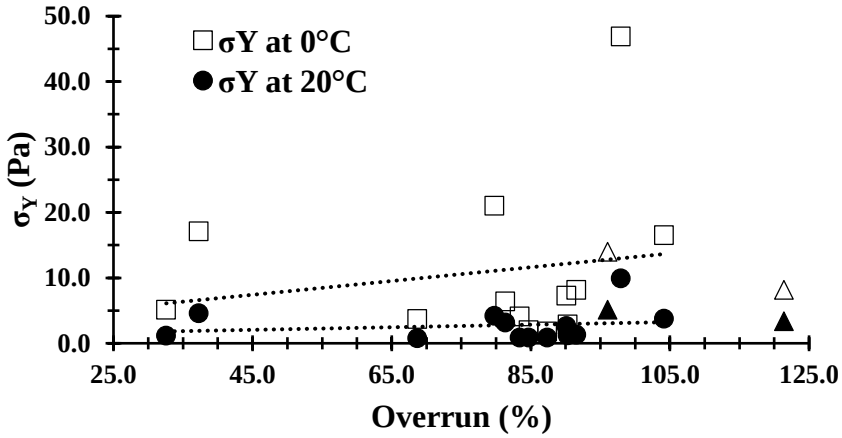

(B)

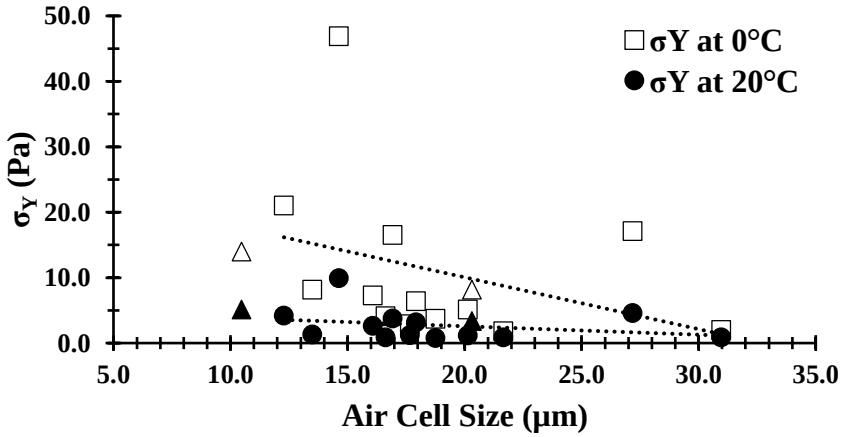

(C)

Figure 4.8: Influence of (A) fat destabilization, (B) overrun and (C) air cell size on residual viscosity (σ_Y) from six-element models at 0 and 20°C. Triangles are ice cream sandwich samples. Lines are linear trend line.

discussed. The greater impact of structural components on σ_y at 0°C than at 20°C was probably due to structure changes with increased temperature. Last, as mix viscosity affected σ_y at 0°C in previous work (Chapter 2), mix viscosity may probably affect $\sigma_{y\ 0°C}$ in commercial ice cream products. However, more studies are required since mix viscosity was not evaluated for commercial ice cream products.

Finally, in previous work (Chapter 2), recovery and $\eta_{0\ 0°C}$ from creep and recovery were compared to $\sigma_{y\ 0°C}$ at 0°C since those measurements were obtained under near transient conditions in the melted ice creams. Here, a very strong linear correlation was found between $\eta_{0\ 0°C}$ and $\sigma_{y\ 0°C}$ at 0°C (R^2=0.79, p<0.0001), while a significatively strong correlation was found between $\eta_{0\ 20°C}$ and $\sigma_{y\ 20°C}$ at 20°C (R^2=0.50, p=0.0034). As the low constant load (within LVR) is applied to the sample, the melted matrix is deformed over time until it reaches the equilibrium (viscous behavior in Figure 4.5C. In this region the sample probably initiated the flow since the highest correlation was found between η_0 and σ_y at both temperatures, 0 and 20°C. In this way, although η_0 and σ_y were obtained from different inputs, constant stress and shear rate, respectively, η_0 and σ_y was obtained in close transient conditions. Therefore, these significant linear correlations also validated σ_y measurements for commercial ice cream products.

4.4.4 Correlations between Rheological Parameters and Drip-Through Rate (DT)

Melting behavior of ice cream is an important quality parameter. Essential melting parameters are commonly obtained from meltdown tests (Wu et al., 2019). Nevertheless, meltdown test has its limitations, such as sample size, heat transfer rate, sample volume and weight, among other external variables. As highlighted in previous work (Chapter 3), structural components and their intrinsic arrangement influence both rheological and meltdown behaviors.

Therefore, correlations between parameters from an instrumental test, such as rheometry, and parameters from meltdown test, such as drip-through rate (DT), may provide important information about melting behavior in ice cream.

Correlations between three rheological parameters at 0°C, $G'_{0°C}$, $\eta_{0\ 0°C}$ and $\sigma_{Y\ 0°C}$, and DT were chosen for comparison purposes with previous work (Chapter 3). The use of the previous model (chapter 3) in this study is limited due to unknown formulation and process of commercial ice cream products. However, common trends were observed between the two studies.

The correlation between $G'_{0°C}$ and DT for commercial ice creams is compared to the exponential model from previous work (Chapter 3) in Figure 4.9A. The exponential decay model has three parameters, growth rate (-1.2E-02Pa^{-1}), scale (7.40$g.min^{-1}$) and asymptote (0.19$g.min^{-1}$) (Equation 3.1 in Chapter 3). Samples with low $G'_{0°C}$ (below 130Pa) presented high DT (above 1.7$g.min^{-1}$). As $G'_{0°C}$ increased in samples up to around 200Pa, an exponential decay in DT was observed**.** Samples with $G'_{0°C}$ above 200Pa showed a plateau with DT below 0.46$g.min^{-1}$. Although the proposed model shows large variability in 95% confidence interval, data from ice cream commercial products for $G'_{0°C}$ fitted well in the model from previous work (Chapter 3). In the model, high DT occurs in samples with low $G'_{0°C}$ and DT shows exponential decay as $G'_{0°C}$ increases slightly and reaches an asymptote, where, further no effect is observed in DT values. Interestingly, other than one commercial sample with the highest $G'_{0°C}$, all observed data from this study fitted well in the 95% confidence interval of the model proposed in Chapter 3 (Figure 4.9A).

The correlation between $\eta_{0\ 0°C}$ and DT is presented in Figure 4.9B, along with the model reported in previous work (Chapter 3). The exponential decay model also presents growth rate (-1.9E-04Pa^{-1}), scale (1.67$g.min^{-1}$) and asymptote (0.17$g.min^{-1}$) (Equation 3.1 in Chapter 3). Also creases.

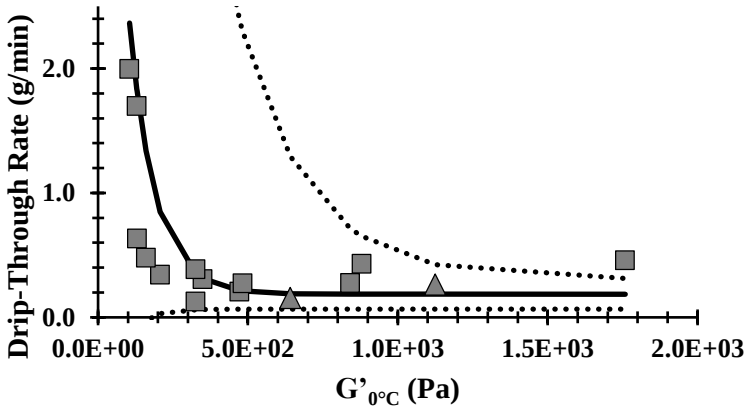

(A)

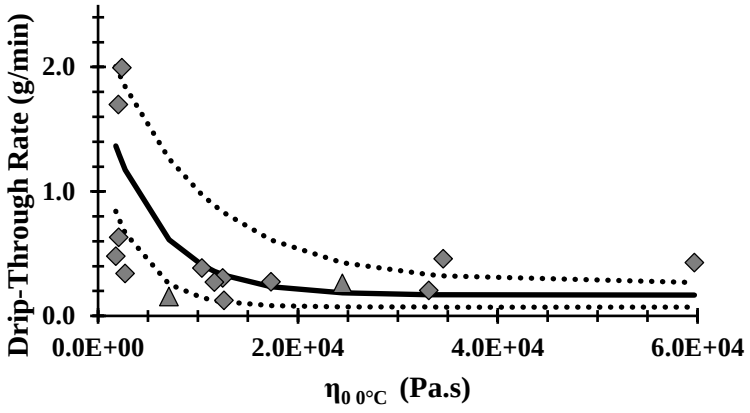

(B)

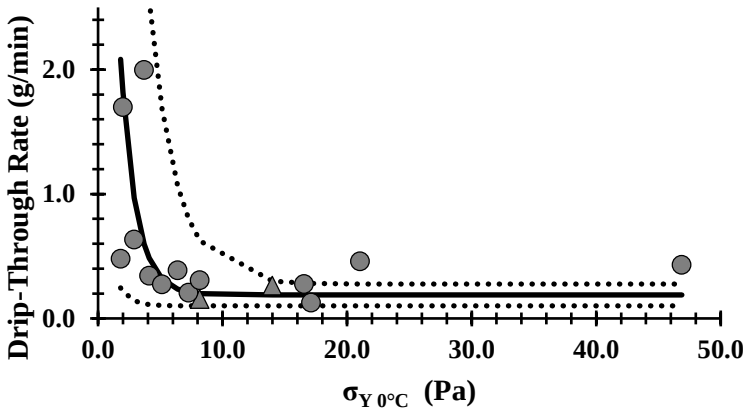

(C)

Figure 4.9 Correlations of drip-through rate with (A) storage modulus ($G'_{0°C}$), (B) residual viscosity **(**$\eta_{0\,0°C}$) and (C) yield stress ($\sigma_{Y\,0°C}$) at 0°C compared to exponential decay models for ice creams with controlled structural formation from previous work (Chapter 3). Triangles are ice cream sandwich samples. Lines and dotted lines are models and their 95% confidence intervals, respectively, from previous work (Chapter 3).

in this case, in general, DT was high with low $\eta_{0\ 0°C}$ and exponentially decayed as $\eta_{0\ 0°C}$ increased. After that, DT reaches a lower asymptote, where, $\eta_{0\ 0°C}$ did not affect DT. However, many commercial samples were out of the 95% confidence interval of the model. In particular, the sample with the lowest value of $\eta_{0\ 0°C}$ showed a relatively low DT (0.48g.min^{-1}). Thus, data from commercial ice cream products for $\eta_{0\ 0°C}$ did not fit well in the model from previous work (Chapter 3).

An exponential decay model for correlation between $\sigma_{Y\ 0°C}$ and DT, which was reported in previous work (Chapter 3), is shown in Figure 4.9C. The exponential model also has three parameters, growth rate (-8.1E-01Pa^{-1}), scale (8.18g.min^{-1}) and asymptote (0.19g.min^{-1}) (Equation 3.1 in Chapter 3). As before, samples with low $\sigma_{Y\ 0°C}$ generally had high DT, which then decayed exponentially and reached a lower asymptote with increasing $\sigma_{Y\ 0°C}$. However, the commercial sample with the lowest $\sigma_{Y\ 0°C}$ (1.8Pa) presented a relatively low DT (0.48g.min^{-1}), so there was not a clear distinction in DT based on $\sigma_{Y\ 0°C}$. Although observed data with low $\sigma_{Y\ 0°C}$ values were within 95% confidence interval, from 1.8 to 3.7Pa, samples presented unstable DT, ranging from 0.48 to 2.00g.min^{-1}. Therefore, although data from ice cream commercial products for $\sigma_{Y\ 0°C}$ did not fit well in the model from previous work (Chapter 3), it was very interesting the common trend in commercial ice cream products and ice creams with controlled structural formation.

4.5 Conclusions

A wide variety of structural components influence the rheological behavior of commercial ice cream products. Fat destabilization was the main parameter to affect rheological properties at 0°C although the effects decreased at 20°C. Fat destabilization was the main parameter that affected elastic (G'), viscous (η_0) and transient (σ_Y) behaviors of melted ice cream matrix, followed

by overrun and air cell size. It is important to note that serum phase also showed effects on rheological parameters through total solids and mix density. However, it was not possible to identify which were the main components that affected serum phase due to unknown formulation of commercial samples. A common exponential decay trend was observed between DT and rheological parameters ($G'_{0°C}$, $\eta_{0\ 0°C}$ and $\sigma_{Y\ 0°C}$) from previous model and observed data of commercial samples. Data from commercial ice creams fitted well in previous model proposed (Chapter 3) for $G'_{0°C}$ of ice creams with controlled structural formation. Commercial ice cream products with $G'_{0°C}$ above 200Pa presented sufficient elasticity to keep DT below 0.46g.min^{-1}. Commercial samples with $\eta_{0\ 0°C}$ and $\sigma_{Y\ 0°C}$ above 7.11Pa.s and 4.1Pa, respectively, also presented DT below 0.46g.min^{-1}. Therefore, responses from DT suggested that $G'_{0°C}$ was a good rheological parameter to indicate melting behavior of commercial ice cream products. Last, the clear common trend in commercial ice cream products and ice creams with controlled structural formation for correlations between DT with $G'_{0°C}$, $\eta_{0\ 0°C}$ and $\sigma_{Y\ 0°C}$ showed that ice cream rheology is important perspective studying meltdown properties.

4.6 Acknowledgements

The authors thank Rachel Fehring for her help in collecting data from meltdown test, particle size distribution and tracing of ice crystals and air cells. D.O. Freire would like to thank his scholarship from CNPq (National Council for Scientific and Technological Development – Brazil) and financial support from FDC (Frozen Dessert Center).

4.7 References

Ahmed, J., 2015. Effect of Barley B-Glucan Concentrate On Oscillatory and Creep Behavior Of Composite Wheat Flour Dough. J. Food Eng. 152, 85–94. https://doi.org/https://doi.org/10.1016/j.jfoodeng.2014.11.018

Bolliger, S., Goff, H.D., Tharp, B.W., 2000. Correlation between colloidal properties of ice cream mix and ice cream. Int. Dairy J. 10, 303–309.

Briggs, J.L., Steffe, J.F., Ustunol, Z., 1996. Vane Method to Evaluate the Yield Stress of Frozen Ice Cream. J. Dairy Sci. 79, 527–531. https://doi.org/https://doi.org/10.3168/jds.S0022-0302(96)76395-6

Chang, Y., Hartel, R.W., 2002a. Stability of Air Cells in Ice Cream during Hardening and Storage. J. Food Eng. 55, 59–70.

Chang, Y., Hartel, R.W., 2002. Measurement of Air Cell Distributions in Dairy Foams. Int. Dairy J. 12, 463–472. https://doi.org/https://doi.org/10.1016/S0958-6946(01)00171-6

Clarke, C., 2004. **The Science of Ice Cream**, First. ed. The Royal Society of Chemistry, Cambridge.

Cook, K.L.K., Hartel, R.W., 2010. Mechanisms of ice crystallization in ice cream production. Compr. Rev. Food Sci. Food Saf. 9, 213–222.

Dogan, M., Kayacier, A., Toker, Ö.S., Yilmaz, M.T., Karaman, S., 2013. Steady, dynamic, creep, and recovery analysis of ice cream mixes added with different concentrations of xanthan gum. Food Bioprocess Technol. 6, 1420–1433.

Dolz, M., Hernández, M.J., Delegido, J., 2008. Creep and recovery experimental investigation of low oil content food emulsions. Food Hydrocoll. 22, 421–427. https://doi.org/https://doi.org/10.1016/j.foodhyd.2006.12.011

Donhowe, D.P., Hartel, R.W., Bradley, R.L., 1991. Determination of ice crystal size distributions in frozen desserts. J. Dairy Sci. 74, 3334–3344.

Eisner, M.D., Wildmoser, H., Windhab, E.J., 2005. Air cell microstructuring in a high viscous ice cream matrix. Colloids Surfaces A Physicochem. Eng. Asp. 263, 390–399.

Elliott, J.H., Ganz, A.J., 1977. Salad dressings—preliminary rheological characterization. J. Texture Stud. 8, 359–371.

Goff, H.D., Freslon, B., Sahagian, M.E., Hauber, T.D., Stone, A.P., Stanley, D.W., 1995. Structural Development in Ice Cream—Dynamic Rheological Measurements. J. Texture Stud. 26, 517–536. https://doi.org/10.1111/j.1745-4603.1995.tb00801.x

Goff, H.D., Hartel, R.W., 2013. **Ice Cream**, Seventh. ed. Springer Science & Business Media, New York.

Granger, C., Leger, A., Barey, P., Langendorff, V., Cansell, M., 2005. Influence of formulation on the structural networks in ice cream. Int. Dairy J. 15, 255–262. https://doi.org/https://doi.org/10.1016/j.idairyj.2004.07.009

Gunasekaran, S., Ak, M.M., 2003. **Cheese Rheology and Texture.** CRC Press LLC, Boca Raton.

Hui, Y.H., 2006. **Handbook of Food Science, Technology, and Engineering.** Taylor & Francis, Boca Raton.

Kaschta, J., Schwarzl, R.R., 1994. Calculation of discrete retardation spectra from creep data — I. Method. Rheol. Acta 33, 517–529. https://doi.org/10.1007/BF00366336

Lucey, J.A., Teo, C.T., Munro, P.A., Singh, H., 1997. Rheological properties at small (dynamic) and large (yield) deformations of acid gels made from heated milk. J. Dairy Res. 64, 591–600. https://doi.org/10.1017/S0022029997002380

Luyten, H., Kloek, W., Van Vliet, T., 1994. Yielding behaviour of mixtures of xanthan and enzyme-modified galactomannans. Food Hydrocoll. 8, 431–440.

Muse, M.R., Hartel, R.W., 2004. Ice Cream Structural Elements that Affect Melting Rate and Hardness. J. Dairy Sci. 87, 1–10. https://doi.org/https://doi.org/10.3168/jds.S0022-0302(04)73135-5

Purkayastha, S., Peleg, M., Normand, M.D., 1984. Presentation of the creep curves of solid biological materials by a simplified mathematical version of the generalized Kelvin-Voigt model. Rheol. Acta 23, 556–563. https://doi.org/10.1007/BF01329288

Rao, M.A.A., 2007. **Rheology of Fluid and Semisolid Foods: Principles and Applications**, Second. ed. Springer Science & Business Media, New York.

Segall, K.I., Goff, H.D., 2002. A modified ice cream processing routine that promotes fat destabilization in the absence of added emulsifier. Int. Dairy J. 12, 1013–1018. https://doi.org/https://doi.org/10.1016/S0958-6946(02)00117-6

Shama, F., Sherman, P., 1966. The Texture of Ice Cream 2. Rheological Properties of Frozen Ice Cream. J. Food Sci. 31, 699–706. https://doi.org/10.1111/j.1365-2621.1966.tb01926.x

Sherman, P., 1966. The Texture of Ice Cream 3. Rheological Properties of Mix and Melted Ice Cream. J. Food Sci. 31, 707–716. https://doi.org/10.1111/j.1365-2621.1966.tb01927.x

Sofjan, R.P., Hartel, R.W., 2004. Effects of overrun on structural and physical characteristics of ice cream. Int. Dairy J. 14, 255–262.

Steffe, J.F., 1996. **Rheological Methods in Food Process Engineering**. Freeman Press, East Lansing.

Toker, O.S., Karaman, S., Yuksel, F., Dogan, M., Kayacier, A., Yilmaz, M.T., 2013. Temperature Dependency of Steady, Dynamic, and Creep-Recovery Rheological Properties of Ice Cream Mix. Food Bioprocess Technol. 6, 2974–2985. https://doi.org/10.1007/s11947-012-1005-4

Warren, M.M., Hartel, R.W., 2018. Effects of Emulsifier, Overrun and Dasher Speed on Ice Cream Microstructure and Melting Properties. J. Food Sci. 83, 639–647. https://doi.org/10.1111/1750-3841.13983

Warren, M.M., Hartel, R.W., 2014. Structural, Compositional, and Sensorial Properties of United States Commercial Ice Cream Products. J. Food Sci. 79, E2005–E2013. https://doi.org/10.1111/1750-3841.12592

Wildmoser, H., Scheiwiller, J., Windhab, E.J., 2004. Impact of disperse microstructure on rheology and quality aspects of ice cream. LWT-Food Sci. Technol. 37, 881–891.

Wu, B., Freire, D.O., Hartel, R.W., 2019. The Effect of Overrun, Fat Destabilization, and Ice Cream Mix Viscosity on Entire Meltdown Behavior. J. Food Sci. 84, 2562–2571. https://doi.org/10.1111/1750-3841.14743

Table 4.1 Comparison of means using Tukey's HSD for total fat, total solids, ice cream mix density (ICM density), overrun, extent of fat destabilization (FD), air cell and ice crystal sizes of commercial ice creams products ($\alpha = 0.05$).

Code	Total Fat (%)	Total Solids (%)	ICM Density (kg L^{-1})	Overrun (%)	FD (%)	Air Cell Size (µm)	Ice Crystal Size (µm)
106	*14.1^{a}	*39.7^{bc}	**1.091^{g}	90.1 ± 0.9^{cde}	36.0 ± 0.7^{cd}	16.1 ± 1.1^{cde}	32.6 ± 2.4^{d}
129	9.9 ± 0.1^{fg}	38.5 ± 0.2^{ef}	1.108 ± 0.001^{a}	104.2 ± 7.1^{b}	39.6 ± 2.1^{c}	16.9 ± 0.3^{cde}	34.4 ± 0.9^{cd}
293	*10.49^{cd}	37.0 ± 0.1^{i}	1.098 ± 0.001^{ef}	83.4 ± 0.4^{e}	54.3 ± 1.9^{b}	16.6 ± 0.3^{cde}	38.0 ± 1.1^{bcd}
297	9.9 ± 0.1^{fg}	38.6 ± 0.2^{e}	**1.108^{a}	79.8 ± 2.6^{ef}	73.7 ± 1.5^{a}	12.3 ± 1.0^{de}	44.6 ± 1.5^{ab}
320	*10.4^{de}	37.5 ± 0.1^{ghi}	1.101 ± 0.001^{de}	87.4 ± 2.0^{cde}	23.7 ± 1.3^{ef}	21. 7 ± 1.8^{bc}	40.8 ± 1.3^{bcd}
325	9.8 ± 0.1^{g}	38.9 ± 0.2^{de}	1.110 ± 0.002^{a}	98.0 ± 3.2^{bc}	62.3 ± 1.5^{b}	14.6 ± 0.7^{cde}	37.7 ± 0.8^{bcd}
347	*10.0^{efg}	37.6 ± 0.1^{ghi}	**1.104^{bcd}	91.6 ± 0.3^{cde}	22.5 ± 1.5^{ef}	13.5 ± 0.2^{cde}	35.2 ± 1.9^{bcd}
[1]358	*10.3^{def}	39.3 ± 0.1^{cd}	**1.101^{a}	96.1 ± 1.3^{bcd}	74.0 ± 2.2^{a}	10.5 ± 0.5^{e}	53.5 ± 4.8^{a}
[1]410	*10.3^{defg}	37.3 ± 0.1^{hi}	**1.101^{de}	121.4 ± 0.3^{a}	58.2 ± 2.0^{b}	20.3 ± 3.2^{bcd}	36.3 ± 1.4^{bcd}
559	14.2 ± 0.1^{a}	37.6 ± 0.1^{gh}	1.082 ± 0.001^{h}	32.6 ± 0.1^{g}	77.0 ± 1.6^{a}	20.2 ± 2.9^{bcd}	40.3 ± 1.3^{bcd}
652	10.1 ± 0.2^{defg}	*37.9^{fg}	1.104 ± 0.001^{bcd}	84.7 ± 0.7^{de}	4.5 ± 0.2^{g}	31.0 ± 3.0^{a}	35.1 ± 0.7^{bcd}
710	10.8 ± 0.2^{c}	39.2 ± 0.1^{cd}	1.106 ± 0.001^{abc}	81.3 ± 0.7^{e}	33.7 ± 1.0^{cd}	17.9 ± 1.1^{cde}	35.3 ± 0.8^{bcd}
880	*14.2^{a}	40.7 ± 0.1^{a}	**1.095^{f}	37.3 ± 0.6^{g}	24.4 ± 0.6^{ef}	27.2 ± 1.7^{ab}	44.2 ± 1.0^{ab}
903	10.4 ± 0.1^{cde}	38.9 ± 0.1^{de}	**1.107^{ab}	90.3 ± 1.9^{cde}	28.6 ± 2.0^{de}	17.7 ± 0.6^{cde}	33.8 ± 1.2^{cd}
957	*12.1^{b}	40.1 ± 0.1^{b}	1.103 ± 0.001^{cd}	68.7 ± 1.5^{f}	19.6 ± 2.4^{f}	18.8 ± 0.5^{cde}	42.7 ± 2.1^{bc}

[1]Samples from ice cream sandwich.

*Values denoted with standard errors lower than 0.1%.

**Values denoted with standard errors lower than 0.001kg L^{-1}.

^{a,b,c,d,e,f,g,h,i} Means denoted with the same letter are not significantly different from each other ($p > 0.05$).

Table 4.2 Parameter estimates, coefficients of determination (R^2 and R^2_{Adj}) of the multiple linear regression models for storage (G') and loss (G") moduli, loss tangent (tanδ), residual viscosity (η_0) and yield stress (σ_y) at 0 and 20°C.

Rheological Test	Y	Coefficients							R^2	R^2_{Adj}	F Ratio
		Intercept	FD	MD	TS	OR	AC	Fat			
OTR	$G'_{0°C}$	-25686*	15.2**	23210*	n/a	n/a	n/a	n/a	0.68	0.63	12.7521
	$G''_{0°C}$	-4430*	3.0**	4010*	n/a	n/a	n/a	n/a	0.71	0.67	14.9252
	$G'_{20°C}$	-2066*	4.1**	n/a	45.8*	2.0*	7.4	n/a	0.71	0.60	6.2461
	$G''_{20°C}$	-470*	1.0***	n/a	10.6*	0.4*	1.9	n/a	0.73	0.62	6.7825
	$tan\delta_{20°C}$	0.338***	-0.0009*	n/a	n/a	n/a	n/a	n/a	0.31	0.26	5.9003
Creep	$\eta_{0\ 0°C}$	-219340	412*	n/a	5638	n/a	n/a	n/a	0.39	0.29	3.8389
	$\eta_{0\ 20°C}$	-73060*	83*	n/a	1746*	74*	n/a	n/a	0.55	0.42	4.4280
Stress Growth	$\sigma_{y\ 0°C}$	-190.7	0.27*	n/a	5.816	n/a	n/a	-3.0	0.44	0.28	2.8372
	$\sigma_{y\ 20°C}$	-52.3*	0.06*	n/a	1.278*	0.041	n/a	n/a	0.52	0.39	4.0137

Legend: FD is fat destabilization, MD is mix density, OR is overrun, AC is air cell size, TS is total solids and Fat is total fat.
$^{*}p<0.05$, $^{**}p<0.01$; $^{***}p<0.001$.

Table 4.3 Comparison of means using Tukey's HSD for storage (G') and loss (G") moduli, loss tangent (tanδ), residual viscosity (η_0) and yield stress (σ_{YS}) at 0 and 20°C of commercial ice cream products ($\alpha = 0.05$).

Code	G'$_{0°C}$ (kPa)	G"$_{0°C}$ (kPa)	Tanδ$_{0°C}$	G'$_{20°C}$ (kPa)	G"$_{20°C}$ (kPa)	Tanδ$_{20°C}$	$\eta_{0\ 0°C}$ (kPa.s)	$\eta_{0\ 20°C}$ (kPa.s)	$\sigma_{Y\ 0°C}$ (Pa)	$\sigma_{Y\ 20°C}$ (Pa)
106	0.47±0.01^{abcd}	[1]0.11^{ab}	**0.23^{bcd}	0.20±0.01^{abc}	[2]0.06^{abcdef}	[3]0.29^{ab}	33.1±3.5^{bc}	5.4±1.9^{bcd}	7.3±0.3^{ab}	2.6±0.2^{abcd}
129	0.84±0.11^{cde}	0.18±0.02^{bc}	0.21±0.01^{abc}	0.20±0.03^{abc}	0.06±0.01^{bcdef}	0.29±0.01^{ab}	17.3±1.3^{abc}	11.4±1.8^{e}	16.5±2.2^{c}	3.8±0.3^{de}
293	0.21±0.01^{ab}	*0.05^{a}	**0.26^{d}	0.08±0.01^{a}	[2]0.02^{a}	0.29±0.01^{abc}	2.7±0.4^{a}	0.9±0.2^{a}	4.1±0.4^{a}	0.9±0.1^{ab}
297	1.76±0.33^{f}	0.32±0.06^{d}	**0.19^{a}	0.23±0.04^{bcd}	0.07±0.01^{def}	0.29±0.01^{abc}	34.6±3.2^{c}	8.6±1.2^{de}	21.1±2.2^{c}	4.2±0.4^{de}
320	0.16±0.01^{ab}	*0.04^{a}	0.25±0.01^{d}	0.07±0.01^{a}	[2]0.02^{a}	0.37±0.02^{c}	1.8±0.1^{a}	***0.6^{a}	1.8±0.1^{a}	0.9±0.1^{ab}
325	0.88±0.07^{de}	0.18±0.01^{bc}	0.20±0.01^{ab}	0.19±0.03^{abc}	0.05±0.01^{abcde}	**0.28^{ab}	59.7±15.1^{d}	7.0±0.6^{cde}	46.9±4.6^{d}	9.9±1.5^{f}
347	0.35±0.06^{abc}	0.07±0.01^{a}	0.20±0.01^{ab}	0.12±0.02^{ab}	0.03±0.01^{abc}	0.28±0.02^{ab}	12.5±1.8^{abc}	1.8±0.2^{ab}	8.2±0.8^{a}b	1.3±0.2^{abc}
[1]**358**	1.12±0.07^{e}	0.24±0.01^{cd}	0.21±0.01^{abc}	0.36±0.04^{d}	0.09±0.01^{f}	0.24±0.01^{a}	24.5±6.4^{abc}	7.6±0.6^{de}	14.0±1.3^{bc}	5.1±0.4^{e}
[1]**410**	0.64±0.09^{bcde}	0.16±0.02^{bc}	**0.26^{d}	0.32±0.06^{cd}	0.08±0.01^{ef}	**0.26^{a}	7.1±0.5^{a}	4.8±0.8^{abcd}	8.2±0.2^{ab}	3.4±0.1^{cde}
559	0.48±0.02^{abcd}	*0.11^{ab}	0.23±0.01^{bcd}	0.19±0.03^{abc}	[2]0.06^{abcdef}	0.31±0.03^{abc}	11.7±1.4^{abc}	***0.9^{a}	5.1±0.1^{a}	1.2±0.1^{abc}
652	0.13±0.01^{a}	*0.03^{a}	0.25±0.01^{cd}	[2]0.08^{a}	[2]0.03^{ab}	0.36±0.02^{bc}	2.0±0.2^{a}	***0.6^{a}	2.0±0.2^{a}	0.9±0.1^{ab}
710	0.33±0.01^{ab}	*0.06^{a}	**0.20^{ab}	0.14±0.01^{ab}	[2]0.04^{abcd}	0.29±0.01^{ab}	10.4±1.1^{ab}	3.0±1.0^{abc}	6.4±0.5^{ab}	3.2±0.4^{bcde}
880	0.33±0.01^{ab}	*0.07^{a}	0.20±0.01^{ab}	0.23±0.02^{bcd}	[2]0.06^{cdef}	0.27±0.01^{a}	12.6±1.8^{abc}	5.3±0.3^{bcd}	17.1±1.7^{c}	4.6±0.4^{de}
903	0.13±0.01^{a}	*0.03^{a}	0.23±0.01^{bcd}	0.08±0.01^{a}	[2]0.03^{ab}	0.31±0.01^{abc}	2.1±0.2^{a}	0.9±0.1^{a}	2.9±0.3^{a}	1.2±0.1^{abc}
957	0.11±0.01^{a}	*0.03^{a}	0.26±0.02^{d}	[2]0.07^{a}	[2]0.02^{a}	0.36±0.04^{bc}	2.4±0.1^{a}	***0.5^{a}	3.7±0.5^{a}	0.8±0.1^{a}

[1]Samples from ice cream sandwich.
*Values denoted with standard errors lower than 0.01kPa.
**Values denoted with standard errors lower than 0.01.
***Values denoted with standard errors lower than 0.1kPa.s.
[a,b,c,d,e,f,g,h,i] Means denoted with the same letter are not significantly different from each other ($p > 0.05$).

Chapter 5

5 Conclusions and Recommendations

5.1 Conclusions

The arrangement of structural components in the ice cream matrix governed not only the rheological behavior but also the ice cream behavior in the meltdown test. No structural component was responsible for a specific rheological behavior; however, the most influential structural component depended on each rheological parameter evaluated, which was obtained by applying different types of shear to the sample. Since the different rheological parameters could be related to structural component rearrangement events, the importance of the different rheological tests used in this study helped understand the mechanisms involved in melting ice cream. Thus, the selected correlations between rheological and meltdown properties provided a still unexplored perspective and shed new light on the different structural rearrangement mechanisms involved in ice cream meltdown.

In the first study, mix viscosity at $50s^{-1}$, fat destabilization extent and overrun provided a wide variety of structures that provided good correlations with the selected rheological parameters. Although the rheological behavior of ice cream was strongly influenced by ice phase presence, the elastic behavior ($G'_{-15°C}$) of the frozen matrix was most influenced by the mix viscosity. In the absence of ice phase and with an intact structure assumed, fat destabilization that the most influence on elastic behavior ($G'_{0°C}$) of the melted matrix. In the transient flow behavior at very low shear rate, a six-element model (generalized Kelvin-Voigt model) provided good representation of the creep behavior of melted ice cream. Moreover, mix viscosity had the greatest effect on the $\eta_{0\ 0°C}$, which illustrated transient flow behavior of the melted matrix, followed by fat destabilization. Although $\eta_{0\ 0°C}$ value was obtained at constant stress load and the stress required to initiate the flow ($\sigma_{Y\ 0°C}$) of the melted matrix was obtained at constant shear rate, mix viscosity had the most influence on the $\sigma_{Y\ 0°C}$, followed by fat destabilization. Moreover, due to these similar

transient flow conditions, the linear correlation between $\eta_{0\ 0°C}$ and $\sigma_{Y\ 0°C}$ values was also used to validate $\sigma_{Y\ 0°C}$ measurements. The rheological destruction ($Thix_{0°C}$), which provided insights about the initial structural formation in the melted matrix, was a promising rheological parameter to characterize the structural development in ice creams. Mix viscosity had the most influence on $Thix_{0°C}$, but fat destabilization also showed strong influence. Moreover, the outstanding correlation between $Thix_{0°C}$ and $tan\delta_{Peak}$ (from OTR) suggested that structure that influenced $tan\delta_{Peak}$ values during ice melting and dilution of serum phase in OTR was similar to that initial structure disrupted during the thixotropic loop.

In the second study, good correlations between rheological and meltdown parameters verified the importance of rheological behavior on meltdown test of ice cream. Although $G'_{0°C}$ provided good correlations with drip-through (DT) and final height (FH), the results suggested that the elastic behavior is important in the melted ice cream, but other rheological parameters were needed to give more insights about DT and FH in meltdown test. The partial flow of ice cream on the top of the screen during meltdown test has a low shear rate. Thus, $\eta_{0\ 0°C}$, which was obtained at a low shear rate, provided good correlations with DT and FH obtained in meltdown test. Although $\sigma_{Y\ 0°C}$ is a different measurement and was measured with a different input, the force required for the melted matrix to yield was obtained in a similar transient flow condition that $\eta_{0\ 0°C}$ was measured. Therefore, $\sigma_{Y\ 0°C}$ also provided good correlations with DT and FH. Furthermore, trends in the correlations of structural components with $\eta_{0\ 0°C}$ were also similar to those trends of structural components with $\sigma_{Y\ 0°C}$, which reaffirm the validation of $\sigma_{Y\ 0°C}$ measurements. The $Thix_{0°C}$ measurements provided outstanding correlations with DT and FH. The suggested initial structural formation by $Thix_{0°C}$ was highly correlated with DT and FH in meltdown test. This thixotropic loop was successfully used for a more accurate structural

characterization of melted ice creams. Finally, the wide structural range created in ice creams by mix viscosity, extent of fat destabilization and overrun as well as outstanding correlations of these structural components with rheological and meltdown properties showed that besides the ice phase, these structural components have great importance in the structural arrangement and physical properties of ice cream.

In the third study, the practical application of the two previous works was verified in commercial ice cream products. A wide range of structural components affected rheological properties and DT of commercial ice cream products. Fat destabilization was the most influential structural component on the DT as well as on the elastic ($G'_{0°C}$), viscous ($\eta_{0\ 0°C}$) and transient ($\sigma_{Y0°C}$) behaviors at 0°C, whereas the influence of fat destabilization on rheological properties decreased at 20°C. After fat destabilization, overrun and air cell size provided the most influence on G', η_0 and σ_Y in the melted ice cream matrix. Although the main components that affected serum phase were not identified due to unknown formulation of commercial samples, it is worth noting that the serum phase also affected rheological properties through total solids and mix density. Furthermore, the strong linear correlations between η_0 and σ_Y reaffirmed the reliable measurements of $\sigma_{Y\ 0°C}$. Last, although formulations and processes were unknown in commercial ice cream products, the observed data in this study had an outstanding fit from the models of Chapter 3, which were obtained from ice creams with controlled structural formation. This consolidated the importance of rheological behavior in meltdown test of ice cream.

5.2 Recommendations

The rheological parameters discussed in this dissertation were selected so that the mechanical performance of an ice cream sample during meltdown test could briefly be highlighted.

Moreover, due to the large volume of data obtained, the discussion of all parameters of each rheological test became redundant. Thus, further studies of other rheological parameters may assist in better understanding the mechanical performance of an ice cream sample during sensory tests and texture analyses.

In oscillatory thermo-rheometry (OTR), storage modulus (G') measures the deformation energy stored and recovered per cycle of deformation in the matrix, while loss modulus (G") measures the deformation energy dissipated and lost in the sample per cycle of deformation. Mix viscosity had the most influence on G' in ice phase presence (-15°C), while extent of fat destabilization was the most influential parameter on G' in ice phase absence (0°C). Moreover, mix viscosity had the most influence in drip-through (DT) rate and final height (FH). A study focused in the G" measurements at -15°C, which evaluate viscous behavior in intact structure, would probably provide insights about sensory and texture properties, such as denseness, scoopability or hardness, of ice cream. Moreover, further studies focused on tanδ (ratio between G" and G') behavior, namely $\tan\delta_{Peak}$, which was most influenced by mix viscosity, as well as G" at 0°C, which was most affected by fat destabilization, can probably provide deeper understanding of flavor release and perception in ice cream. The values of $\tan\delta_{Peak}$ were reached at different temperatures, which was very strongly affected by mix viscosity and fat destabilization, in this study. It is known that fat destabilization and mix viscosity can affect sensory properties in ice cream (Amador et al., 2017); also, fat is a good flavor carrier in ice cream and temperature affects the partitioning of flavor compounds between lipidic and serum phases (Berg and Rankin, 2005) in dairy products. Therefore, a study focused on fat destabilization and mix viscosity combined with rheological parameters, such as $\tan\delta_{Peak}$ and $G"_{0°C}$, and dynamic sensory evaluation may provide interesting insights about flavor perception in ice cream.

Structural components similarly affected elastic modulus (G_0) from creep tests and G' (from OTR). Beyond the residual viscosity, η_0, obtained at low shear rate, the creep test is an important method to evaluate internal structure of food products. The internal structure is also responsible for the viscoelastic behavior, which may affect textural properties in ice cream. Therefore, a study focused on internal structure parameters, such as retarded elastic moduli, G_1 and G_2 (springs in six-element model) and internal viscosities, η_1 and η_2 (dashpots in six-element model), textural properties in ice cream may present important information about the mechanical performance during texture analyses.

In stress growth test, the structural components that affected shear modulus (G) similarly affected G_0 and G'. Equilibrium viscosity (η_∞) showed similar trend to η_0. Mix viscosity was the most influential component on yield stress (σ_y). Moreover, the most influential structural component on both the work required for yield stress of the melted ice cream and excess work of structure breakdown (W) was mix viscosity, but with also strong effects from fat destabilization. The work required to reach the yield stress of the sample as well as W may present significant correlations with textural properties, namely parameters from texture profile analysis.

In flow ramp test, the time-dependency behavior, assessed as stress peak (σ_{Peak}), had very strong correlations with the initial structure formation, which was characterized by the rheological destruction (Thix) in this test. Thix showed to be a promising rheological parameter in ice cream research, which may have outstanding correlations not only with textural properties, but also with sensory properties of ice cream.

Last, some observed outliers in Chapter 3 (seen clearly in Figures 3.12A, 3.16A), namely samples S1A1P3-S1A3P3 (see codes back in Table 2.1), with high fat destabilization and low mix viscosity, showed low FH as well as low σ_Y and Thix, which could be explained by percolation

events that occur during the meltdown test of the ice cream. Furthermore, in Chapter 2, correlations between $\tan\delta_{Peak}$ and Thix suggested that the structure that affected $\tan\delta_{Peak}$ magnitude during ice melting and dilution of serum phase was similar to the initial structure that was disrupted during the thixotropic loop. Therefore, a study focused on structural components, such as mix viscosity, fat destabilization and overrun, combined again with rheological parameters, such as $\tan\delta_{Peak}$, σ_Y and Thix, as well as experiments to evaluate diffusion and percolation events, may provide deeper understanding of melting mechanisms in ice cream.

Amador, J., Hartel, R., Rankin, S., 2017. The Effects of Fat Structures and Ice Cream Mix Viscosity on Physical and Sensory Properties of Ice Cream. J. Food Sci. 82, 1851–1860. https://doi.org/10.1111/1750-3841.13780

Berg, D.P., Rankin, S.A., 2005. Partitioning Behavior of Alkan-1-ols between Milkfat and Aqueous Phases As Influenced by Temperature. J. Agric. Food Chem. 53, 2646–2651. https://doi.org/10.1021/jf048263q